INVESTIGATING THE NUCLEAR IMPORT PROTEIN KPNβ1 AS A CANCER THERAPEUTIC TARGET

Aderonke Fopesaye Ajayi-Smith

Thesis presented for the Degree of

DOCTOR OF PHILOSOPHY

In the Division of

Medical Biochemistry and Structural Biology

Department of Integrative Biomedical Sciences

UNIVERSITY OF CAPE TOWN

January 2019

Declaration

I, **Aderonke Fopesaye Ajayi-Smith**, hereby declare that the contents of this thesis are based on my original work, except where acknowledgements indicate otherwise; and that neither the whole work nor any part of it has been, is being, or is to be submitted for another degree in this or any other University. I am now submitting this thesis for academic examination towards the Degree of Doctor of Philosophy in Medical Biochemistry.

Signed by candidate

Signed: Date: 18/January/2019

Acknowledgements

Words are not enough to express my deepest appreciation to the following people:

My supervisor, Prof Virna Leaner for her immeasurable support and guidance during the course of this project. I see clearly because I was privileged to stand on your shoulder.

A/ Prof Denver Hendricks for his constant encouragement and constructive feedbacks.

Dr Pauline Van der Watt for always giving amazing suggestions that contributed immensely to the success of this work.

Dr Zenda Woodman for her emotional support and positive energy.

Our laboratory manager, Mrs Hajira Guzgay for keeping the lab running, and for the motherly care.

Our laboratory technician, Mr Robert Samuels for his dedication and diligence, you made our work a lot easier.

I would also love to appreciate my present and past colleagues in the cancer lab, you guys were available to share your time, protocols and a shoulder to cry on, Dr Cherise Dunn, Sarah Carden and Dr Tamara Stelma and Dr Erin Strydom.

To the past and present members of the Zenda Woodman lab: Bahiah Meyer, Alessandra Unterpertinger and Riley Traviss, for their constant support and friendly chats.

Mr Rodney Lucas for his patience and assistance with the animal study.

Mrs Susan Cooper for her assistance with the fluorescent microscope.

Mrs Sylva Schwager for the assistance with the biophysical assay.

Mr Ronnie Dreyer for the assistance with flow cytometry analysis.

Pastors Aderemi and Mopelola Adelusi for the spiritual support and encouragement.

Dr Henry Adeola for the friendship, brotherly support and inspiration.

Dr Omolaja Osoniyi for the career mentorship.

National Research Foundation (NRF) and the University of Cape Town for the financial assistance.

To IUBMB for awarding me the funding to travel to the conference in Seoul, South Korea

To my special friends who have walked this road with me, Babatunde Akinoso, Mofoluke Oluleye, Tolulope Eunice, Temilade Aina, Oluwatosin Ojo, Ursula-Claire Andong, Christian Polorigni, Adetunji 'Teejay' Adesina, Olabanji Alo-Steven, Abigail Osiki, Olanrewaju and Titilayomi Kunnuji, Prisca Osiki, Nonku Mkwanazi, Bianca Abrahams, Michael Okpara, Mateen Wagiet and Jamie Pillaye. True friends are indeed a man's best possession.

My siblings, Abayomi, Omolola and Omokolade Ajayi-Smith, thanks a lot for believing in me and for being my biggest supporters. I have come this far because I have you all by my side.

My parents, Otunba Abayomi and Yeye Olusola Ajayi-Smith, I cannot appreciate you both enough for the sacrifices and prayers. You both are my backbone.

“Known unto God are all his works

From the beginning of the world”

Acts 15:18

Contents

Abbreviations

5-FU	5-Fluorouracil
~	Approximately
˚C	Degree Celsius
%	Percentage
AC	Adenocarcinoma
ADMET	Absorption, Distribution, Metabolism, Excretion, Toxicology
AP-1	Activator Protein 1
APS	Ammonium Persulphate
ARM	Armadillo
ATCC	American Type Culture Collection
BBB	Blood-Brain Barrier
BCA	Bicinchoninic Acid
BCL-2	B-Cell Lymphoma Leukemia 2
BLI	Bio-Layer Interferometry
BSA	Bovine Serum Albumin
CAS	Cellular Apoptosis Susceptibility Protein
CCK-8	Cell Counting Kit-8
CD	Circular Dichroism
CDDP	Cisplatin
CDK4	Cyclin-Dependent Kinase 4
CHX	Cycloheximide
CI	Confidence Interval
CIN	Cervical Intraepithelial Neoplasia
CL	I*n vitro* Intrinsic Clearance
CML	Chronic Myeloid Leukemia
cNLS	classical NLS
C60	Compound 60
CRM1	Chromosomal Region Maintenance 1
CREB	cAMP Response Element Binding
CYP	Cytochrome P450
DAD	Diode array detector
DAPI	4',6-diamidino-2-phenylindole dihydrochloride
DME	Drug Metabolising Enzyme
DMEM	Dulbecco's Modified Eagle's Medium
DMSO	Dimethyl sulfoxide

DNA	Deoxyribonucleic acid
EC_{50}	Half maximal Effective Concentration
EDTA	Ethylenediaminetetraacetic acid
EGFR	Epidermal Growth Factor Receptor
EGTA	Ethylene glycol-bis(β-aminoethyl ether)-N,N,N',N'-tetraacetic acid
EMT	Epithelial-Mesenchymal Transition
FOBT	Faecal Occult Blood Test
G	Gravitational force
GAPDH	Glyceraldehyde 3-Phosphate Dehydrogenase
GFP	Green Fluorescent Protein
GI	Gastrointestinal
GIST	Gastrointestinal stromal tumour
GORD	Gastro-Oesophageal Reflux Disease
GST	Glutathione-S-Transferase
HEPES	4-(2-hydroxyethyl)-1-piperazineethanesulfonic acid
HNSCC	Head and Neck Squamous Cell Cancer
HPLC	High Performance Liquid Chromatography
HPV	Human Papillomavirus
HSFAEC	Health Sciences Faculty Animal Ethics Committee
HSILs	High Grade Intraepithelial Lesions
IBB	Importin Beta Binding
INI-43	Inhibitory of Nuclear Import-43
i.p.	Intraperitoneal
IPTG	Isopropyl β-D-1-thiogalactopyranoside
ITC	Isothermal Titration Calorimetry
JNK	c-Jun N-terminal kinase
K_a	Equilibrium association constant
KCl	Potassium Chloride
K_d	equilibrium dissociation constant
kDa	Kilo Dalton
Kpnα2	Karyopherin Alpha 2
Kpnβ1	Karyopherin Beta 1
LMB	Leptomycin B
LSILs	Low Grade Intraepithelial Lesions
Log	Logarithm
Log D	Log of Distribution coefficient
Log P	Log of Partitioning coefficient
MCL-1	Myeloid Cell Leukemia 1

$MgCl_2$	Magnesium Chloride
MS/MS	Tandem Mass Spectrometry
MTT	3-[4,5-dimethylthiazol-2-yl]-2,5-diphenyltetrazolium bromide
Na_3VO_4	Sodium Orthovanadate
NaCl	Sodium Chloride
NaF	Sodium Fluoride
NCI	National Cancer Institute
NE	Nuclear Envelope
NES	Nuclear Export Signal
NFAT	Nuclear Factor of Activated T cells
NFκB	Nuclear Factor Kappa B
NLS	Nuclear Localization Signal/Sequence
NMR	Nuclear Magnetic Resonance
NPC	Nuclear Pore Complex
NSCLC	Non-small cell lung cancer
NTF2	Nuclear Transport Factor-2
Nups	Nucleoporins
OBA	Oral Bioavailability
OD	Optical density
PAHs	Polycyclic Aromatic Hydrocarbons
PAMPA	Parallel Artificial Membrane Permeability Assay
PARP	Poly (ADP-Ribose) Polymerase
PBS	Phosphate Buffered Saline
PCD	Programmed Cell Death
PD	Pharmacodynamics
PFA	Paraformaldehyde
PI	Propidium Iodide
PK	Pharmacokinetics
PMA	Phobol 12-Myristate 13 Acetate
PPB	Plasma Binding Protein
PPI	Protein-Protein Interaction
pRb	Retinoblastoma Protein
PS	Phosphatidyl Serine
PSA	Prostate Specific Antigen
PTHrP	Parathyroid Hormone Related Protein
RanBP	Ran Binding Protein
RanGAP	RanGTP-Activating Protein
RanGDP	Ran-Guanosine Diphosphate

RanGEF	Ran-Guanosine Nucleotide Exchange Factor
RanGTP	Ran-Guanosine Triphosphate
RCC1	Regulator of Chromosome Condensation-1
RIPA	Radioimmunoprecipitation assay
RNA	Ribonucleic acid
RNase	Ribonuclease
rpm	Revolutions per minute
SAR	Structural Activity Relationship
SCC	Squamous Cell Carcinoma
SDS	Sodium Dodecyl Sulphate
SDS-PAGE	SDS polyacrylamide gel electrophoresis
SEM	Standard Error Mean
SINE	Selective Inhibitors of Nuclear Export
siRNA	Small-interfering RNA
SMIs	Small Molecule Inhibitors
SPR	Surface Plasmon Resonance
SREBP2	Sterol Regulatory Binding Protein 2
SSA	Super Streptavidin
SSHR	Signal Sequence Hydrophobic Region
SV-40	Simian Virus 40
STAT	Signal Transducers and Activators of Transcription
$T_{1/2}$	Half-life
TB	Terrific Broth
TBP	TATA-Binding Protein
TBS	Tris Buffered Saline
TBST	Tris Buffered Saline-Tween-20
U	Unit
VDSS	Volume of Distribution at Steady State
VEGFR	Vascular Endothelial Growth Factor Receptor
V	Volts
XPO1	Exportin 1

Units

M	Molar
mM	Millimolar
µM	Micromolar
nM	Nanomolar

g	Gram
kg	Kilogram
µg	Microgram
mg	Milligram
ng	Nanogram
L	Liter
µL	Microliter
mL	Milliliter
m	meter
µm	Micrometer
mm	Millimeter
nm	Nanometer

Abstract

The dysregulation of numerous genes has been associated with the development and progression of cancer, many of which are being investigated as potential therapeutic targets. Previous work in our laboratory and others reported the elevated expression of the nuclear import protein Karyopherin Beta 1 (Kpnβ1) in various cancers. The inhibition of Kpnβ1 by siRNA silencing inhibited the proliferation of cancer cells and induced cell death via apoptosis while having little effect on non-cancer cells. These findings suggested that Kpnβ1 has potential as an anti-cancer therapeutic target. Using an *in silico* screening approach to identify small molecule inhibitors of Kpnβ1 with anti-cancer activity, a number of compounds were selected for further investigation in our laboratory. The aim of this study was to investigate a novel small molecule, Compound 60 (9-[(1-methyl-3-piperidinyl)methoxy]-4-[(6-methyl-2-pyridinyl)methyl]-7-(5-methyl-2-thienyl)-2,3,4,5-tetrahydro-1,4-benzoxazepine); by monitoring (i) its effect on cancer cell biology using cervical and oesophageal cancer cell lines, (ii) its effect on nuclear import activities associated with Kpnβ1, (iii) its *in vitro* ADME pharmacokinetics and *in vivo* anti-cancer properties and (iv) performing biophysical analysis of Kpnβ1:C60 interactions.

Cervical and oesophageal cancer cells were found to be more sensitive to C60 treatment compared to non-cancer epithelial cell. C60 treatment resulted in the inhibition of cancer cell proliferation, colony formation, migration and invasion. G1/S cell cycle arrest and a reduced expression of cell cycle regulatory proteins such as Cyclins D1, B1 and A as well as CDK4 was observed on treatment with C60. C60 induced cell death via apoptosis as observed PARP cleavage. These results suggest that C60 has an inhibitory effect on cancer cell biology.

Immunofluorescent analysis and nucleo-cytoplasmic western blot analysis showed that C60 treatment resulted in the cytoplasmic retention of Kpnβ1. Immunofluorescent analysis and luciferase reporter assays showed that C60 inhibited the nuclear entry and transcriptional activity of a Kpnβ1 cargo, NFκB. Similarly, the transcriptional activity of cargo proteins NFAT and AP-1 were also inhibited. This suggests that C60 inhibits the nuclear entry of Kpnβ1 and thus its function as a nuclear importer of cargo proteins.

In vitro ADME pharmacokinetics analysis found C60 to have high solubility, permeability and plasma protein binding properties and a short half-life. These findings suggest that C60 may have good oral absorption but rapid clearance in living systems. *In vivo* toxicology studies showed that C60 is tolerable, allowing for its testing in a xenograft nude mouse model. Intraperitoneal injection of C60 selectively inhibited the growth of oesophageal tumour cells with a significant effect observed on KYSE 30 oesophageal tumours.

To investigate Kpnβ1:C60 binding interactions, Kpnβ1 was purified using the GST-tagged purification technique. Purified Kpnβ1:C60 interactions were monitored using the Bio-layer interferometry technique. Our preliminary data suggest an interaction between C60 and Kpnβ1 with K_d values in the micromolar range. We obtained varying K_d values, hence further optimisation is required to arrive at a conclusive K_d value.

In conclusion, this study is a first to show that Compound 60 (9-[(1-methyl-3-piperidinyl)methoxy]-4-[(6-methyl-2-pyridinyl)methyl]-7-(5-methyl-2-thienyl)-2,3,4,5-

tetrahydro-1,4-benzoxazepine), a small molecule identified to bind Kpnβ1 in an *in silico* screening approach interferes with the subcellular localisation of Kpnβ1, inhibits the localisation and transcriptional activity of Kpnβ1 cargo proteins and inhibits cancer cell biology *in vitro* and *in vivo*. *In vitro* ADME pharmacokinetics shows that C60 has tolerable drug properties. Biophysical analysis shows that C60 appears to bind Kpnβ1 in the micromolar range. Together, these results provide evidence for C60 as a compound that warrants further investigation as an anti-cancer agent.

Chapter 1: Literature review

1.1. Cancer and its hallmarks

Carcinogenesis in humans consists of multiple stages, and each stage has genetic alterations that drive the stepwise transformation of normal cells into highly malignant cells[1]. Berenblum and Schubik initially described the idea of multi-stage carcinogenesis in 1948 and it has been validated by other studies. Modern-day oncology identifies three major phases in carcinogenesis: initiation, promotion and progression and each of these phases may be made up of numerous stages [2,3]. The hallmarks of cancer are made up of biological abilities gained during the multi-step development of tumours. The hallmarks make up an organising principle for describing the complicated nature of neoplastic diseases and are well described by Hanahan and Weinberg, 2011 [4]. These hallmarks are important changes in cell physiology that contribute to malignancy. They include characteristics such as evading growth suppression, inducing angiogenesis, activating invasion and metastasis, sustaining proliferative signalling and resisting cell death (Figure 1.1). Genomic instability and tumour promoting inflammation are essential to these hallmarks as they create the genetic diversity that accelerates their acquisition and promotes several hallmark functions respectively [1,4].

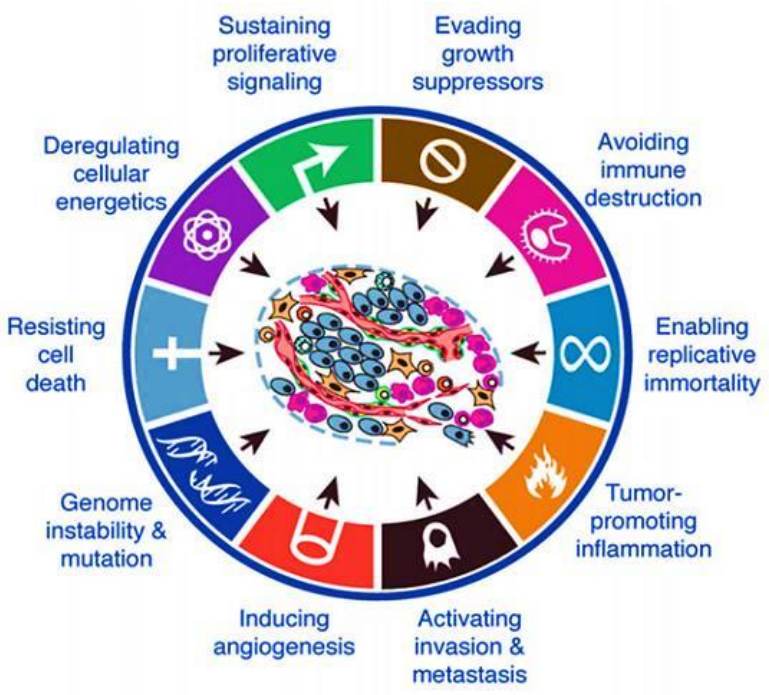

Figure 1.1. The hallmarks of cancer. These acquired abilities are essential for tumour growth and progression. Adapted from Hanahan and Weinberg (2011) [4].

1.2. The global burden of cancer

Cancer is the primary cause of mortality worldwide and it accounted for 8.2 million deaths in 2012, with most of these deaths arising from cancers of the oesophagus, lung, stomach, colon, liver, and breast [5]. The incidence of cancer increased from 12.7 million in 2008 to 14.1 million in 2012, and a 75% increase is expected over the next two decades with the estimated number of cancer cases expected to rise to 25 million [5,6]. Over 60% of global cancer cases are in the developing countries of South America, Africa, and Central Asia with these regions accounting for about 70% of global cancer mortality [6]. Figure 1.2 shows the approximated incidence and mortality rate of the top 10 cancers in both males and females worldwide, and highlights the global burden of oesophageal and cervical cancers. Cervical and oesophageal cancers have high prevalence and high mortality rates in South Africa [7], and this formed the rationale for choosing them for this study. Cervical

cancer is the fourth most common cancer in women and it ranks as the seventh most common cancer when cancer incidences in both sexes are considered. Oesophageal cancer is the eighth most common cancer globally and the sixth most common cause of mortality [7]. The global rise in cancer incidence is a major human health challenge, which demands actions on multiple fronts including improved treatment options, prevention and early detection [8].

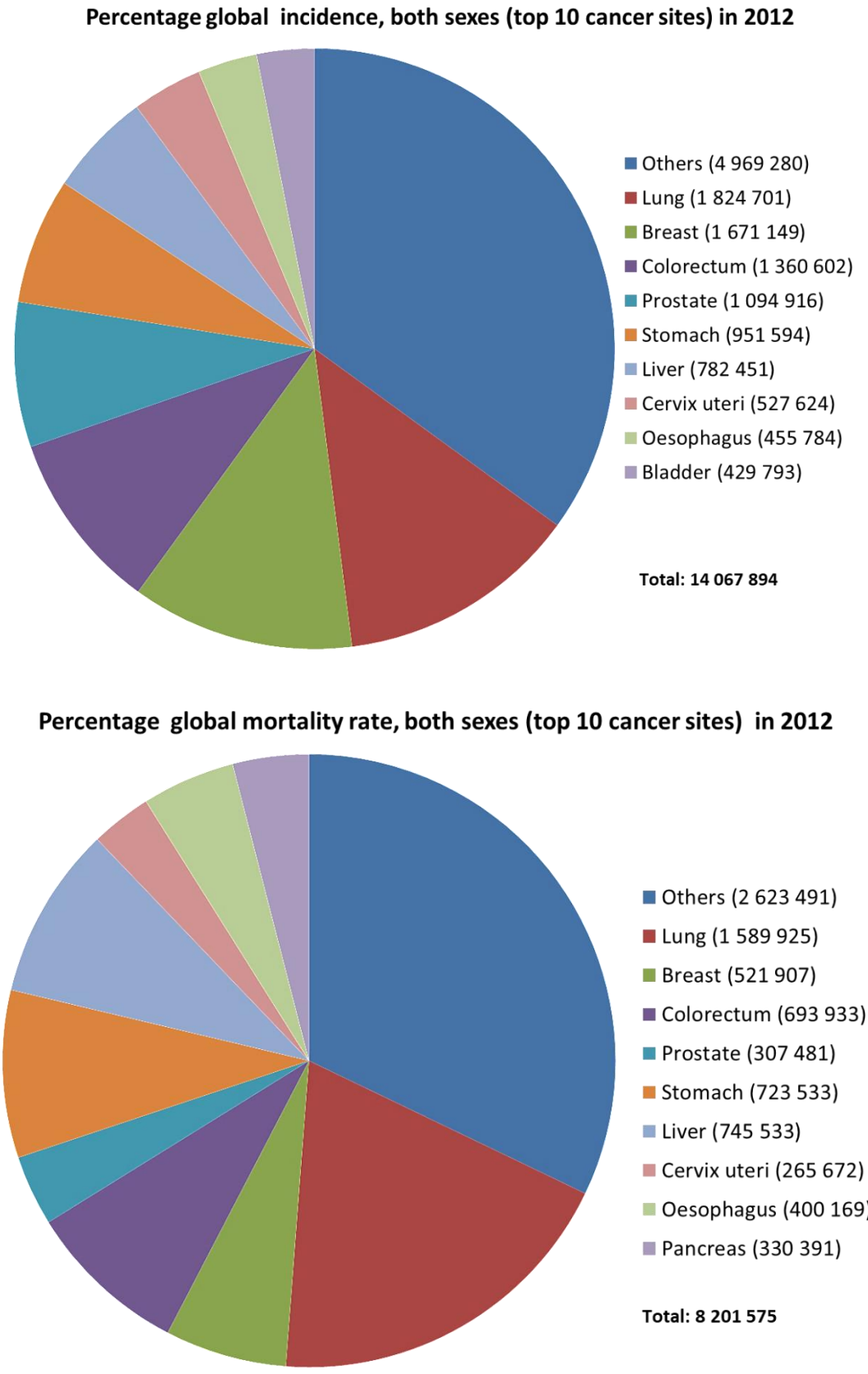

Figure 1.2. Global estimated incidence and mortality of cancer in both males and females. Adapted from WHO cancer today [9].

1.2.1. Cervical cancer

Approximately 85% of cervical cancer cases are diagnosed in developing countries, where it accounts for approximately 12% of all female cancers [7]. Cervical cancer is the second most common cancer among South African women [10]. There is a convincing association between cervical cancer and incessant infection with high-risk Human Papillomavirus (HPV) 16 and 18 [11,12]. HPV DNA is found in 99.7% of all cervical cancer cases and HPV 16 and 18 account for 70% of these cases [13]. In addition to persistent HPV infection, other factors that affect the progression from infection to Cervical Intraepithelial Neoplasia (CIN) include behaviours such as smoking, multiple partners, use of contraceptives, former pregnancies, immunosuppression and infection with other sexually transmitted pathogens such as *Chlamydia trachomatis* [12,14].

Functionally high-risk HPV infection promotes cellular transformation and tumour progression via the activity of two viral oncogenes: E6 and E7. These two oncogenes interfere with the activity of significant cell cycle regulatory proteins such as p53 and Retinoblastoma protein (pRb) [11]. The E6 oncogene deregulates the cell cycle through inhibiting p53 function. The interaction of E6 with p53 is one of the major causes of chromosomal instability in cells transformed by HPV E6. The association between pRb and E7 is critical for HPV-facilitated cancer development. E7 binds pRb and other members of pocket protein family resulting in the deregulation of the G1/S checkpoint [15,16]. The natural sequence of cervical cancer involves reversible alterations in normal cervical tissues from a state in which neoplastic changes are absent in the squamous epithelium to different states of cellular abnormalities that result in the development of cervical cancer. This sequence of transformation forms the basis for the cytological

screening for cervical cancer and corresponds with the basic multistep carcinogenic process in the development of CIN [17].

All sexually active women are at risk of HPV infection with about 80% being infected with HPV in their lifetime. The realisation that the infection of the cervix by oncogenic HPV is essential but not sufficient for the development of cervical cancer led to the development of effective prophylactic vaccines [13]. The United States Food and Drug Administration (FDA) endorsed the prophylactic quadrivalent HPV (types 6, 11, 16, 18) vaccine (Gardasil) for use in women aged 9-26 years old in 2006. The prophylactic bivalent HPV (types 16 and 18) vaccine (Cervarix) was approved for use in women between age 10-25 years [14]. Both vaccines have shown 100% efficiency against vulvar, cervical and vaginal intraepithelial neoplasias in virus-naive individuals [18]. Gardasil showed preventive efficacy against pre-malignant genital lesions, external genital warts and cervical cancer caused by specific HPV types [18,19]. As effective as the bivalent and quadrivalent vaccines were, they have limitations, as they were ineffective against unspecified HPV types that account for about 30% of all cervical cancers. This insufficient protection led to the license of a 9-valent HPV vaccine (types 16, 18, 31, 33, 45, 52, 58, 6 and 11) named Gardasil-9. Gardasil-9 has demonstrated 90% protective efficacy against cervical cancer and genital warts [18].

Although these vaccines are valuable, they do not have beneficial effects in women that are already infected with HPV. Studies have shown that women infected with high-risk HPV types 16 and 18 have a higher chance of developing invasive cervical cancer over a period of years [20]. Cervical cancer is mostly a preventable disease owing to the fact that

its causal agent is known. Its identified viral activator and the well-known stages of disease progression makes cervical cancer an ideal model for investigating new potential therapies [21].

1.2.2. Oesophageal cancer

Approximately 80% of oesophageal cancer cases occur in less developed countries [7]. Oesophageal Squamous Cell Carcinoma (SCC) is the most frequent and malignant type of oesophageal cancer [22,23] with high prevalence in developing nations including South Africa [24]. Oesophageal SCC arises from epithelial cells in the upper and middle portion of the oesophagus [25,26]. Another type is oesophageal Adenocarcinoma (AC) which arise from the glandular cells that are found in the lower third of the oesophagus (the junction of the oesophagus and stomach) [25,26]. The oesophagus has a distinct anatomy that makes the behaviour of its malignancy different from other gastrointestinal malignancies. The wall of the oesophagus has no serosa and this increases the invasive property of oesophageal cancer. In addition, it has an extensive network of lymphatics which allows for early local tumour advancement [27]. Oesophageal cancer if not detected and treated early has the ability to metastasize to nearby lymph nodes and to other body parts such as the liver through the bloodstream [28].

Risk factors for oesophageal SCC include malnutrition, alcohol, tobacco, chemical carcinogens such as Polycyclic Aromatic Hydrocarbons (PAHs) [25,28,29]. Smoking and alcohol consumption are some of the major risk factors for oesophageal cancer among South Africans [30]. The primary risk factors for oesophageal AC are Gastro-Oesophageal Reflux Disease (GORD) and Barrett's oesophagus [28,29]. GORD is a common gastrointestinal disorder

which develops when there is a reflux of stomach contents which ultimately leads to disturbing symptoms or complications including heartburn and regurgitation [31,32]. GORD can consequently lead to the development of a spectrum of injury which includes esophagitis, Barrett's oesophagus and AC [31]. The association between carcinogenesis and GORD suggests that this condition must be treated early [32]. Barrett's oesophagus can develop as a result of GORD over an extended period, which leads to the damage of the inner lining of the oesophagus. In Barrett's oesophagus, squamous cells lining the oesophagus are substituted with glandular cells that are more resistant to stomach acid. Individuals with Barrett's oesophagus are more likely to develop oesophageal AC compared to those without, although, only a few people with Barrett's oesophagus will develop AC [33]. The understanding of the risk factors and multiple stages of various cancers is critical for accurate diagnosis, and development of novel and effective therapeutic strategies.

1.3. Cancer and therapeutic strategies

In spite of the new discoveries and development in the field of oncology, cancer remains a difficult disease to treat. This is largely due to the late detection of this disease. Diagnosis and accurate measurement of cancer progression are thus essential for the successful management of cancer [34]. Patients who were diagnosed with advanced cases of either lung, colorectal or breast cancer had 5-year survival rates of 3%, 5%, and 27% respectively compared to patients with early-stage lung, colorectal or breast cancer who had 5-year rates of 50%, 90% and 98% respectively [35]. These figures show that the early stages of cancer carry the highest potential for therapeutic intervention; however, this stage is mostly asymptomatic resulting in delayed diagnosis [34]. Various tests such as Faecal Occult Blood Test (FOBT) for colon cancer, Prostate-Specific Antigen (PSA) for prostate cancer, annual

mammogram for breast cancer and Pap smear for cervical cancer have been used for the detection of cancers [35]. However, most of these tests are not efficient at detecting tumours at early stages.

Cancer is a disease that has a vast molecular diversity among different individuals, so patients with the same clinically diagnosed cancer often have different responses to the same treatment because each case of cancer has a unique molecular signature [36]. The conventional therapeutic approaches for cancer are surgery, irradiation, and chemotherapy [37,38]. Surgery and radiation therapy are used for treating primary tumours and metastases while chemotherapeutic approaches are generally used for disseminated tumours such as breast, prostate and colorectal [38]. Conventional chemotherapeutic agents function by inhibiting cell division and DNA replication and could also affect microtubule spindle assembly; however, they are not efficient at treating all cancer types [38]. A limitation of many chemotherapies is their lack of specificity for cancer cells resulting in systemic toxicity and also the frequent development of drug-resistant cancer cells [39]. Treatment options such as immunotherapy, signal transduction therapy, angiogenesis therapy, nucleic acid-based therapy and apoptosis regulation therapy are all under investigation with recent studies focusing on novel approaches that involve target specific treatments [38]. With advances in technology allowing for target identification, the field of cancer research has moved from a "one-size-fits-all" treatment approach to a customised medicine strategy that concentrates on the discovery and development of molecularly targeted drugs that take advantage of the specific genetic requirements and susceptibilities of cancer cells [40].

1.4. Targeted therapy in the treatment of cancers

Targeted therapy refers to the generation of cancer drugs developed to interfere with unique molecular targets that are considered to play important roles in tumour growth and survival [38]. Targeted therapies are hypothesised to be more effective in cancer treatment and have reduced side effects. The recognition of suitable targets relies on a detailed understanding of the molecular changes that accompany cancer development [38,39]. Targeted therapy focuses on delivering drugs to specific genes or proteins that are essential to cancer cells or the tissue environment that facilitates the growth of cancer [39]. Targeted therapies utilize various mechanisms such as inhibition of proliferation, promotion of cell cycle regulation, apoptosis or autophagy induction, metastasis suppression and reversal of multidrug resistance [38,39]. Targeted therapy includes the use of monoclonal antibodies or oral small-molecule drugs [41–43].

i. Monoclonal antibodies

Monoclonal antibodies that target specific tumour surface markers provide tumour specific and less toxic alternatives for cancer treatment [42]. The conjugation of monoclonal antibodies to cytotoxic drugs increases the cell killing activity of these antibodies as well as conferring increased tumour selectivity on the cytotoxic drugs [42]. Gemtuzumab, a CD-33 specific monoclonal antibody linked to calicheamicin was used for the treatment of Acute Myeloid Leukemia (AML) [39]. Other monoclonal antibodies that have been licensed for use include Trastuzumab (Herceptin), the anti-Her2 monoclonal antibody that has been successfully used in the treatment of Her2-positive breast cancer [39,42], Campath (Alemtuzumab) for specific leukemias, Avastin (Bevacizumab), Vectibix (Panitu-mumab) and Erbitux (Cetuximab) for the treatment of colorectal cancer [42]. Monoclonal antibodies are

used for the direct delivery of chemotherapeutic drugs and radioactive substances to cancer cells [39].

ii. Small molecule inhibitors

Small Molecule Inhibitors (SMIs) are smaller than monoclonal antibodies and are readily absorbed by the body. They can be directed against molecular targets that are necessary for proliferation, angiogenesis and metastasis of cancer cells [39]. Protein kinases seem to exemplify essential molecular targets for cancer therapy. They are frequently found to be activated via mutation and/or amplification and this highlights their function in various forms of human cancers [37]. Such targets have become the focus in the search for newer anticancer treatments. Examples include, the use of Imatinib, a multi-kinase inhibitor in the treatment of acute promyelocytic leukemia caused by translocations in the RARα retinoic acid receptor gene [39], Chronic Myeloid Leukemia (CML) caused by BCR-ABL genetic reshuffling and Gastro-Intestinal Stromal Tumour (GIST) [37]. The success of Imatinib provided the evidence for the use of small molecules in targeting pathogenic driver anomalies in clinical settings [39].

Other SMIs of cancer targets include Gefitinib, an inhibitor of Epidermal Growth Factor Receptor (EGFR) kinase that has been approved for the treatment of lung cancer [39,44], Erlotinib- inhibitor of EGFR in Non-Small Cell Lung Cancer (NSCLC) patients, Lapatinib- inhibitor of EGFR/ERBB2 for ERBB2-positive breast cancer and Sorafenib- inhibitor of Vascular Endothelial Growth Factor Receptor (VEGFR) kinase in renal cancer [39]. Newer additions include Abiraterone- the CYP171A1 inhibitor, which blocks androgen synthesis and has been approved for the treatment of castration-resistant prostate cancer, Crizotinib, an

inhibitor of the protein kinase ALK approved for the treatment of NSCLC patients and Vemurafenib, an inhibitor of BRAF kinase for metastatic melanoma [39].

The success of Imatinib in the treatment of CML was remarkable as it showed a 90% success rate in comparison to 35% that can be achieved with conventional chemotherapy. Furthermore, most patients taking Imatinib showed complete cytogenetic remission [41]. Similarly, NSCLC patients treated with Gefitinib have a higher response rate and longer disease-free survival of 75% and 11 months respectively in comparison to those treated with conventional chemotherapy showing a response rate of 30% and disease-free survival of 5 months [41]. In some cases, the extent of clinical success is minimal as seen with the use of Erlotinib for the treatment of late-stage pancreatic cancer. The addition of Erlotinib to conventional chemotherapy increased the one-year survival rate from 17% to 24% [43]. Apart from increasing patients' survival, targeted therapy also provides treatment alternatives for patients who cannot be treated with conventional chemotherapy. For example, NSCLC and non-Hodgkin's lymphoma affects elderly individuals with health conditions that prevent the use of conventional chemotherapy. Targeted therapies such as Rituximab and Erlotinib are better tolerated and mostly less toxic giving these patients a better treatment option [43].

While significant progress has been made with the development of molecularly targeted therapies, there are limited therapeutic options for many patients as the process of developing a new drug is time-consuming with high failure rates [39]. Although molecular profiling provides guidance on appropriate treatment options for patients, the challenge of identifying disease-specific molecular targets still exists [45]. Following the identification of potential new therapeutic targets, the next process involves selecting and validating

the most suitable targets, while establishing a relationship between target modulation and a therapeutically significant biological effect in an appropriate experimental prototype [39].

1.5. Conventional and targeted therapeutic strategies for the treatment of cervical and oesophageal cancers

1.5.1. Therapeutic strategies for the treatment of cervical cancer

Cervical cancer is the fourth most common cancer in women globally, with an estimated incidence of 570,000 cases and mortality of 311,000 in 2018 [46]. In spite of the advances in screening, vaccination, treatment of early-stage tumour, a fraction of patients will be diagnosed with late-stage, recurrent cervical cancer. For this population of patients, chemotherapy is the major treatment option [47]. Cisplatin is the most studied single agent for cancer treatment. Data from the Gynaecologic Oncology Group showed an overall response rate of 38% with Cisplatin treatment. Overall survival with the use of cisplatin alone was 6.5 to 9 months with a progression-free survival of approximately three months [48]. Cisplatin in combination with radiation therapy has been studied widely and is phase 2 clinical trials. Other cytotoxic agents used alone or in combination with radiation therapy are carboplatin, fluorouracil, etoposide, bleomycin and paclitaxel [49].

Since the growth of cancer cells is largely dependent on oncogenic signal transduction pathways, new therapeutics are developed to alter these pathways by interfering with intracellular protein such as tyrosine kinases [47]. A recombinant monoclonal antibody, bevacizumab has been targeted against VEGF-A, it inhibits VEGFR-1 and VEGFR-2 signal transduction pathways. Increased VEGF expression has been linked to poor prognosis

and early recurrence in cervical cancer [46]. The tyrosine kinase inhibitors, sunitinib and pazopanib inhibit c-KIT, VGFR and PDGFR, however, they have not shown significant beneficial effect in overall survival in advanced cervical cancer [46]. The increased expression of EGFR in cervical cancer is associated with poor clinical outcomes, based on this, cetuximab, a monoclonal antibody against EGFR-1 has been evaluated in preclinical studies. Phase 2 clinical trial data showed that cetuximab alone was not maximally beneficial to patients [47]. Similarly, targeting EGFR with gefitinib or erlotinib did not have objective responses in cervical cancer patients [47].

Some of the targeted therapies used alone did not have significant benefit in the treatment of cervical cancer; hence, they have been used in combination with chemotherapy. In patients with recurrent or metastatic cervical cancer, treatment with Bevacizumab, an inhibitor of VEGF and chemotherapy was linked to increased survival [48]. Cetuximab and matuzumab, both monoclonal antibodies have been used in combination with cisplatin or cisplatin and topotecan in the treatment of persistent cervical carcinoma [48]. The combination of erlotinib, cisplatin and radiotherapy was used in a study involving 36 patients, 34 patients responded positively and had a 3-year progression-free survival [47].

1.5.2. Therapeutic strategies for the treatment of oesophageal cancer

Oesophageal cancer is the eight most common cancer and the sixth cause of cancer-associated mortality globally [50,51]. Most people are diagnosed with oesophageal cancer after the tumour has spread, and when cure is mostly impossible [51]. The traditional standard treatment for localised oesophageal SCC and AC is surgery, especially in

patients with early-stage disease. However, survival rates when surgery alone is used remains low with a median 5-year overall survival of approximately 20% [50]. Chemotherapeutic agents such as 5-FU, mitomycin C, cisplatin, vinorelbine, etoposide, irinotecan and the taxanes have been used as single agents or in combination for the treatment of oesophageal cancer. The response rates for the use of single agents ranged from 15% to 30%. Combination therapy containing cisplatin has been shown to produce better response rates [52]. The development of resistance has been associated with the use of chemotherapeutic agents [53], hence the need for more effective therapeutic strategies for treating oesophageal cancer.

The goal of targeted therapy in the treatment of oesophageal cancer is to improve the response rate and minimise metastasis. Some markers that have been associated with oesophageal cancer phenotype include EGFR, Ki-67, VEGF and HER-2 [52]. The overexpression of EGFR has been discovered in about 92% of oesophageal cancer cases and is associated with poor prognosis and disease progression. Cetuximab targets EGFR and is currently used in the treatment of oesophageal cancer [52]. Lapatinib, a small molecule and Trastuzumab are targeted against HER-2[53]. The use of targeted therapy in the treatment of oesophageal cancer is still in the early stage, promising results have been obtained with the use of antibodies directed against targets such as EGFR and VEGF[52].

For both cervical and oesophageal cancers, there is a need to discover more molecular targets that will be used in the development of novel targeted therapies. Currently, in the targeted therapies for both cancers are centred mostly on the use of monoclonal

antibodies. This current research is focused on discovering new molecular targets that be targeted with the use of small molecule inhibitors.

1.6. Gene Expression analysis in the identification of therapeutic targets

Microarray technology has been used extensively in different fields including basic biology and medical science. It is used particularly in the field of cancer research where a number of important genes involved in cancer progression have been identified [54]. Deoxyribonucleic Acid (DNA) microarray allows the expression pattern of multiple genes to be monitored in a single experiment making it possible to get the molecular portrait of both normal and cancer tissues [55]. Alizadeh *et al* (2000) used DNA microarray technology to carry out a systematic classification of gene expression in B-cell malignancies. They identified two molecularly different forms of Diffuse Large B-Cell Lymphoma (DLBCL) - germinal centre B-like DLBCL and activated B-like DLBCL. Furthermore, they showed that patients with germinal centre B-like DLBCL had considerable better overall survival than individuals with activated B-like DLBCL [56]. cDNA microarray analysis was used to compare the gene expression profiles of breast cancer tissues in comparison to normal breast tissues [57]. Furthermore, the FDA has endorsed a custom microarray of 70 genes for the prognosis of breast cancer [58].

Gene expression microarray analysis was previously used in our laboratory to profile non-cancer and cancer tissue of the cervix to identify novel cancer targets. Members of the Karyopherin superfamily of proteins were among the genes that showed significant differential expression in the cancer tissues compared to normal tissues. Included were,

Chromosome Region Maintenance 1 (CRM1), Karyopherin Beta 1 (Kpnβ1) and Karyopherin Alpha 2 (Kpnα2) which all showed elevated expression in cervical cancer tissue in compared to normal cervical tissue [55]. The Karyopherin proteins have key roles in nuclear transport and in other important cellular activities such as Nuclear Envelope (NE) and Nuclear Pore Complex (NPC) assembly, and mitotic and cell cycle regulation [59,60]. Sub-cellular localisation is important for proper protein function as it determines the access of proteins to their binding partners as well as their incorporation into biological networks. Abnormally localised proteins have been implicated in various human diseases such as kidney stones, Alzheimer's disease and cancer [61]. Hence, the nucleo-cytoplasmic transport system has received attention in recent years especially for their roles in cancer development and progression.

1.7. Karyopherin proteins and nucleo-cytoplasmic transport

The nucleo-cytoplasmic transport of proteins and ribonucleic Acids (RNAs) which occurs through the NPC is vital for their function [62,63]. There are four major role players involved in nucleo-cytoplasmic transport; transport receptors (also known as Karyopherins), Ran-Guanosine Triphosphate (RanGTP), Nucleoporins (Nups-proteins of the NPC) and cargoes [63]. The nucleo-cytoplasmic transport of proteins can alter gene expression and modify cell function, morphology, and composition [64].

Access to the nucleus is restricted by the NE which is a double membrane structure containing large pore structures known as NPCs [64–66]. The NPC is cramped with nucleoporins, which are defined by the presence of FG dipeptide (phenylalanine-glycine) repeats. These FG repeats are present throughout the NPC [67]. The nucleoporins are direct

facilitators of nucleo-cytoplasmic transport [68]. Various nucleoporins have been linked to CRM1-mediated nuclear export. The nucleoporin, Tpr serves as a primary binding site for CRM1-containing export complexes. Antibodies targeting Tpr resulted in the inhibition of nuclear export [69]. Studies using human cells showed that Nup358 promotes Karyopherin α/β and Transportin-mediated nuclear import. Furthermore, reduced nuclear import has been observed in Drosophila cells lackingNup358 [69].

The transport of small molecules, proteins and nucleotides required for the synthesis of DNA and RNA occurs through the NPC. The transport of macromolecules is mediated by a large family of transport receptors known as Karyopherins [63,70–73]. The Karyopherins are involved in different cellular processes such as gene expression, signal transduction, immune response and some pathologic processes including tumorigenesis [74]. The Karyopherin protein family is divided into alpha and beta subfamilies. The Karyopherin beta family members are responsible for mediating most import and export activities, while Karyopherin alpha family members act as adaptors [65]. There are more than 20 members of the Karyopherin beta family in mammals. Nine have been shown to act as export receptors (Exportins) while the others function as import receptors (Importins) [65,70,75,76]. A few members of this family act as both importins and exportins and are therefore referred to as Transportins [76]. Members of the Karyopherin beta family have molecular weights ranging between 90-150 kDa, and a tandem HEAT repeat structure formed by antiparallel helices that are connected by a short intra-repeat loop [59,77,78]. Importins bind their cargoes in the cytoplasm through the recognition of the Nuclear Localisation Sequence (NLS), while Exportins bind cargoes via recognition of the Nuclear Export Sequence (NES) [70].

Elevated expression of Karyopherin family members has been associated with cancers of different cell origin. The most implicated of these family are Kpnβ1, CRM1, Kpnα2 and Cellular Apoptosis Susceptibility Protein (CAS) [78]. Adam and Adam (1994) initially discovered Kpnβ1 as a cytosolic factor necessary for the NLS-mediated binding to the NE [79]. Chi *et al* (1995) later described its sequence and mechanism of action using *in vitro* nuclear import assays [80]. Since Kpnβ1 is the focus of this study, its structure, mechanism of action and role in cancer development will be expanded on in the latter part of this review.

Kpnα (an adaptor protein) recognises the classical NLS (cNLS) and also interacts with Kpnβ1 and together they form a classical trimeric complex [72,77]. Kpnα has two functional domains; an Importin Beta-Binding (IBB) domain at the amino terminus, and an NLS binding site which is made up of eight to ten Armadillo (ARM) repeats[72,81,82]. After recognising and binding cargoes containing cNLS, Kpnα binds Kpnβ1 through its IBB domain. The cargo: Kpnα: Kpnβ complex is transported across the NPC into the nucleus. In the nucleus, the complex dissociates on binding with RanGTP [65,73,77,83,84]. Kpnα binds to CAS which is responsible for its nuclear export [63,65,70]. The Kpnβ-RanGTP complex is transported back to the cytoplasm for a new round of import [63,65]. The classical nuclear import pathway is illustrated in Figure 1.3

Seven Kpnα isoforms, which bind differently to specific substrates, have been characterised and divided into 3 subfamilies: α1, α2 and α3. The α1 subfamily consists of Kpnα2 and Kpnα7, the α2 subfamily comprises Kpnα4 and Kpnα3 while the members of α3 subfamily include Kpnα1, Kpnα5 and Kpnα6 [78,85]. Two human Kpnα, α1, and α2 have been shown to bind the same β1: Kpnβ1. The binding domain of Kpnα1 and α2 contain binding sites for Kpnβ1 [86]. However, not all import cargoes contain a cNLS and therefore do not require an

adaptor protein such as Kpnα for nuclear import but rely directly on Kpnβ1 or other Karyopherin β members [70,77,83,87]. Direct Karyopherin β: cargo transport has been found to be faster (has more stable nuclear accumulation and initial import rate) compared to karyopherin β: α: cargo transport [74].

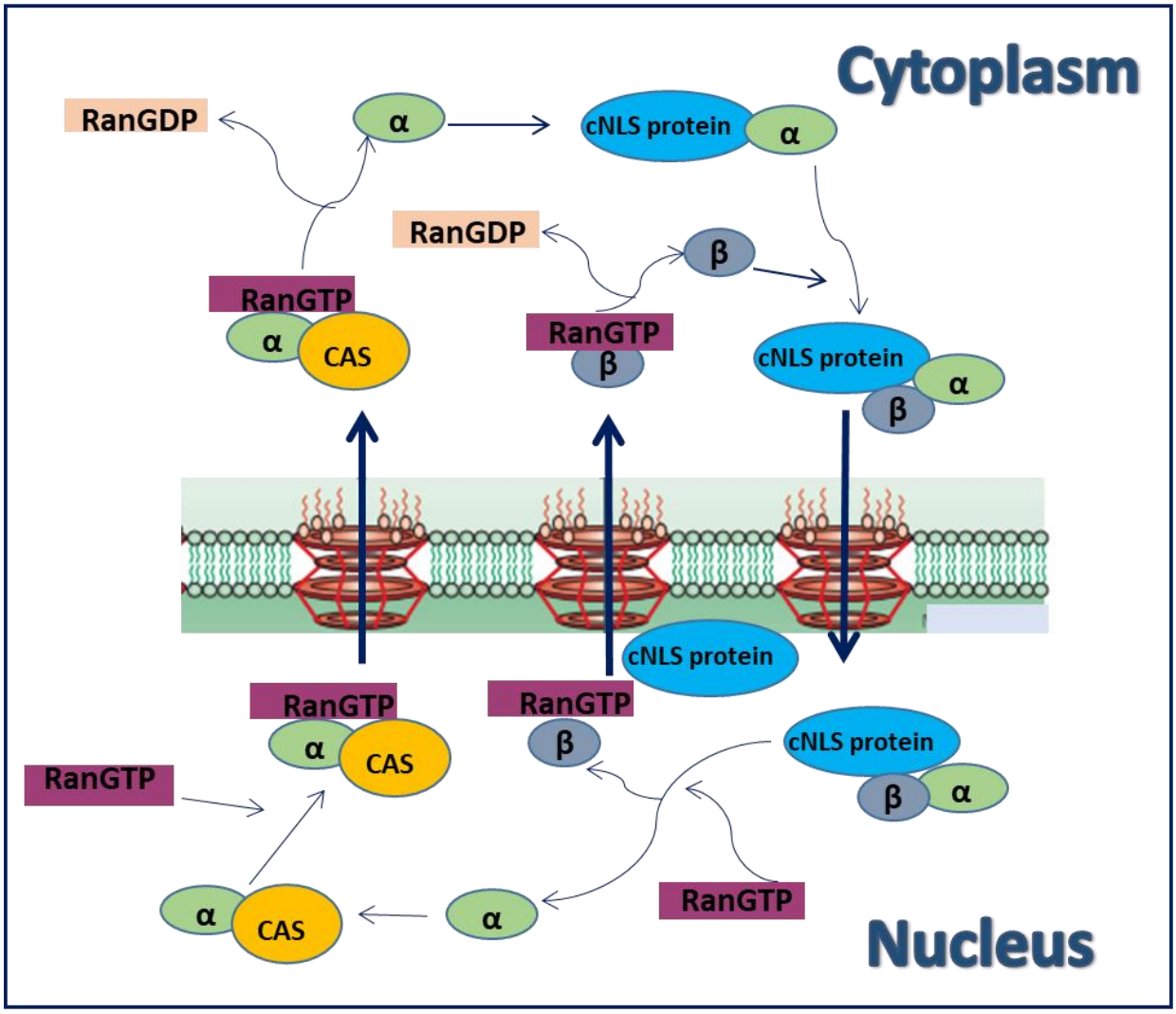

Figure 1.3. Graphic representation of the classical nuclear import pathway. Kpnα (α) recognises and binds to cargo containing NLS. This complex binds Kpnβ (β) and forms a trimeric complex that passes through the NPC into the nucleus. The binding of RanGTP causes a dissociation of the complex. Kpnβ-RanGTP complex is recycled into the nucleus while Kpnα is transported out of the nucleus by the export receptor CAS. Within the cytoplasm, the hydrolysis of RanGTP to RanGDP causes the dissociation of Kpnβ-RanGTP and Kpnα-CAS complexes, after which CAS is imported back into the nucleus. Adapted from Tau *et al*, 2004 [63].

CRM1 also known as Exportin 1 (XPO1) is the most extensively characterised nuclear export protein [83,88]. It is essential for the maintenance of correct chromosome structure [86]. It belongs to the Karyopherin beta family of export receptors; it exports proteins containing leucine-rich NES from the nucleus to the cytoplasm [83,87,88]. CRM1 binds to NES-containing cargo and then forms a complex with RanGTP. The complex moves out of the nucleus, the hydrolysis of RanGTP to RanGDP (Ran-Guanosine Diphosphate) by RanGAP (RanGTP-Activating Protein) results in the dissociation of the complex and causes cargo to be released into the cytoplasm [63,83]. The nuclear export pathway is illustrated in Figure 1.4. CRM1 has 20 HEAT domains that permit its binding to RanGTP, cargo binding occurs outside this HEAT domain ring [83]. The bond between the cargo and CRM1 is weak, however, the collective binding of cargo protein and RanGTP to CRM1 increases CRM1 binding affinity by 500-1000 fold [89].

Nuclear transport is dependent on the energy provided by Ran, a small nuclear GTP of the Ras family [65,83]. Ran has a molecular weight of about 25 kDa [83], and it switches between a GDP-bound state or GTP-bound state through nucleotide hydrolysis and exchange [77,82] . Ran functions in nuclear transport by maintaining the compartment-specific binding and release of transport cargoes [63,90,91]. RanGTPase has been described to be involved in mitotic spindle formation and organisation. It also functions in the reorganisation of the NE after cells enter interphase after exiting mitosis [92–94].

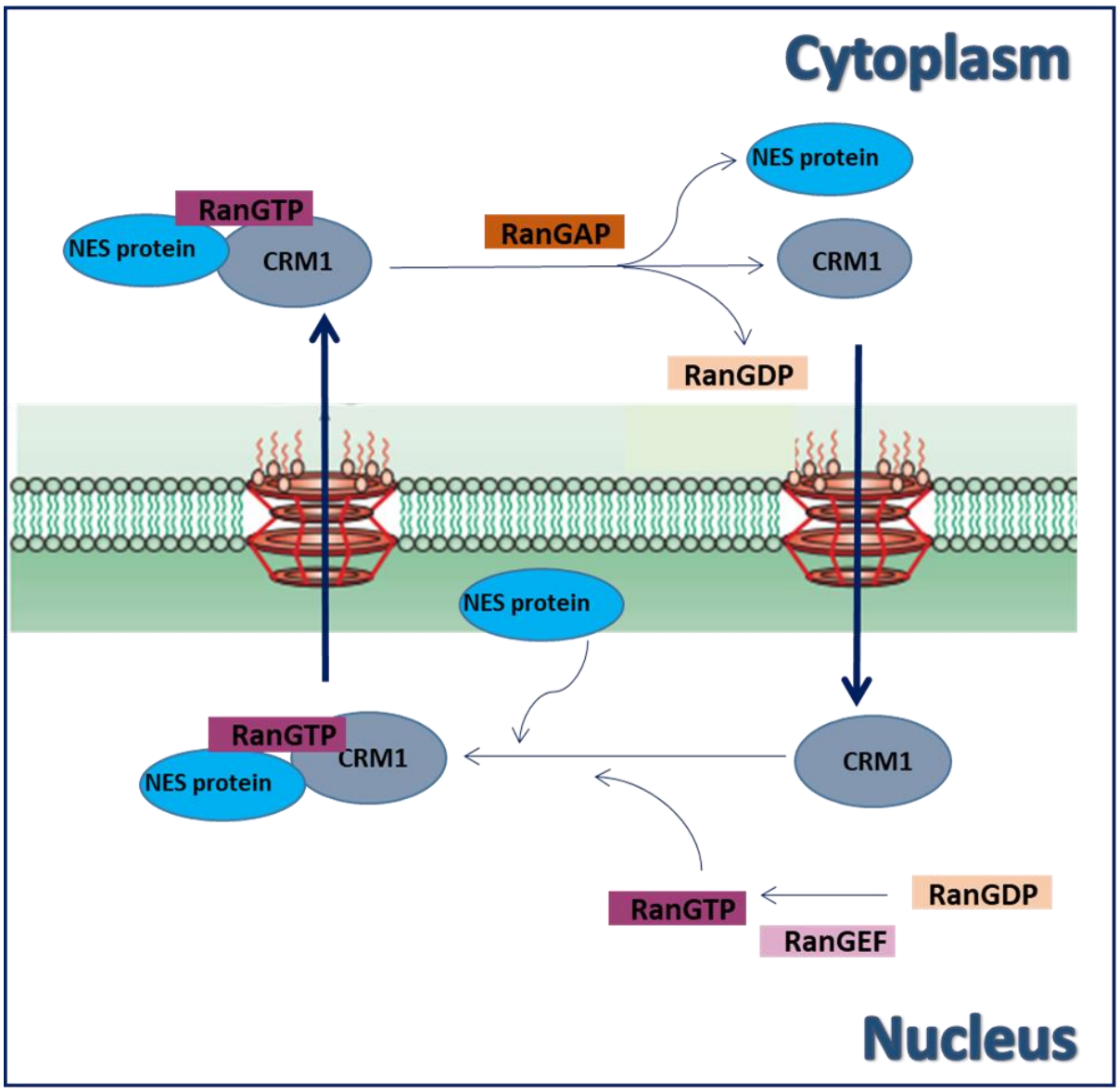

Figure 1.4. Graphic representation of the nuclear export pathway. Within the nucleus, CRM1 recognises and binds to cargo bearing NES in the presence of RanGTP. The ternary complex passes through the NPC into the cytoplasm. The conversion of RanGTP to RanGDP results in complex dissociation and cargo is released. CRM1 is then taken back into the nucleus to repeat a new export cycle. Adapted from Tau *et al*, 2004 [63].

1.7.1. Dysregulation of nuclear transport and cancer

The nucleo-cytoplasmic transport of proteins is necessary for the regulation of cell cycle and proliferation in both healthy and cancerous tissues. Dysregulation of the process may thus affect numerous cellular processes such as tumour growth, inflammatory response, and

apoptosis [95]. As correct sub-cellular localisation of proteins is essential, it is not surprising that disruptions in the nuclear transport pathway have been associated with oncogenesis and for the ability of cancer cells to evade and develop resistance to chemotherapeutic drugs [96]. Nuclear transport in cancer cells is deregulated and it has been observed that as cells move a dormant to proliferating and transformed state, the rate of nuclear transport increases [65]. Alterations in the nuclear transport pathway can occur through a variety of ways which include: alteration in the expression of transport receptors, alteration in the localisation of transport receptors, alteration of RanGDP/RanGTP gradient and disruption of endogenous inhibitors of nuclear transport [64,78].

Nucleo-cytoplasmic shuttling of cargoes in and out of the nucleus usually starts with the recognition of the cargo by its receptor, accompanied by docking and movement through the NPC. RanGTPase and its regulators control the rate of cargo movement through the NPC as well as the loading and unloading of cargoes. Changes in this process have been seen in many cancers [97,98]. Studies have reported the overexpression of RanGTPase in a variety of cancers such as prostate [99], breast [99], ovarian [100], kidney [101] and colon [99] cancers. Low levels of RanGTPase have been reported to be necessary for normal cell survival while its overexpression causes deregulation in normal cell activity which might contribute to cancer development [93]. Kpnα2 overexpression has been observed in breast cancer and melanoma where it is associated with poor prognosis and reduced disease-free survival [65,96]. The endogenous nuclear export protein, CAS which mediates the nucleo-cytoplasmic translocation of Kpnα is found to be overexpressed in several cancers such as colon, breast and liver cancers [96,102]. This aberrant expression activates the nuclear accumulation of Kpnα-dependent transcription factors which results in pathological cell proliferation [102]. Likewise,

overexpression of CRM1 has also been linked to various cancers such as cervical [55], ovarian [103], glioma [104] and oesophageal cancer [105]. Similarly, it has been linked to some haematological malignancies such as CML and Mantle Cell Lymphoma (MCL) [106]. There is evidence in the literature showing that Kpnβ1: Kpnα-mediated nuclear transport pathways play significant roles in development, adaptation and disease [107]. Previous work done in our laboratory identified multiple members of the Karyopherin family of proteins having elevated expression in cervical cancer cells in comparison to non-cancer cells [55]. As Kpnβ1 is the focus of this study, its role in cancer development will be expanded on in section 1.7.

1.7.2. Targeting nuclear transport for cancer therapy

Strategies that target host cell proteins that are essential to normal and malignant cells raise concerns as they may have side effects on the proliferation of non-cancer cells [65,102]. It is thus important to determine whether targeting a specific protein presents a therapeutic window where the malignant cells are more affected than non-malignant cells. There are reports showing that cancer cells are more responsive to nuclear transport inhibition compared to normal cells [55,105]. These studies suggest that cancer cells are more dependent on nuclear transport receptors for their increased proliferation and that therapies specifically targeting the transport machinery of tumour cells have promise as anti-cancer agents [64].

Therapeutic agents such as small molecules targeting nucleo-cytoplasmic transport can interfere with the binding of transport receptors to cargoes, binding of transport receptors to Ran regulators and with the interaction of these with the NPC [96]. The interaction between nucleoporins and transport receptors presents a target for the inhibition of nuclear

transport, and monoclonal antibodies against nucleoporins have been effectively used to inhibit the binding of cargo to the NPC in rat liver nuclear envelopes [108]. A peptidomimetic inhibitor of Kpnα/Kpnβ nuclear import that imitates the FXFG structure has also been reported to prevent the binding of Kpnβ to nucleoporins [96].

Competitive inhibition of cargo to receptor binding is also an unconventional method of altering the nucleo-cytoplasmic transport of proteins. The use of peptides having transport sequences to displace the nuclear import or export cargoes from their transport receptors is a prospective therapeutic approach [96]. Bimax1 and Bimax2 are two peptide inhibitors that have been identified as inhibitors of the classical nuclear import by Kosugi *et al* (2008). The experimental technique used was the activity-based profiling of systemically mutated NLS peptide templates. These peptides bind strongly to Kpnα independently of Kpnβ1 thereby inhibiting cargo release in the nucleus [64,96,109].

CRM1 is responsible for the nuclear export of most cargoes; it controls the export of a reported 220 proteins to date [110]. Elevated expression of CRM1 is common in many cancers and its inhibition results in the death of cancer cells [110,111]. Leptomycin B (LMB) is a first generation CRM1 inhibitor while Selective Inhibitors of Nuclear Export (SINE) are second generation CRM1 inhibitors [111]. The discovery of LMB as a cellular target of CRM1 was a key innovation. The binding of LMB to CRM1 occurs at a conserved cysteine residue, which matches the position 528 of the human protein. Disruption of CRM1-cargo binding occurs when LMB causes the alkylation of the cysteine residue in the hydrophobic groove of CRM1 [96]. The use of LMB was discontinued in phase 1 clinical trials as it displayed severe cytotoxicity and absence of obvious efficacy at tolerable doses [78,112]. More recently, newer

inhibitors of CRM1 known as SINEs have been developed and include KPT-330 (selinexor), KPT-335 (verdinexor), KPT-185, KPT-276 and KPT-251 [110]. Selinexor, a small molecule inhibitor of CRM1 as well other SINEs were developed using known structural activity relationship (SAR) and innovative computational methods [113]. SINEs have high selectivity for CRM1 and form a covalent bond that is slowly reversible with the cysteine-528 residue in the binding pocket of CRM1 [112,113]. These SINEs have shown anti-cancer activity in various solid and haematologic tumour xenograft models [112]. Selinexor is currently being tested as an anti-cancer drug in phase 2 and 3 clinical trials [114]. Ryan *et al* (2018) reported that Selinexor had clinical activity but poor tolerability in metastatic castration-resistant prostate cancer patients' refractory to second-generation anti-androgenic therapies [115]. There is thus sufficient evidence in the literature that targeting members of the Karyopherin protein family present as novel anti-cancer targets. Research into investigating multiple members in this family is currently underway.

1.8. Karyopherin Beta 1 (Kpnβ1), a nuclear transport protein that associates with cancer.

1.8.1. Kpnβ1 structure and functions

Kpnβ1 also known as Importin B or p97 is a transport protein that is involved in the nuclear import process [59,73,107,116]. Kpnβ1 can facilitate nuclear import autonomously [107,117] or by associating with adaptor proteins of the Karyopherin α family such as Kpnα2 [55,90,118]. Kpnβ1 imports certain cargoes on its own, examples of these include Sterol Regulatory Element Binding Protein-2 (SREBP2) and Parathyroid Hormone-related Protein (PTHrP) [119]. Examples of Kpnβ1 cargoes that require an adaptor include GATA3 and Signal Transducers and Activators of Transcription (STAT) family member [120].

Kpnβ1 is composed of 876 amino acids and has a molecular weight of 97 kDa [121]. Kpnβ1 is composed of 19 HEAT repeats [59,75,122], 13 of these HEAT repeats are used for its interaction with Kpnα in the classical nuclear import [59]. HEAT repeats 1-8 are used for the binding of Kpnβ1 to RanGTP, while HEAT repeats 7-19 (C-terminal) interact with the IBB domain of Kpnα. Additionally, Kpnβ1 binds to the FG-rich repeats of Nups using HEAT repeats 4-8 [65,121]. Kpnβ1 mediates the nuclear import of numerous proteins and many signalling networks. Several transcription factors such as Nuclear Factor Kappa B (NFκB) [117], Nuclear Factor of Activated T-Cell (NFAT) [123], STAT3 [124] and Snail [125] are dependent on Kpnβ1 for their entry into the nucleus. Kpnβ1 is also involved in neuronal regeneration, which occurs in response to axonal injury. Kpnβ1 functions in transmitting damage signals from axons of damaged neurons to the cell body [126]. Importantly, Kpnβ1 is a global regulator of cell cycle transitions. It plays key roles in mitosis (involved in mitotic spindle assembly) and replication [127,128].

1.8.2. Association between Kpnβ1 and cancer

Normal cell homeostasis depends on proper Kpnβ1 function, strict regulation, and expression [65]. The cell cycle regulatory role of Kpnβ1 implies that its expression is associated with proliferation [71]. Kpnβ1 has been shown to have elevated expression in tissues that replicated actively such as lymphocytes, testis and tumours [71]. The overexpression of Kpnβ1 has been observed in both transformed and cancer cells. The elevated expression of Kpnβ1 has been reported in several cancers, including cervical [55], glioblastoma [129], breast [130], multiple myeloma [131], hepatocellular carcinoma [132] and malignant peripheral nerve sheath tumour [133]. At the mRNA level, elevated Kpnβ1 expression in ovarian cell cancer cells in comparison to their normal counterparts has been reported [134].

The efficacies and rates of Kpnα2/Kpnβ1 and Kpnβ1-dependent nuclear import are increased in transformed cells in comparison with normal cells [135]. Kpnβ1 might also be involved in cancer-related inflammation; this is because of its activity in transporting transcription factors associated with inflammation such as GATA3, NFκB, STAT (1, 2, 3, and 6), Smad3 and Activator Protein 1 (AP-1) [120]. The nuclear import of cAMP-Response Element Binding (CREB) protein, a nuclear transcription factor that has been shown to be involved in tumour initiation, progression and metastasis [136] is also dependent on Kpnβ1 [137].

Research previously done in our laboratory reported that Kpnβ1 expression in cervical cancer patient tissue was found to be substantially higher than what was observed in normal cervical tissue and, expression levels were similarly elevated in cervical cancer cell lines compared to non-cancer cells [55]. Kpnβ1 has been shown to have elevated levels in Hepatocellular Cancer (HCC) and it had a significant correlation to tumour size, metastasis and histological grade[132]. Zhu *et al* (2016), reported that Kpnβ1 was significantly upregulated in gastric cancer patient tissues in comparison to adjacent non-cancer tissues [138]. A recent study by Kodama *et al* (2017) also demonstrated that ovarian cancer patients with increased levels of Kpnβ1 had worse prognosis than patients with lower expression [139]. In addition, it is one of the genes essential for the survival of NSCLC and Head and Neck Squamous Cell Carcinoma (HNSCC) [140].

The increased expression and functional reliance on Kpnβ1 in both transformed and cancer cells suggest that this nuclear importer might be a therapeutic target for cancers [65]. There is evidence in the literature to support this hypothesis. Sekimoto *et al* (2017) identified Kpnβ1 as a likely target for lung adenocarcinoma. Their study showed that inhibition of Polo-Like

Kinase 1 (PLK1), an important mitotic kinase decreased the expression level of Kpnβ1 which resulted in decreased cell proliferation and cell death via apoptosis [141].

1.8.3. Kpnβ1 as an anti-cancer target

The significance of targeting Kpnβ1 as an anti-cancer target derives from the fact that Kpnβ1 is necessary for the survival and progression of tumours as many processes associated with tumorigenesis depend on Kpnβ1-mediated nuclear import [142]. Lin *et al* (1995) in a search for inhibitors of Kpnα/Kpnβ1 report that cell-permeable peptides having the NLS of NFκB/p50 subunit inhibited the nuclear import of NLS-bearing transcription factors such as NFκB, NFAT, AP-1 and STAT1 [143,144]. This peptide was named cSN50.1 and has been found to inhibit both SREBP/Kpnβ1 and Kpnα/NLS-cargo mediated import via two different mechanisms. It is assumed that cSN50.1 inhibits SREBP/Kpnβ1-mediated import via the binding of its Signal Sequence Hydrophobic Region (SSHR) motif to Kpnβ1 [78]. Ivermectin, an anti-parasitic agent has been shown to inhibit only Kpnα/Kpnβ1 mediated nuclear import with no effect on other nuclear import pathways including nuclear import mediated by Kpnβ1 alone [145,146].

The concentration of RanGTP controls the dissociation of the nuclear import complex as well as the assembly of the export complex in the nucleus. Various studies have identified small molecules that are capable of inhibiting Kpnβ/RanGTP binding. Karyostatin 1A, a pyrrole compound was identified using affinity-based screening by confocal nanoscanning. This small molecule was able to impede the binding between Kpnβ1 and RanGTP and this resulted in the inhibition of the nuclear import of Green Fluorescent Protein-NFAT (GFP-NFAT). Ambrus et al (2010) identified another potential inhibitor of Kpnβ1, 58H 5-6 [147]. It was identified via the analysis of peptidomimetic libraries and was reported to inhibit

Kpnβ1/Kpnα mediated nuclear import without affecting Transportin-mediated nuclear import. However, this compound lacks *in vivo* efficacy, which is probably due to inadequate cell permeability [147].

Soderholm *et al* (2011) identified Importazole, a 2,4 diaminoquinazoline through a FRET-based, high throughput screen for small molecules that had the potential to inhibit the binding between RanGTP and Kpnβ1 [123]. Importazole inhibited the binding of RanGTP to Kpnβ1 specifically without disrupting CRM1-mediated nuclear export or Transportin-mediated nuclear import [78,96]. Yan *et al* (2015) reported that Importazole inhibited the nuclear import of NFκB/p65 in multiple myeloma cells [131]. The preliminary data obtained from these various inhibitors are encouraging and support the investigation of novel inhibitors of Kpnβ1 with anti-cancer potential.

1.8.4. Identification of novel Kpnβ1 inhibitors

Previous work done in collaboration with researchers at the Brown Cancer Centre (University of Louisville, Kentucky, USA) used a structure-based computational screen to identify novel small molecules that may bind and inhibit Kpnβ1 function. A library of 12,662,570 compounds in the 2010 ZINC database was screened to identify small molecules that had the ability to bind the overlapping RanGTP and Kpnα2 binding region of Kpnβ1 [142] (Figure 1.5). This region is necessary for the proper functioning of Kpnβ1 and has been shown to be between amino acids residue 331-364 of Kpnβ1 which is the common binding region of RanGTP, Kpnα2 and SREBP-2 [148,149]. The search yielded 74 hits and 47 top scoring compounds were chosen for further investigation. A total of 16 compounds were found to have cancer cell killing effects and of this, C43 (now known as INI-43), C53 and C60 had

effects on the nuclear import functions of Kpnβ1 using an NFAT activity assay to monitor inhibitory effects. 3-(1H-1, 3-benzimidazol-2-yl)-1-[3-(dimethylamino) propyl]-1H-pyrrolol[2,3-b]quinoxalin-2-amine, which has been named Inhibitor of Nuclear Import-43 (INI-43) interfered with the nuclear localisation of Kpnβ1 and its known cargoes, which include AP-1, NFkB, NFAT and NFY. It also had inhibitory effects on the proliferation of cancer cells, showed reduced effects on non-cancer cells at the same concentration with which it killed cancer cells and reduced tumour growth in *in vivo* mouse models [142,150].

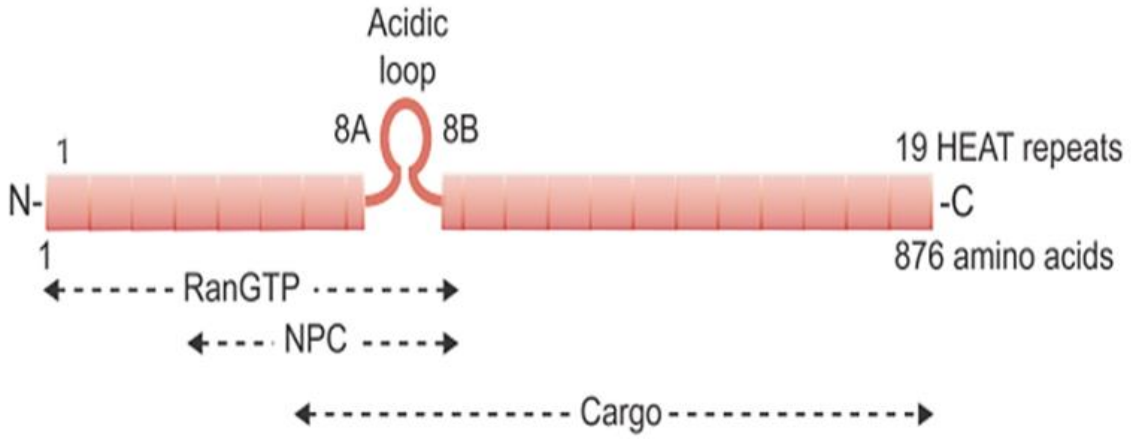

Figure 1.5. Structure of Kpnβ1 showing the overlapping binding site of Kpnα2 and RanGTP. Kpnβ1 is made up of 19 HEAT repeats, each consisting of A and B helices that are connected by a short run. HEAT repeat 8 is replaced by an acidic loop, which is important for substrate binding and release. The HEAT repeats 1-8 are necessary for its binding to RanGTP while HEAT repeats 7-19 are for its binding to Kpnα. The binding sites for nucleoporins which lie between HEAT repeats 4-8 [122].

The focus of this study is on one of the three compounds identified as having the potential to kill cancer cells and inhibit Kpnβ1-mediated nuclear import, Compound 60 (9-[(1-methyl-3-piperidinyl)methoxy]-4-[(6-methyl-2-pyridinyl)methyl]-7-(5-methyl-2-thienyl)-2,3,4,5-tetrahydro-1,4-benzoxazepine) (Figure 1.6). Compound 60 (C60) is a derivative of piperidine and benzoxazepine. Benzoxazepine is a bi-cyclic heterocyclic compound made up of

benzene ring fused to an oxazepine ring. Different benzoxazepine derivatives have been used for numerous biological activities some of its derivatives have displayed good biological activities and have been considered as a lead molecule for the synthesis of future drugs. Benzoxazepine derivatives are well-known pharmacophores in medicinal chemistry and have been used in anticonvulsants, antimicrobials, antipsychotic agents and anti-cancer drugs [151,152]. One of the benzoxazepine derivatives has been discovered to target microtubule assembly to induce anti-cancer activity [152–154]. A benzoxazepine derivative has been shown recently to have synergistic antitumour effect when used with Oxaliplatin and 5-Fluorouracil (5-FU) in colorectal cancer cells [155]. There is thus evidence in the literature that benzoxazepine derivatives have anti-cancer activity. Although, another compound (INI-43) from the same *in silico* screening has been previously described, the rationale for investigating C60 in this current study based on the need for the development of more targeted therapies that can be used alone or in combination with other therapies. Furthermore, data obtained from this study might result in the development of small molecule inhibitors that will be used in the treatment of cervical and oesophageal cancers, which currently are largely dependent on the use of monoclonal antibodies.

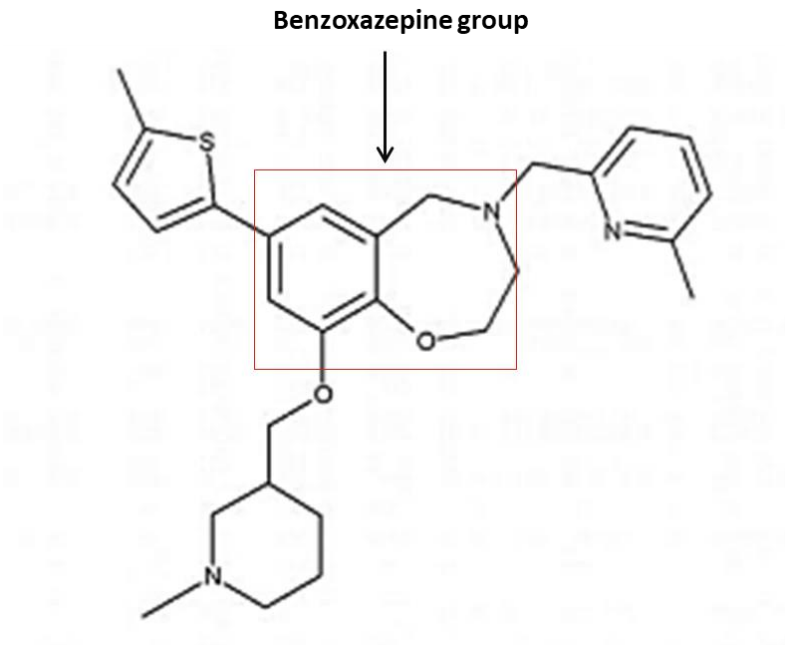

Figure 1.6. Structure of the small molecule inhibitor Compound 60 (C60).

1.9. Significance

This project is based on the hypothesis that the nuclear import protein Kpnβ1 is necessary for the growth and survival of cancer cells and that identified small molecule inhibitors of Kpnβ1 may have potential as anti-cancer therapies. Novel Kpnβ1 inhibitors can be further developed for use in clinical settings for the treatment of cancers of different tissue origins either as a monotherapy or in combination with other drugs.

1.10. Project aims

This project aims to:

(i) Investigate the effect of C60, a potential inhibitor of Kpnβ1 on the biology of cancer cells.

(ii) Investigate the ability of C60 to interfere with the cellular localisation of Kpnβ1 and on the nuclear import and function of some of its known cargoes.

(iii) Investigate the *in vitro* ADME pharmacokinetic properties of C60 to determine its solubility, lipophilicity, permeability, plasma protein binding and metabolic stability.

(iv) Investigate the *in vivo* toxicity of C60 and its effect on tumour growth using a mouse xenograft model.

(v) Purify Kpnβ1 for investigating Kpnβ1: C60 binding kinetics using Bio-layer interferometry.

Chapter 2: Effect of C60, a potential small molecule inhibitor of Kpnβ1 on the biology of cancer cells

2.1. Introduction

Cancer is a disease with molecular heterogeneity and there are various tumour types with diverse histopathologies, genetic and epigenetic differences and even clinical outcomes. All these factors make the understanding of cancers difficult [156]. Molecularly targeted therapies take advantage of the major addictions and vulnerabilities of cancer cells [40]. Targeted drugs are classified according to their individual effects on one or more hallmarks of cancer [4]. The efficacy of an anti-cancer drug is a validation of a particular hallmark; if a hallmark is necessary for cancer survival, then targeting it should result in the inhibition of tumour proliferation and growth. Most anti-cancer drugs targeting hallmarks of cancer have been aimed at specific molecular targets that drive tumour growth [4].

The transition from the use of anti-cancer drugs that display broad cytotoxicity to the discovery and use of molecularly targeted drugs has resulted in an increased number of therapies anticipated to improve treatment outcome. The BCR-ABL inhibitor Imatinib, usually referred to as a trailblazer drug validated the idea of designing small molecule drugs to treat a classified population of patients [40]. This development was followed by the discovery of other small molecules inhibiting important cancer targets such as EGFR kinase which is inhibited by gefitinib and is used for patients with NSCLC; VEGFR kinase which is targeted by Sorafenib and is used in treating renal cancer [40].

Our laboratory has an interest in identifying genes that associate with cancer as novel anti-cancer targets. We identified Kpnβ1 a nuclear import receptor, which has been shown to have elevated expression in cervical and oesophageal cancers at both the mRNA and protein levels. Furthermore, the inhibition of Kpnβ1 using small interfering RNA (siRNA) silencing resulted in significantly reduced cell proliferation as well as cell death via apoptosis. This was observed in cancer cells with minimal effect on normal cells [55,142]. The elevated expression of Kpnβ1 in cancer cells, as well as the effect of its inhibition on their biology suggests that cancer cells are functionally dependent on the elevated expression of Kpnβ1.

As very few inhibitors of Kpnβ1 are commercially available, our laboratory in collaboration with researchers at the University of Louisville, Kentucky, used a computational screening approach to identify potential small molecule inhibitors of Kpnβ1. A number of compounds were identified including compounds C43 (now known as INI-43) and C60. INI-43 has shown anti-cancer properties *in vitro* and *in vivo* as well as nuclear import inhibitory properties [142]. In this study, the anti-cancer potential of C60 will be investigated in cervical and oesophageal cancer cell culture models. This will be done by determining the half-maximal effective concentration (EC_{50}) of C60 and monitoring its effect on cancer cell proliferation, colony-forming ability and cell cycle progression. Furthermore, the mode of cell death induced by C60 will be investigated by PARP cleavage.

2.2. Results

To examine the effects of C60 on cancer cell biology, its effect on cell proliferation, cell cycle progression and its mechanism of inducing cell death were analysed using a cervical and oesophageal cancer cell lines.

2.2.1. Investigating C60 cytotoxicity and its effect on cancer cell proliferation and survival

2.2.1.1. Determination of the cytotoxicity of C60

The 3-(4,5-Dimethylthiazol-2-yl)-2,5-diphenyltetrazolium bromide (MTT) assay was used to determine the Effective Concentration $_{50}$ (EC_{50}) value of C60. EC_{50} is the concentration of an agent that is needed to obtain 50% of the maximum response [157]. The anti-proliferative effect of C60 was tested in a panel of cervical (HeLa, CaSki and SiHa), oesophageal (WHCO1, WHCO5, WHCO6, KYSE 30 and KYSE 150) cancer cell lines. Normal epithelial cells (ARPE-19 and hTERT RPE-1) were used as non-cancer control cells. Cells were treated with increasing concentrations of C60 for 24 or 48 hours, surviving cells monitored using the MTT assay and EC_{50} values with 95% Confidence Intervals (CIs) calculated using GraphPad Prism Software.

Representative EC_{50} hill curves of experiments performed at least three independent times for every cell line at 24 hours and 48 hours of treatment are shown in Figure 2.1 and Figure 2.2 respectively. The EC_{50} values obtained for the cancer cells at 24 hours ranged between 11-14 µM (Table 2.1). In the normal epithelial cells, EC_{50} was in the range of 40-60 µM (Table 2.1). At 48 hours, the EC_{50} values ranged between 6-10 µM in cancer cell lines and between ~25 -36 µM in normal epithelial cells (Table 2.1). At both 24 and 48 hours, the selectivity

index (SI, obtained by dividing the EC_{50} value of normal cells by that of cancer cells) was between 2.5-4. SI of less than 2 is reported as suggestive of general toxicity, while the greater the SI value is thought to be indicative of a more selective drug [158]. SI values of 2.5-4 for C60 suggest that C60 has more selective cytotoxicity for cancer cells.

Alongside EC_{50} calculations for C60, we performed similar experiments using HeLa, ARPE-19 and hTERT RPE-1 cells for Importazole, a commercially available Kpnβ1 inhibitor. The EC_{50} value of Importazole at 24 hours was 30.55 µM, 81.50 µM and 72.41 µM in HeLa, ARPE-19 and hTERT RPE-1 respectively. At 48 hours, values were 19.99 µM, 62.08 µM and 55.18 µM in HeLa, ARPE-19 and hTERT RPE-1 respectively (Table 2.2). Importazole showed selectivity for cancer cells with SI of ~2.3-3 at both time points. This is in line with what was determined for C60 showing that a higher dose of this drug (2-3 fold) was required to kill non-cancer in comparison to cancer cells.

For comparative purposes, the EC_{50} value of Cisplatin, a commercially available platinum-based anti-cancer drug in clinical practice was determined at 24 and 48- hour time points in HeLa cervical cancer cell and two non-cancer epithelial cells (ARPE-19 and hTERT RPE-1). The EC_{50} value of Cisplatin at 24 hours was 28.01 µM, 152.8 µM and 147.75 µM in HeLa, ARPE-19 and hTERT RPE-1 respectively. At 48 hours, values were 10.33 µM, 73.8 µM and 46.6 µM in HeLa, ARPE-19 and hTERT RPE-1 respectively (Table 2.3). At both time points, the EC_{50} value of Cisplatin in HeLa cells was about 1.5-2 fold higher than that obtained in C60, suggesting that lower concentrations of C60 have similar cell killing effects to that of Cisplatin. Cisplatin

showed good selectivity for HeLa cancer cell in comparison to the non-cancer cells with SI of ~4.5-7.

Together, these results suggest that lower doses of C60 results in cervical and oesophageal cancer cell killing effects compared to a commercially available Kpnβ1 inhibitor, Importazole as well as the alkylating agent, Cisplatin.

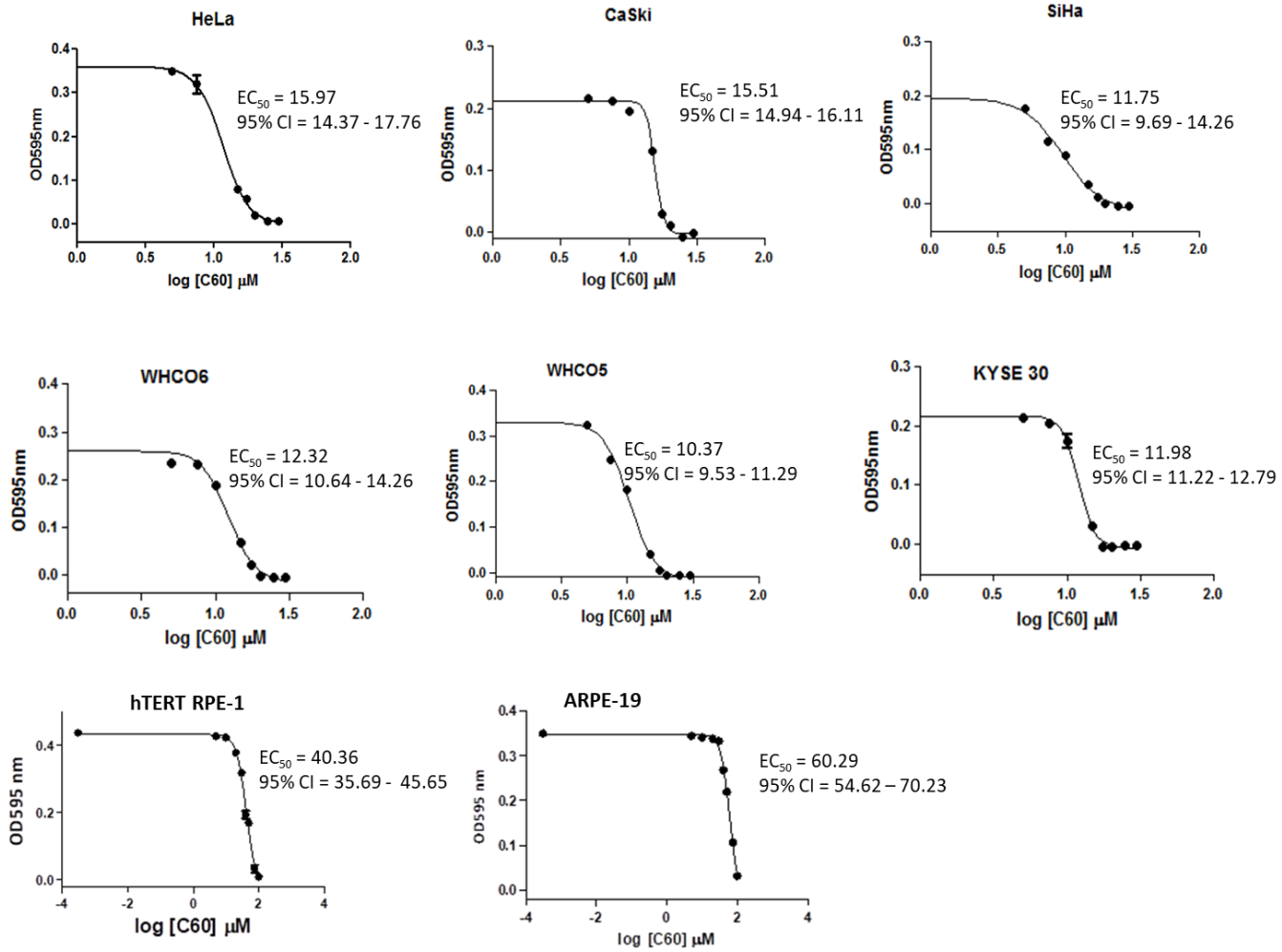

Figure 2.1: EC_{50} curves showing the sensitivity of cervical cancer, oesophageal cancer and non-cancer epithelial cells to C60 after 24 hours treatment. Cervical cancer cells (HeLa, CaSki and SiHa), oesophageal cancer cells (WHCO6, KYSE 30 and WHCO1), immortalised epithelial cells (hTERT RPE-1) and normal epithelial cells (ARPE-19) were treated with increasing concentration of C60 for 24 hours after which MTT assay was carried out. EC_{50} values and hill plots were calculated using GraphPad Prism software. Hill plots shown are representative of the mean ± SEM of experiments performed in triplicate and repeated at least three independent times.

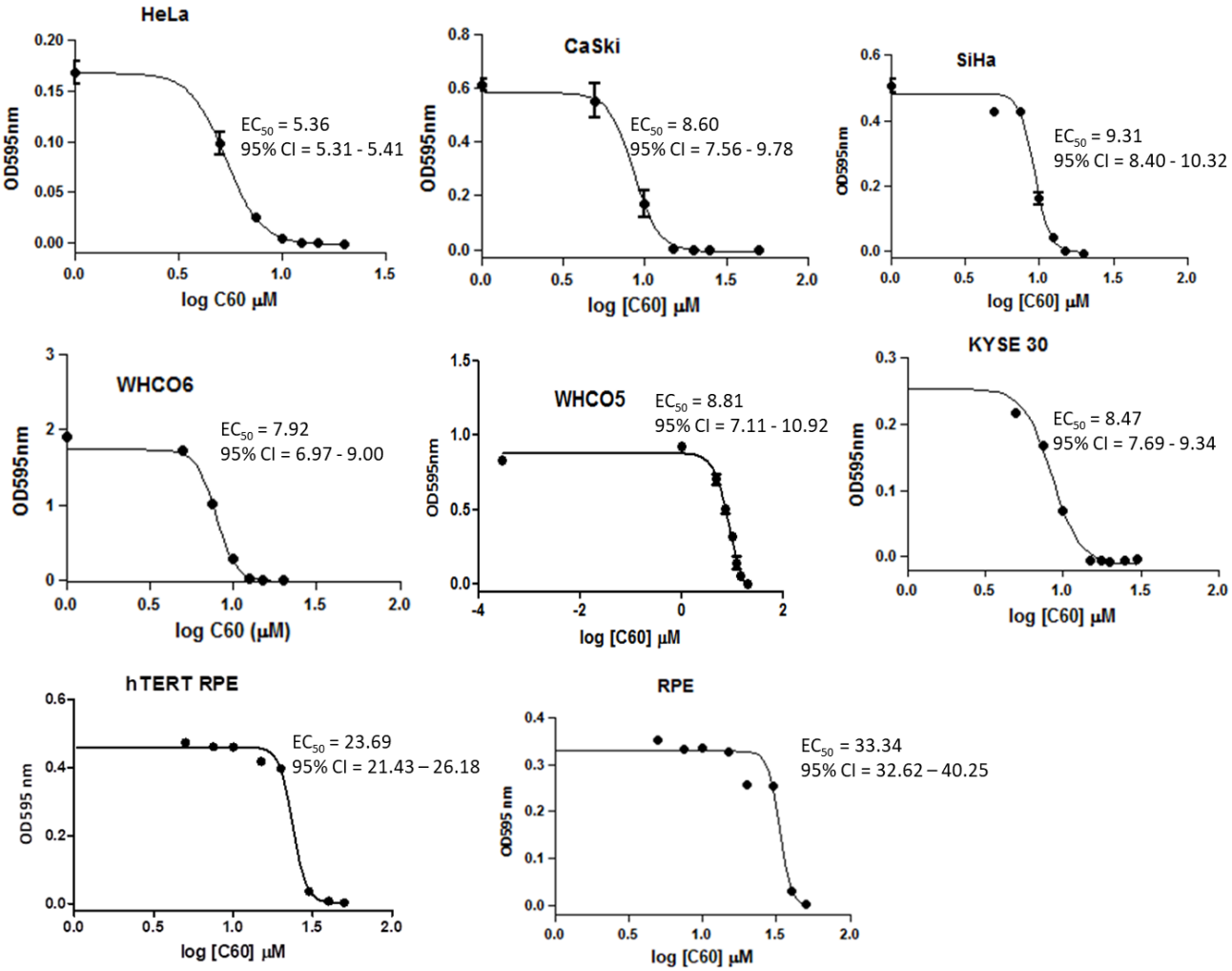

Figure 2.2: EC_{50} curves showing the sensitivity of cervical cancer, oesophageal cancer and non-cancer epithelial cells to C60 after 48 hours treatment. Cervical cancer cells (HeLa, CaSki and SiHa), oesophageal cancer cells (WHCO6, KYSE 30 and WHCO1), immortalised epithelial cells (hTERT RPE-1) and normal epithelial cells (ARPE-19) were treated with increasing concentration of C60 for 48 hours after which MTT assay was carried out. EC_{50} values and hill plots were calculated using GraphPad Prism software. Hill plots shown are representative of the mean ± SEM of experiments performed in triplicate and repeated at least three independent times.

Table 2.1: Average EC_{50} values of C60 in a panel of cervical and oesophageal cancer cells (24 and 48 hours)

MTT assay and GraphPad Prism software were used to determine the EC_{50} values and the 95% confidence interval of C60 in a panel of cervical and oesophageal cancer cell lines as well non-cancer epithelial cells after 24 and 48 hours treatment. Cells were plated in triplicate and each experiment was performed at least three independent times.

		24 hours		48 hours	
Origin	**Cell line**	**EC_{50} (µM)**	**95% Confidence interval**	**EC_{50} (µM**	**95% Confidence interval**
Cervical cancer	HeLa	13.82	12.58 -15.19	6.66	6.09 -7.34
Cervical cancer	SiHa	10.70	9.00 -12.73	10.06	9.02 -11.23
Cervical cancer	CaSki	13.03	12.02 -14.09	9.61	8.10 -11.55
Oesophageal cancer	WHCO5	14.50	11.92 -17.77	8.14	6.26 -10.59
Oesophageal cancer	WHCO6	10.01	9.14 -11.09	7.94	7.24 - 8.53
Oesophageal cancer	KYSE 30	11.45	10.85-12.08	8.40	7.65 -11.47
Oesophageal cancer	KYSE 150	11.98	11.08 -13.00	7.77	5.65 -10.86
Oesophageal cancer	WHCO1	10.30	9.35 -11.33	8.94	6.97 -11.73
Primary epithelial cell	ARPE-19	61.37	50.72-74.27	36.04	32.32-40.40
Immortalised epithelial cell	hTERT RPE-1	41.43	35.46 - 48.45	25.44	23.27-27.81

Table 2.2: Average EC_{50} values of Importazole in HeLa cervical cancer cells and non-cancer epithelial cells.

MTT assay and GraphPad Prism software were used to determine the EC_{50} values and the 95% confidence interval of Importazole in HeLa cervical cancer cells and two non-cancer epithelial cells after 24 or 48 hours of treatment. Cells were plated in triplicate and experiment was performed three independent times.

		24 hours		48 hours	
Origin	**Cell lines**	**EC_{50} (µM)**	**95% Confidence Interval**	**EC_{50} (µM)**	**95% Confidence Interval**
Cervical cancer	HeLa	30.55	24.39 - 38.49	19.99	13.36 - 30.23
Primary Epithelial cell	ARPE-19	81.50	70.60 - 94.39	62.08	56.19 - 68.60
Immortalised epithelial cell	hTERT RPE-1	72.41	58.29 - 90.03	55.18	43.24 - 71.60

Table 2.3: Average EC_{50} values of Cisplatin in HeLa cervical cancer cells and non-cancer epithelial cells.

MTT assay and GraphPad Prism software were used to determine the EC_{50} values and the 95% confidence interval of Cisplatin in HeLa cervical cancer cells and two non-cancer epithelial cells after 24 or 48 hours of treatment. Cells were plated in triplicate and experiment was performed three independent times.

		24 hours		48 hours	
Origin	**Cell lines**	**EC_{50} (µM)**	**95% Confidence Interval**	**EC_{50} (µM)**	**95% Confidence Interval**
Cervical cancer	HeLa	28.01	20.88 - 37.71	10.33	4.22- 25.99
Primary Epithelial cell	ARPE-19	152.8	114.69 - 212.05	73.8	31.93 - 174.3
Immortalised epithelial cell	hTERT RPE-1	147.75	91.49 - 268.4	46.6	31.09 - 73.80

2.2.1.2. Effect of C60 on anchorage-dependent proliferation

Having established the EC_{50} values of C60 in a panel of oesophageal and cervical cancer cell lines, anchorage-dependent proliferation assay was performed. The proliferation of C60 or Dimethyl Sulphoxide (DMSO, vehicle control) treated cells was monitored over a period of five days. Cells were treated with 5 µM C60 or 10 µM C60 (10 µM was chosen as it was the closest to the EC_{50} value obtained across the panel of cell lines considered).

A significant reduction in proliferation on treatment with 10 µM C60 was observed in all cancer cell lines; HeLa, CaSki, WHCO6, KYSE 30) while little to no effect was observed on normal epithelial cells, hTERT RPE-1 and ARPE-19 (Figure 2.3.A). A bar graph representation of the effects of C60 on all the cell lines on day 5 of treatment is shown in Figure 2.3.B. Results show that C60 at 10 µM had a significant effect on the proliferation of cancer and transformed cells in comparison to normal cells. These results provide evidence that cervical and oesophageal cancer cells lines are more sensitive to C60 treatment compared to normal cells.

A

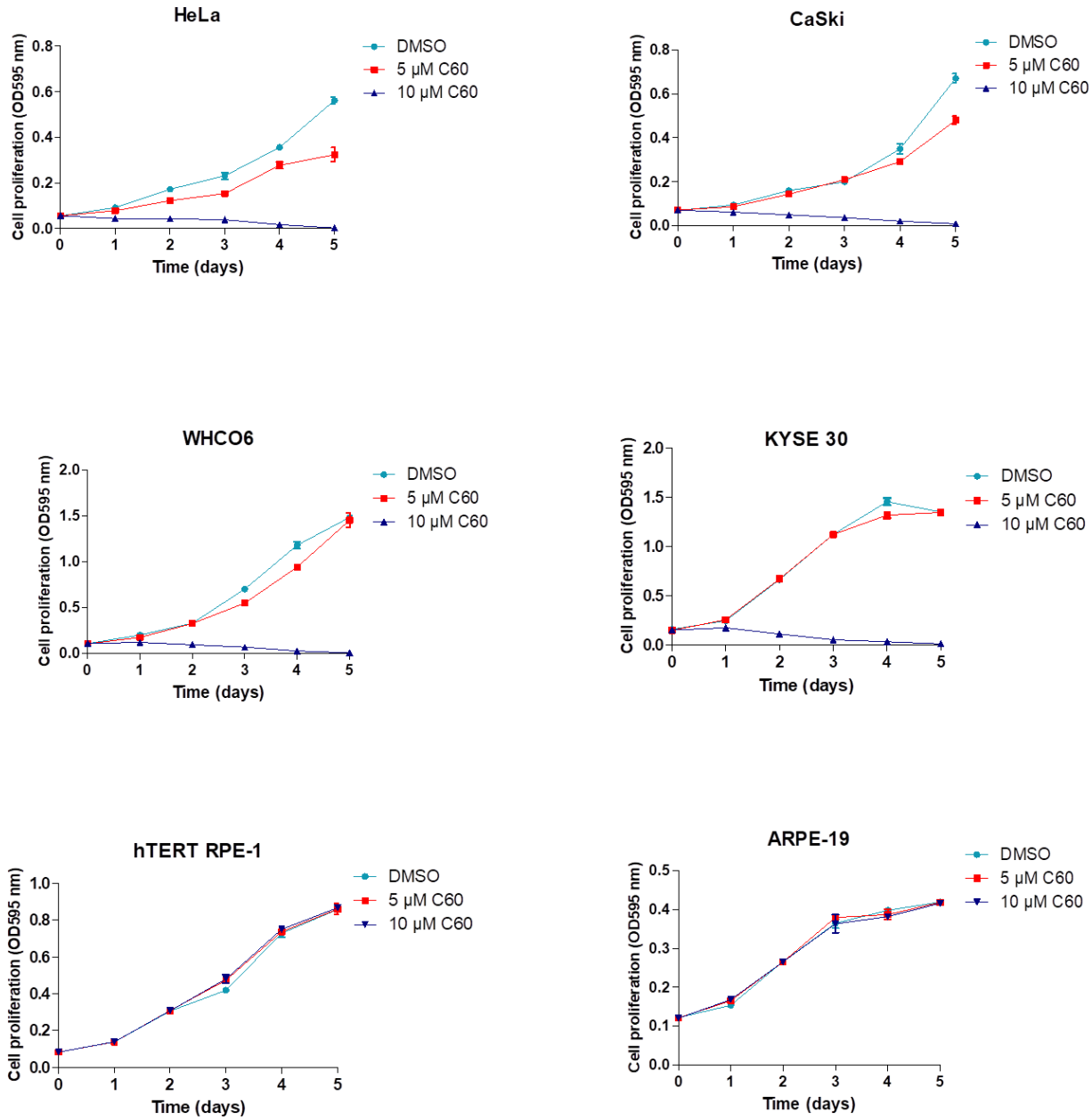

Figure 2.3.A. C60 inhibits anchorage-dependent cancer cell proliferation. Adherent cells were plated at 1000 per well in each well of a 96-well plate and allowed to settle overnight prior to treatment with either DMSO (vehicle control), 5 µM or 10 µM C60. Proliferation was monitored every 24 hours using the MTT reagent for a period of 5 days. Results displayed are mean ± SEM of 4 replicates, and each experiment was repeated at least two independent times, *p≤0.05

B

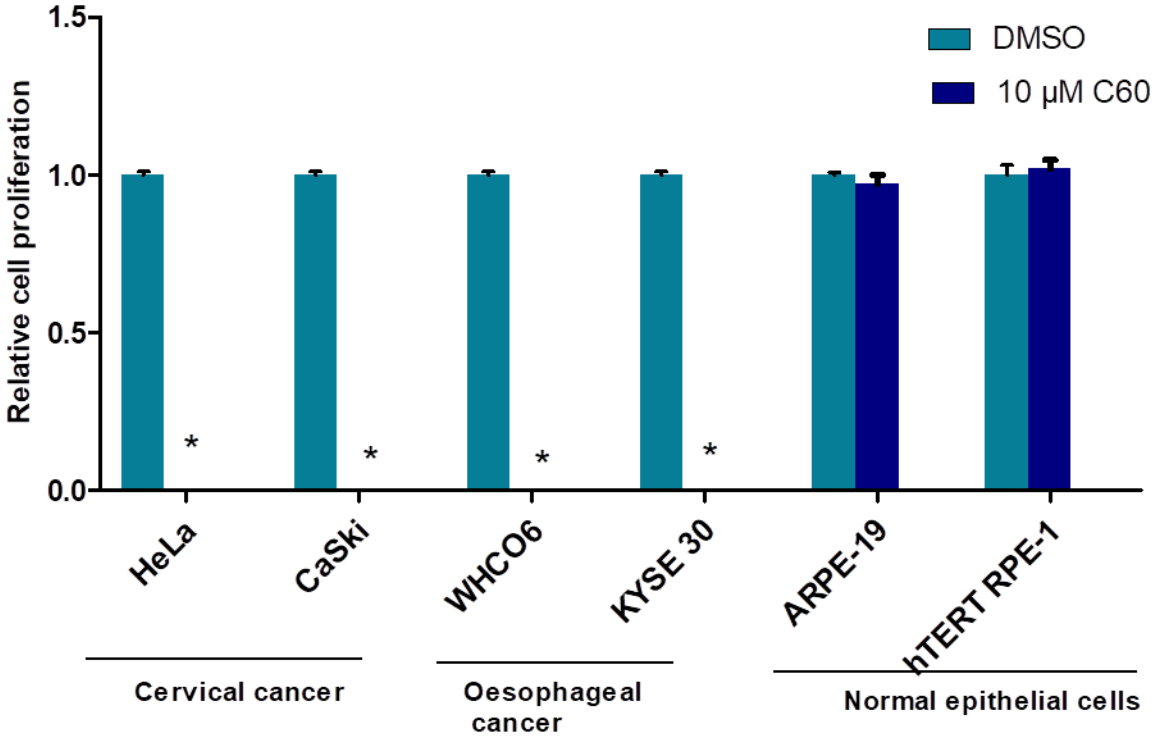

Figure 2.3.B Relative cell proliferation on Day 5. Proliferation in each treated cell line was expressed relative to its untreated counterpart for day 5 of proliferation assay. Results displayed are mean ± SEM of 4 replicates, and each experiment was repeated at least two independent times. Statistical significance was determined using student paired t-test, *p≤0.05

2.2.1.3. Effect of C60 on anchorage-dependent colony formation

Having observed a significant reduction in the proliferation of cancer cells after C60 treatment, the effect of C60 on the colony forming ability of cancer cells was investigated using the colony formation assay. The colony formation assay was established based on the ability of a single cell to proliferate indefinitely thus maintaining its ability to form a colony. This assay has been used to investigate the cytotoxicity induced by different chemotherapeutic agents [159,160]. Experiments were set up as described in the materials and method section (Section 7.2.6). Cells were grown for 8 days with media changes every two

days. Cells were fixed, stained with 0.5% crystal violet and colonies photographed. Area covered by cells was measured to determine colony number. Colony area determined using Colony Area ImageJ plugin as described in the literature [161]. A significant reduction in colony formation in response to C60 treatment was observed (Figure 2.4.A). A bar graph representation of the effects of C60 on colony formation in the cancer cell lines is shown in day 5 of treatment is shown in Figure 2.4.B.

The colony formation assay was also performed using a different approach where DMSO and C60 treatment was retained in cells for a period of 8 days without media change. The results showed that C60 completely inhibited colony formation (Figure 2.4.C).

A

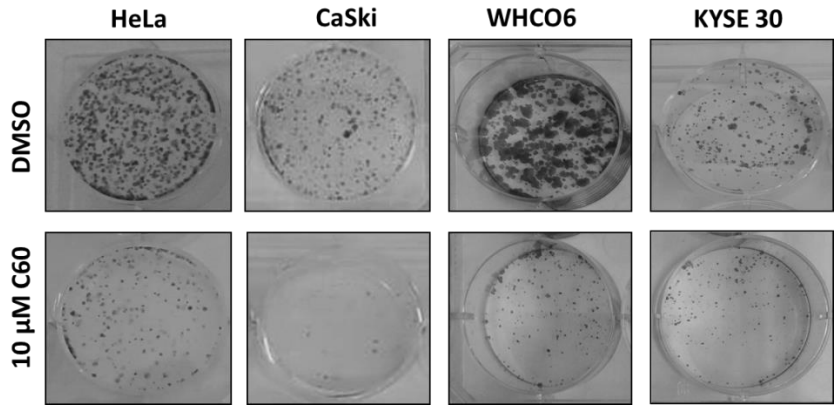

B

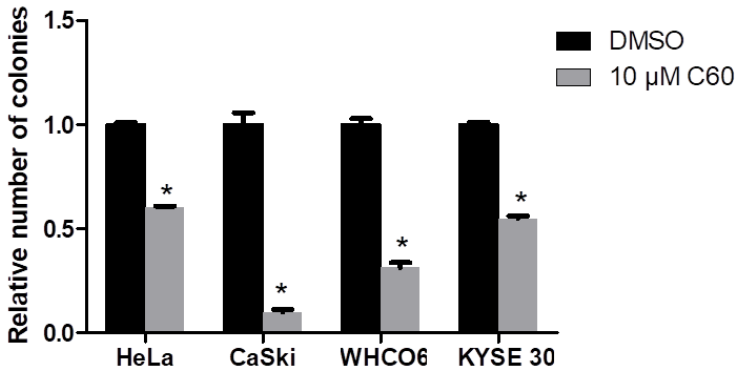

C

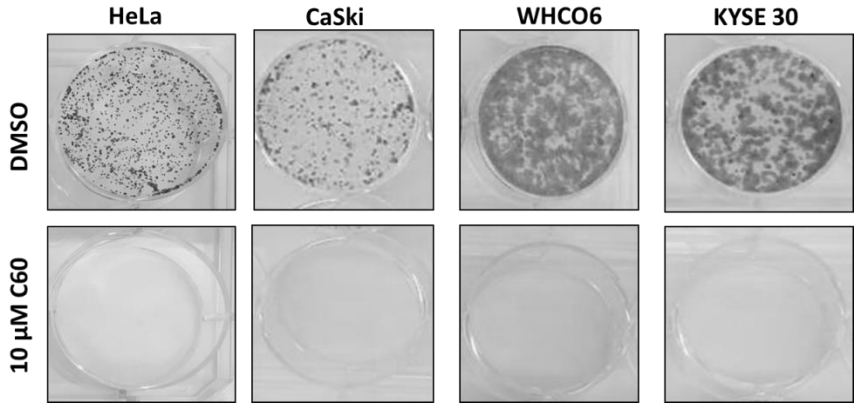

Figure 2.4. C60 reduces colony formation in cancer cells. Significant reduction in colony formation was observed when cells were treated with 10 µM C60 for 24 hours and media replaced every second day over a period of 8 days (A). Graphs represent relative survival fraction in treated compared to untreated cells (B). Complete inhibition of colony formation was observed when cells were treated with 10 µM C60 without media change for a period of 8 days (C). Results are the mean ± SEM of experiments done in triplicate and performed three independent times. Statistical significance was determined using student paired t-test, *p≤ 0.05.

2.2.1.4. C60 induces G1 cell cycle arrest in cancer cells

Components of the cell cycle machinery are often times altered in most human cancers. As cancerous cells develop, both genetic and epigenetic mechanisms alter the expression of cell cycle regulatory proteins, which confers a selective growth advantage on cancer cells [162]. Some anti-cancer agents prevent cancer cell proliferation via the initiation of cell cycle arrest [159].

In order to determine if the reduced proliferation observed after C60 treatment associated with changes in cell cycle progression, DNA based flow cytometry analysis was performed after CaSki and HeLa cervical cancer and WHCO6 oesophageal cancer cells were treated with 10 µM or 15 µM C60 for 6, 12 or 24 hours. No significant change in cell cycle progression of CaSki cells was observed at 6 hour treatment with C60 (Figure 2.5.A). At 12 hours C60 treatment, a significant increase in the percentage of cells at the G1 phase with a concurrent significant decrease in the percentage of cells at S phase was observed (Figure 2.5.B). At 24 hours, C60 treatment similarly showed a significant increase in the percentage of cells at the G1 phase and a significant decrease in the percentage of cells at S and G2/M phases of the cell cycle (Figure 2.5.C).

HeLa cells showed similar results to that obtained for CaSki cells with treatment for 6 hours having no effect on cell cycle progression (Appendix, Figure A.1.A.A). A 12-hour treatment resulted in an increase in the percentage of cells in G1 phase and a concurrent decrease in the percentage of cells at S and G2/M phases of the cell cycle (Appendix, Figure A.1.A.B). 24 hours treatment with C60 resulted in a significant increase in the percentage of cells in sub

G1, G1 phase, and a simultaneous increase in the cells at S and G2/M phase of the cells cycle (Appendix, Figure A.1.A.C).

Results obtained in WHCO6 cells showed a trend towards an increase in the percentage of cells in G1 phase, a significant decrease in the percentage of cells in S phase at 6 hours treatment (Appendix, Figure A.1.B.A). The treatment of cells for 12 hours resulted in an increase in the percentage of cells in G1 and a decrease in the percentage of cells in the S phase (Appendix, Figure A.1.B.B). At 24 hours, there was an increase in the percentage of cells in sub-G1 and G1 phase. This was accompanied by a decrease in the percentage of cells in S and G2/M phases of the cell cycle (Appendix, Figure A.1.B.C). Together, these results suggest that C60 treatment induces G1/S cell cycle arrest.

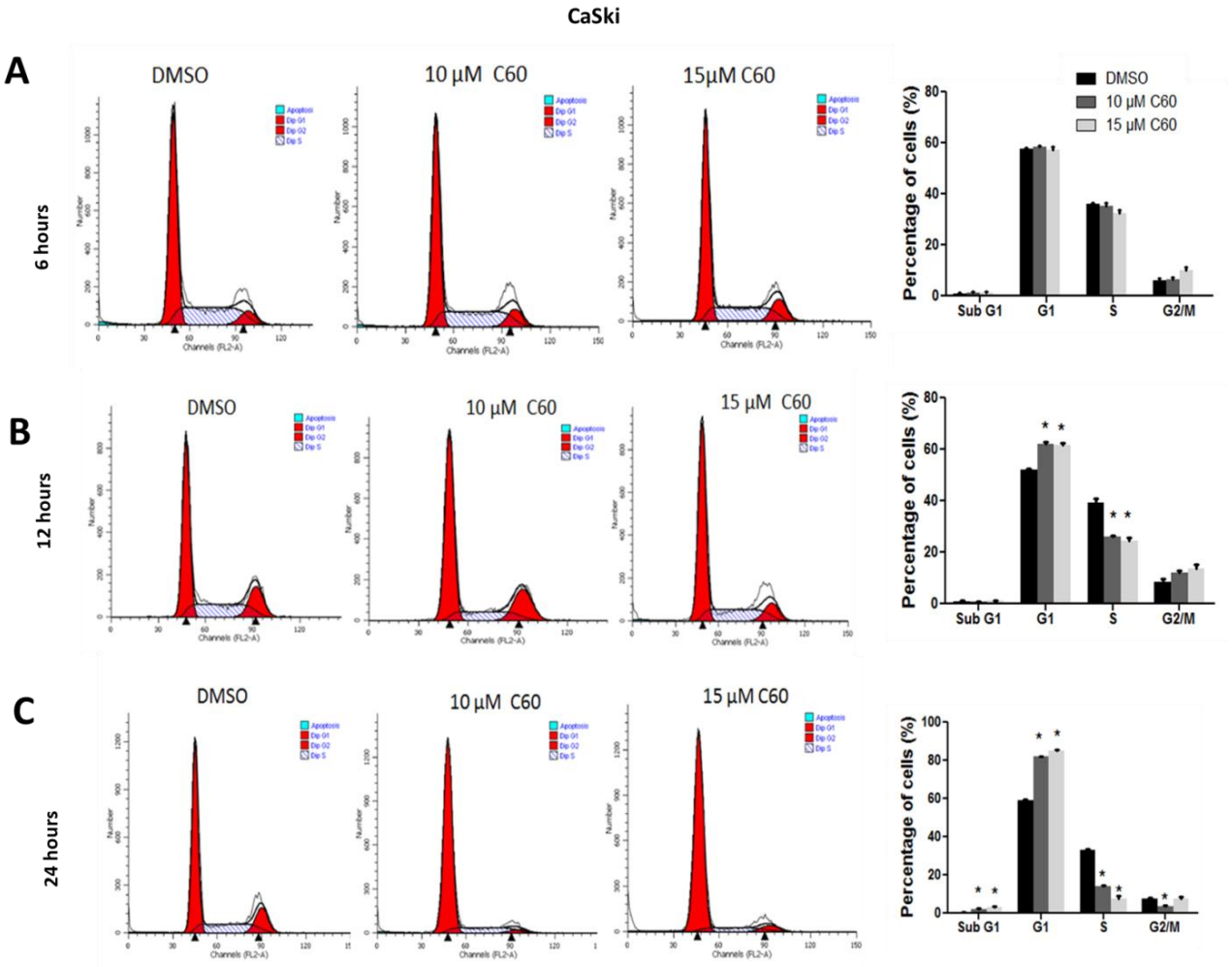

Figure 2.5. C60 suppresses cell cycle progression. Cell cycle analysis was done after Propidium iodide staining in cell treated with C60 for 6 hours (A), 12 hours (B) and 24 hours (C). Modfit software was used to generate cell cycle profile and student paired t-test was used to calculate statistical significance. Results are shown as a mean ± SEM of experiments performed in triplicate and repeated at least three independent times (*$p \leq 0.05$).

2.2.1.5. Effect of C60 on cell cycle regulatory proteins

As C60 had effects on cell cycle progression, we next monitored its effects on cell cycle regulatory proteins including cyclin B1, cyclin D1, Cyclin-Dependent Kinase 4 (CDK4) and cyclin A. In CaSki cervical cancer cells, 6 hours treatment resulted in an increase the levels of cyclin D1, CDK4 and cyclin A, with no effect on cyclin B1 level (Figure 2.6). At 12 hours, a decrease in cyclin D1 was observed with no noticeable effect on cyclin B1, CDK4 and cyclin A levels. At 24 hours, C60 treatment in CaSki cells resulted in a decrease in cyclin B1, cyclin D1, CDK4 and cyclin A levels (Figure 2.6).

In HeLa cervical cancer cells, 6 hours treatment had no effect on cyclin B1, cyclin D1, CDK4 and cyclin A levels. At 12 hours, C60 treatment caused a decrease in cyclin B1, CDK4 and cyclin A levels but no apparent difference in the level of cyclin D1. 24 hours C60 treatment resulted in a decrease in cyclin B1, cyclin D1, CDK4 and cyclin A levels (Appendix, Figure A.2.A).

In WHCO6 oesophageal cancer cells, 6 hours treatment with C60 resulted in an increase in cyclin B1 and cyclin D1 levels but there was no noticeable change observed in CDK4 and cyclin A levels. At 12 hours, C60 treatment caused a decrease in cyclin B1, cyclin D1, CDK4 and cyclin A levels. C60 treatment for 24 hours resulted in a decrease in cyclin B1, cyclin D1, CDK4 and cyclin A levels (Appendix, Figure A.2.B). These results suggest that the G1/S cell cycle arrest induced by C60 associated with changes in the expression of cell cycle regulatory proteins predominantly 24 hours after treatment with changes in the cell cycle proteins varying between the cell lines.

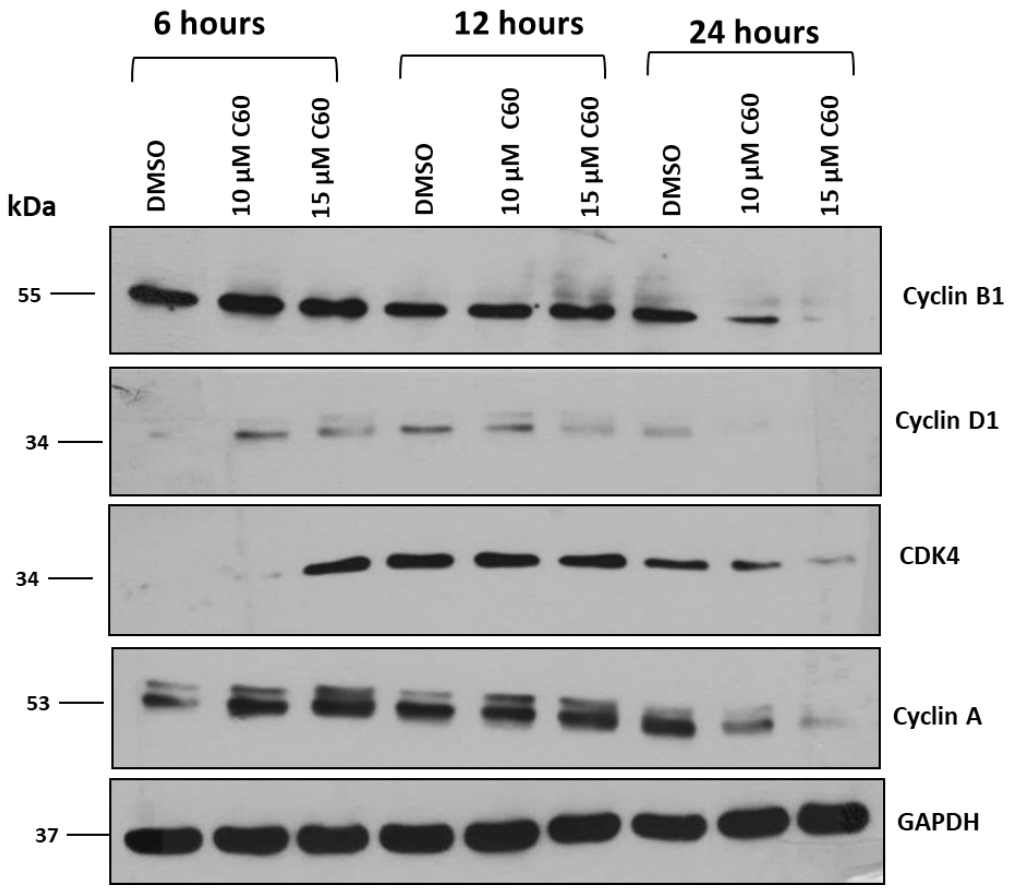

Figure 2.6. Effect of C60 treatment on cell cycle regulatory proteins. CaSki cells were treated with DMSO (vehicle control), 10 µM or 15 µM C60 for 6, 12 or 24 hours. The effect of treatment on cell cycle markers was investigated via western blot analysis with GAPDH as the loading control. Results shown are representative of experiments performed three independent times.

2.2.2. C60 treatment results in cell death via apoptosis

Apoptotic cell death is a cell-specific and well-described mode of cell death also named as type 1 Programmed Cell Death (PCD)[163]. Apoptosis is distinguished by a number of morphological characteristic such as cell shrinkage, nuclear condensation and fragmentation, DNA fragmentation and presence of apoptotic bodies [163,164]. It is further defined by Phosphatidyl Serine (PS) exposure on cell membranes [164]. Apoptosis occurs through two distinct pathways; extrinsic and intrinsic pathways both of which result in the activation of Caspase 3 and 7 (executioner caspases) via proteolytic cleavage [165]. These caspases are involved in the subsequent cleavage of Poly (ADP) Ribose Polymerase (PARP) which is involved in DNA damage repair [166].

2.2.2.1. C60 induced morphological changes in cancer cells

We observed that C60 treatment of CaSki cervical cancer cells resulted in the appearance of rounded cells, which showed signs of dying via apoptosis such as cytoplasmic shrinkage (Figure 2.7). HeLa (Appendix, Figure A.3.A) and WHCO6 (Appendix, Figure A.3.B) cancer cell lines showed similar changes in morphology following treatment with C60.

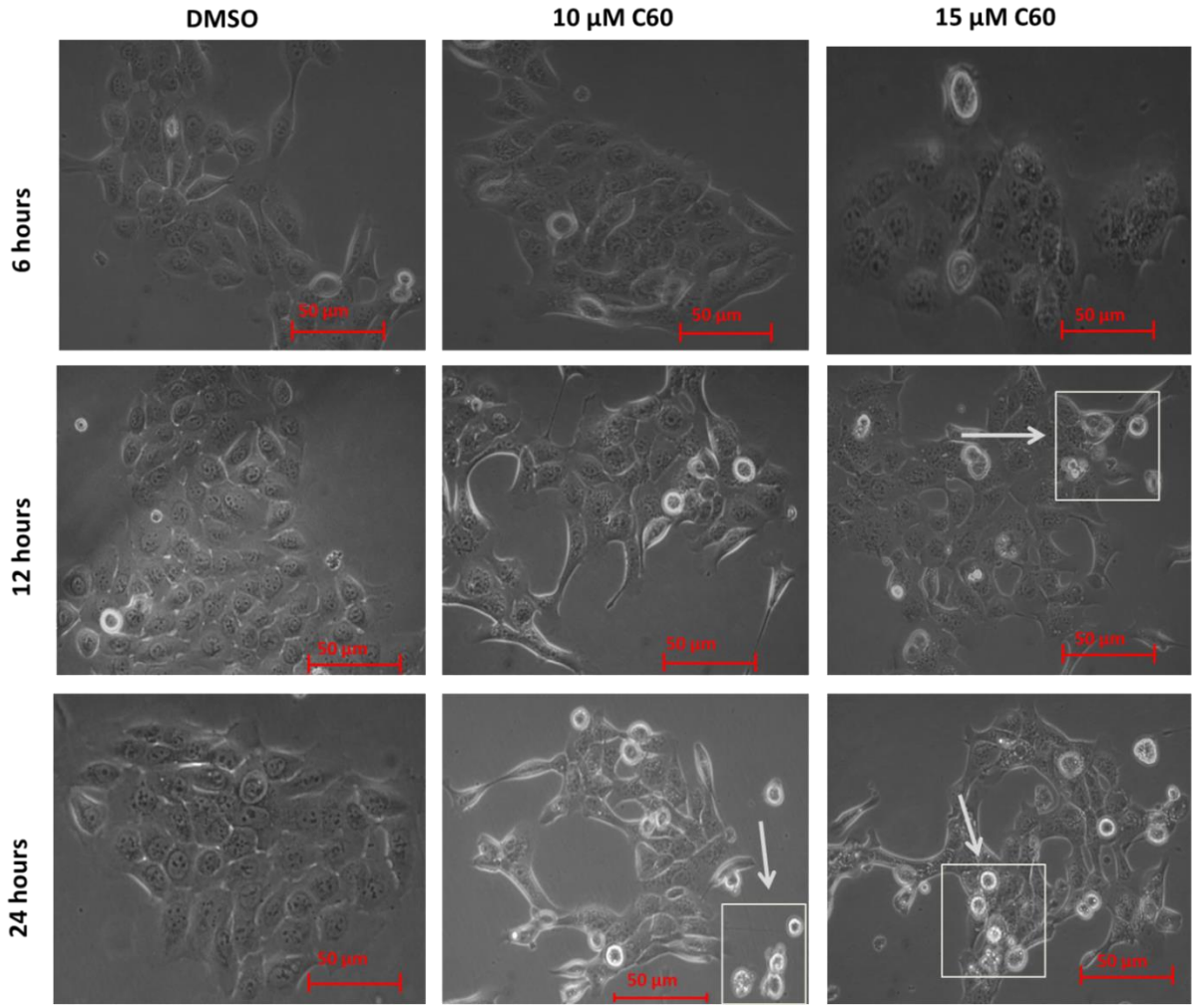

Figure 2.7. Effect of C60 treatment on cell morphology. Images of CaSki cells treated with 10 µM and 15 µM C60 or DMSO (vehicle control) at different time points were captured using Primovert inverted microscope with Axio cam ERC 5s (Zeiss, Göttingen, Germany) at 20X magnification.

2.2.2.2. C60 induces apoptotic cell death

PARP cleavage monitored by western blot analysis

To further investigate the mechanism of cell death induced by C60, PARP cleavage was monitored after 24 hours of treatment. PARP is a nuclear enzyme with a molecular weight of 116 kDa [167]. During apoptosis, Caspases 7 and 3 cleave PARP into two fragments of molecular weight 89 and 24 kDa. The cleavage of PARP suppresses its activity because the 89 and 24 kDa fragments cannot bind to DNA [167,168]. Cleaved PARP was observed after treatment with 10 µM C60 for 24 hours in CaSki, HeLa, WHCO6 and KYSE 30 cells (Figure 2.8.A). 5 µM and 10 µM C60 had no effect on PARP in the normal epithelial, ARPE-19 cell cultures (Figure 2.8.B). These results further suggest that the cancer cell lines monitored in our study are more sensitive to C60 treatment than non-cancer cells.

We also monitored the effects of C60 on Myeloid Cell Leukemia 1 (MCL-1). MCL-1 is a B-cell Lymphoma Leukemia 2 (BCL-2) homologue and it is a known anti-apoptotic protein [169]. A decrease in the expression level of MCL-1 was observed after C60 treatment in the cervical and oesophageal cancer cell lines (Figure 2.9)

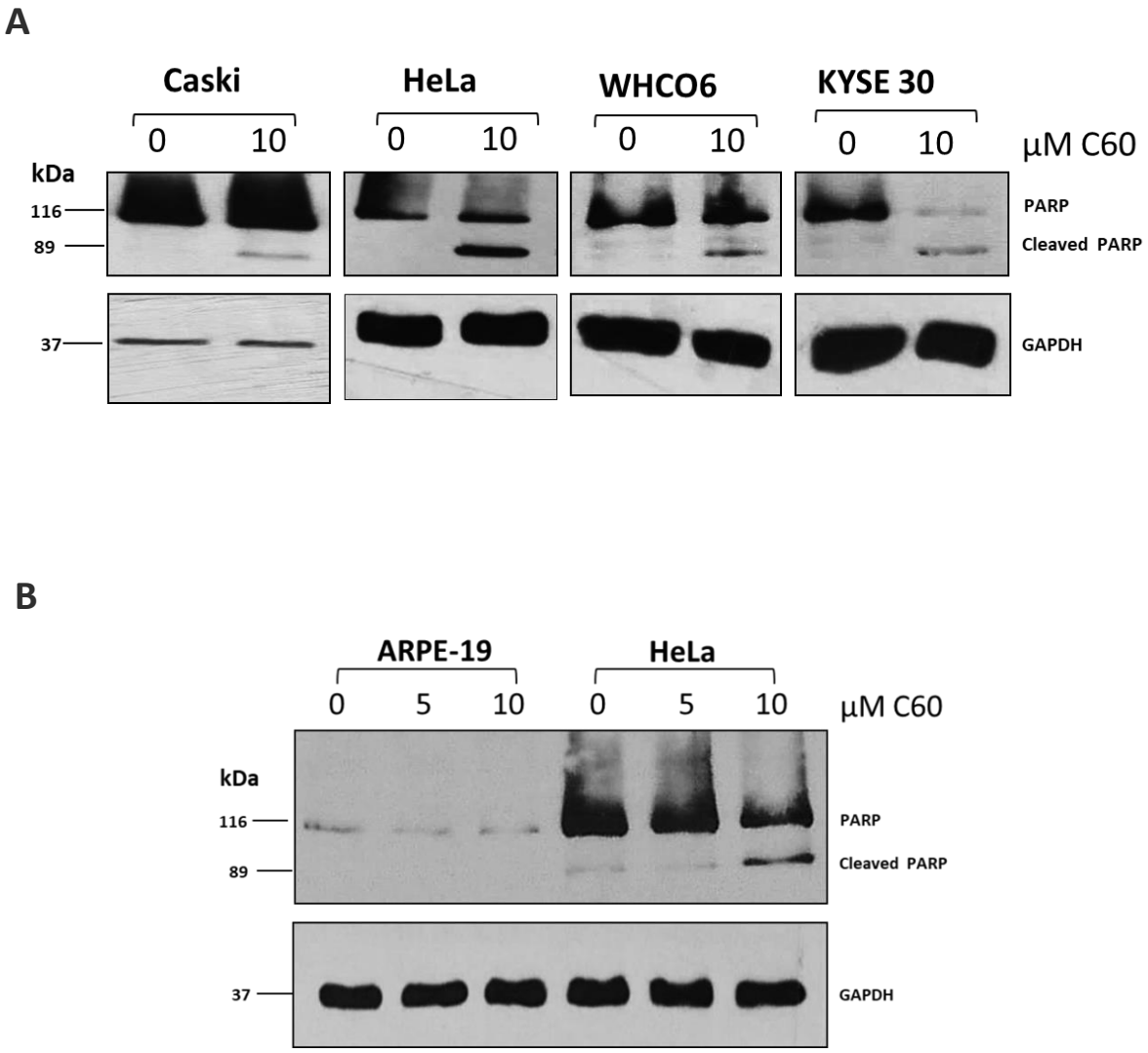

Figure 2.8. C60 induces PARP cleavage in cancer cells. Cervical (HeLa and CaSki) and oesophageal (WHCO6 and KYSE 30) cancer cells were treated with 10 µM C60 for 24 hours (A). The effect of 5 µM or 10 µM C60 treatment for 24 hours on PARP cleavage in HeLa cells was compared to ARPE-19 non-cancer epithelial cells (B). Results shown are representative of experiments performed at least three independent times.

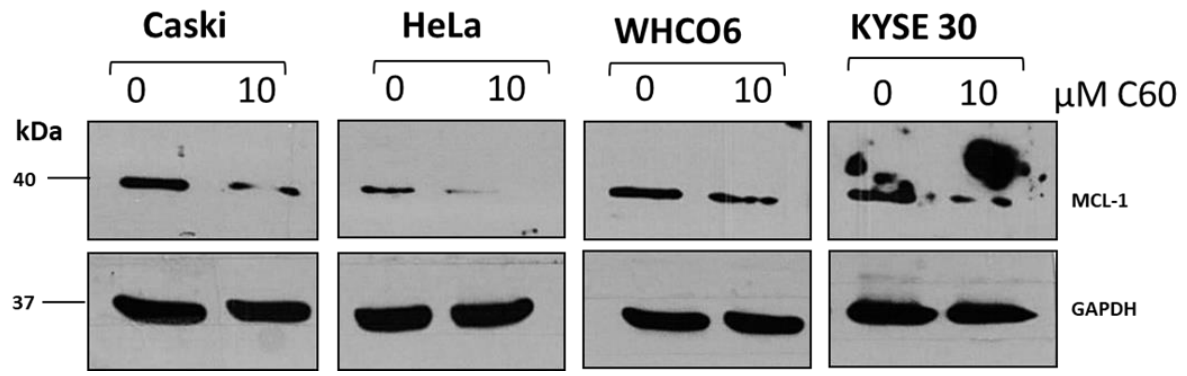

Figure 2.9. Effect of C60 on MCL-1 expression. Cervical (HeLa and CaSki) and oesophageal (WHCO6 and KYSE 30) cancer cell lines were treated with 10 μM C60 for 24 hours. MCL-1 level was analysed by western blot. Results shown are representative of experiments performed at least three independent times.

2.2.3. The effect of C60 on migration and invasion of cancer cells

In addition to monitoring the effect of C60 on cancer cell phenotypes such as proliferation, survival and cell cycle progression, we also investigated its effect on other biological phenotypes associated with cancer cells such as migration and invasion.

2.2.3.1. Effect of C60 on the migration of cancer cells

The migration of cells is important for physiological development, immune response, tissue homeostasis, tissue repair and renewal [170]. Migration is also involved in metastasis which is the major cause of mortality in cancer patients [171]. The effect of C60 on the migratory ability of cancer cells was investigated using the transwell migration assay. This assay permits the movement of cells with migratory capacity to move from the upper chamber of the transwell plate through the 8 μm to the lower chamber containing a chemoattractant e.g.

high serum concentration growth medium. Cervical and oesophageal cancer cells were pre-treated with C60 for 6 hours and migration through the transwell monitored after 24 hours. A 6-hour treatment time was selected, as at this timepoint C60 did not cause significant cytotoxic effects as shown by its effect on cell morphology and cell cycle progression. MTT cell viability assays were performed alongside migration assays to correct for migration relative to viable cells. Migrated cells were stained with crystal violet, photographed and quantified. Visual images and quantification of the results showed that C60 significantly reduced HeLa and Caski cervical cancer cell migration (Figure 2.10. A,B). Similar results were obtained in WHCO6 and KYSE 30 oesophageal cancer cell lines (Figure 2.10.C, D).

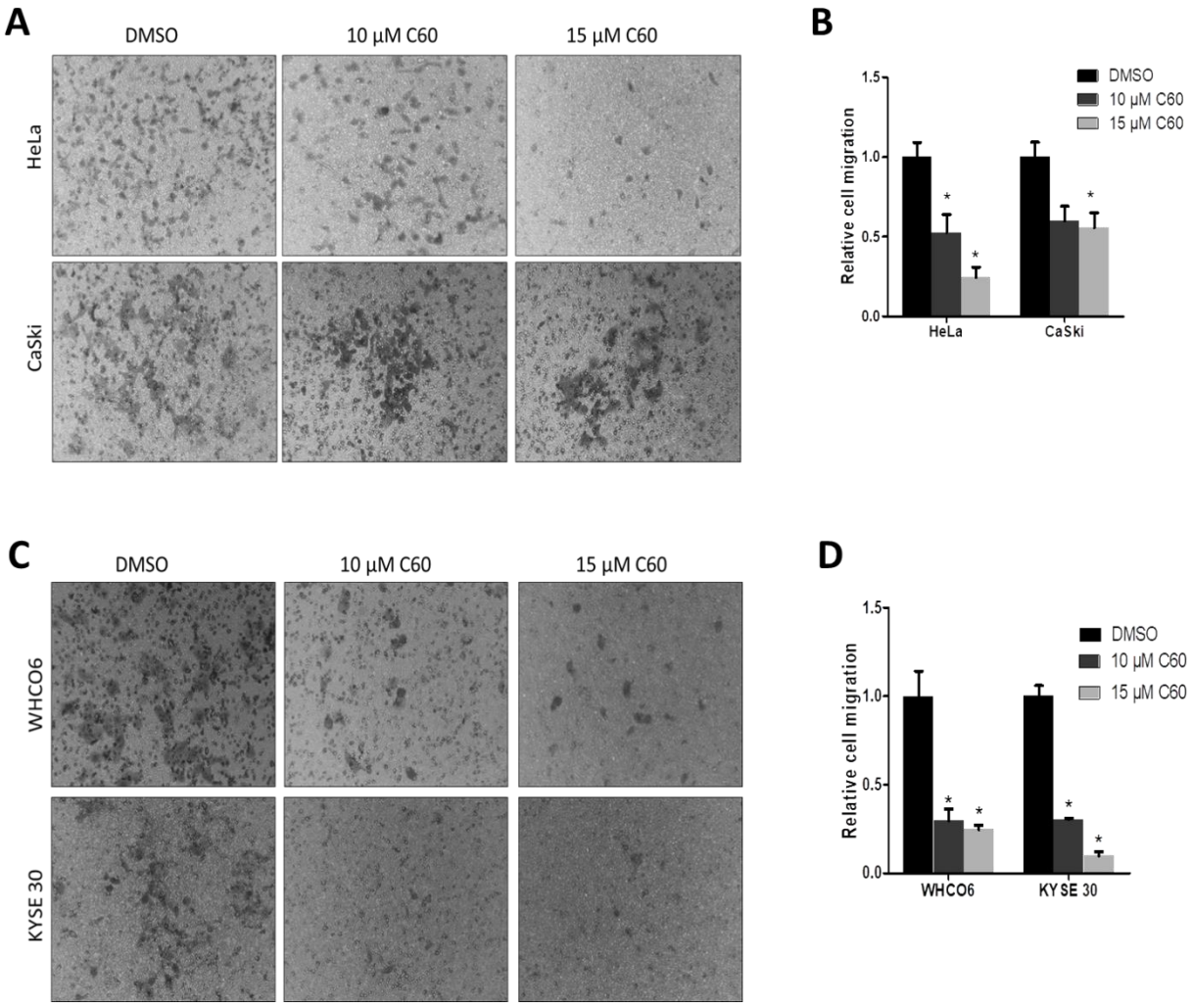

Figure 2.10. C60 inhibits migration of cancer cells. Representative images from the transwell migration assay showing reduced migration of cells after 10 or 15 µM C60 treatment for 6 hours (x100 magnification) in HeLa and CaSki cervical cancer cells (A) and WHCO6 and KYSE 30 oesophageal cancer cells (C). Quantification of relative migrated cells normalised to viable cells as measured by MTT assays for the cervical cell lines (B) and oesophageal cancer cell lines (D). Results are the mean ± SEM of experiments performed in triplicate and repeated two independent times. Statistical significance was determined by student paired t-test (*$p \leq 0.05$).

2.2.3.2. Effect of C60 on cancer cell invasion

The invasiveness of cancer cells is a critical attribute that differentiates benign lesions from malignant ones [172]. A malignant progression involves the invasion of cells into surrounding tissues which results in the development of distant metastasis [173]. The effect of C60 on the invasiveness of cancer cells was investigated using an *in vitro* invasion assay using matrigel covered transwell membranes and experimental conditions as for migration assays. 15 µM C60 was found to significantly inhibit the invasiveness of HeLa, CaSki cervical cancer cell lines (Figure 2.12.A) and WHCO6, KYSE 30 oesophageal cancer cell lines (Figure 2.12.B).

A

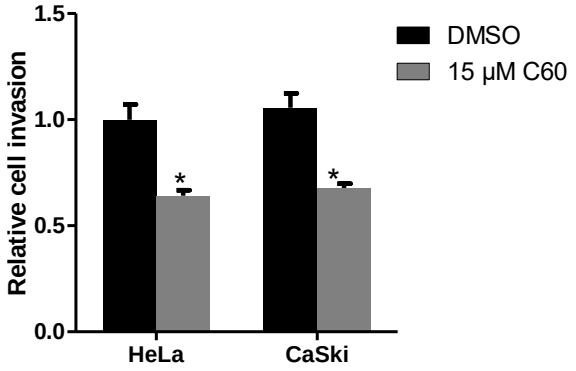

B

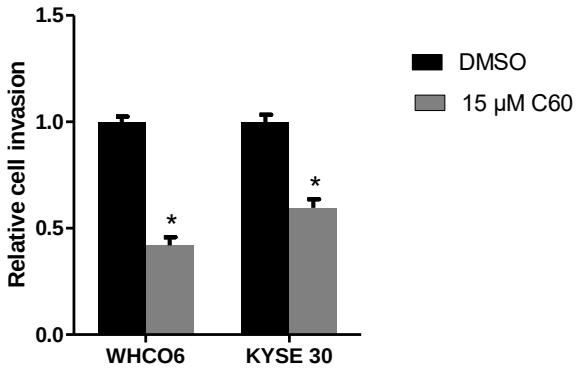

Figure 2.11. C60 inhibits invasion of cancer cells. Quantitative graph of the invasion assay following 6 hours 15 µM C60 treatment of cervical (HeLa and CaSki) cancer cells (A) and oesophageal (WHCO6 and KYSE 30) cancer cells (B). Results are the mean ± SEM of experiments performed in triplicate, Statistical significance was determined by student paired t-test (*$p \leq 0.05$).

2.3. Discussion

An association between the nuclear transport family of proteins and cancer development has been described in many cancers [55,132,174] and newer therapies that target members of this family are under investigation as anti-cancer treatments. Selinexor (KPT-330), a selective inhibitor of CRM1 has been tested in phase I clinical trials as a therapy for solid tumours including prostate, ovarian, cervical and colorectal cancer [175]. Selinexor has also been tested in phase I clinical trials in children with refractory leukemia [176]. The potential for the treatment of various cancers via the inhibition of the nuclear export protein, CRM1 has generated much interest in targeting other nuclear transport proteins for cancer treatment. Previous studies in our laboratory identified Kpnβ1 and CRM1 as the genes necessary for the survival of cervical cancer cells [55]. Van der Watt *et al* (2016) showed that non-cancer fibroblasts; WI38, CCD-1068SK, FG_0 and EPC2 epithelial cells were largely unaffected by Kpnβ1 inhibition via siRNA interference [55,142].

In the present study, we investigated the anti-cancer properties of C60 a small molecule identified via *in silico* screening of the ZINC 2010 drug-like database as a potential inhibitor of Kpnβ1[142]. Our results showed that C60 was significantly more toxic to cancer cells in comparison to non-cancer epithelial cells. The effect of C60 on cancer cell survival was investigated using multiple techniques. EC_{50} values of C60 obtained in different cancer cell lines were significantly lower than that obtained in non-cancer epithelial cell lines showing a selectivity index of 2.5–4. A selectivity index of less than 2 is an indicator that a drug is likely to have general toxicity [158]. Other studies reporting selectivity indexes for potential anti-cancer drugs include a study by He *et al* (2015) showing that FPB, a novel bifunctional mitochondria-targeted anti-cancer agent had selective cytotoxicity for the human gastric

carcinoma cells in comparison to its non-cancer counterpart, a selective index of 6.58 was reported [177]. Similarly, Liu *et al* (2015) showed that RY-2F, an isoflavone analogue has selective cytotoxicity for ovarian cancer cells in contrast to non-cancer ovarian cells with a selective index of approximately 6.9 [159]. Our data showed that C60 was more effective at killing cancer cells compared to the commercially available Kpnβ1 inhibitor Importazole at comparable doses. Soderholm *et al* (2011) reported that Importazole had an EC_{50} value of 22.5 µM in HeLa cells after 24 hours treatment [123] while our results found an EC_{50} value of 30.55 µM with a confidence interval of 24.39-38.49. Our results showed that Importazole had a selectivity index of 2-3 similar to that of C60.

EC_{50} values obtained for C60 showed that a lower concentration was required to kill 50% of the cells when treatment time was extended from 24 to 48 hours. These results are similar to that reported by Deepa *et al* (2011) reporting that the IC_{50} of three anti-lipogenic inhibitors of Fatty Acid Synthase (FASN); cerulenin, triclosan and orlistat reduced when treatment time was increased from 48 to 96 hours [178].

C60 showed significant inhibitory effects on anchorage-dependent cell proliferation and colony formation, which are key hallmarks of cancer cells. Other determinants of cancer spread include invasion and migration as these play important roles in the ability of cancer cells to metastasise [179]. Our results showed that C60 significantly reduced the migratory and invasive ability of cervical and oesophageal cancer cells. In addition to inhibiting key biological features of cancer cells, C60 altered the progression of cells through the different phases of the cell cycle. In most cancers, cell cycle progression is altered, resulting in uncontrolled proliferation [180]. Progression of cells through the cell cycle is controlled by checkpoints that recognize potential defects during DNA synthesis. The activation of these

checkpoints results in cell cycle arrest which allows for the repair of defects thereby preventing their transmission to new daughter cells [181]. Our study found that C60 induced G1 cell cycle arrest with a corresponding decrease in the percentage of cells at the S and G2/M phase of the cell cycle after 12 and 24 hours treatment. The G1 cell cycle arrest was accompanied by a dose-dependent down-regulation of Cyclins D1, A, B and CDK4 at 24 hours. The binding of Cyclin D to CDK has been reported to be necessary for the entry of cells into the next phase of the cell cycle [180]. Cyclin A/ CDK2 complex is required for the progression of cells from late S phase into G2 phase [159]. CDK1/Cyclin B complex is involved in controlling the progression of cells from mitosis to the next phase in the cell cycle [181]. The results obtained in this study are similar to a study by Yim *et al* (2005) showing that Decursin, a coumarin compound induced G1 cell cycle arrest in human prostate cancer cells after 24 and 48 hours treatment. Decursin did not alter the level of CDK4 and cyclin D1 at 24 hours; however, treatment for 48 hours showed a dose-dependent decrease in the expression CDK4 and cyclin D1 [182].

Most anti-cancer drugs display their cytotoxic effects by inducing cell cycle arrest at precise checkpoint thereby provoking apoptosis [162]. Apoptosis is a form of programmed cell death, which is controlled by various signalling cascade. Cleavage of PARP, as well as the effect on the morphology of cells, showed that C60 induced cancer cell death via apoptosis. Additionally, the decreased expression of MCL-1 in C60 treated cells further confirmed the induction of cell death via apoptosis. MCL-1 is an anti-apoptotic member of the BCL-2 family [183]. Cisplatin has also been shown to decrease the expression of MCL-1 in a time and dose-dependent manner and this reduced expression is associated with proteasome-dependent degradation. This proteasomal degradation of MCL-1 is important in the cisplatin-mediated

apoptosis through the mitochondrial apoptotic pathway [184,185]. The elimination of MCL-1 results in the initiation of cytochrome c release and caspase activation, which precedes cell death via apoptosis evidenced by the cleavage of PARP [186,187]. While the data in this study suggests that C60 did not induce PARP cleavage in the non-cancer cell line, ARPE-19, it is important to note that there is a vast difference between the expression level of PARP in cancer and non-cancer cells. The overexpression of PARP has been reported in numerous human cancers including breast cancer [188]. The effect of C60 on non-cancer cells can be investigated in an Annexin V assay to confirm that C60 does not induce apoptotic cell death in non-cancer cells.

In this chapter, the concentration of C60 was changed from 5 µM and 10 µM concentrations initially used in the proliferation assay to 10 µM and 15 µM in other assays such as cell cycle analysis, migration and invasion since a shorter treatment time of 6 hours was included in these assays, therefore, a higher treatment concentration was required. Data obtained showed that while 10 µM and 15 µM C60 treatment for 6 hours did not have obvious effects on cell cycle progression and morphology, it was sufficient to inhibit migration and invasion of cancer cells. Collectively, the results described in this chapter using data from *in vitro* experiments showed that C60 had greater cytotoxicity in oesophageal and cervical cancer cells in comparison to non-cancer cells; it induced cell death via apoptosis, caused a G1 cell cycle arrest and significantly reduced cell migration and invasion. These anti-cancer effects of C60 suggest it has potential as a candidate for further development as a chemotherapeutic drug.

Chapter 3: Investigating the effect of C60 on Kpnβ1 sub-cellular localisation and on the nuclear activity of Kpnβ1 cargo proteins.

3.1. Introduction

Various studies have demonstrated that Kpnβ1 has elevated expression in cancer and transformed cells. There is also evidence that supports a requirement of Kpnβ1 for maintaining aspects of the cancer phenotype[142] most likely via its role in the nuclear transport of oncogenic transcription factors and its involvement in cell cycle transition, mitosis and replication. It has also been reported that the frequency of nuclear transport is increased in transformed and cancer cells in order to maintain increased metabolism and proliferation [65]. Inhibition of Kpnβ1 expression resulted in cell death via apoptosis in cancer cells which further emphasises its role in carcinogenesis [142]. In the previous chapter, we showed that C60, a potential inhibitor of Kpnβ1 has inhibitory effects on the proliferation of cancer cells of oesophageal and cervical origin. Here, we set out to investigate the effects of C60 on the sub-cellular localisation of Kpnβ1 and on the nuclear activity of known Kpnβ1 cargo proteins including that of oncogenic transcription factors.

Kpnβ1 imports numerous transcription factors including NFκB, NFAT, AP-1 and STAT into the nucleus. NFκB plays a crucial role in cell proliferation, apoptosis and inflammation. Aberrant activation of NFκB is associated with various cancers [117]. The NFκB family is made up of five distinct members: c-Rel, p65 (Rel A), Rel B, p50/p105 (NFκB1) and p52/p100 (NFκB2) with the p50/p65 heterodimer being the most common NFκB complex [117]. The nuclear import of NFκB complexes occurs after the degradation of its inhibitor protein IκB [131,189]. Stimulation of NFκB nuclear translocation and activity can be triggered by various agents such as

Tumour Necrosis Factor α (TNF-α) and Phorbol 12-Myristate 13-Acetate (PMA) [190]. Fagerlund *et al* (2005) showed that Importin α3 and Importin α4 are the major Importins involved in the nuclear import of TNF-α induced NFκB p50/p65 heterodimer [191]. NFκB nuclear import has been reported to occur via Kpnβ1, XPO7 and IPO8 [117].

Another known cargo of Kpnβ1 is NFAT. NFAT is a family of transcription factors that have a role in the regulation of immune response and include four calcium/calcineurin-responsive proteins (NFATc1-c4) [192,193]. The NFAT pathway is calcium-dependent and when activated, NFAT is dephosphorylated by the phosphatase Calcineurin. This results in the nuclear translocation of NFAT and transcriptional activation of its downstream target genes [192]. Dephosphorylation of NFAT exposes its NLS and allows its translocation via interaction with nuclear transport proteins [194]. The NFAT signalling pathway controls many parts of cellular functions by acting as a calcium sensor and it also involved in growth and development, inflammatory and immune responses [195]. Multiple studies have implicated the NFATs in various aspects of cancer such as proliferation, metastasis, angiogenesis and drug resistance [194,195]. NFAT is imported into the nucleus in the classical nuclear import pathway by Kpnβ1 and Kpnα and exported by CRM1 [123,196].

As C60 was discovered via a rational drug design approach to identify small molecules with the potential to bind and interfere with Kpnβ1 activity, we investigated its effects on Kpnβ1 itself and on the nuclear activity of known Kpnβ1 cargo proteins, NFκB, NFAT and AP-1.

3.2. Results

3.2.1. Expression of Kpnβ1 and Kpnα2 in cancer cells versus non-cancer cell lines

Previous studies in our laboratory and others reported the elevated expression of Kpnβ1 in cervical [55], gastric [71] and breast [130] cancer cell lines and tissues in comparison to non-cancer cell cultures and tissue. In this study, we independently validated the expression of Kpnβ1 and its adaptor protein Kpnα2 in HeLa (cervical) and WHCO6 (oesophageal) cancer cell lines in comparison to that in normal primary retinal epithelial cell culture, ARPE-19 and its immortalised counterpart hTERT RPE-1.

Western blot analysis showed that both Kpnβ1 and Kpnα2 expression levels were higher in the HeLa and WHCO6 cancer cells in comparison to the non-cancer epithelial cells (Figure 3.1.A). Quantification by densitometric analysis of Kpnβ1 and Kpnα2 band intensities normalised to GAPDH as a loading control of western blot analysis performed three independent times is shown in Figure 3.1.B and C. These results support previous studies reporting that cancer cell lines have elevated Kpnβ1 and Kpnα2 expression.

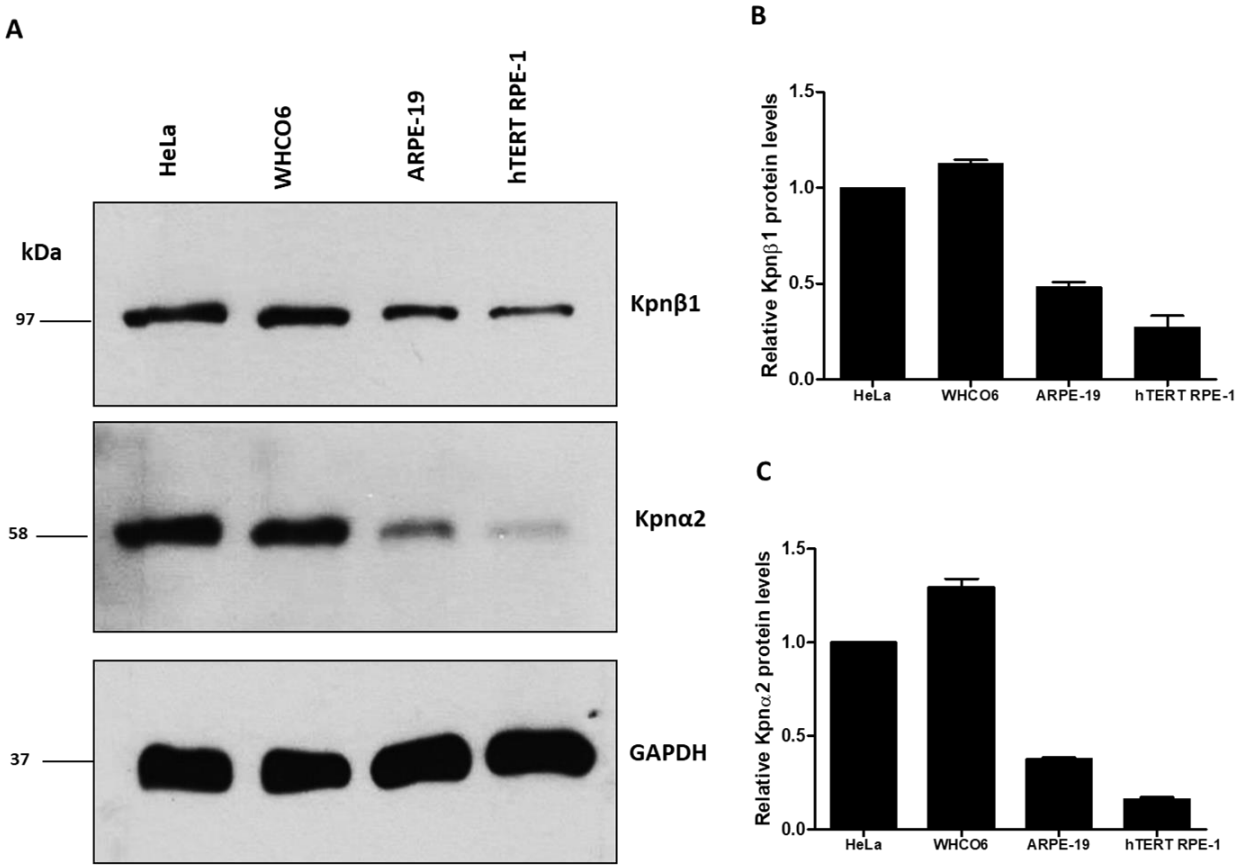

Figure 3.1. Kpnβ1 and Kpnα2 expression in cancer cells versus non-cancer cells. Western blot analysis was done to determine the expression levels of Kpnβ1 and Kpnα2 expression in cancer cells (HeLa and WHCO6) in comparison to non-cancer cells (ARPE-19 and hTERT RPE-1) (A). Densitometric analysis of Kpnβ1 (B) and Kpnα2 (C) relative to GAPDH (loading control). Densitometric values of WHCO6, ARPE-19 and hTERT RPE-1 were normalised to that of HeLa. Results are representative of experiments performed at least three independent times.

3.2.2. Investigating the effect of C60 on Kpnβ1 and Kpnα2 nuclear localisation

3.2.2.1. The effect of C60 on Kpnβ1 and Kpnα2 using nucleo-cytoplasmic separation

To determine whether C60 acts on Kpnβ1, we investigated its effect on the sub-cellular localisation of Kpnβ1. HeLa cervical cancer cells were treated with 10 µM or 15 µM C60 for 6 hours and cytoplasmic and nuclear proteins were harvested. Western blot analysis showed a noticeable decrease in nuclear, and an associated increase in cytoplasmic Kpnβ1 (Figure 3.2). The effect of C60 on the localisation of Kpnα2, the adaptor protein of Kpnβ1 was also investigated. Result showed that the nuclear entry of Kpnα2 was not inhibited by C60; instead, there was a dose-dependent increase in nuclear Kpnα2 and a concurrent decrease in cytoplasmic Kpnα2. The TATA-Binding Protein (TBP) served as the loading control for the nuclear fraction while GAPDH served as the loading control for the cytoplasmic and whole cell fractions.

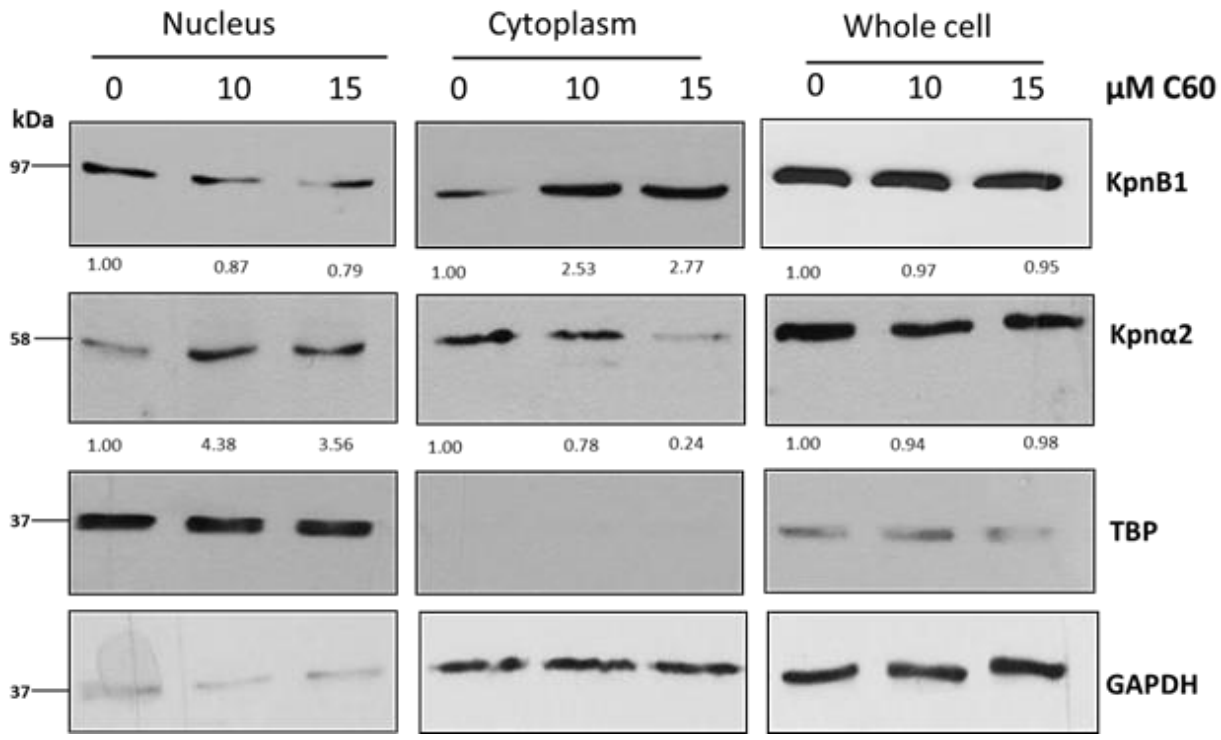

Figure 3.2. Effect of C60 on the sub-cellular localisation of Kpnβ1 and Kpnα2. Nuclear and cytoplasmic protein fractions were harvested from HeLa cells after C60 treatment for 6 hours. Kpnβ1 and Kpnα2 levels in the two fractions were examined via western blot. TBP and GAPDH served as the loading controls for the nuclear and cytoplasmic fractions respectively. Densitometric analysis was normalised to loading controls for each fraction. Results shown are representative of western blot analysis done three independent times.

3.2.2.2. The effect of C60 on Kpnβ1 and Kpnα2 monitored using immunofluorescent microscopy

To independently monitor the effect of C60 on Kpnβ1 sub-cellular localisation, Kpnβ1 was immunofluorescently labelled and its localisation viewed using confocal microscopy. Control cells showed a strong nuclear localisation of Kpnβ1, which became cytoplasmic after treatment with 10 µM and 15 µM C60 (Figure 3.3.A). Fluorescent intensities of Kpnβ1 (Cy3) and DAPI (nucleus) across single cells confirmed a reduction in nuclear Kpnβ1 fluorescent intensity in 10 and 15 µM C60 treated cells (Figure 3.3.B). We also confirmed the effect of C60 on Kpnα2 sub-cellular localisation. C60 resulted in an increase in Kpnα2 nuclear staining (Figure 3.4.A). Fluorescent intensities of Kpnα2 (Alexa Fluor 647) and DAPI (nucleus) across single cells confirmed increased nuclear Kpnα fluorescent intensity in 10 and 15 µM C60 treated cells (Figure 3.4.B). The fluorescent intensities of various cells representative of each treatment were measured for random cells for three independent experimental repeats however; images shown in results are illustrative images from one experiment. Together, these results show that C60 treatment altered the sub-cellular localisation of Kpnβ1, making it more cytoplasmic while altering the localisation of Kpnα2 to being more nuclear.

A

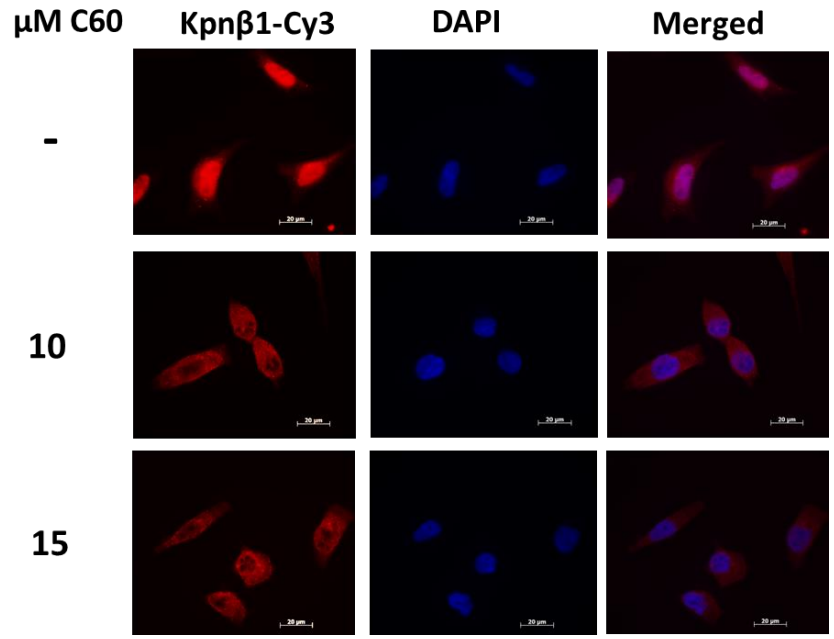

B

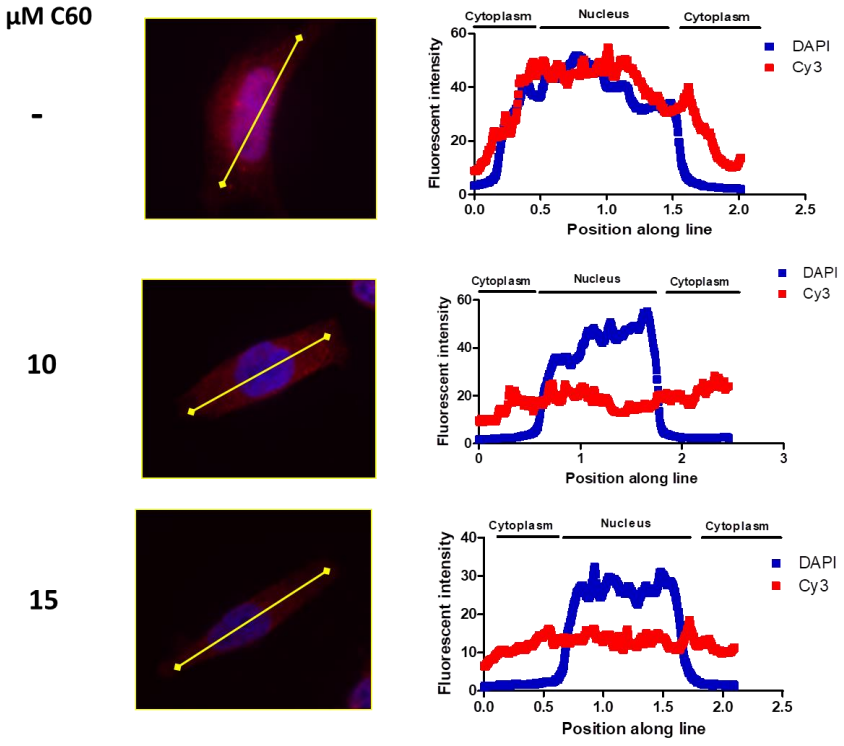

Figure 3.3. C60 treatment inhibits the nuclear accumulation of Kpnβ1. HeLa cells were treated with C60 for 6 hours prior to fixation and staining with Cy3 (Kpnβ1) and DAPI (nucleus). Images were captured using a fluorescent microscope (A). Association between Kpnβ1-Cy3 and DAPI (nucleus) fluorescent intensities was done using Image J software (B). Experiment was performed three independent times and an illustrative image from one experiment is shown.

A

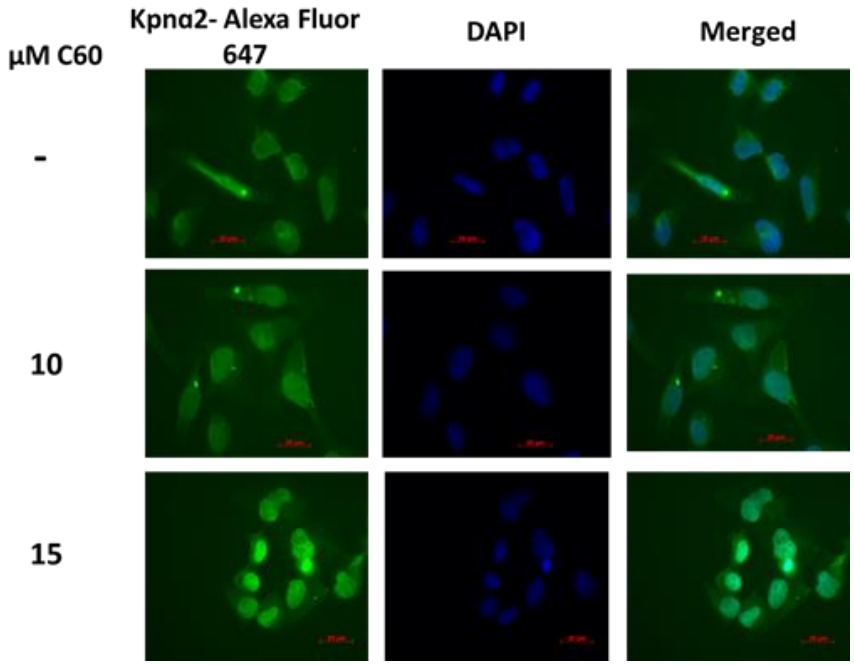

B

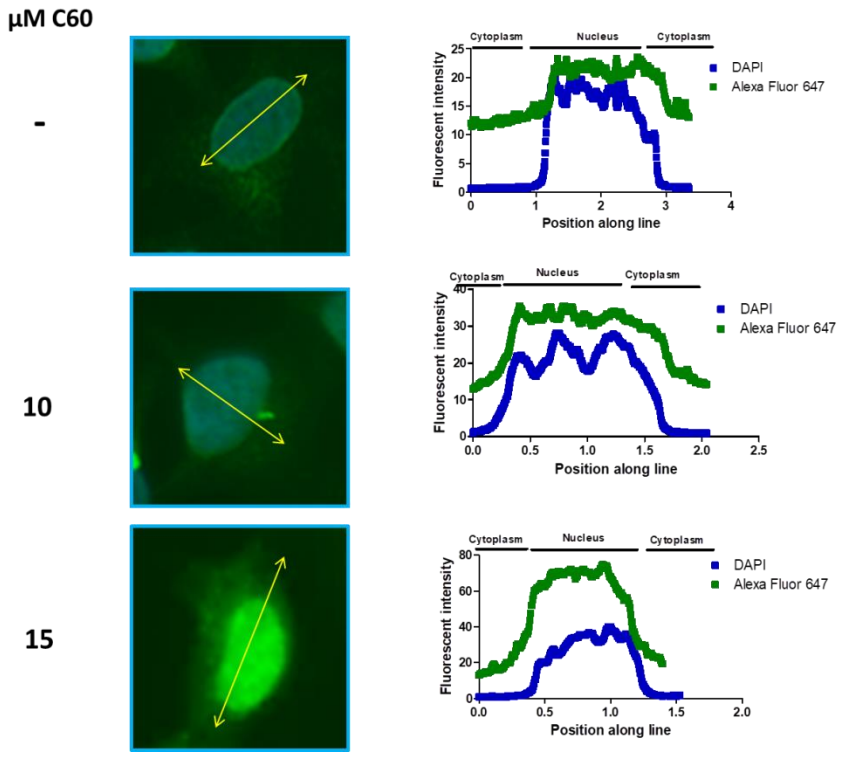

Figure 3.4. C60 treatment induced nuclear accumulation of Kpnα2. HeLa cells were treated with C60 for 6 hours prior to fixation and staining with Alexa Fluor 647 (Kpnα2) and DAPI (nucleus). Images were captured using a fluorescent microscope (A). Association between Kpnα2-Alexa Fluor and DAPI (nucleus) fluorescent intensities was done using Image J software (B). Experiment was performed three independent times and an illustrative image from one experiment is shown.

3.2.3. Effect of C60 on the half-life of Kpnβ1 and Kpnα2

To investigate the effect of C60 on the stability of Kpnβ1, half-life assays using cycloheximide to inhibit new protein synthesis was performed. HeLa cells were pre-treated with DMSO (vehicle) or 5 µM C60 for 3 hours prior to treatment with 50 µg/mL Cycloheximide (CHX). 5 µM C60 concentration was chosen for this experiment as it showed a less cytotoxic effect in the proliferation assay experiment (Figure 2.3.A) in comparison to the 10 µM concentration, thus allowing us to monitor the effect of C60 on Kpnβ1 half-life over a long period. CHX is a known inhibitor of de novo protein synthesis and it has been reported to inhibit the elongation phase of eukaryotic translation [197]. Protein was harvested at different time points after CHX treatment and western blot analysis used to monitor the effect of C60 on Kpnβ1 stability. Since Kpnα2 was accumulating in the nucleus, we investigated the possibility of increased protein stability following C60 treatment. The expression of Kpnα2 was monitored alongside that of Kpnβ1 (Figure 3.5.A). Quantification of Kpnβ1 or Kpnα2 levels expressed relative to GAPDH was done and its half-life (Log2/slope) determined by plotting band intensities relative to time. In the absence of C60, the half-life of Kpnβ1 was approximately 67 hours which was reduced by roughly 2.3 fold to 29 hours in the presence of C60 (Figure 3.5.B). The reduction in the half-life of Kpnβ1 suggests that C60 causes increased degradation of Kpnβ1. Interestingly, C60 treatment resulted in a 2.5 fold increase in the half-life of Kpnα2 from approximately 18 hours to 45 hours (Figure 3.5.C). Since Kpnα2 was accumulating in the nucleus of C60-treated cells, it is likely that this nuclear accumulation protected it from degradation thereby increasing its half-life.

A

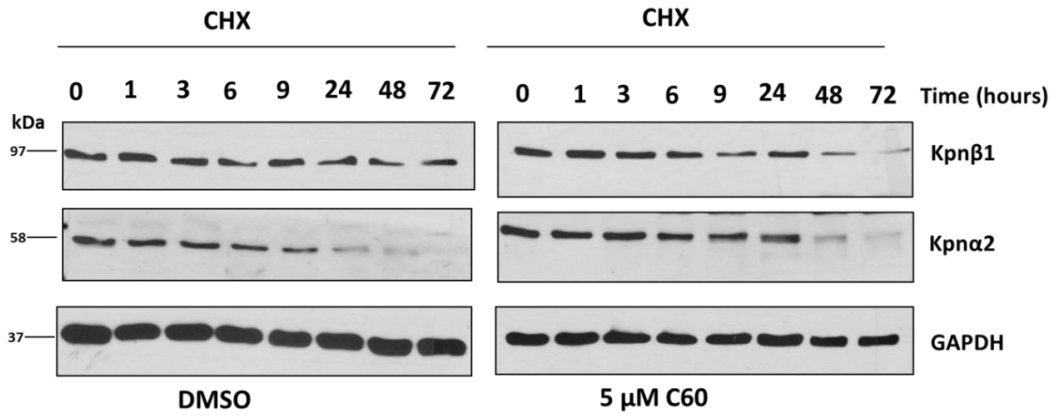

B

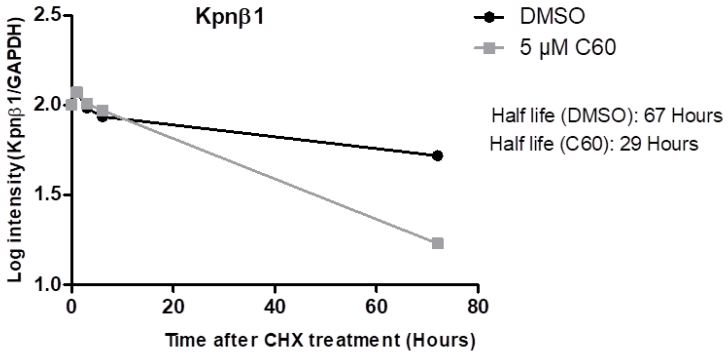

C

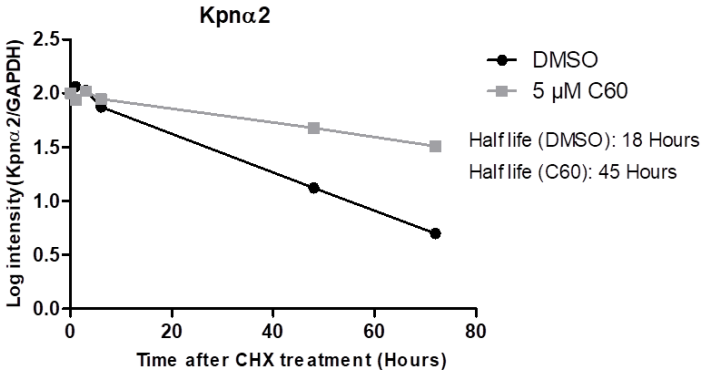

Figure 3.5. Effect of C60 on the stability of Kpnβ1 and Kpnα2. The half-life of Kpnβ1 and Kpnα2 was determined after HeLa cells were treated with 5 µM C60 or DMSO (vehicle) for 3 hours followed by treatment with 50 µg/mL CHX. Proteins were harvested at various time points after CHX treatment, Kpnβ1 and Kpnα2 expressions were analysed by western blot. GAPDH served as loading control (A). Quantitative analysis of Kpnβ1 and Kpnα2 was done using densitometric scanning and band intensities were plotted in log scale relative to Kpnβ1(B) or Kpnα2 (C) at time 0 hour. Half-life was determined using the equation (Log2/ slope). Graph shown is representative of single experiment. Half-life is the average of experiments done three independent times.

3.2.4. Effect of C60 on the sub-cellular localisation of Kpnβ1-dependent cargo proteins

3.2.4.1. C60 inhibits the nuclear import of NFκB/p65

Previous studies have shown that Kpnβ1 is a major nuclear import receptor of the transcription factor NFκB/p65 and this import is reliant on the NLS of NFκB/p65 [117].

i. Effect of C60 on NFκB/p65 nuclear import using immunofluorescent microscopy

We investigated the ability of C60 to interfere with the nuclear import of NFκB/p65 in response to PMA (phorbol ester) stimulation. HeLa and WHCO6 cells were pre-treated with 10 µM or 15 µM C60 for 6 hours and treated with 0.5 µM PMA for 1 hour to stimulate NFκB/p65 nuclear entry before the termination of C60 treatment. NFκB/p65 localisation was monitored using immunofluorescence.

Our results show that NFκB/p65 (Cy3) is predominantly localised to the cytoplasm of untreated cells (Figure 3.6.A). Stimulation with PMA led to the nuclear translocation of NFκB/p65 and C60 treatment resulted in the cytoplasmic retention of NFκB/p65 in HeLa cells. Quantification of NFκB/p65 fluorescent intensity (Cy3) across randomly selected single cells showed elevated intensities that it overlapped with DAPI staining of the nucleus in PMA stimulated cells (Figure 3.6.B). In the 10 µM and 15 µM C60 treated cells, the NFκB/p65 intensity was significantly reduced in the nuclear compartment (Figure 3.6.B). Similar observations were made in WHCO6 cells where PMA stimulation resulted in the nuclear localisation of NFκB/p65, which was inhibited by C60 treatment (Figure 3.7. A). Fluorescent intensities were measured for random cells representing each treatment condition (Figure 3.7.B). The fluorescent intensities of various cells representative of each

treatment were measured for random cells for three independent experimental repeats however; images shown in results are illustrative images from one experiment. These results support that Kpnβ1 is required for the nuclear import NFκB/p65 in cervical and oesophageal cancer cells.

A

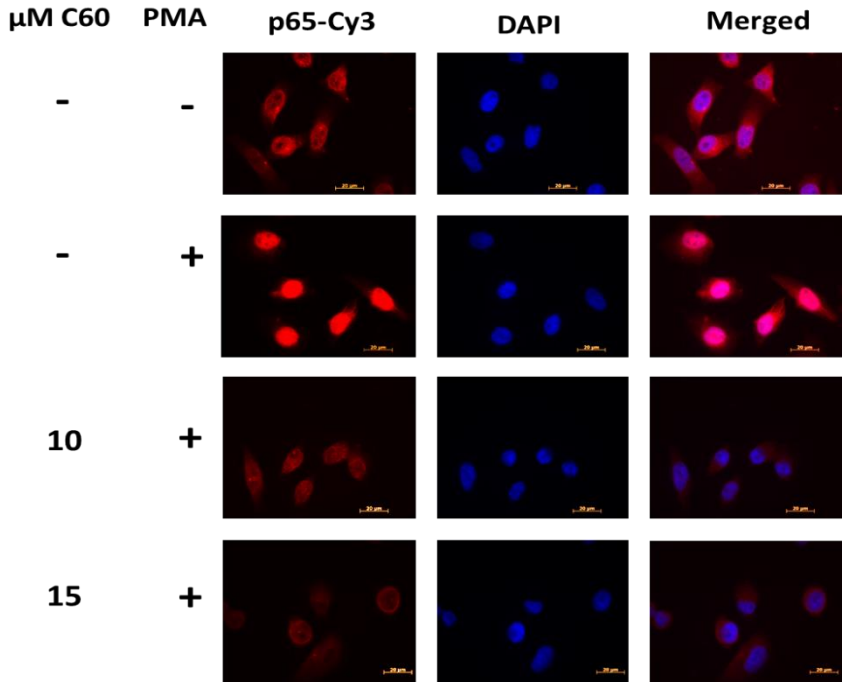

B

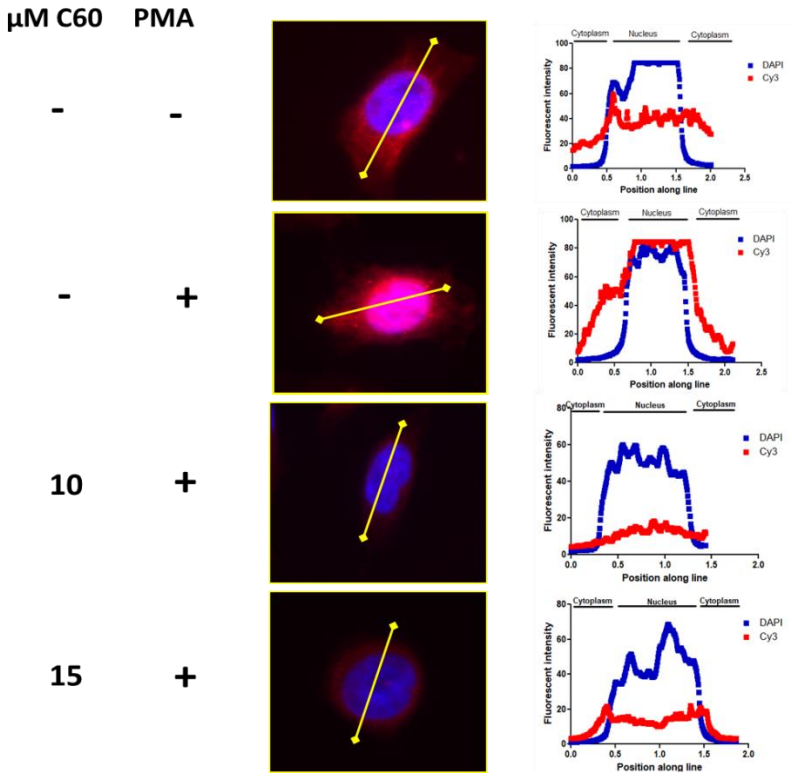

Figure 3.6. The effect of C60 on NFκB/p65 cellular localisation in HeLa cervical cancer cells. Immunofluorescent microscopy was used to monitor the effect of 6 hours C60 treatment on PMA-induced NFκB/p65 nuclear import in HeLa cells. An illustrative image for each treatment type is shown (A). Fluorescent intensities for NFκB/p65-Cy3 and DAPI (nucleus) are plotted as previously described (B).

A

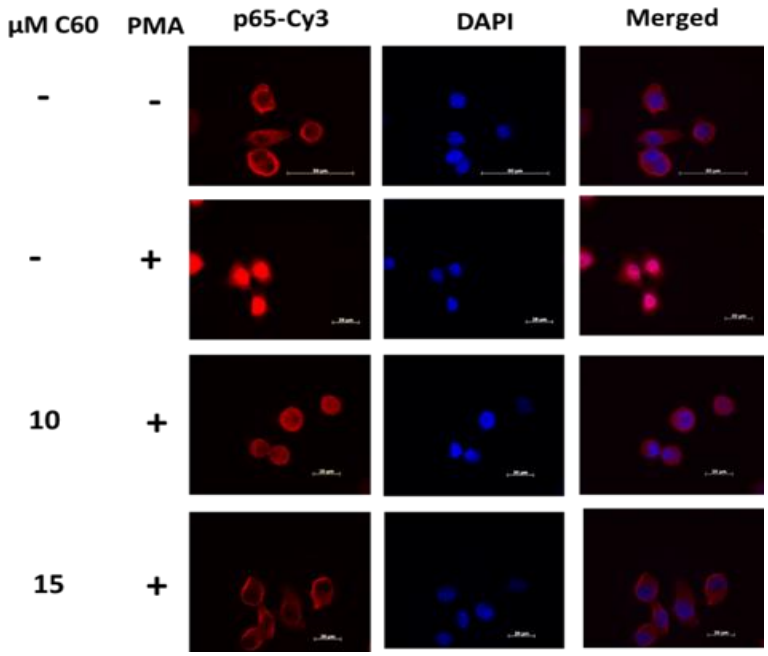

B

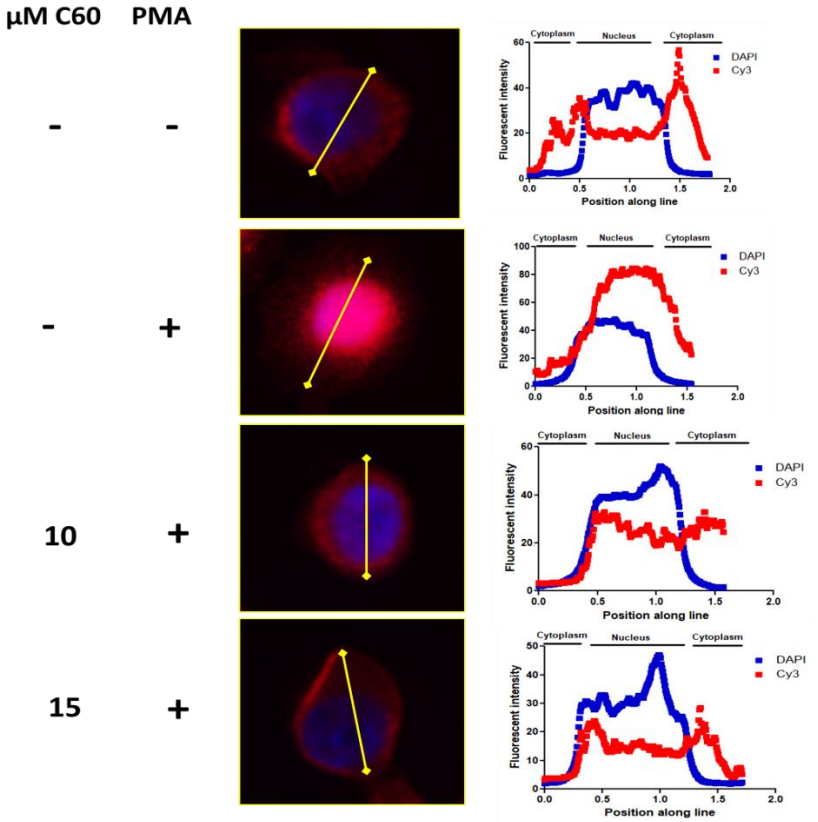

Figure 3.6. The effect of C60 on NFκB/p65 cellular localisation in WHCO6 oesophageal cancer cells. Immunofluorescent microscopy was used to monitor the effect of 6 hours C60 treatment on PMA-induced NFκB/p65 nuclear import in WHCO6 cells. An illustrative image for each treatment type is shown (A). Fluorescent intensities for NFκB/p65-Cy3 and DAPI (nucleus) are plotted as previously described (B).

i. Monitoring the effect of C60 on NFκB/p65 nuclear activity using luciferase reporter assays

Luciferase reporter assays were used to monitor the effect of C60 on the functional activity of NFκB/p65. Treatment of cells with 10 μM and 15 μM C60 resulted in a significant reduction in PMA-induced NFκB/p65 luciferase activity in HeLa (Figure 3.8.A) and WHCO6 (Figure 3.8.B) cancer cells. C60 treatment in ARPE-19 normal epithelial cells had no significant inhibitory effect on PMA-induced NFκB/p65 transcriptional activity (Figure 3.8.C).

Importazole, a commercially available inhibitor of Kpnβ1/Kpnα2 mediated nuclear import had no inhibitory effect on NFκB/p65 transcriptional activity when using the same concentration and time points at which C60 inhibited NFκB/p65 transcriptional activity (Figure 3.9.A). Increasing Importazole concentrations to 20 μM or 40 μM similarly had no significant effect on NFκB/p65 transcriptional activity (Figure 3.9.B). However, a significant reduction in NFκB/p65 transcriptional activity was only observed when cells were treated with 40 μM Importazole for a longer period of 24 hours (Figure 3.9.C). These results suggest that C60 is more effective at inhibiting the activity of Kpnβ1 cargo such as NFκB.

A

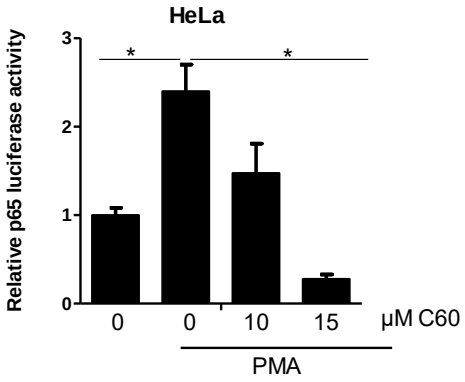

B

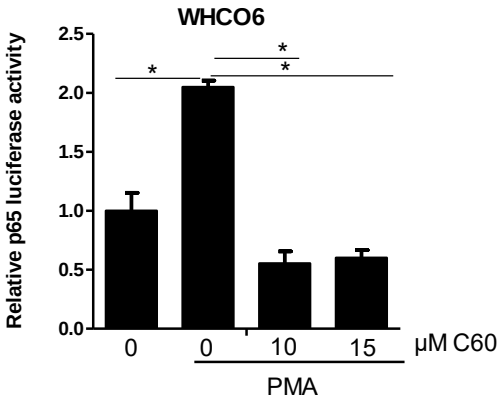

C

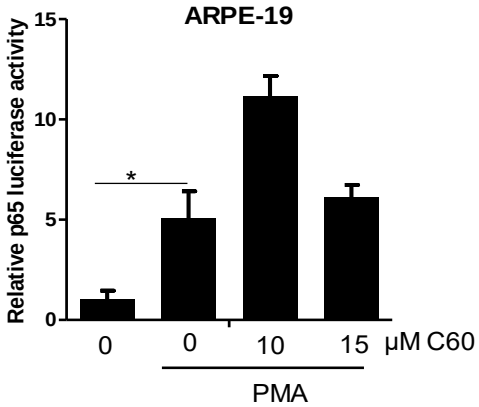

Figure 3.8. Effect of C60 on NFκB/p65 transcriptional activity in cancer cell lines versus non-cancer epithelial cell line. NFκB/p65 transcriptional activity using NFκB binding site luciferase reporter was measured after transient transfection in cells. Cells were pre-treated with C60 followed by 0.5 µM PMA stimulation for 3 hours (6 hours overall treatment time). The effect of C60 treatment on NFκB/p65 transcriptional activity was monitored in HeLa (A) and WHCO6 (B) and ARPE-19 non-cancer epithelial cell line (C). Results shown are representative of the mean ± SEM of experiments done in quadruplicate and repeated at least twice. Statistical significance was determined by student paired t-test, *p≤ 0.05.

A

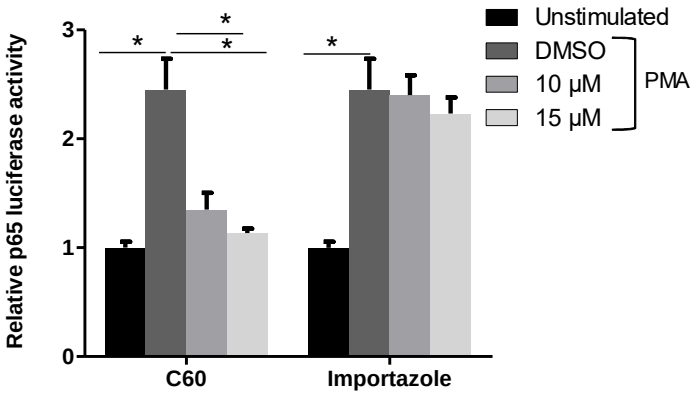

B

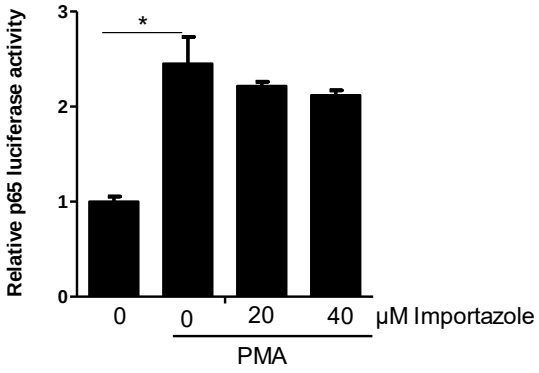

C

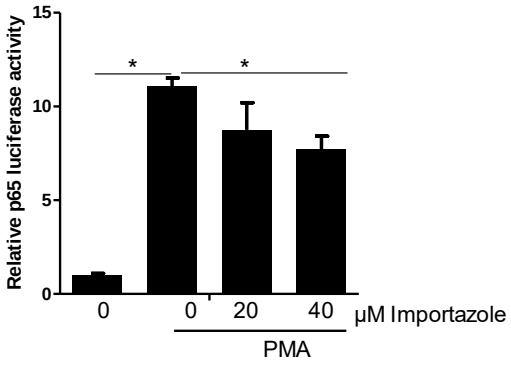

Figure 3.9. Comparison of the effect of C60 or Importazole on NFκB/p65 transcriptional activity. Comparison of the effect of 10 µM or 15 µM C60 versus Importazole treatment for 6 hours in HeLa cells (A). Treatment of HeLa cells with 20 µM or 40 µM Importazole for 6 hours did not result in the inhibition of NFκB/p65 transcriptional activity (B). Exposure of HeLa cells to 40 µM Importazole treatment for 24 hours resulted in a significant reduction in NFκB/p65 transcriptional activity (C). Results shown are representative of the mean ± SEM of experiments done in quadruplicate and repeated at least twice. Statistical significance was determined by student paired t-test, *p≤ 0.05.

3.2.4.2. C60 inhibits the nuclear import of NFAT

We investigated the effect of C60 on NFAT transcriptional activity, as it is a reported Kpnβ1 cargo. A NFAT-luciferase reporter plasmid was transfected into cells and Ionomycin used to increase intracellular calcium levels that stimulate NFAT nuclear translocation as previously described [123,198]. PMA and ionomycin were used to co-stimulate NFAT as their combination has been previously used to induce synergistic stimulation of NFAT luciferase activity [142] and cells were exposed to 10 μM or 15 μM C60 treatment for 6 hours. Results show that C60 significantly reduced PMA-induced NFAT activation in HeLa and WHCO6 cell lines (Figure 3.10.A and B). In comparison, Importazole the commercially available inhibitor of Kpnβ1/Kpnα2 mediated nuclear import had no inhibitory effect using the same concentration and time point (Figure 3.10.C). Importazole significantly reduced NFAT activity at 40 μM concentration after 6 hours treatment (Figure 3.10.D).

These results provide evidence that C60 has a significant inhibitory effect on the nuclear activity of NFAT, a Kpnβ1 cargo protein.

3.2.4.3. C60 inhibits the nuclear activity of AP-1

The effect of C60 on the transcriptional activity of AP-1 was investigated using AP-1 luciferase reporter construct comprising four artificial AP-1 binding sites fused to the luciferase reporter. For AP-1 to be activated, its cJUN component must undergo phosphorylation by JNK within the nucleus. However, the nuclear import of JNK does not rely on Kpnβ1 as it is NLS-independent [150]. In addition to investigating AP-1 activity in response to C60, we also investigated whether C60 had an effect on the phosphorylation of cJUN. Our results show that C60 significantly inhibited PMA-induced AP-1 transcriptional

activity as well as PMA-induced phosphorylation of cJUN in WHCO6 cells (Figure 3.11.A and B). Interestingly, C60 had no effect on AP-1 transcriptional activity and cJUN phosphorylation in HeLa cervical cancer cells (Figure 3.11.C and D). Similar to what was observed in HeLa cells, C60 did not inhibit AP-1 transcriptional activity in another cervical cancer cell line, CaSki (Figure 3.11.E).

Together, these results show that C60 inhibits the nuclear import and activity of AP-1 in a differential manner depending on the cancer type. While AP-1 is negatively affected by C60 in oesophageal cancer cells, C60 had no effect on the cervical cancer cells analysed in this study. This suggests that for cervical cancer cells in this study the nuclear translocation of AP-1 occurs via mechanisms not reliant on Kpnβ1.

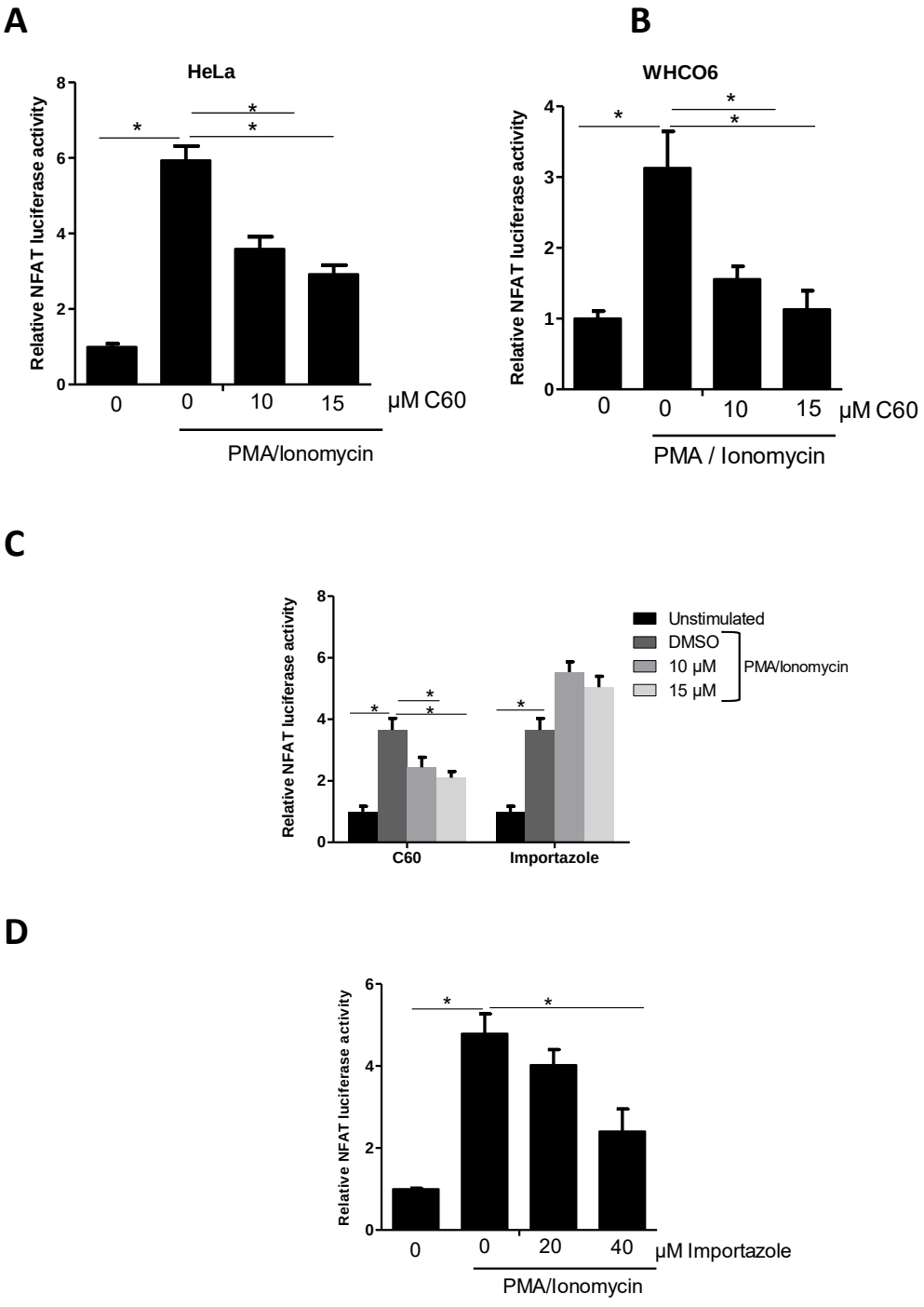

Figure 3.10. Effect of C60 on NFAT transcriptional activity. Cells were transiently transfected with NFAT reporter and expression plasmids after which they were treated with DMSO (vehicle control), 10 µM or 15 µM C60 for 6 hours. Cells were stimulated with 0.5 µM PMA and 1.3 µM Ionomycin for 3 hours before termination of drug treatment. The effect of C60 on PMA and ionomycin induced NFAT activity was monitored in HeLa (A) and WHCO6 (B) cells. The effect of 10 µM or 15 µM C60 treatment for 6 hours on NFAT activity was compared to that of Importazole in HeLa cells (C). Exposure of HeLa cells to 40 µM Importazole treatment for 6 hours resulted in a significant reduction in NFAT promoter activity (D). Results shown are representative of the mean ± SEM of experiments done in quadruplicate and repeated at least twice independently. Statistical significance was determined by student paired t-test, (*p≤ 0.05).

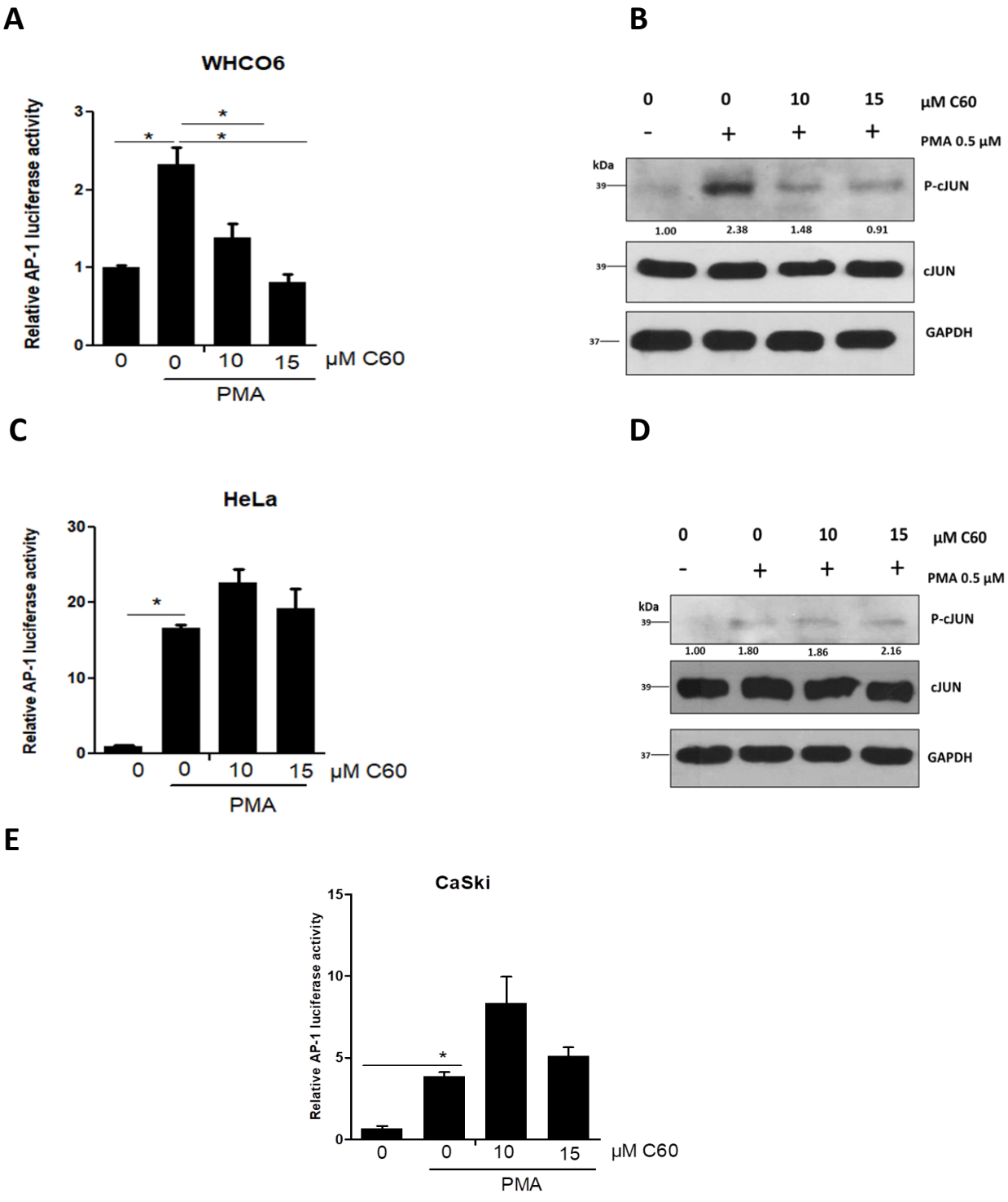

Figure 3.11. Effect of C60 on AP-1 transcriptional activity. AP-1 transcriptional activity was monitored after 0.5 µM PMA stimulation for 3 hours and 3 hours pre-treatment with 10 µM or 15 µM C60 (6 hours total treatment time) in WHCO6 (A), HeLa (C) and CaSki (E)cancer cells. Western blot was used to analyse the effect of C60 on PMA induced P-cJUN levels in WHCO6 cells (B) and HeLa cells (D). Densitometry analysis shows phosphorylated levels of cJUN (P-cJUN) normalised to total cJUN. Results shown are representative of the mean ± SEM of experiments done in quadruplicate and repeated at least twice. Statistical significance was determined by student paired t-test, *p≤ 0.05.

3.3. Discussion

Our data in the previous chapter demonstrated that C60, a potential novel small molecule inhibitor of Kpnβ1 had inhibitory effects on the biology of cancer cells that were similar to the effects obtained when Kpnβ1 was knocked down using siRNA [127,150]. This suggested that C60 might be inhibiting cancer cell biology by targeting Kpnβ1. In this chapter, we investigated the effect of C60 on the sub-cellular localisation of Kpnβ1 and some of its cargo proteins. We investigated the level of Kpnβ1 and Kpnα2 expression in cervical, oesophageal and non-cancer epithelial cells. Our result showed that both Kpnβ1 and Kpnα2 had elevated expression in the cancer cells in comparison with normal epithelial cells which supports what has been reported in the literature that nuclear transport proteins have elevated expression in cancer cells [55,71,73].

Our results using western blot analysis and immunofluorescent analysis showed that C60 inhibited the nuclear entry of endogenous Kpnβ1. A decrease in the nuclear localisation of Kpnβ1 and a concurrent increase in cytoplasmic Kpnβ1 level was seen in C60-treated cells. The altered sub-cellular localisation of Kpnβ1 as a result of C60 might be due to the binding of C60 to the functional sites of Kpnβ1. C60 was identified based on its predicted potential to bind to the RanGTP and Kpnα2 binding sites on Kpnβ1, thereby acting as a Kpnβ1 inhibitor. These results are similar to previous studies done in our laboratory on INI-43 that has inhibitory effects on the nuclear translocation of Kpnβ1 [142]. However, we also observed a dose-dependent increase in the nuclear level of Kpnα2, the adaptor protein of Kpnβ1. These results suggest that although C60 was able to inhibit the nuclear entry of Kpnβ1 it did not have a similar effect on Kpnα2.

A study by Miyamoto *et al* (2002) showed that Kpnα2 is capable of being constitutively translocated into the nucleus in an Importin Beta Binding (IBB)-domain independent manner when it is not bound to a basic-type NLS cargo protein [199]. Another study by Kose *et al* (1997) showed that a mutant of Kpnβ1, which was known to inhibit the nuclear import of Kpnβ1/Kpnα2-NLS cargo and that of Kpnβ1-cargo, had no effect on the nuclear translocation of Kpnα2 [200]. This further implied that C60 was able to inhibit nuclear import mediated by Kpnβ1 alone or in association with Kpnα2 but it was unable to prevent the nuclear import of Kpnα2. A likely explanation for the dose-dependent nuclear accumulation of Kpnα2 following C60 treatment is that since both Kpnα2 [199] and Kpnβ1 [200] get into the nucleus through the gated channels of the NPC, the binding of C60 to Kpnβ1 not only inhibited its binding to its cargoes, but also to the nucleoporins of the NPC thereby making more sites available for the nuclear entry of Kpnα2. Furthermore, C60 was identified based on its potential to bind Kpnβ1 therefore, it might not have an inhibitory effect on the nuclear translocation of Kpnα. Immunoprecipitation experiments can be performed to investigate the effect of C60 on Kpnα2.

Our result revealed that the half-life of Kpnβ1 was decreased by 2-fold in response to C60 treatment. Quensel *et al* (2004) showed that Kpnβ1 was stable after 48 hours cycloheximide treatment [201], which is similar to our results which showed Kpnβ1 stability after 67 hours cycloheximide treatment, however, C60 reduced this half-life to 29 hours. The half-life of Kpnα2 was increased from 18 to 45 hours in C60-treated cells. These results suggest that C60 prevented the nuclear entry of Kpnβ1 and over time resulted in the degradation of cytoplasmic Kpnβ1. A recent study in our laboratory showed that INI-43 similarly decreased

the stability of Kpnβ1 while CRM1 and Kpnα2 remained mostly unaffected (S. Carden, MSc Dissertation, 2017[ǂ1]). Our results further imply that the increased stability of Kpnα2 might be because of its nuclear accumulation, which resulted in its protection from protein degradation. Previous study in our laboratory showed that the inhibition of CRM1 via siRNA silencing resulted in the nuclear accumulation p53 as well an increased protein half-life (P. van der Watt, PhD Dissertation, 2009[ǂ2]).

NFκB, NFAT and AP-1 are transcription factors that have been reported to be dependent on Kpnβ1 for their import into the nucleus[117,123,137]. We hypothesised that if these transcription factors are dependent on Kpnβ1 for their nuclear entry, inhibiting Kpnβ1 by C60 treatment will interfere with their nuclear activities. Our results suggest that C60 inhibited the nuclear entry of NFκB/p65 and its transcriptional activity. In addition, C60 significantly reduced NFAT promoter activity in a dose-dependent manner. C60 was found to be more effective than Importazole, a previously described inhibitor of Kpnβ1-mediated nuclear import NFAT [123]. The effects of C60 on NFκB and NFAT activity was similar to that described for INI-43 [142,150].

C60 treatment had differing effects on AP-1 activity depending on the cell type. Our results showed that AP-1 transcriptional activity and nuclear translocation of cJUN might take place via different nuclear import mechanism in different cancer types. While AP-1 activity was

[ǂ1] S. **Carden**, "Modulating the expression and activity of the nuclear import protein, Karyopherin B1, in cancer cells". MSc Dissertation, University of Cape Town, 2017

[ǂ2] P. **van der Watt**, "Expression and regulation of nuclear transport proteins Crm1 and Kpnβ1 in cervical and transformed cell lines". PhD Dissertation, University of Cape Town, 2009

inhibited by C60 treatment in the oesophageal cancer cell line this was not observed in the cervical cell lines assayed. cJUN is capable of translocating into the nucleus through multiple pathways; therefore, its import is independent of the availability of individual importins, which assures its efficient transport under all conditions. cJUN has been reported to be imported by Kpnβ1, Transportin, Importin 5, Importin 7, Importin 9 and Importin 13 [202]. Furthermore, cJUN may dimerize with other cellular proteins that contain basic leucine zipper such as cFOS and travel into the nucleus using the interacting importins of its binding partners [202]. This suggests that the oesophageal cancer line might be more dependent on Kpnβ1 for the nuclear import of cJUN while cervical cancer cells imports cJUN via other importins other than Kpnβ1 or through the importins responsible for the nuclear import of its binding partners.

In conclusion, the results presented in this chapter supports that C60 acts on Kpnβ1 as it altered the sub-cellular localisation of Kpnβ1 by preventing it from entering the nucleus. Furthermore, C60 decreased the half-life of Kpnβ1 and had an inhibitory effect on the nuclear activity of Kpnβ1 cargo proteins such as NFκB/p65, NFAT and AP-1. These findings are in line with that of Togerson *et al* (1998), showing that SN50 an inhibitory peptide interfered with the nuclear import of NFκB, AP-1 and NFAT by disrupting the Importin α/β-transcription factor binding [143]. Although our data showed that C60 had inhibitory effects on the nuclear import and activity of NFκB, AP-1 and NFAT, conclusions cannot be drawn from this data as the total level of these proteins are not known, and therefore it is impossible to state that only nuclear import is affected. Our findings also provide evidence that C60 is capable of inhibiting nuclear import of Kpnβ1; however, it is unable to inhibit the nuclear import of Kpnα2 into the nucleus. Although C60 did not inhibit the nuclear localisation of

Kpnα2, we do not know if there was a form of direct or indirect interaction between them. Investigation of the biophysical interaction between purified Kpnα2 and C60 might provide insight into the C60-induced Kpnα2 nuclear translocation. Taken together, these results suggest a possible specificity of C60 for Kpnβ1. Investigation of the biophysical interaction between Kpnβ1 and C60 will thus be explored in subsequent chapters.

Chapter 4: Investigating the *in vivo* toxicity and *in* vitro pharmacokinetic properties of C60

4.1. Introduction

For drugs or chemical compounds to reach clinical testing they require three major properties; a primary action on the therapeutic target, a promising Absorption, Distribution, Metabolism, Excretion and Toxicology (ADMET) properties to enter and stay in the body to provoke an effect; and a safety boundary that ensures that the drug causes no harm [203]. ADMET studies are important at the early drug discovery stage [204]. The aim of drug therapy is to achieve a specific pharmacologic response of required intensity and duration while preventing harmful drug reactions [205].

The principal causes of failure in drug discovery have been linked to poor PK/ADME, toxicological properties and undesirable effects rather than the lack of therapeutic efficiency [206]. In the past decade, the assessment of the ADMET properties and the efficacy of New Chemical Entities (NCEs) have been generally accepted as a necessity for the discovery of novel drugs and for the optimisation of the ADME properties of drug candidates [206]. An ideal drug candidate should be able to provide prolonged exposure, go through steady clearance pathways having numerous enzymes and not hinder the action of Drug-Metabolizing Enzymes (DMEs) and transporters [207].

Absorption of a drug refers to the procedures involved in the transfer of the drug from the Gastrointestinal (GI) fluid across segments of the small intestine into the portal blood system. Therefore, a drug must go through a layer or layers of membranes either via

passive diffusion or active transport to get to the systemic circulation [207]. The rate at which drugs reach and leave the site of action determines the total concentration in that compartment [203]. The degree and frequency of absorption are reliant on physicochemical properties, drug formulation and the anatomy and physiology of the site of absorption [207]. **D**istribution of a drug refers to the reversible transmission of a drug from one position to another within the body. The compound is circulated to various tissues of the body after entering into the systemic circulation. The Volume of Distribution at Steady State (VDSS) is used in most cases to describe the distribution of a compound in the body. The distribution of a drug is an essential factor in determining its pharmacological action [207]. **M**etabolism of a drug refers to the biochemical procedure through which pharmacologically inactive compounds are transformed to pharmacologically active metabolites which increases their removal from the body [207,208]. A wide class of hydrolytic enzymes such as esterases, amidases and phosphatases generally facilitates these reactions. Cytochrome P450 (CYP) enzymes are the most important enzymes necessary for the pharmacological activation of many drugs; however, the transformation of a prodrug to its resultant active drug can happen non-enzymatically [208]. Metabolism occurs majorly in the liver and can take place in other organs such as lung, kidney and intestinal epithelium. The rate and degree of the metabolism of a drug determine the dose of the drug as well the duration of its effect [207]. **E**xcretion of a drug refers to the irreversible removal of a drug from the body under the control of the liver, kidney and other organs. Following oral absorption, drugs are removed from the body through excretion as unchanged forms in urine and bile. For drugs whose clearance is based on metabolism, its intrinsic metabolic stability determines the unbound drug concentrations and the length of its pharmacological effects [207].

It is unreasonable to assume that excessive amounts of virtually any substance will not be harmful and according to Paracelsus (1493-1541) which states; ". . . all things are poison and nothing is without poison. Solely the dose determines that a thing is not poison . . ."[203]. Toxicity and adverse reactions of small molecules present a public health risk and result in severe attrition rates in advanced stages of drug development. Toxicity and harmful effects of small molecules cause a serious drawback in drug development [209]. The toxicity of a substance can be investigated by *in vitro* studies using cell lines, *in vivo* studies using experimental animal models or by studying the effect of accidental exposure to such substance [210]. These studies are done with a control group, low dose, intermediate dose and high doses. The intermediate and high dose helps to determine dose responsiveness and organ toxicity respectively. Safety studies are anticipated to give an idea of the range between efficacy and toxicity, maximum achievable dose and expected toxicity [203].

In this chapter, the ADME pharmacokinetic properties of C60 was investigated *in vitro* by carrying out kinetic solubility, metabolic stability, lipophilicity, permeability and plasma protein binding assays. The *in* vivo toxic side effects of C60, as well as its effect on tumour growth in a nude mouse model were also investigated.

4.2. Results

In vitro ADME assays done to determine the pharmacokinetic properties of C60 were performed with assistance from H3D Africa based at the University of Cape Town. The *in vivo* toxicology study and tumour xenograft studies were performed using a nude mouse model.

4.2.1. C60 shows high kinetic solubility

Solubility and permeability are the determining factors of a compound's absorption following its oral administration as well as determining its Oral Bioavailability (OBA) [207]. The kinetic solubility assay was carried out to establish the degree of solubility of C60. The solubility ranking of a 200 µM preparation in 2% DMSO is shown in Table 4.1 and was used to determine the solubility class of C60. Results obtained showed that C60 had a solubility ranking of 180 µM, which indicates high solubility. This suggests that C60 has a high bioavailability.

Table 4.1. Solubility ranking based on 200 µM preparation in 2% DMSO

Solubility class	Concentration (µM)	C60
High	≥150	180 µM
Moderate	50-150	
Low	5-49	
Very low	<5	

4.2.2. Investigating the metabolic stability of C60 using liver microsome assay

A major hindrance to achieving a stable steady-state drug concentration for treatment is metabolic degradation [203]. Liver microsome assay was used to determine the stability of the parent drug in the presence of transforming enzymes from the liver. Briefly, the compound of interest, which is C60, was incubated in liver microsomes containing concentrated liver enzymes. Following the incubation of the compound in liver microsomes, HPLC-MS/MS (Tandem Mass Spectrometry) was used to establish the percentage of untransformed C60. The microsomal stability of C60 was determined in human, rat and mouse liver microsomes and the percentage of the parental C60 remaining was used to calculate its half-life. Results obtained were used to predict the *in vivo* intrinsic clearance of C60 in humans, rats and mice. As shown in Table 4.2, C60 has a predicted *in vivo* clearance of 106 mL/min/kg protein and a half-life 19 minutes in humans. In rats, the predicted clearance was 158 mL/min/kg protein and half-life of 19.8 minutes, while in mice it has a predicted clearance of > 250 mL/min/kg protein and half-life of 15 minutes. The results showed that C60 has a high hepatic extraction ratio which ranged between 0.7- 0.8. The results obtained from this *in vitro* assay suggest that C60 would likely have a short half-life and rapid clearance *in vivo*.

Table 4.2. Metabolic stability of C60 in human, rat and mouse liver microsomes

Liver microsomal species	Half-life (min)	Predicted *in vivo* CL (mL/min/kg protein)	Hepatic extraction ratio (E_H)
Human	19.0	106	0.8
Rat	19.8	158	0.7
Mouse	15.0	>250	0.8

4.2.3. C60 showed moderate lipophilicity

Lipophilicity refers to the ratio of the compound's concentration between an organic and an aqueous phase at equilibrium [207]. It is a measure of the ability of a drug to dissolve in lipids or organic solvents such as octane in contrast to water [203]. Lipophilicity values are termed Log P and Log D. Log P is the Log of the partitioning coefficient of the compound between an organic phase and an aqueous phase at a pH where all of the compound molecules are in the neutral form. Log D refers to the distribution coefficient of the compound between an organic phase and an aqueous phase at a pH where a part of the compound's molecules may be in the ionic form and a part in the neutral form [211]. Generally, a LogP of < 1 implies that a compound or drug will have good solubility but poor permeability [207]. Table 4.3 shows the influence of Log $D_{7.4}$ on drug-like properties in drug development and discovery [211]. The lipophilicity of C60 was determined using a sealed down shake flask method. Briefly, octanol was added to C60 followed by the addition of PBS. Incubation was done followed by centrifugation. HPLC was used to determine the concentration of C60 in each phase. Results obtained showed that C60 had a Log $D_{7.4}$ of 1.6, which suggests that C60 has moderate solubility and permeability. Based on this value, its oral absorption and BBB (Blood-Brain Barrier) penetration are viewed to be favourable *in vivo*.

Table 4.3. Impact of Log $D_{7.4}$ on drug-like properties [211]

Log $D_{7.4}$	Common impact on drug-like properties	Common impact *in vivo*
<1	Solubility high Volume of distribution low Permeability low by passive trans-cellular diffusion Permeability possible via Para cellular if MW < 200 Metabolism slow.	Volume of distribution low Oral absorption blood brain barrier (BBB) penetration unfavourable Renal clearance may be high
1 to 3	**Solubility moderate** **Permeability moderate** **Metabolism slow**	**Balanced volume of distribution** **Oral absorption and BBB penetration favourable** **Renal clearance may be high**
3 to 5	Solubility low Permeability high Metabolism moderate to high	Oral bioavailability moderate to low Oral absorption variable
>5	Solubility low Permeability high Metabolism high	High volume of distribution (especially amines) Oral absorption unfavourable and variable

4.2.4. C60 displayed high permeability

Solubility and permeability are important factors that determine a drug's absorption and oral bioavailability. Various cell-free and cell-based systems have been used to study permeability and the role of transporters in permeability of new chemical entities. The Parallel Artificial Membrane Permeability Assay (PAMPA) has been used extensively as a high throughput, inexpensive and straightforward tool for screening discovery compounds for their capacity for passive permeability [207]. For passive lipid membrane diffusion, this assay measures the rate of passage through a phospholipid-coated filter [211]. PAMPA results showed that C60 has a passive permeability of -4.7 at pH 6.5, which is considered a high permeability value. This result suggests that C60 would be easily absorbed in a living system and should be suitable for oral absorption.

4.2.5. C60 displayed high plasma protein binding affinity

Plasma Protein Binding (PPB) is a necessary factor in predicting drug distribution because it may result in reduced bioactivity and insufficient drug-drug interactions [204]. PPB has a major influence on the rate of drug diffusion between plasma and tissues and therefore affects the *in vitro* intrinsic clearance (CL) and Volume of Distribution at Steady State (VDSS) of drugs. Drugs with high PPB are generally avoided since small changes in the PPB can result in significant changes in the free fraction. PPB information is also necessary to estimate the effective concentration of drugs that facilitate inhibition of DMEs and transporters [207]. PPB assays showed that C60 has a protein binding affinity of 98% with a free drug fraction of 0.02%. This suggests that C60 will be more retained in the vascular system thereby having a lower volume of distribution.

In summary, the results of the ADME pharmacokinetic studies showed that C60 has high solubility, permeability and protein binding affinity; it also has moderate lipophilicity, short half-life and rapid *in vivo* clearance. Results suggest that while C60 might be soluble and useful as a potential oral drug, its short half-life and rapid clearance might interfere with its therapeutic efficacy in a living system.

4.2.6. Investigating the toxic side effect of C60 in athymic nude mice

The potential toxic side effects of C60 were investigated in nude mice over a period of 28 days. Nude mice were used for investigating the *in vivo* toxic side effect of C60 because it was important for us to use immunocompromised mice for the downstream tumour xenograft study. The use of nude mice for the toxicity study was to minimise experimental variations. Vehicle (7.5% DMSO in PBS) or C60 were administered via the intraperitoneal (i.p.) injection twice in a week for 4 weeks (8 treatments). Body mass was measured 4 times per week and welfare monitoring was carried out daily to detect any side effects. In this experiment, treated mice received 10 μg/g, 30 μg/g or 50 μg/g C60, while control mice received 7.5% DMSO in PBS. Throughout the course of the study, the animals showed no abnormal behaviour and signs of distress; however, we observed that animals receiving the 30 μg/g and 50 μg/g C60 doses showed signs of slight discomfort. Animals showed signs of discomfort by raising their legs at the site of injection following which recovery was observed. Fluctuations in body mass were observed between the control, 10 μg/g and 30 μg/g C60 mice. The control mice showed an approximate 10% gain in body mass and the 10 μg/g, 30 μg/g and 50 μg/g treated groups, had a 27%, 20%, and 12% gain in body mass respectively (Figure 4.1. A, B, C). The gain in body mass at the end of the study showed an increase in body mass for 10 μg/g and 30 μg/g C60 treated mice compared to control mice, while the 50 μg/g mice showed a similar gain in body mass to the control (Figure 4.2). Overall, mice that received C60 gained more weight in comparison to control mice; however, the gain in body mass was not significant. The difference in the body mass gain between the groups may have been due to the different eating and drinking habits of individual animals within the different groups. Therefore,

body mass was not the only factor used for evaluating the toxicity of C60 and animal welfare.

Post mortem analysis of the internal organs of control and C60 treated mice was done with assistance from a trained animal technician. No abnormalities such as discolouration or inflammation of organs (including liver, spleen, heart, lung, kidneys and ovaries) were detected. No visible difference was observed in the appearance of internal organs between the control and C60- treated animals (Figure 4.3.A). The liver is a vital target for foreign substances such as drugs which are metabolised and excreted by the liver [212]. An enlargement of the liver as a result of drug toxicity has been reported [213]. We measured the liver mass of control and treated animals at the end of the study. Relative liver mass was calculated by normalising liver mass to body mass for each animal ($Liver\ \mathrm{mass} \div \mathrm{body\ mass}$). Results of the relative liver mass showed no substantial difference between the control and C60-treated animals (Figure 4.3.B). Together, these results suggest that nude mice tolerated C60 up to the 50 μg/g dose.

A

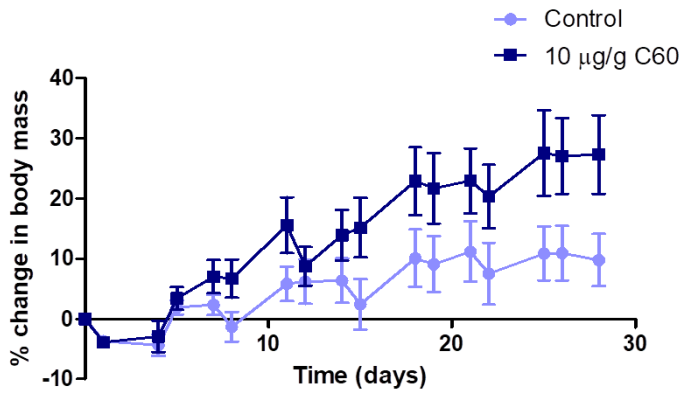

B

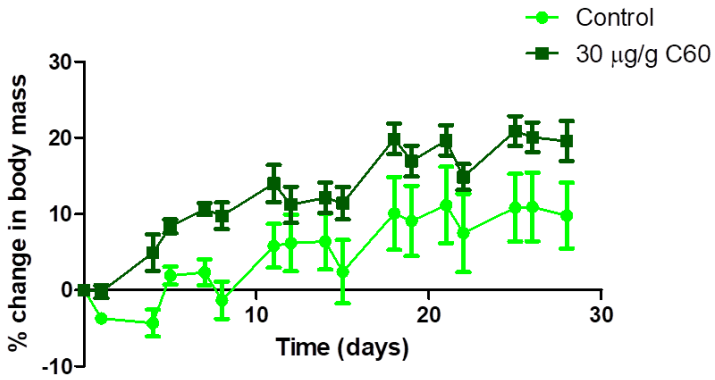

C

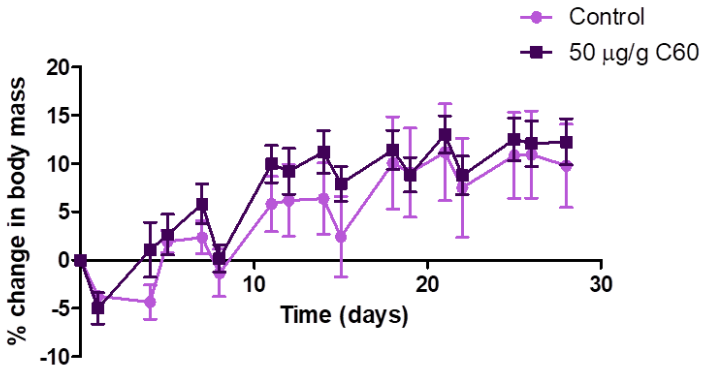

Figure 4.1. Effect of C60 on body mass in nude mice. The toxic side effect of C60 was monitored by investigating the effect of C60 on body mass over a period of 28 days (4 weeks). Mice were randomly divided into 4 groups (control, 10 µg/g C60, 30 µg/g C60 and 50 µg/g C60) of 6 animals per group. Change in body mass was calculated as a percentage increase from the first day of treatment for control mice versus 10 µg/g (A), 30 µg/g (B) and 50 µg/g (C) C60-treated mice. Results shown are the mean ± SEM for each group (n=6). Statistical significance was determined using the non-parametric Mann-Whitney U test.

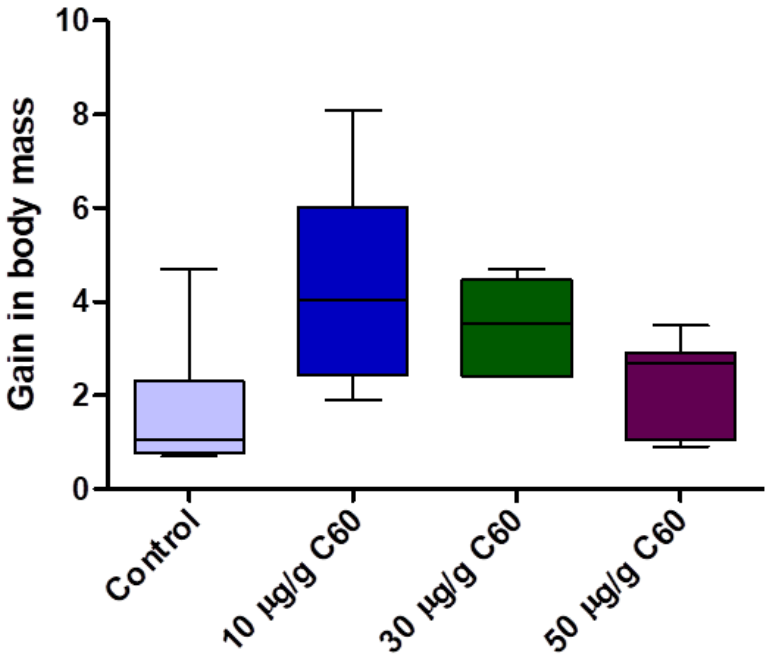

Figure 4.2. Gain in body mass on the final day. The overall gain in body mass was calculated as a fold change in body mass between the first and last day of measurement for each treatment group. Box and whisker plot showing minimum, median and maximum values represents the gain in body mass at the end of the study for each group. Results shown are the mean ± SEM for each group (n=6). Statistical significance was determined using the non-parametric Mann-Whitney U test.

A

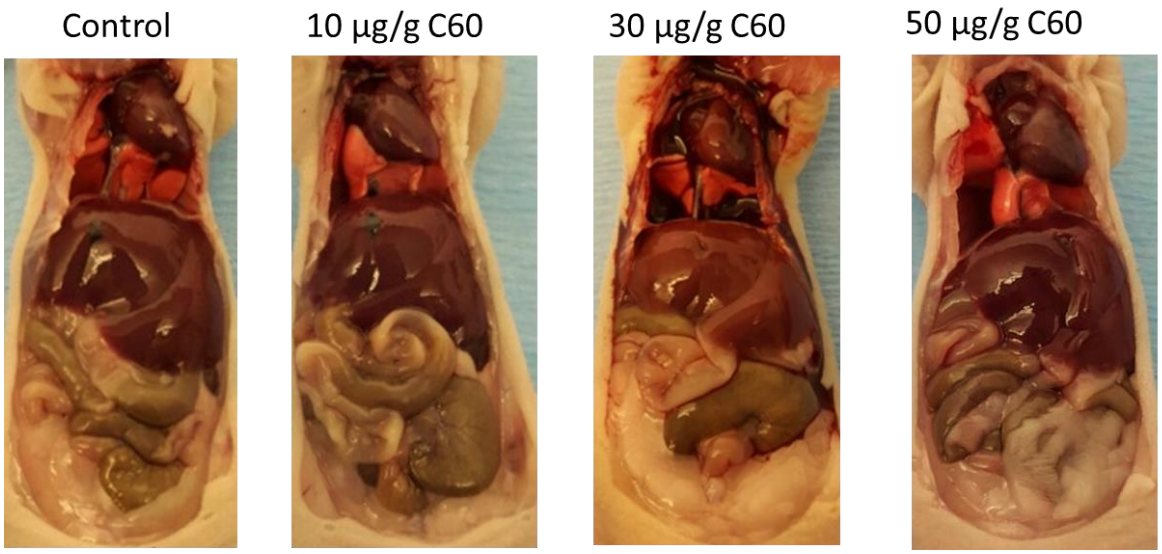

B

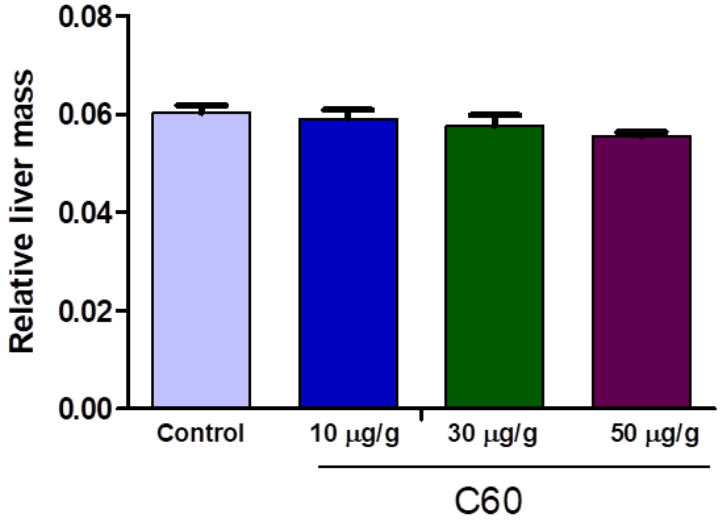

Figure 4.3. **Post-mortem analysis of and liver size measurement.** Images representative of mice from each group indicate that there was no difference in organ morphology between the mice in treatment groups and those in the control group (A). Mice livers were weighed at the end of the study, and liver mass was normalised to the body mass of each mouse. Bar graph represents the relative liver mass for each group, which showed no significant difference (B). Statistical significance was determined using the non-parametric Mann-Whitney U test.

4.2.7. The effect of C60 treatment on xenograft tumour growth in nude mice

An ectopic xenograft model approach was used to determine the *in vivo* effects of C60 on the growth of oesophageal (KYSE 30 and WHCO6) and cervical (CaSki) cancer tumour growth. Five million cancer cells have been previously described as the optimal number of cells to be inoculated to induce tumour formation (A. Chi, PhD thesis, 2016[ǂ3]). The hind flanks of mice were subcutaneously inoculated with 5 million cancer cells, allowed to reach palpable size before treatment commenced. While investigating the toxic side effects of C60, we observed that mice receiving the30 μg/g or 50 μg/g doses of C60 showed signs of discomfort after C60 was injected into them, hence 10 μg/g dose of C60 was used for the tumour xenograft study. Tumour-bearing mice of each cancer type were randomised into control and 10 μg/g C60 treatment group. The rate of tumour formation for the different cell lines varied, therefore day 0 was marked as the first day of treatment for each cell line. Tumour measurement, as well as treatment, was done twice a week for 19 days, 26 days and 16 days for KYSE 30, WHCO6 and CaSki-tumour bearing mice respectively.

Body mass was measured four times a week and welfare monitoring was done daily. No abnormal behaviour was observed in both control and C60-treated mice. Fluctuations in body mass were similar between the control and C60-treated mice in KYSE 30, WHCO6 and CaSki (Figure 4.4.A, B, C). The overall change in body mass was within the tolerable range and was not statistically different between control and C60-treated mice for KYSE 30, WHCO6 and CaSki (Figure 4.4.D, E, F) tumours.

ǂ[3] A. Chi "Investigating a novel small molecule inhibitor of nuclear import as an anti-cancer approach" PhD Thesis, University of Cape Town, 2016.

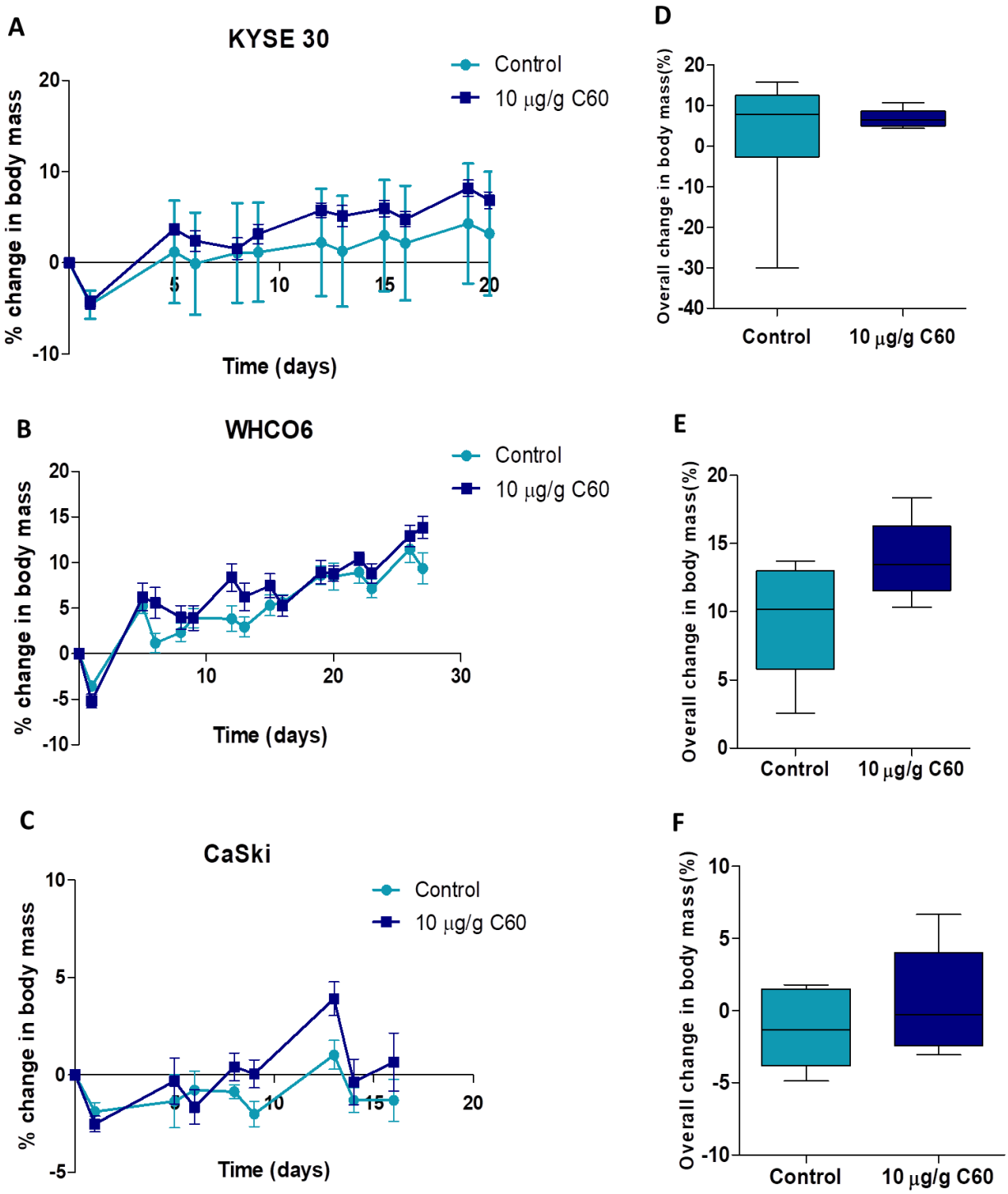

Figure 4.4. **Change in body mass.** In the course of the tumourigenesis assay, change in body mass was monitored in both control and C60 treatment groups for KYSE 30 (A), WHCO6 (B) and CaSki (C) tumour bearing mice. Body mass was calculated as percentage change to the body mass measured on day 0 of each experiment. The percentage overall gain in body mass for control and C60-treated mice are shown for each cell line (D -F). Results are shown as mean ± SEM for 6 mice in each group. Statistical significance was determined using the non-parametric Mann-Whitney U test.

Our results showed that C60 treatment of KYSE 30 oesophageal tumours resulted in a significant decrease in tumour volume (Figure 4.5.A). A trend towards a decrease in tumour volume was observed for WHCO6 (Figure 4.5.B) while no change was observed with the CaSki tumours (Figure 4.5.C). The fold change in tumour volume on the last day relative to day 0 of the study for each tumour type showed a significant decrease in KYSE 30 tumour volume. In the mice bearing KYSE 30 tumours, the control mice had an 18.4-fold increase in tumour volume while the C60-treated mice had a 9.4-fold increase. While not significant, mice bearing WHCO6 tumours showed a trend towards a decrease in tumour volume (Figure 4.6.A). Comparisons of tumour mass at the end of the study also showed a significant reduction in tumour mass in the KYSE 30 and a trend towards a decrease for WHCO6 tumours (Figure 4.6.B). Images of the control and C60-treated tumours on the last day of the study for each cancer type are shown in Figure 4.7. These results show that C60 has selective effects on tumour growth *in vivo,* with KYSE 30 oesophageal tumour cells being the most responsive of the cell types analysed.

A

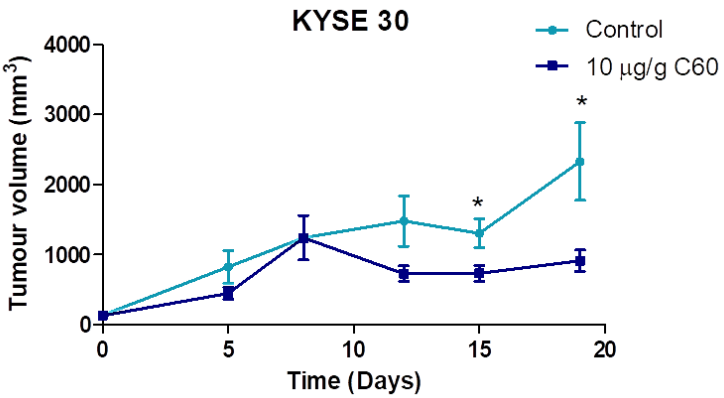

B

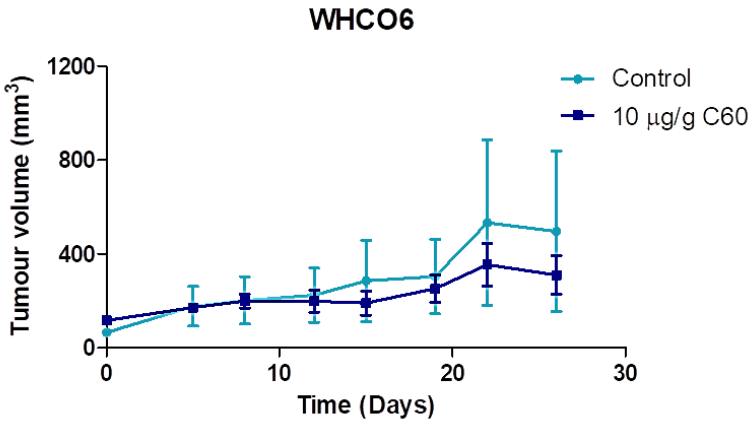

C

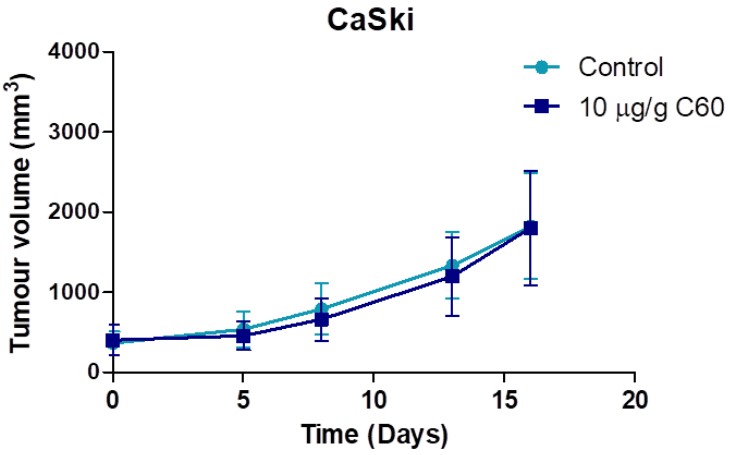

Figure 4.5. The effect of C60 treatment on oesophageal xenograft tumour growth in nude mice. Tumour growth for control (DMSO) and C60- treated mice bearing KYSE 30 (A), WHCO6 (B) and CaSki (C) tumours. Results shown are the mean ± SEM for 6 mice in each group. Statistical significance was determined using the non-parametric Mann-Whitney U test, *p ≤0.05.

A

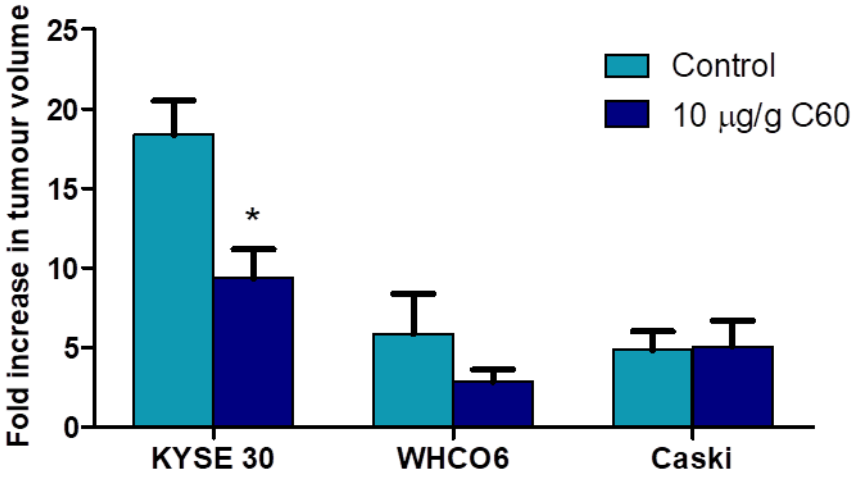

B

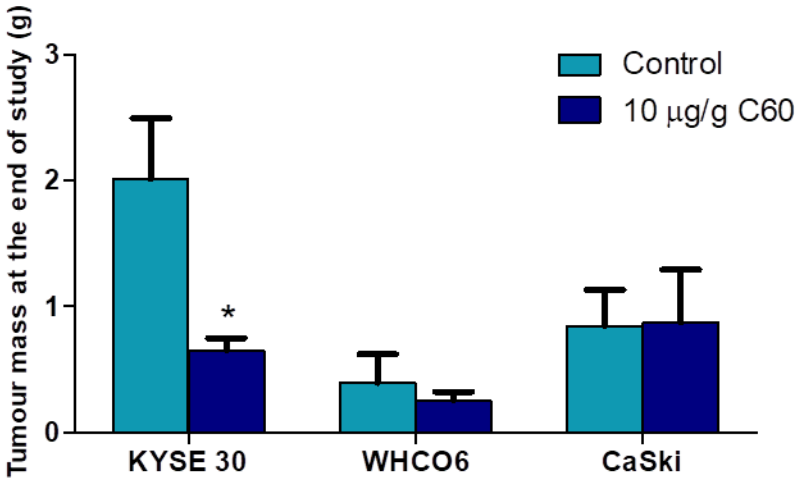

Figure 4.6. Evaluation of tumour size at the end of the study. Fold increase in tumour size on the last day of the study relative to the starting tumour size on Day 0 (A). Tumour mass at the end of the study (B). Results shown are mean ± SEM for 6 mice in each group. Statistical significance was determined using the non-parametric Mann-Whitney U test, *p≤ 0.05.

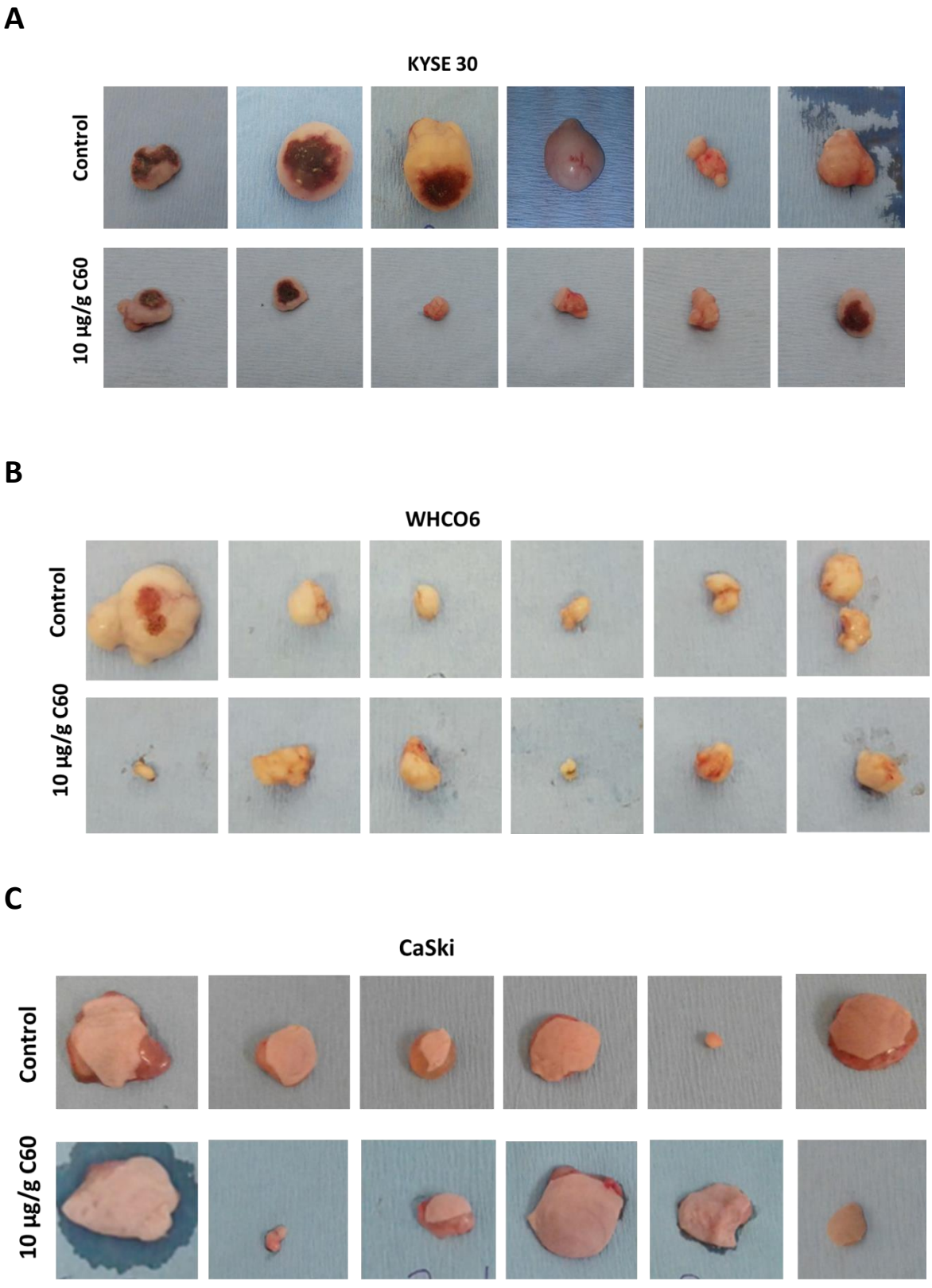

Figure 4.7. Images of tumours at the end of the study. On the last day of the study, mice were euthanised and tumours were excised. Images of tumours from both control and C60- treated groups were taken for KYSE 30 (A), WHCO6 (B) and CaSki (C) tumours. Asterisk marks indicate the presence of necrosis in the tumour mass.

4.3. Discussion

A review by van de Waterbeemd and Gifford (2003) describe that 39% of failure in drug development can be attributed to poor pharmacokinetics, while 11% was attributed to animal toxicity, hence pharmacokinetic and pharmacodynamic assessment early on in the drug discovery process is required [214].

In this study, we investigated the ADME pharmacokinetic properties of C60 by examining its *in vitro* solubility, metabolic stability, lipophilicity, permeability and plasma protein binding. Our results showed that C60 has high solubility and optimal lipophilicity as well as a high permeability. The significance of solubility as a pharmacokinetic property was established in the BCS (Biopharmaceutical Classification System), a scientific framework for grouping drugs based on their aqueous solubility and intestinal permeability. According to this classification system, drugs are classified as Class 1 drugs if they have high solubility and high permeability [215].

Metabolic studies done using liver microsomes showed that C60 has high hepatic clearance, and a short half-life in human, mouse and rat. The half-life is the time it takes to achieve a 50% reduction in the plasma concentration or the amount of drug in the body. It also describes the time it takes for drug concentration to reach 50% of the expected steady-state concentration [216,217]. Metabolic stability is one of the major determinants of drug concentration and has been used to evaluate bioavailability and toxicokinetics. Metabolically unstable drugs have limitations in that the desired therapeutic concentration may not be achieved. On the other hand, a measure of instability is advantageous for a prodrug where a metabolite is more effective than its parent compound [218].

For example, the half-life of N-desmethyl-imatinib the metabolite of imatinib significantly exceeds that of its parent compound [219]. The short half-life obtained for C60 could be as a result of the metabolic breakdown of the parent compound. Therefore, future analysis of the metabolic products of C60 may lead to the discovery of pharmacologically effective metabolites with significantly longer half-lives. In addition, to note is that the half-life of a drug may not necessarily have an influence on its degree of potency. Alavijeh *et al* (2005) reported a group of Benzodiazepines with varying potencies not associated with their half-lives. They report that Alprazolam, Lorazepam and Triazolam all have short half-lives but display high potency while Diazepam, Flurazepam and Clorazepate have long half-lives but show low potency [220].

Clearance refers to the capacity of the body to eliminate a drug and, can be classified as plasma clearance, blood clearance or clearance dependent on the concentration of unbound or free drug. The extraction ratio of an organ is described as the ratio of the rate of elimination to the rate of presentation. The ratio of 1 occurs when no drug is released into the venous blood after passing through the eliminating organ. Drugs with a ratio of more than 0.7 are regarded as high extraction ratio drugs [216]. C60 has an extraction ratio that ranged between 0.7-0.8, which makes it a drug with a high extraction ratio. The plasma protein binding of C60 was shown to be 98%. This is in line with that of some commercially available chemotherapeutics. Literature reports have shown a few clinically used anti-cancer drugs that have high plasma protein binding. Small molecule inhibitors of EGFR used in the treatment of NSCLC such as Gefitinib, Erlotinib, and Dacomitinib have plasma protein binding of 90%, 95% and 98% respectively [221].

Clinically, the differences between the pharmacokinetic properties of drugs are important because they influence the possibility of drug-drug interaction, and consequently the efficacy, ideal dose and tolerability of treatment [221]. For example, development of resistance has been reported for Imatinib, hence, detailed pharmacokinetic data associated with clinical response is required for the likelihood of identifying mechanisms of resistance in non-responders [219].

We investigated the potential toxic side effects of C60 *in vivo.* Results indicated that nude mice tolerated C60 up to a dose of 50 µg/g; however, the dose of 10 µg/g was found to be more suitable for tumour-bearing mice as there was no sign of discomfort at this dose. An increase in body mass was within tolerable range and internal organs were not affected by C60 treatment. Subsequent tumorigenesis assays done using an ectopic xenograft mouse model showed that C60 had anti-tumour effects on the more aggressive KYSE 30 oesophageal cancer tumours *in vivo*, but not all tumour types assayed in this study. There are thus similarities and dissimilarities between C60 and INI-43 a small molecule inhibitor of Kpnβ1 recently described by our laboratory. While C60 inhibited *in vivo* tumour development in a cell/tissue-specific manner, INI-43 significantly reduced *in vivo* growth of both cervical and oesophageal tumours cells. C60 like INI-43 had no significant adverse toxic effect on the animals [142]. Other *in vivo* studies showing that targeting nuclear import pathways in tumour development include a study by Kodama *et al* (2017) reporting Ivermectin, an anti-parasitic that also inhibits Importin α/β-mediated nuclear import reduced ovarian cancer tumour growth in nude mice [139]. Ivermectin, however, does not specifically target Kpnβ1 and may have other cellular targets.

The inhibition of other Karyopherins such as CRM1 has been shown to have *in vivo* inhibitory effects on cancers of different origin. Selective inhibitors of nuclear export, KPT-276 and KPT-330 significantly reduced melanoma growth *in vivo* in nude mice [222].

In brief, this chapter showed that C60 has a high solubility, permeability and lipophilicity *in vitro* which translates to good oral absorption; however, it had high plasma protein binding and a short half-life that indicate that it could be readily cleared from the body which might prevent it from been a therapeutically relevant drug if used in a living system. The *in vitro* and *in vivo* half–life of Importazole, a commercially available inhibitor of Kpnβ1 has not been reported in any literature to the best of our knowledge. Selinexor, an inhibitor of CRM1, which is currently in phase 1 clinical trials for the treatment of Acute Myeloid Leukemia (AML), was reported to have an *in vitro* half-life of 6 hours [223]. Further investigation is required to identify the pharmacologically active metabolites of C60, which may possibly have longer half-lives. Since the lipophilicity range of C60 predicted that it might have a short half-life, the use of Quantitative Structure-Activity/Property Relationships (QSAR) models may provide guidance towards identifying the positions on compounds where metabolically inert lipophilicity may be included to improve half-lives while making sure unbound clearance remains low [224]. The lack of adverse effects and reduced *in vivo* tumour growth of certain tumour types suggest that C60 may have value as a therapeutic agent for specific tumours. Further investigation into its efficacy on tumour types of different tissue origin and aggressiveness is required.

Chapter 5: Kpnβ1 purification and investigating Kpnβ1: C60 binding kinetics

5.1. Introduction

An *in silico* screening approach was used to identify C60 as a potential small molecule inhibitor of Kpnβ1. Our results in the previous chapters presented data showing that C60 alters Kpnβ1 sub-cellular localisation and may inhibit the nuclear import of Kpnβ1 cargoes. This suggested that C60 inhibits cancer cell biology by targeting Kpnβ1. In this chapter, we describe the purification of Kpnβ1 in sufficient quantities for the investigation of the potential of C60 to interact directly with Kpnβ1 via protein-drug (Kpnβ1: C60) interactions.

There are various techniques for protein purification including chromatographic and non-chromatographic methods [225]. The method of purification used in this study was an affinity chromatography technique, which uses a precise interaction that takes place between a molecule in the solute phase and another in the stationary phase. This method is suitable for exploiting the high affinity binding that occurs between protein molecules and their individual ligands [226,227]. Affinity chromatography is based on the molecular recognition of a target molecule by a molecule bound to a column [228]. It makes use of affinity tags, which range from single amino acid to entire proteins and are often attached to the N-terminus or C-terminus of the target protein. The target protein can then be selectively trapped and purified through association with the tag-specific affinity resin, aside from aiding protein purification, these tags also enhance protein solubility and stability [229,230].

Kpnβ1 fused with GST was purified using affinity chromatography spin columns. Different biological ligands such as Glutathione S-Transferase (GST) have been used as tags. GST is a 26 kDa protein that is found naturally in eukaryotic cells. GST binds reversibly to glutathione attached to a Sepharose matrix. The engineering of a unique protease site between the GST moiety and the protein of interest which allows the GST moiety to be removed from the target recombinant protein [230–232].

Protein-protein interactions are a wide class of therapeutic and biological targets that were initially thought to be resistant to small molecule modulation [233]. A key challenge in the identification of compounds capable of interfering with protein-protein interaction is the development of efficient techniques to investigate such interactions. There are multiple complexities involved in carrying out binding measurements that underlie drug-protein interactions [234]. Biophysical and computational techniques for investigating small ligand screening and drug design are available. These biophysical methods allow the qualitative identification of a small molecule to target binding as well as the quantitative determination of physical factors related to binding [235]. Biophysical methods that have been used in drug discovery process include Surface Plasmon Resonance (SPR), Mass Spectrometry (MS), Nuclear Magnetic Resonance (NMR), Bio-layer Interferometry (BLI), Circular Dichroism (CD) and Isothermal Titration Calorimetry (ITC) [234,236].

In this study, Bio-layer Interferometry (BLI) was used to investigate the binding kinetics between C60 and Kpnβ1. BLI is an exceptionally sensitive method for investigating protein-small molecule interactions [234]. The Octet Red system (FortéBio, Pall Life Sciences, Menlo Park, CA, USA) uses BLI, a label-free technique that measures molecular interactions in real time. BLI measures interference patterns between waves of light [237]. This technique utilises fibers (biosensors) which have an upper surface and a lower surface. The lower surface of the tip is coated with a unique material, creating an optical layer that can bind various molecules. The binding of a molecule to the lower surface of a biosensor causes a shift in the interference pattern, which can be measured in real-time [238]. The instrument moves the biosensor into a well containing assay buffer to obtain a baseline after which it moves it into a well containing the compound. If binding occurs; the instrument detects the difference in light reflected from the target surface relative to the response in the assay buffer, and response is reported as a change in wavelength shift for the interference pattern. The biosensor is moved back into a well containing assay buffer and the dissociation of the compound from the sensor is examined [239].

Kinetic analysis of protein-protein and small molecule interaction is an important application upon which the Octet instrument family were designed. It is used to measure the affinity of an interaction and quantify association and dissociation rate constants for reversible, non-covalent binding [237,240]. The Octet platform is presently being used in many sectors of the pharmaceutical and biotherapeutic drug development processes such as early discovery, process development and late-stage clinical trials [240] The equation below is used to describe the interaction between two biomolecules [237].

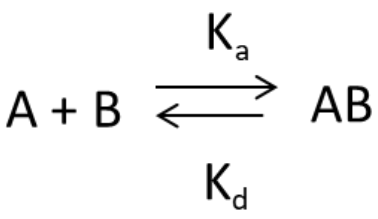

Where,

A represents the ligand molecule immobilised on the surface of the biosensor

B represents the analyte in solution

K_a represents the equilibrium association constant

K_d represents the equilibrium dissociation constant [241]

The K_d, which is the affinity constant or equilibrium constant, measures how tightly the ligand binds to its analyte (small molecule). The number of ligand molecules with analyte bound equals the number of ligand molecules without analyte bound at this concentration. There is an inverse relationship between K_d and affinity- the smaller the K_d value the tighter the affinity of the analyte to the ligand. It is expressed in molar units (M) [237,242].

At the time of this study, purified Kpnβ1 was commercially available but it was not cost-effective to purchase it for the biophysical analysis. For the purpose of our study, Kpnβ1 was purified in sufficient quantities using the GST tag system for the biophysical investigation of Kpnβ1: C60 binding interaction using the BLI technique.

5.2. Results

5.2.1. Kpnβ1 protein purification using GST-tag affinity chromatography

To prepare purified Kpnβ1, a plasmid pGEX-6P1-Kpnβ1 was prepared and transformed into *E. coli* (JM109) bacteria cells as previously described (E. Strydom, PhD thesis, 2016[ǂ4]). The pGEX vector is an expression vector that makes up the core of the GST expression system[243]. *E. coli* bacterial cells containing pGEX-6P1-Kpnβ1 grown in Terrific Broth were treated with IPTG (Dioxane-Free, Promega™) to induce GST-Kpnβ1 expression. Protein purification was done using the batch-binding technique according to the manufacturer's instructions. GST-Kpnβ1 was eluted by adding reduced glutathione to the equilibration buffer (Materials and Methods) and eluates containing GST-Kpnβ1 alongside flow-through and washes were electrophoresed using SDS-PAGE followed by staining the gels with coomassie brilliant blue to assess the efficacy of purification.

Our results showed the induction of Kpnβ1-GST expression as a result of IPTG stimulation in the crude lysate compared to the unstimulated lysate (Figure 5.1.A). Eluates were collected and quantified alongside BSA standards. A predominant band at ~123 kDa was observed, which corresponds to the molecular weight of Kpnβ1 fused to GST (Figure 5.1.B).

The GST tag was also cleaved off using HRV 3C Protease (Thermoscientific, Rockford, IL, USA). The efficacy of purification and GST-cleavage was assessed via SDS-PAGE and coomassie blue staining (Figure 5.2.A). Kpnβ1 obtained. A predominant band at ~97 kDa was observed, which corresponds to the molecular weight of Kpnβ1 (Figure 5.2.B).

ǂ[4] E. Strydom "Investigating Karyopherin B1:Small molecule interactions for cancer therapy" PhD Thesis, University of Cape Town, 2016.

A

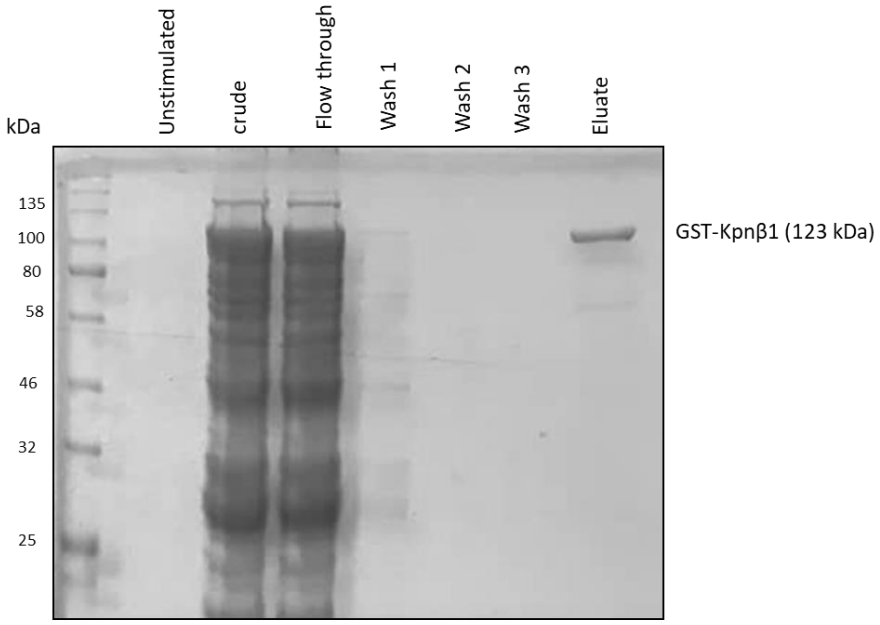

B

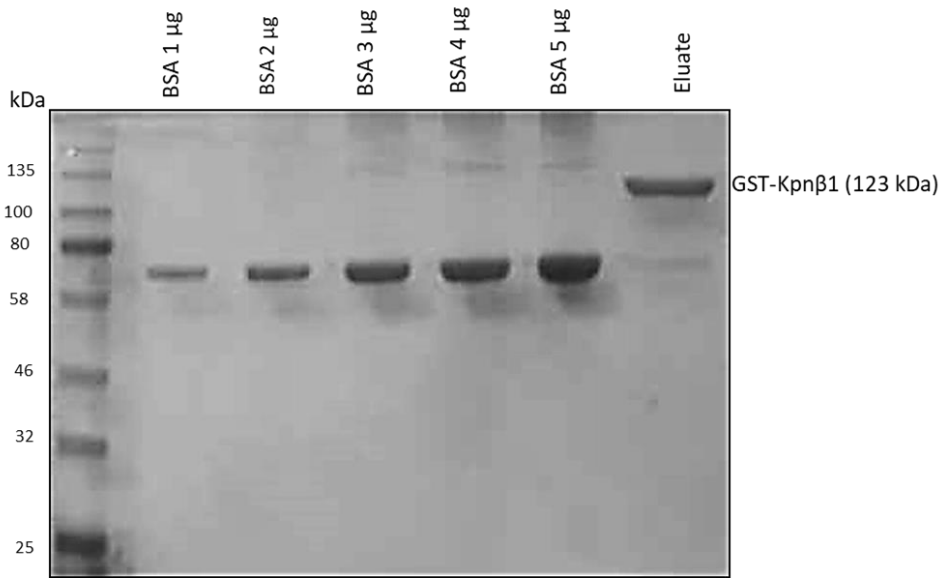

Figure 5.1: SDS-PAGE gels showing GST-Kpnβ1 staining. Fractions from the batch binding were analysed via SDS-PAGE (A). Eluate containing purified GST-Kpnβ1 and BSA standards electrophoresed on SDS-PAGE gel (B).

A

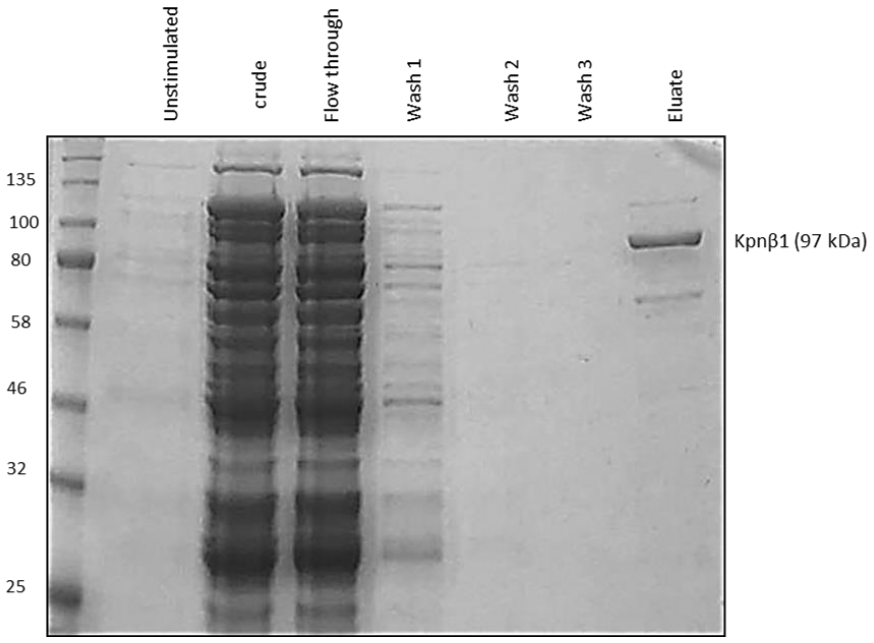

B

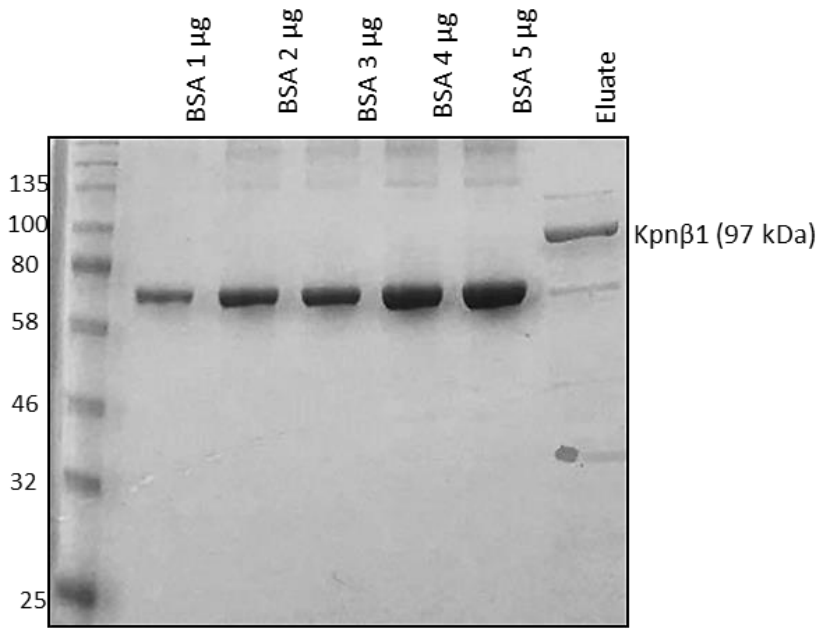

Figure 5.2: SDS-PAGE gels showing Kpnβ1 staining. Fractions from the batch binding were analysed via SDS-PAGE (A). Eluate containing purified Kpnβ1 and BSA standards electrophoresed on SDS-PAGE gel (B).

BSA standards run alongside eluates on SDS-PAGE gels allowed for the quantification of GST-Kpnβ1 and Kpnβ1 in samples using Image J software. Table 5.1 shows the quantity of GST-Kpnβ1 and Kpnβ1 purified for a batch of the purification process. The GST-Kpnβ1 purification table (Table 5.2) shows the nanodrop quantification of the various fractions. GST-Kpnβ1 quantity obtained in Table 5.1 was used to determine the percentage purity of each fraction shown in Table 5.2. Result showed that Eluate contained 82.6% pure GST-Kpnβ1. The Kpnβ1 purification table (Table 5.3) shows the nanodrop quantification of the various fractions. GST-Kpnβ1 quantity obtained in Table 5.1 was used to determine the percentage purity of each fraction in Table 5.3. Result showed that Eluate contained 85.2% pure GST-Kpnβ1.

The total protein obtained was used to determine the purity as only the bands ascertained to be GST-Kpnβ1 or Kpnβ1 bands were quantified. Data obtained for GST-Kpnβ1 and Kpnβ1 in Table 5.1 are from the same batch purification as data contained in Table 5.2 and Table 5.3 for GST-Kpnβ1 and Kpnβ1 respectively. The purification process was repeated until sufficient quantities of protein were obtained for downstream biophysical analysis.

Table 5.1. Table showing the quantity of GST-Kpnβ1 and Kpnβ1. Figures in the table are based on the densitometric analysis of SDS-PAGE gel using Image J software. Results are representative of protein quantities obtained for a round of purification.

Sample	Intensity	µg in sample (20 µL)	µg/µL	µg/mL	Total protein (µg /2 mL)
GST-Kpnβ1	14351.4	4.71	0.235	235	470
Kpnβ1	8139.9	3.46	0.173	173	346

Table 5.2. Purification table of the various stages of purification of GST-Kpnβ1 using affinity tag chromatography. Results in the table are based on nanodrop quantification are representative of protein quantities obtained for a round of purification.

Fraction	µg/mL	Volume (mL)	Total protein (µg)	% Yield	% Purity
Crude	17716	5	88580	100	0.53
Flowthrough	15957	5	79785	90.07	0.59
Wash 1	4232.5	2	8465	9.56	5.55
Eluate (containing GST-Kpnβ1)	284.5	2	569	0.64	82.6

Table 5.3. Purification table of the various stages of purification of Kpnβ1 using affinity tag chromatography. Figures in the table are based on nanodrop quantification are representative of protein quantities obtained for a round of purification.

Fraction	µg/µL	Volume (mL)	Total protein (µg)	% Yield	% Purity
Crude	14770	5	73850	100	0.23
Flowthrough	13798	5	68990	93.42	0.25
Wash 1	2862	2	5724	7.75	3
Eluate (containing Kpnβ1	203	2	406	0.55	85.2

5.2.2. Western blot analysis to confirm purified protein as Kpnβ1

To confirm that Kpnβ1 is present in the eluates, purified protein at different concentrations were electrophoresed on an SDS-PAGE gel and western blot analysis for Kpnβ1 carried out. An increased GST-Kpnβ1 after IPTG induction was observed in comparison to the unstimulated lysate (lanes 1 and 2, Figure 5.3.A). The prominent band in lanes 1-4 had a molecular weight of ~123 kDa, which corresponds to the molecular weight of the GST-Kpnβ1 fusion protein while the predominant bands in lanes 7-9 had a molecular weight of ~97 kDa corresponding to the molecular weight of Kpnβ1 (without the GST tag) which was obtained after GST has been cleaved off. The protein eluates in lanes 7-9 were incubated with HRV 3C Protease to remove the GST tag. HeLa cell lysates were used as a positive control in western blot analysis and results showed that the purified Kpnβ1 had a comparable size to that of Kpnβ1 in HeLa lysates (Figure 5.3.B).

Purified Kpnβ1, both the fusion protein, GST-Kpnβ1 and Kpnβ1 with the GST tag removed were used in the biophysical analysis.

A

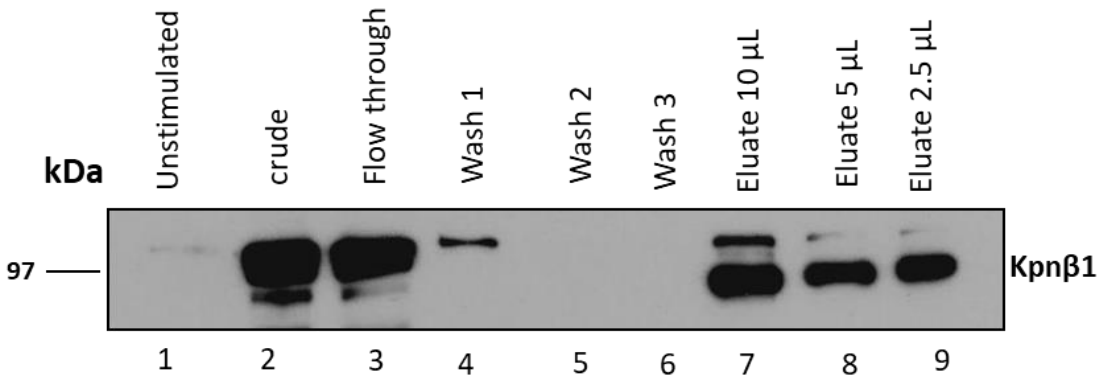

B

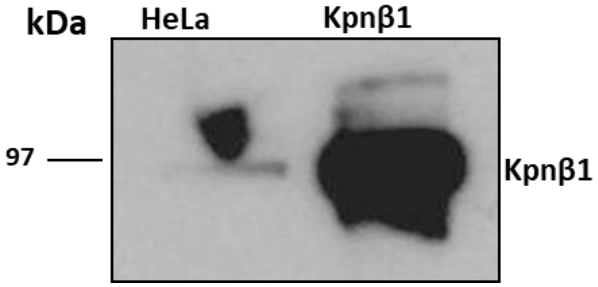

Figure 5.3: Western blot analysis of purified Kpnβ1. Different fractions from the batch binding were analysed via SDS-PAGE and probed for Kpnβ1 (A). Western blot comparing purified eluate to HeLa cell lysate, both bands appeared at ~97 kDa (B).

5.2.3. Bio-layer Interferometry (BLI) technology for investigating Kpnβ1: C60 binding

In this study, we used the Octet instrument platform to perform biophysical analysis of Kpnβ1: C60 interactions. The Octet Red system enables binding kinetics to be analysed in multiples ways, including the use of a GST biosensor or Super Streptavidin (SSA) biosensor. We used both approaches to determine the binding affinity of C60 to Kpnβ1.

5.2.3.1. Measuring GST-Kpnβ1:C60 binding kinetics using a GST biosensor

The binding affinity between purified GST-Kpnβ1 and C60 was investigated using the GST biosensor kinetics assay. The Octet anti-GST biosensor consists of a high affinity anti-GST antibody pre-immobilised on the biosensor. Purified GST-Kpnβ1 at a concentration of 100 µg/mL was loaded onto the anti-GST biosensors, followed by dipping the biosensors into wells containing C60 at different concentrations (0.1, 1, 10 and 100 µM). A response from ~0.4 to ~2.0 nm was observed as a result of GST-Kpnβ1 binding to the anti-GST biosensor (Sensors C1 and D1). Sensor C1, the ligand sensor was loaded into C60 while sensor D1 the reference sensor (control) was loaded into binding assay buffer. A dose-dependent binding of C60 to GST-Kpnβ1 was detected with Sensor C1.

A control for non-specific binding between the anti-GST biosensor (not loaded with Kpnβ1) and C60 was also included with two other sensors (Sensors C2 and D2) were included in the experiment. Sensor C2 (Ligand sensor) was loaded into assay buffer followed by placing it in C60 wells while sensor D2 (Reference Ligand) served as the control and was not placed in C60 wells (Figure 5.4).

Analysis of the data to calculate the binding kinetics was done using the Octet FortéBio analysis software. Non-specific interactions were taken into account and a 1: 1 fitting model with full local fitting of the curves as well as double reference subtraction was performed. A K_d value of 4.4E-05 M (~44 µM) with a R^2 value of 0.93 was obtained for GST-Kpnβ1: C60 interaction. The R^2 value is an indicator of how well the curve fits and our experimental data correlate with an R^2 of 0.95 considered to be a good fit [237]. A K_d of 44 µM and an R^2 of 0.95 suggests that C60 binds to GST-Kpnβ1 with weak affinity. We performed similar experiments for Importazole, a commercially available inhibitor of Kpnβ1 alongside the GST-Kpnβ1: C60 experiments. A K_d value of 1.3E-06 M (~1.3 µM) and an R^2 value was 0.99 was obtained for GST-Kpnβ1-Importazole interaction.

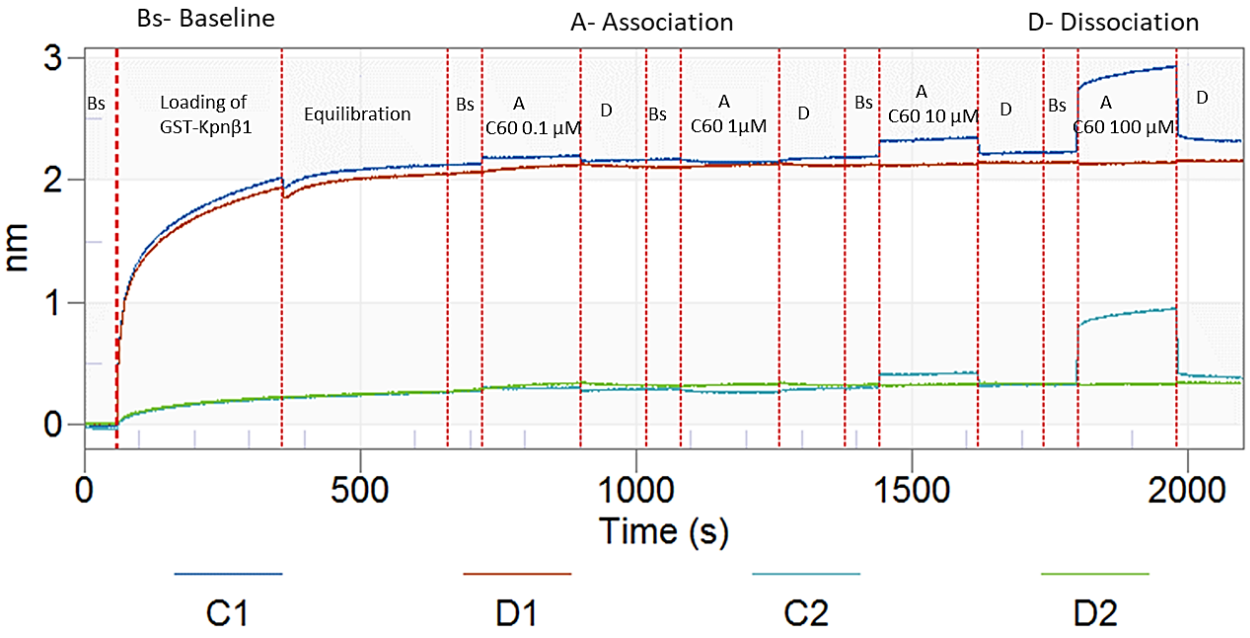

Figure 5.4: Sensorgram of GST-Kpnβ1 binding to anti-GST biosensor, followed by binding of C60. The Y-axis shows the response in nanometer (nm), and the X-axis shows the time in seconds. Sensor C1 (ligand sensor) and Sensor D1 (reference sensor) were loaded with GST-Kpnβ1 before association with C60 or assay buffer respectively. As negative controls, Sensors C2 and D2 were loaded with assay buffer prior to association with C60 or assay buffer respectively, and were subjected to the same experimental steps as Sensors C1 and D1.

5.2.3.2. Kpnβ1: C60 binding kinetics using a Super Streptavidin (SSA) biosensor

The binding affinity between purified Kpnβ1 (GST tag removed) and C60 was investigated using the Super Streptavidin (SSA) biosensor kinetics assay. In this assay, biotinylated Kpnβ1 was immobilised onto a high-capacity SSA biosensor surface. The SSA biosensors were loaded with 100 µg/mL biotinylated Kpnβ1. Blocking was done in 10 µg/ mL biocytin (Sigma) prior to dipping the biosensors in wells containing C60 (0.1, 1, 10 and 100 µM) for association. A response at ~0.4 to ~3.5 nm as a result of Kpnβ1 binding to the SSA biosensors (Sensors E1 and F1) was observed. Significant binding was only observed between C60 and Kpnβ1 at 100 µM C60 concentration (Sensor E1-Ligand sensor). As previously described sensors E2 and F2 were included as controls for non-specific binding of the sensor to C60. Sensor E2 (Ligand sensor) was loaded into assay buffer followed by placing it in C60 wells while sensor F2 (Reference Ligand) served as the control and was not placed in C60 wells (Figure 5.5). Analysis of data was done using the Octet FortéBio analysis software as previously described. A K_d value of 3.1E-06 M (~3.1 µM) with an R^2 value of 1 was obtained for Kpnβ1: C60 interaction. The binding of Importazole, the commercially available inhibitor of Kpnβ1 had a K_d value of 1.8E-07 M (~0.18 µM) and an R^2 value of 1 using the SSA method.

A comparison of K_d values obtained from using the GST and SSA biosensors methods is shown in Table 5.2. K_d values obtained using purified protein where the GST tag was removed were approximately 10 fold lower for both C60 and Importazole compared to that obtained for GST-Kpnβ1.

Together these results suggest that C60 interacts with Kpnβ1 in the micromolar range. Importazole, the commercially available inhibitor similar interacts with Kpnβ1 in the micromolar range albeit at lower K_d values than that for C60. Further optimisation of experimental conditions is required to obtain data that is more conclusive.

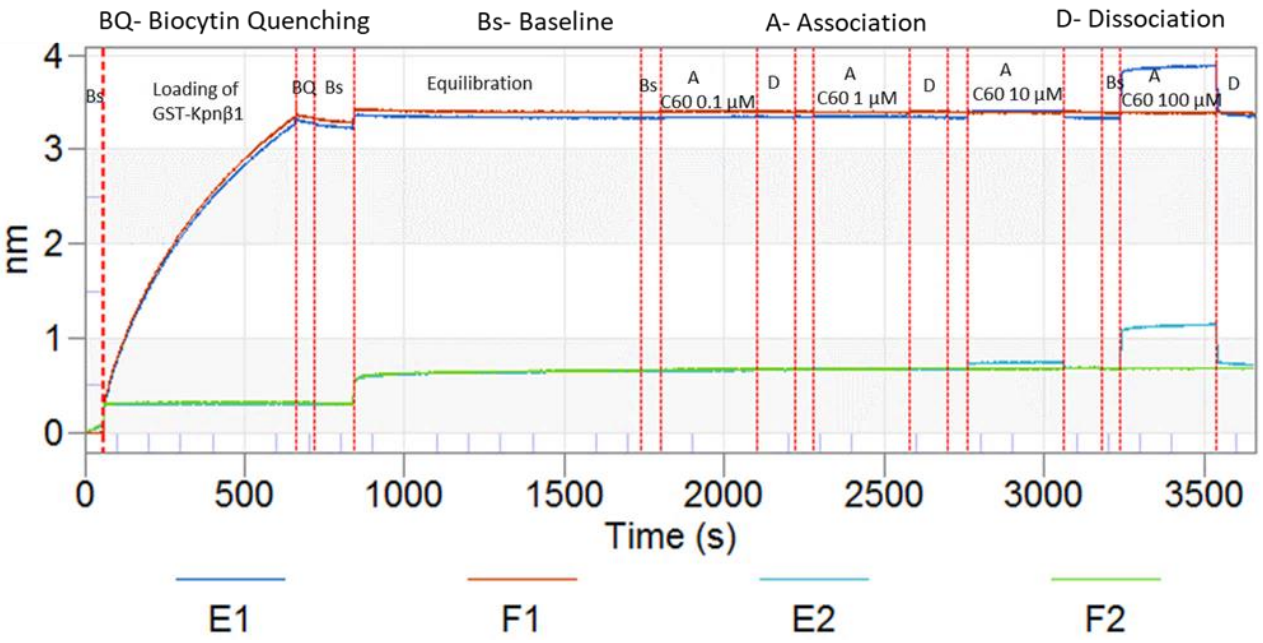

Figure 5.5: Sensorgram of Kpnβ1 binding to SSA biosensor, followed by binding of C60. The Y-axis shows the response in nanometer (nm), and the X-axis shows the time in seconds. Sensor E1 (ligand sensor) and Sensor F1 (reference sensor) were loaded with Kpnβ1 before association with C60 or assay buffer respectively. As negative controls, Sensors E2 and F2 were loaded with assay buffer prior to association with C60 or assay buffer respectively, and were subjected to the same experimental steps as Sensors E1 and F1.

Table 5.2. Binding kinetics of C60 and Importazole using GST and SSA biosensors on the Octet Red.

	GST Biosensor		SSA Biosensor	
Compounds	**K_d**	**R^2**	**K_d**	**R2**
C60	44 µM	0.929	3.1 µM	1
Importazole	1.3 µM	0.998	0.18 µM	1

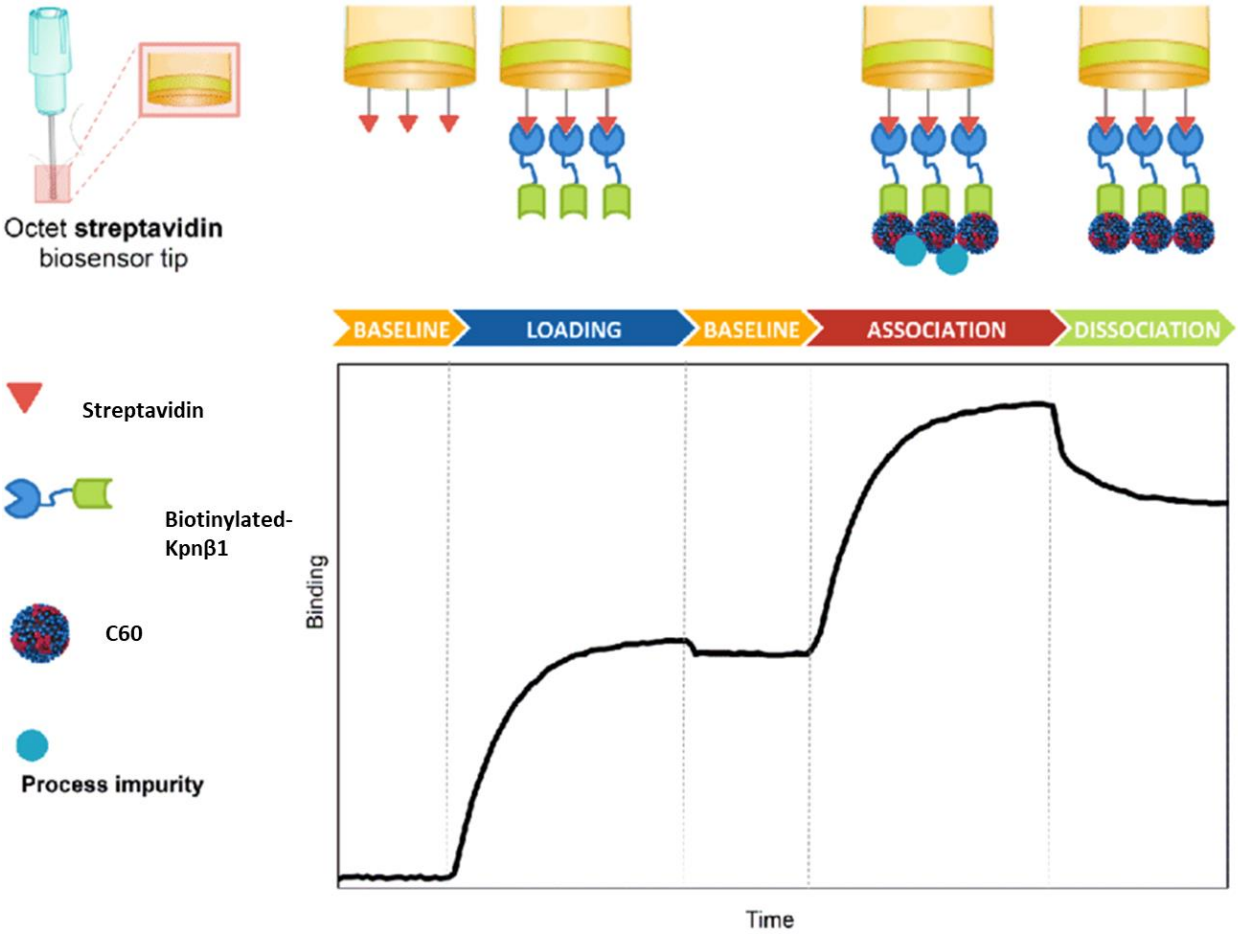

Figure 5.6: A cartoon depicting the use of SSA biosensors in the BLI technique. Graphic representation of the binding of C60 to immobilised biotinylated-Kpnβ1 on SSA biosensor. Image is adapted from Carvalho *et al* (2011) [244]

5.3. Discussion

In this chapter, we used the GST-affinity tag purification method to obtain purified Kpnβ1 (GST-tagged and untagged). Using this technique, we were able to purify Kpnβ1 that was quite stable after about 3-4 cycles of freeze thawing (data not shown). Purified Kpnβ1 was prepared in sufficient quantities to perform biophysical analysis of either GST-Kpnβ1 or Kpnβ1 interaction with C60.

Protein-protein interaction (PPI) underlies various physiological cellular processes. PPIs are also involved in the pathogenesis of multiple diseases. Targeting protein-protein interactions via small molecules has multiple issues related to the 'druggability' of a target. Druggability refers to the alteration of a target protein's function by small molecules with high affinity [245]. The contemporary drug discovery process involves three major steps; discovery of potential drug target, investigation of its properties and development of a compatible ligand. Hence, the knowledge of protein-protein interaction is valuable in the development of agents that can target protein complexes involved in different diseases [245].

Information regarding PPI domains for Kpnβ1 has been reported in the literature. In an earlier investigation, the crystal structure of Kpnβ1 bound to Kpnα2 and Ran was used for the *in silico* identification of small molecules with the potential to bind Kpnβ1. C60 was one of a number of small molecules identified and further characterised for its inhibitory activity on Kpnβ1 associated functions. In the previous chapters, we reported that C60 had anti-cancer activities *in vitro and in vivo* and inhibited the nuclear import of Kpnβ1 and that of some of its known cargoes e.g. NFAT, NFκB and AP-1.

In this chapter, we investigated whether the cancer cell killing effect and interference of C60 with Kpnβ1 localisation relates to the ability of this small molecule to bind Kpnβ1 directly. For the biophysical analysis of a potential Kpnβ1: C60 interaction, we used the Octet biosensor system, which relies on the Bio-layer Interferometry technique. Real-time, label-free biosensors are important biophysical tools in the biopharmaceutical industry and are currently being used in various stages of drug discovery and development [246].

Our results showed binding between C60 and Kpnβ1 in the micromolar range. K_d values of 44 µM and 3.1 µM were obtained for C60 using the GST and SSA biosensors respectively. We also investigated the binding kinetics of Importazole, a commercially available inhibitor of Kpnβ1 with its target-Kpnβ1. Our result showed that Importazole had K_d values of 1.3 µM and 0.18 µM using the GST and SSA-biosensors respectively. In both cases, removal of the GST tag improved the binding kinetics suggesting that the GST tag negatively affects binding kinetics in this instance. Since GST-Kpnβ1 was used with the GST biosensor, there is a possibility that C60 was interacting with the GST-dimers (formed between GST-Kpnβ1 and GST immobilised on the sensor). The binding of GST alone to the GST-biosensors will be a good control.

Previous work done in our laboratory using Isothermal Titration Calorimetry (ITC) and Circular Dichroism (CD) found another small molecule, INI-43 had K_d values in the micromolar range (E. Strydom, PhD thesis, 2016[ǂ5]). It has been reported in the literature that most small molecules developed from non-natural products generally have K_d values in the micromolar range indicating weak affinity [247]. Biologically significant non-covalent interactions have K_d values ranging from picomolar to nanomolar for the strongest interactions, and up to a millimolar range for the weakest ones. Small molecule drugs generally display tight binding to their target proteins with K_d values in the nanomolar to picomolar range [242].

Although, we were able to generate K_d values using the BLI technique further optimisations must be done since non-specific binding of the target protein to the sensors was observed for both anti-GST and SSA techniques. Furthermore, the ligand (Kpnβ1) loading step requires optimisation as the excess binding of the ligand to the biosensor can result in data artifacts. Over-saturation of the sensor may also cause weaker non-specific binding at higher analyte (small molecule) concentrations. The timing of the loading step also plays an important role in the kinetic analysis of drug-small molecule binding; slow loading for a longer period is preferred to rapid ligand binding [237]. In addition to optimising the BLI techniques, solution competition experiments can also be performed using the Octet Red instrument. Abdiche *et al* (2008) reported that the Octet does not have the highest precision in determining the direct binding of small molecules, however, it can detect their affinities indirectly through solution competition experiments [248].

ǂ[5] E. Strydom "Investigating Karyopherin B1: Small molecule interactions for cancer therapy" PhD Thesis, University of Cape Town, 2016.

Our results showing binding of C60 to Kpnβ1, albeit in the micromolar range is promising. However, further optimisation of biophysical analysis will have to be performed to arrive at more conclusive data of Kpnβ1: C60 binding kinetics.

Chapter 6: Conclusion

6.1. Main conclusion

Targeted therapy is a treatment approach that is based on the identification of the molecular vulnerability of cancer cells. The nuclear transport apparatus in eukaryotic cells plays an important role in maintaining normal cell physiology and deregulation in this system has been linked to carcinogenesis amongst other diseases. Previous studies in our laboratory identified Kpnβ1, Kpnα2 and CRM1 as potential therapeutic targets for cancer. In this study, we investigated the effect of C60 on cancer cell biology *in vivo* and *in vitro,* its effect on nuclear import pathway associated with Kpnβ1, its *in vitro* ADME pharmacokinetic properties as well as its binding kinetics with Kpnβ1.

The anti-cancer effects of C60 were demonstrated via different cell culture based assays, which included proliferation, colony formation and cell cycle assays. Our results show that cancer cells tested in this study showed greater sensitivity to C60 treatment in comparison to non-cancer epithelial cells. This was further confirmed by MTT proliferation assays where non-cancer cells were largely unaffected by C60 at concentrations that caused a significant reduction in the proliferation of cancer cells. While the MTT assay has high reproducibility and provides information on cytotoxicity and proliferation [249], it has the disadvantage of providing inaccurate data, therefore, it should be accompanied with other assays such as cell counting kit-8 (CCK-8 assay) [250]. While C60 resulted in a significantly reduced anchorage-dependent proliferation, the effect of C60 on anchorage-independent proliferation would paint a more reliable picture of what goes on in a tumour *in vivo*. The ability of cancer cells to display anchorage-independent cell growth has been considered to be an important hallmark in cancer biology because it has been linked to tumour aggressiveness *in vivo* [251].

The selectivity of C60 for cancer cells may originate from the increased dependence of cancer cells on Kpnβ1 [130]. The non-cancer cells used in this study were of retinal origin, and may not be the best normal controls since cervical and oesophageal cancers were the focus of the study. The use of more non-cancer epithelial cells of the cervical and oesophageal origins will be appropriate controls that might further highlight the selectivity of C60 for cancer cells.

The reduced proliferative ability of cancer cells after C60 treatment was shown to be associated with a G1 cell cycle arrest. This arrest was linked to a decrease in the expression of cell cycle regulatory proteins such as cyclin D1 and CDK4 whose interaction is necessary for the progression of cells from G1/S phase into the G2/M of the cell cycle [180]. In this study, cell cycle analysis was not done in non-cancer cells. The use of non-cancer cells as positive controls in the investigation of the effect of C60 on cell cycle regulation will provide more evidence for the selective toxicity of C60. PARP cleavage, which is a classical molecular marker of apoptosis and decreased levels of the anti-apoptotic protein MCL-1 associated with C60 treatment. Previous work in our laboratory showed that inhibiting Kpnβ1 via siRNA silencing similarly showed the degradation of MCL-1 and cell death via apoptosis [127]. Cleavage C60 also caused a significant reduction in migration and invasion of cancer cells, which is comparable with what was observed when cancer cells were treated with INI-43, another small molecule inhibitor of Kpnβ1 [150].

The elevated expression of Kpnβ1 and that of its adaptor protein Kpnα2 have been shown in cervical cancer tissues and cell lines [55]. The results presented in this thesis support the findings showing that Kpnβ1 and Kpnα2 have significantly higher expression in cervical and

oesophageal cancer cell lines in comparison to non-cancer epithelial cell lines, which indicate that the overexpression of these proteins is not limited to cervical cancer only. The elevated expression of Kpnβ1 has been reported in diffuse large B-cell lymphoma [71], breast cancer [130] among others. Likewise, the overexpression of Kpnα2 has been reported for numerous cancers including breast [174], oesophageal [23], endometrial [252] and ovarian [253] cancers.

Using western blot analysis and immunofluorescent microscopy, we investigated the effect of C60 on the localisation of endogenous Kpnβ1. Results demonstrated that the localisation of Kpnβ1 became altered from the nucleus to the cytoplasm in the presence of C60. In addition to causing the cytoplasmic retention of Kpnβ1, C60 also resulted in a shorter protein half-life, suggesting increased Kpnβ1 degradation in the presence of C60. These results are similar to previous data that showed that for another small molecule, INI-43 which resulted in the cytoplasmic accumulation of and degradation of Kpnβ1 (S. Carden, MSc Dissertation, 2017). Cycloheximide half-life assay showed that C60 reduced the half-life of Kpnβ1, thermal stability shift assay using purified Kpnβ1 (which was done in this study) can be used to test the effect of C60 on Kpnβ1 stability *in vitro.*

We also investigated the effect of C60 on the nuclear import of transcription factors that have been associated with increased cancer invasiveness and are known cargoes of Kpnβ1. Transcription factors, NFκB, NFAT and AP-1 have been implicated in the development and progression of cancer [254–256]. These set of proteins have been shown to be reliant on Kpnβ1 for their nuclear import. Using immunofluorescent microscopy and luciferase reporter assays, we showed that C60 treatment inhibited the nuclear entry of NFκB. C60 caused a

significant reduction in the transcriptional activity of NFκB in the cervical and oesophageal cancer cells, and no significant effect was observed in the ARPE-19 non-cancer cell line. A dose dependent decrease in NFAT transcriptional activity in C60 treated cells was also observed.

Furthermore, the transcriptional activity of AP-1, as well as the nuclear import of its cJUN component, was inhibited by C60. The inhibitory effect of C60 on the activity of these transcription factors was compared to that of Importazole, a commercially available inhibitor of Kpnβ1 nuclear import. C60 was found to be more efficient at inhibiting nuclear import in comparison to Importazole. Together these results suggest that C60 interferes with the sub-cellular localisation of Kpnβ1 and thus with the nuclear localisation and activity of its cargo proteins. The data on the inhibition of Kpnβ1 cargoes is inconclusive as the effect of C60 on the total expression level of these proteins have not been tested, therefore it is difficult to determine if nuclear inhibition is as result of Kpnβ1 inhibition or reduced expression of the level of the cargo proteins as a result of C60 treatment. The *in vitro* data in this study suggests that C60 has potential as an anti-cancer agent by acting on Kpnβ1.

The early stage of drug discovery involves making predictions of pharmacological and toxicological properties of a compound from *in vitro* cellular and *in vivo* animal models [257]. We investigated the *in vitro* ADME pharmacokinetic properties of C60 by via five major parameters; solubility, permeability, lipophilicity, metabolic stability and plasma protein binding. The results of these assays provided information, which suggested that C60 is readily soluble, and ideal for oral absorption; however, it had the potential of being rapidly cleared from the body due to its short half-life. The rapid clearance and short half-life of C60

may compromise its use therapeutic drug in its current form, however, it must be noted that the ADME studies were performed using *in vitro* methods. Prediction of *in vivo* clearance from the results of *in vitro* metabolism assay has been inadequate for many studies, as most compounds display no correlation between *in vitro* stability and *in vivo* clearance [257]. *In vivo* ADME studies are thus required to accurately measure the clearance of C60 in an animal model system. Furthermore, the investigation of the metabolites formed after the metabolic breakdown of C60 may provide information on its pharmacologically active metabolites, which may have longer half-lives and less rapid clearance. These metabolite data may provide a lead to the necessary structural modifications that are necessary to improve the drug-like properties of C60.

Toxicity studies in nude mice showed that C60 was tolerated up to a dose of 50 µg/g; however, the dose of 10 µg/g was used for the xenograft study as tumour bearing mice showed signs of discomfort to higher doses of C60. Our results demonstrated that in the ectopic xenograft mouse model, C60 injection via the intraperitoneal route inhibited tumour growth of KYSE 30 oesophageal cancer cells. KYSE 30 tumours developed necrosis, which is a feature of aggressive tumours that have been strongly associated with invasiveness [258]. To our knowledge, studies showing the effect of inhibiting nuclear import *in vivo* are limited however; the effect of inhibiting nuclear export *in vivo* has been reported.

The Selective Inhibitors of Nuclear Export, KPT-251 and KPT- 330 have significant inhibitory effect on tumour growth in a renal cell carcinoma xenograft mouse model [259,260]. KPT-330 is currently being tested in clinical trials in a wide range of cancers including prostate, breast, ovarian, gastric, cervical and pancreatic cancers [145]. Our study and those on inhibiting

nuclear import suggest that there is promise in investigating inhibition of nuclear transport pathways as an anticancer approach.

Small molecules inhibit protein-protein interaction via three different mechanisms- allosteric regulation, interfacial binding and orthosteric inhibition [245]. Allosteric regulation involves the binding of small molecules to target proteins at sites different from the macromolecular interface. Interfacial inhibitors bind to a pocket at the macromolecular interface and cause the complex to be locked in a non-functional conformation while orthosteric inhibition involves the binding of small molecules to target proteins at sites that overlap with areas used for interacting with partner proteins [245].

C60 was identified using in an *in silico* screen to bind to the overlapping site of Ran and Kpnα2 on Kpnβ1, suggesting it as an orthosteric inhibitor. We used Bio-layer Interferometry to investigate the binding kinetics between C60 and Kpnβ1. The knowledge of binding interaction between drugs and target proteins is essential in order to avoid the side effects of drug action. This is achieved by ensuring that the affinity (K_d) between the protein target and the drug is as tight as possible. Small molecules have been reported to generally display tight binding to their target proteins with K_d values in the nanomolar to picomolar range. For example, Imatinib binds to its target with a K_d value of ~10 nM [242]. Preliminary data obtained from BLI assay showed that C60 binds to Kpnβ1 in the micromolar range. Similarly, the binding kinetics for Importazole, the commercially available inhibitor of Kpnβ1 was found to be in the micromolar range in our investigation. This suggests the weak binding of these small molecules to Kpnβ1. A possible reason for weak binding could be that C60 was

identified using the *in silico* crystal structure of Kpnβ1, which may not completely reveal what the interaction would look like *in vitro*.

Binding kinetics studies done in our laboratory previously with another potential inhibitor of Kpnβ1, INI-43 was done using CD and ITC. ITC has been reported to have high accuracy and reproducibility with the error of binding constant in the range of 5%. It has the ability to measure binding affinities as low 10^{-2}-10^{3} μM and high affinity interactions with binding coefficients as large as 10^{8}-10^{9} M^{-1} [261]. These techniques can also be used to further investigate the binding kinetics between C60 and Kpnβ1. We also observed that the K_d values obtained from the SSA biosensors were lower than that obtained from the GST biosensors. Possible explanations for this is that GST monomers are able to dimerise and have been shown to have K_d values in the nanomolar range [262], the use of GST only protein bound to the GST-biosensor can be used to test this. Furthermore, the use of GST immobilisation technique has been shown to have a lower overall signal output strength in comparison to other immobilisation technique [263]. The SSA biosensor generated lower K_d values possibly because of the strong interaction between the biotinylated Kpnβ1 and SSA biosensors. The streptavidin/biotin interaction has been reported to have low dissociation constant of about 10^{-15} M. The advantage of this approach is the guarantee that the orientation of proteins immobilised on the sensor will remain unchanged [263].

In conclusion, this study provides evidence showing C60, a novel small molecule has potential as an inhibitor of Kpnβ1, as it has anti-cancer effects *in vitro* and *in vivo* and interfered with Kpnβ1-mediated nuclear import functions. Our results demonstrate that C60 has value as a parent compound for the further development of novel inhibitors of Kpnβ1.

6.2. Summary of key findings

- The small molecule C60 inhibited cancer cell proliferation and induced cell death via apoptosis while having little or no effect on the viability of non-cancer cells at a concentration of 10 µM.
- Data suggested that C60 inhibited the nuclear import of Kpnβ1 and had inhibitory effects on the nuclear translocation and activity of known Kpnβ1 cargoes.
- C60 decreased tumour growth in oesophageal cancer xenograft mouse model.
- *In vitro* ADME pharmacokinetics studies showed that C60 has high solubility, permeability and plasma protein; however, liver microsomal assay predicted rapid clearance.
- Preliminary data obtained using the Bio-layer interferometry technique suggest that C60 binds Kpnβ1 in the micromolar range.

6.3. Limitation and recommendation

1. In this study, primary and immortalised epithelial cells of the retinal origin were used as non-cancer controls. The use of non-cancer cervical and oesophageal epithelial cells is recommended for future studies. Furthermore, these cells can be used as controls for assays such as cell cycle analysis.
2. Results in this study suggested that the inhibition of Kpnβ1 by C60 resulted in the inhibition of the nuclear import of Kpnβ1 cargoes such as NFκB, NFAT and AP-1; however, the effect of C60 on the total expression of these cargoes was not investigated. This data will provide a confirmation that C60 was indeed inhibiting the nuclear import of these cargoes via Kpnβ1 rather than on the cargoes themselves.
3. The ADME *in vitro* data suggests that C60 is ideal for oral absorption but has a short half-life and rapid clearance. Investigating the products of the metabolic breakdown of C60 might reveal the presence of metabolites with longer half-lives. I*n* vivo ADME assays should be performed to determine the behaviour of C60 in a living system.
4. Binding kinetics data obtained using the BLI technique suggested that C60 binds to Kpnβ1 in the micromolar range. Variations were observed between K_d values obtained with the use of GST and SSA biosensors. While this data provides information that C60 might be binding Kpnβ1, the technique must be optimised for conclusive K_d value to be generated. Other techniques such as CD and ITC can be used to confirm data obtained from BLI.

Chapter 7: Materials and methods

7.1. Materials

7.1.1. Cell lines

The following cancer cell lines were obtained from the American Type Culture Collection (ATCC) (Rockville, MD, USA): human cervical cell lines, HeLa, SiHa and Caski. The oesophageal carcinoma cell lines KYSE 30 and KYSE 150 were previously established by Shimada and colleagues [264] and obtained from DSMZ (Berlin, Germany). The oesophageal carcinoma cell lines WHCO1, WHCO5 and WHCO6 were originally established from biopsies of South African patients with oesophageal squamous cell carcinoma [265] and were obtained as a gift from Dr R. Veale at the University of Witwatersrand, South Africa. Cells were grown in Dulbecco's Modified Eagle's Medium (DMEM, Gibco, Life Technologies, Carlsbad, CA, USA) supplemented with 10% Fetal Calf Serum (FCS, Gibco, Life Technologies, CA, USA), 100 U/mL penicillin and 100 µg/mL streptomycin.

Primary retinal pigmented epithelial cells - ARPE-19 and its hTERT immortalised counterpart, hTERT RPE-1 cells were obtained from ATTC (Rockville, MD, USA) and maintained in DMEM: F12 (Gibco, Life technologies, Paisley, UK) supplemented with 10% FCS, 100 U/mL penicillin and 100 µg/mL streptomycin. hTERT RPE1 cells were grown in the presence of 0.01 mg/mL hygromycin B (Sigma-Aldrich).

7.1.2. Compounds

7.1.2.1. Compound 60 (C60)

C60 (chemical name 9-[1-methyl-3-piperidinyl)methoxy]-4-[6-methyl-2-pyridinyl)methyl]-7-(5-methyl-2-thienyl)-2,3,4,5-tetrahydro-1,4-benzoxazepine), an inhibitor of Kpnβ1 was obtained in powder form from Ambinter (Amb10224332, Orleans, France) and stored as a 20 mM stock in DMSO at -20 ˚C.

7.1.2.2. Importazole

Importazole, an inhibitor of nuclear import was purchased from Sigma-Aldrich (St. Louis, MO, USA). It was dissolved in DMSO to a stock concentration of 25 mM and stored 4 ˚C.

7.1.2.3. Cisplatin (CDDP)

Cisplatin was purchased from Sigma-Aldrich (St. Louis, MO, USA) in powder form and dissolved to a concentration of 1 mg/mL in 0.9% NaCl. Solutions were filtered using a 0.22 μm filter and stored in the dark at room temperature.

7.1.2.4. Phorbol-12-myristate-13-acetate (PMA)

PMA (Phorbol ester) was purchased in powdered form from Sigma-Aldrich (St Louis, MO, USA) and was dissolved to a stock concentration of 1 mM in DMSO and stored at -80 ˚C.

7.1.3. Plasmids

The NFκB/p65 reporter construct in a pGL4 vector containing five copies of the p65 binding site responsible for driving the transcription of the luciferase reporter gene *luc2P* was

purchased from Promega (Madison, WI, USA). GFP-NFAT plasmid (Addgene plasmid # 24219) was a gift from Jerry Crabtree [198]. The NFAT-luciferase reporter plasmid containing three tandem repeats of a 30-base pair fragment of the IL2 promoter known to bind NFAT (Addgene plasmid # 10959) was a gift from Toren Finkel [266]. The AP-1 reporter plasmid, which contains four AP-1 Luc binding sites (TGAC/GTCA) upstream of the minimal promoter sequence from the albumin gene and the firefly luciferase reporter gene [267] was a gift from Professor M. Birrer (Harvard Medical School, MA, USA).

7.1.4. Animals

Animals used in this study were obtained from the animal breeding unit of the research animal facility of the Health Sciences Faculty, University of Cape Town South Africa. Male and female athymic nude mice (UCT 21) within the age of 6-8 weeks were used. Prior to starting the study, animal ethics approval was obtained from the HSFAEC (Health Sciences Faculty Animal Ethics Committee-protocol number 016/014). 6 mice were housed per cage in autoclaved polysulfone cages with sterile wood shaving as bedding material. A 12-hour light and dark cycle was maintained in a room with constant temperature and humidity. Mice were fed regularly with autoclaved chow diet and water containing antibiotics and multivitamins. All procedures used in the study were in accordance with the guidelines of the HSFAEC.

7.2. Methods

7.2.1. Cell culture

Cells were grown in their respective growth medium (section 6.1.1) in 100 mm tissue culture dishes. Prior to trypsinisation, cells were washed with PBS. After cells detached from the bottom of the dish, fresh culture medium was used to neutralize trypsin-Ethylenediaminetetraacetic acid (EDTA). Cell suspension, medium and trypsin-EDTA was collected into a 12 mL tube. Suspension was centrifuged at 500 x Earth's gravitational force (G) for 3 minutes at room temperature. Supernatant was aspirated to waste and cell pellet was resuspended in fresh culture medium. Cell resuspension was introduced into new culture dish and incubated in a humidified chamber at 37 ˚C in 5% CO_2.

7.2.2. Cryopreservation and reconstitution of cells

Cells were grown to 70-80% confluency and pellet was collected as described above. Cell pellet was resuspended appropriately in cold freezing medium. Cell suspension was transferred into properly labelled cryotubes and stored at -80˚C for 3 days before final storage in liquid nitrogen. Cells were recovered by thawing frozen cell suspension in a water bath at 37 ˚C and introduced into 100 mm cell culture dish containing fresh growth medium.

7.2.3. Mycoplasma test

Cells were checked regularly to ensure that they were free of mycoplasma infection. Cells were grown in Penicillin/ Streptomycin-free medium for 2 days after which they were plated on coverslips. Cells were fixed in cold methanol and stained with 4',6-diamidino-2-phenylindole dihydrochloride (DAPI) nuclear fluorescent stain. Coverslip was mounted on a

microscope slide using mowiol. Cells were visualised using a Zeiss Axiovert fluorescent microscope (Carl Zeiss, Jena, Germany). DAPI is a DNA stain that is capable of staining DNA-containing microorganisms. Hence, mycoplasma contamination is indicated by the presence of small blue specks around the cytoplasm of infected cells. The absence of blue specks in the cytoplasm is indicative of mycoplasma-free cells.

7.2.4. EC_{50} determination

EC_{50} is the concentration at which the half-maximal response of a drug is observed. The EC_{50} concentration of drugs (C60 and Importazole) in different cancer cell lines and normal cells were determined using the MTT (3-[4.5-dimethylthiazol-2-yl]-2, 5-diphenyltetrazolium bromide, Sigma-Aldrich, USA) assay. 5000 cells in 90 µL of culture media were introduced into each well of a 96-well tissue culture plate and allowed to adhere overnight. Cells were plated in triplicate for each drug concentration and cells treated with DMSO were used as control. Cells were treated with various concentrations of the compound ranging from 0.5-100 µM. Incubation with drugs was done for 24 or 48 hours at 37 ˚C. Effect of drug on cell viability was assayed by adding 10 µL MTT reagent (5 mg/mL) to each well, formazan crystals formed were solubilised after the addition of 100 µL solubilisation solution 4 hours after. Plates were incubated overnight and absorbencies were measured at OD595 nm using a microplate reader (BioTek, Winooski, VT, USA). Absorbance readings of drug treated cells were normalised to the absorbance of DMSO-treated cells and were used to plot dose-response curve. The EC_{50} value was calculated using GraphPad Prism V5.0 software. (Graph Pad Software Inc., USA).

7.2.5. Proliferation assay

The effect of small molecule inhibitor (C60) on cell proliferation was determined using the MTT assay. 1000 cells were plated in 96-well tissue culture plates in triplicate, treated with 5 µM or 10 µM C60, and incubated at 37 ˚C for 5 days. The effect of treatment on proliferation was assayed using the MTT reagent (Sigma). 4 hours later, formazan crystals formed were solubilised using solubilisation solution. Absorbances were read at OD595 nm using a microplate reader (BioTeK, Winooski, VT, USA).

7.2.6. Colony formation assay

1 x 10^3 cells were plated in 6-well plates and left to adhere overnight. The following day, cells were incubated in the presence of C60 for 24 hours while DMSO-treated cells served as control. Drug-containing media was replaced with fresh media. Growth media was replaced every 48 hours and viable cells were allowed to grow for 8 days. In another case, drug-containing media was left on for a period of 8 days. At the end of both experiments, cells were rinsed with cold PBS and fixed with fixation solution (see section 7.3 for composition) for 5 minutes at room temperature. Colonies were stained with 0.5% crystal violet (Sigma-Aldrich) solution and incubated at room temperature for 2 hours, following which stain was removed and plates were rinsed in tap water. Plates were left to air-dry overnight before images were captured with a standard camera. Colony areas were measured using Image J software (National Institute of Health, USA)

7.2.7. Migration assay

Transwell migration assay was used to monitor the effect of C60 on the migration of cells. This assay is an *in vitro* technique of monitoring the effect of treatment on the motility of

metastatic cells. 100 x 10^4 cells were plated in 35 mm dishes and allowed to adhere overnight. Cells were treated appropriately before being trypsinised and resuspended in fresh media containing 0.1 % FCS. Cells were plated at a density of 3 x 10^4/well into the upper chamber of the 12-well Transwell migration chambers (Greiner Bio-One, Austria). Chambers were placed into lower chambers containing 20% FCS-containing fresh media (chemoattractant). Cells were allowed to migrate through the membrane over a period of 24 hours. Cells that did not migrate were removed with cotton swab while migrated cells were fixed in 70% methanol and subsequently stained with crystal violet (0.2% w/v in 2% methanol). Inserts were rinsed with water and allowed to air dry properly. Stained cells were counted and images were taken using Zeiss Primovert inverted phase microscope (Carl Zeiss, Jena, Germany. Results were normalised to readings of MTT cell viability assay by dividing the number of migrated cells by absorbance readings from MTT assay.

7.2.8. Invasion assay

Tumour invasion system (Corning, BioCoat™, Bedford, MA) was used to monitor the effect of C60 on cancer cell invasion, and the experiment was done according to manufacturer's instruction. Briefly, cells were grown to ±70% confluency in 100 mm dish before they were stained using 1,1'-Dioctadecyl-3,3,3',3'-tetramethylindocarbocyanine perchlorate (DiI, Sigma). Cells were stained with filtered media containing 10 µg/mL DiI for 1 hour at room temperature. After staining, cells were replated in 35 mm and allowed to adhere overnight. The following day, cells were treated accordingly before trypsinisation and resuspension in fresh media containing 0.1 % FCS. 3 x 10^4 cells in 500 µL of media were added to the apical chamber and 750 µL of 20 % FCS containing fresh media (chemoattractant) was added to the basal chamber. Cells were allowed to invade through the matrigel matrix over a period

of 24 hours. Fluorescence was read OD549 nm and OD565 nm excitation and emission wavelengths respectively using Cary Eclipse Fluorescent Spectrophotometer (Agilent, Australia). Results were normalised to readings of MTT cell viability assay by dividing the absorbance readings of invasive cells by absorbance readings from MTT assay performed in unstained cells exposed to the same treatment procedure. Dil has excitation and emission wavelengths of 549 nm and 565 nm respectively [268].

7.2.9. Cell cycle analysis

To analyse the effect of C60 on cell cycle distribution, 300 x 10^4 cells were plated in 60 mm dishes and treated with C60. Cells were harvested for flow cytometry analysis. Media containing floaters was collected into a 12 mL tube and plates were washed twice with 1X cold PBS after which cells were trypsinised. Cell pellets obtained after 5 minutes of centrifuging at 500 x G were resuspended in 2 mL media and fixed in 8 mL of ice-cold 100% ethanol. Cells in ethanol were stored for up to 2 weeks at -20 ˚C. For flow cytometry processing, cells were removed from ethanol by centrifuging for 5 minutes at 500 x G at room temperature. Cell pellets were rinsed twice with ice-cold PBS. Cell pellets were resuspended in a solution of 50 µg/mL of RNase (Sigma-Aldrich) in PBS and incubated at room temperature for 30 minutes to remove RNA. Cells were finally stained with staining solution containing propidium iodide (PI- 1mg/mL) and incubated at room temperature for 20 minutes. PI has a maximum excitation wavelength at 535 nm and a maximum emission wavelength at 617 nm. Analysis of cell cycle profile was done using BD Accuri C6 Flow Cytometer (BD Biosciences NJ, USA). Quantification of the percentage of cells at each stage of the cell cycle was done using Modfit software.

7.2.10. Protein harvesting and quantification

7.2.10.1. Protein harvesting from whole cell (Live cells)

Cells in culture were grown to 80% confluency and subjected to the appropriate treatment conditions. To harvest live cells only, cells were rinsed twice with ice-cold PBS after which Radioimmunoprecipitation Assay (RIPA) buffer containing complete protease inhibitor cocktail (Roche, Basel, Switzerland) and 0.1 M Sodium Orthovanadate for the inhibition of phosphatases was added to the dish. Cell lysates were removed using a cell scraper and were collected into properly labelled eppendorf tubes. Lysates were sonicated for 10 seconds to shear the DNA strands and immediately placed on ice. Cell lysates were centrifuged at 4˚C for 10 minutes at 10000 x G. Supernatants were carefully collected into new properly labelled eppendorf tubes. Harvesting was done entirely on ice.

7.2.10.2. Protein harvesting from whole cell (Live and dead cells)

In order to analyse cell death via apoptosis, which involves the cleavage of PARP, protein was harvested from live and dead cells. After cells have been exposed to different treatment conditions, culture medium containing floaters was collected into 12 mL tube after which cells were washed twice with ice-cold PBS. PBS washes were collected into the 12 mL tube and spun at 500 x G for 5 minutes at room temperature. Cell pellets were resuspended in RIPA buffer containing complete protease inhibitor cocktail (Roche, Basel, Switzerland) and 0.1 M Sodium Orthovanadate for the inhibition of phosphatases. RIPA buffer was added to the culture dishes and scraper was used to collect cells. Cell lysates were collected into eppendorf tubes in addition to cell pellet resuspended in RIPA buffer. Lysates were

sonicated for 10 seconds to shear the DNA strands. Cell lysates were centrifuged at 4˚C for 10 minutes at 10000 x G. Supernatants were carefully collected into new properly labelled eppendorf tubes. Harvesting was done entirely on ice.

7.2.10.3. Nuclear and cytoplasmic fractionation

To assess the variations between the nuclear and cytoplasmic expression of proteins after C60 treatment, nuclear and cytoplasmic fractionation was done. Cells were plated in 60 mm dishes and exposed to different treatment conditions. For harvesting, cells were rinsed twice with ice cold PBS after which trypsinisation was done. Centrifugation was done at 1000 x G for 5 minutes at 4˚C. Cell pellet was resuspended in harvest buffer and incubated on ice for 5 minutes followed by another round of centrifugation at 3000 x G for 10 minutes. Supernatant, which contains the cytoplasmic fraction, was collected into a new eppendorf tube and stored at -80˚C. The pellet was washed in buffer A and centrifuged at 3000 x G for 5 minutes. The supernatant was discarded and pellet was resuspended in buffer C and vortexed for 15 minutes at 4˚C after which centrifugation was done at 18000 x G for 10 minutes. Supernatant containing the nuclear fraction was collected in new eppendorf tube at stored at -80˚C. See section 7.3 for the composition of buffers.

7.2.10.4. Protein quantification

The concentrations of the proteins were determined using the Bicinchoninic Acid (BCA) protein assay kit (Pierce, Thermo Scientific, USA) according to the manufacturer's instructions. The BCA assay is dependent on the conversion of Cu^{2+} to Cu^{+} under alkaline conditions. The Cu^{+} is identified by upon reaction with BCA which results in the

development of a deep purple colour [269]. In this assay, absorbance reading was measured at OD595 nm using a BioTek microplate spectrophotometer (Winooski, VT, USA) and protein concentrations were determined using a set of established BSA (Bovine Serum Albumin) protein standards. Protein samples were stored at -80 ˚C.

7.2.11. Western blot analysis

7.2.11.1. SDS-Polyacrylamide gel electrophoresis

Using the Mini Protean II system (Bio-Rad, CA, USA), 20 µg of proteins were separated on Sodium Dodecyl Sulphate-Polyacrylamide Gel Electrophoresis (SDS-PAGE) gels. 4 x Laemmli loading dye was first added to protein samples after which they were denatured by heating at 90 ˚C for 5 minutes on a heating block. The samples were subsequently loaded into the wells SDS-polyacrylamide gels. 5 µL of a protein molecular weight marker (Kaleidoscope, BioRad) was used for the determination of protein sizes. Protein electrophoresis was done for an hour at 180 V.

7.2.11.2. Immunoblotting and immunodetection

After electrophoresis, proteins were transferred to a Hybond™ ECL™ nitrocellulose membrane (Amersham Biosciences, UK) using a tank transfer system. Transfer was done for 70 minutes at 100 V. Following transfer, membrane was blocked in 5 % (w/v) fat-free milk in TBST (Tris-buffered saline with 0.1% Tween) for 2 hours at room temperature in order to prevent non-specific bindings after which primary antibody (refer to Table 7.1. for antibody conditions) incubation was done overnight at 4 ˚C with shaking.

Membranes were washed thrice at 5-minute intervals with TBST the following day after which secondary antibody was added and incubation was done at room temperature for an hour with shaking. Membranes were washed thrice at 5-minute interval after secondary antibody incubation. Relevant protein bands were detected by chemiluminescence using Lumiglo (KPLinc, Gaithersburg, MD, USA) or Clarity western ECL substrate (Bio-Rad, United States) depending on signal strength. Protein bands were visualised by exposing nitrocellulose membrane to X-ray films (AGFA) at different times, followed by dipping the film in developer (AGFA G128), water, fixer (AGFA G333C) and finally water.

7.2.11.3. Stripping and reprobing of membranes

For investigating more than one protein on the same membrane, stripping and reprobing were done. Stripping is done for the removal of primary and secondary antibodies from membranes to permit for investigation of another protein. Membranes were stripped by immersing in 10% acetic acid for 10 minutes at room temperature with shaking. Membranes were washed thrice at 5 minutes interval with TBST after which blocking was done with 5 % milk in TBST for 2 hours and subsequently, primary antibody incubation followed.

Table 7.1: Antibody concentrations and incubation conditions for western blot analysis

Primary antibody	Primary antibody condition	Secondary antibody	Secondary antibody condition	Substrates
Rabbit anti-PARP-1 (H-250)[sc-7150, Santa Cruz Biotechnology]	1:1000 in TBST	Goat anti-rabbit [Bio-Rad]	1:5000 in TBST	LumiGlo® chemiluminescent system (KPL)
Mouse anti-GAPDH (0411) [sc-47724,Santa Cruz Biotechnology]	1:10000 in 5 % Milk-TBST	Goat anti-mouse [Bio-Rad]	1:5000 in 5 % Milk-TBST	LumiGlo® chemiluminescent system (KPL)
Rabbit anti-Kpnβ1 (H-300) [sc-11367, Santa Cruz Biotechnology]	1:2000 in 5% Milk TBST	Goat anti-rabbit [Bio-Rad]	1:5000 in TBST	LumiGlo® chemiluminescent system (KPL)
Mouse anti-cyclin D1 (HD11) [sc-246,Santa Cruz Biotechnology]	1:200 in TBST	Goat anti-mouse [Bio-Rad]	1:2000 in 5 % Milk-TBST	Clarity™ Western ECL substrate
Rabbit anti-CDK4 (H-22) [sc-601, Santa Cruz Biotechnology]	1:500 in 2. 5 % BSA-TBST	Goat anti-rabbit [Bio-Rad]	1:2000 in 5 % Milk-TBST	LumiGlo® chemiluminescent system (KPL)
Rabbit anti-TFIID (TBP) (N-12) [sc-204, Santa Cruz Biotechnology]	1:1000 in TBST	Goat anti-rabbit [Bio-Rad]	1:5000 in 5 % Milk-TBST	Clarity™ Western ECL substrate
Rabbit anti-MCL-1 (H-260) [sc-20679, Santa Cruz Biotechnology]	1: 250 in TBST	Goat anti-rabbit [Bio-Rad]	1:2500 in 5 % Milk-TBST	LumiGlo® chemiluminescent system (KPL)
Goat anti-Kpnα2 (C-20) [sc-6917, Santa Cruz Biotechnology]	1: 1000 in 2.5 % Milk-TBST	Donkey anti-goat [sc-2020, Santa Cruz Biotechnology]	1: 2500 in 2.5 % Milk	LumiGlo® chemiluminescent system (KPL)
Mouse anti-cyclin B1 (GNS1) [sc-245,Santa Cruz Biotechnology]	1:500 in TBST	Goat anti-mouse [Bio-Rad]	1:2000 in 5 % Milk-TBST	LumiGlo® chemiluminescent system (KPL)

Table 7.1: Antibody concentrations and incubation conditions for western blot analysis (continued)

Primary antibody	Primary antibody condition	Secondary antibody	Secondary antibody condition	Substrates
Rabbit anti-cJUN (D) [sc-44, Santa Cruz Biotechnology]	1:500 5 % BSA in TBST	Goat anti-rabbit [Bio-Rad]	1:5000 in 5 % Milk-TBST	LumiGlo® chemiluminescent system (KPL)
Rabbit anti-phospho-cJUN (Ser63/73) [sc-16312-, Santa Cruz Biotechnology]	1:250 5 % BSA in TBST	Goat anti-rabbit [Bio-Rad]	1:2500 in 5 % Milk-TBST	LumiGlo® chemiluminescent system (KPL)
Rabbit anti-cyclin A (H-432) [sc-751, Santa Cruz Biotechnology]	1:500 in TBST	Goat anti-rabbit [Bio-Rad]	1:2000 in 5 % Milk-TBST	LumiGlo® chemiluminescent system (KPL)

7.2.12. Cycloheximide half-life experiment

In order to determine the half-life of Kpnβ1 and Kpnα2, HeLa cells were treated with 5 µM C60 for 3 hours prior to treatment with 50 µg/mL CHX. Protein harvesting was done 0, 1, 3, 6, 9, 24, 48 and 72 hours after CHX treatment. Protein quantification was done using BCA kit as previously described. Expression of Kpnβ1 and Kpnα2 was monitored through western blotting; GAPDH (Glyceraldehyde 3-Phosphate Dehydrogenase) served as the loading control. Bands were quantified by densitometric scanning using image J software. Band intensities were plotted in log scale relative to time and half-life ($T_{1/2}$) was determined using the equation $T_{1/2}$= Log2/ Slope.

7.2.13. Immunofluorescence microscopy

Cells were plated on coverslips in 6-well plates and subjected to appropriate treatment. Cells were washed twice with ice cold PBS prior to fixation with 4% PFA (Paraformaldehyde) in PBS for 15 minutes. Cells were washed twice with PBS and permeabilisation was done for

10 minutes using 0.25% Triton X-100 in PBS at room temperature. Cells were washed thrice at 5-minute intervals with PBS, after which blocking was done in 1% BSA in PBST and 0.3 M glycine for 30 minutes. Cells were subsequently incubated with primary antibody (Table 7.2) diluted in 1 % BSA in PBST for 1 hour at room temperature, following which washing with PBS was done thrice at 5-minute intervals. Secondary antibody diluted in 1 % BSA in PBST was added to the cells and incubation was done for 1 hour at room temperature in the dark. Washing was done thrice at 5-minute intervals using PBS. DAPI (200 µg/mL, Sigma Aldrich, USA) was diluted to 1:400 in PBS was used to stain the nuclei of cells. Coverslips were mounted on microscope slides using moviol. Visualisation and capturing of images was done at 100x in oil immersion using Zeiss Axiovert 200M fluorescent microscope with AxioVision 4.8 Zeiss software and an AxioCam HRm (Carl Zeiss, Jena, Germany). Cy3 Goat anti Rabbit antibody has an excitation wavelength of OD548 nm and an emission wavelength of OD561 nm while DAPI has an excitation wavelength of OD359 nm and an emission wavelength of OD461 nm [270].

Table 7.2: Antibody concentrations and incubation conditions for immunofluorescent microscopy

Primary antibody	**Primary antibody condition**	**Secondary antibody**	**Secondary antibody condition**
Rabbit anti NFκB/p65 [Santa Cruz]	1:100, 1% BSA in PBST	Cy3 Goat anti Rabbit [Jackson ImmunoResearch	1:300, 1% BSA in PBST
Rabbit anti-Kpnβ1 (H-300) [sc-11367, Santa Cruz Biotechnology]	1:100, 1% BSA in PBST	Cy3 Goat anti Rabbit [Jackson ImmunoResearch]	1:300, 1% BSA in PBST
Rabbit anti-Kpnα2 [Ab97580, Abcam]	1:100, 1% BSA in PBST	Alexa Fluor 647 Chicken anti Rabbit IgG (Molecular Probes)	1:150, 1% BSA in PBST

7.2.14. Luciferase assay

Luciferase assays have been used to study transcriptional gene expression. Typically, a reporter gene is cloned alongside the DNA sequence of interest into an expression vector, which is then transfected into cells. Consequently, the cells are examined for the presence of the reporter by quantifying the reporter protein itself or its enzymatic activity [271]. To assay for NFAT luciferase activity, 3 x 10^3 cells were plated in each well of a 24-well plate. Cells were allowed to settle overnight. Cells were transfected with 50 ng GFP-NFAT plasmid (Addgene, Cambridge, Massachusetts, USA, Plasmid #24219 gift from Jerry Crabtree)[198], 50 ng NFAT-luciferase (Addgene plasmid # 10959, gift from Toren Finkel) [266], 5ng PRL-TK Renilla and 0.4 µL Genecellin™ transfection reagent (Celtic Molecular Diagnostic, South Africa). Renilla was used as the internal control for measuring the transfection efficiency of the Dual luciferase assay. Cells were then subjected to various treatment conditions treated and stimulated with 500 nM PMA (Sigma) and 1.3 µM Ionomycin (Santa Cruz Biotechnology, Santa Cruz, CA, USA) for 3 hours prior to lysis using 100 µL 1 x passive lysis buffer (Promega, USA). Luciferase firefly activity was measured using the Dual Luciferase kit (Promega, USA) on the Glomax 96 microplate luminometer (Promega, USA.

To assay for NFκB/p65 and AP-1 luciferase activities, cells were plated in 24-well plates and transfected with 100 ng of p65 luciferase reporter which contains five copies of the p65 binding site (Promega, USA) or 100ng AP-1 luciferase reporter which contains four copies of the AP-1 binding site [272] and 10 ng pRL-TK Renilla using 0.4 µL Genecellin™ transfection reagent (Celtic Molecular Diagnostic, South Africa) overnight. Cells were then subjected to various treatment conditions. 3 hours before reading luciferase activity, cells were stimulated with 500 nM PMA (1 hour stimulation for AP-1) after which they were lysed

using 100 µL 1 x passive lysis buffer (Promega, USA). Luciferase firefly activity was measured using the Dual Luciferase kit (Promega, USA) on the Glomax 96 microplate luminometer (Promega, USA). Luciferase reading was normalised to Renilla luciferase activity in the same extract.

7.2.15. ADME pharmacokinetic assays

In Vitro ADME pharmacokinetic assays were done with support from H3D Africa at the University of Cape Town.

7.2.15.1. Kinetic solubility assay

Kinetic solubility assay was done to examine the solubility of C60 in an aqueous medium. This assay was done using a mini shake flask technique. C60 was dissolved to a stock concentration of 10 mM in DMSO, which was subsequently used to prepare calibration standards ranging between 10-220 µM. Standards were diluted in PBS (pH 7.4) to a final DMSO concentration of 2%. Solutions were stirred continuously at 25 ˚C for 2 hours to permit solubilisation of C60. Solutions were filtered and analysed by HPLC-DAD (Agilent 1200 Rapid Resolution HPLC with diode array detector). A best-fit standard curve was constructed using the calibration standards, which were then used to calculate the aqueous solubility of C60.

7.2.15.2. Plasma protein binding assay

Plasma protein binding assay was employed to examine the percentage of C60 that is able to bind the human plasma protein. Briefly, this assay was done in a 96-well microplate

containing pooled human plasma (blood bank K3 EDTA). 10 mM stock of C60 in 100% DMSO was diluted to 1 µM which was eventually used in spiking human plasma. Total plasma concentration samples were prepared by removing an aliquot of plasma spiked with C60 and quenching it with ice-cold acetonitrile containing 0.1 µM carbamazepine (internal standard control) and storing it in the freezer. Duplicate aliquots of spiked plasma were incubated at 37 ˚C for 30 minutes with shaking following which they were transferred into ultracentrifuge tubes for centrifugation (Beckman Optima L-80XP) at 37 ˚C for 4 hours at 42000 rpm. Duplicate dilution of the control drugs was done in plasma and incubation was done at 37 ˚C for 4 hours with shaking. Shaking and ultracentrifugation steps were necessary for ensuring the separation of free drug from plasma protein-bound drug. After 4 hours, C60 samples and control drugs were transferred into the wells of the 96-well plate and quenched with ice-cold acetonitrile with carbamazepine (0.1 µM). All samples were centrifuged (Digtor OR/CE115, United Scientific) for 10 minutes at 3000 rpm and the supernatant was filtered. Analyte concentration of C60 and control drugs were determined by LC-MS/MS (Agilent Rapid Resolution HPLC, AB SCIEX 4000 QTRAP MS). The peak areas/ internal standard peak area were referenced to the total plasma concentration samples in order to determine the percentage of the plasma-bound compound.

7.2.15.3. Parallel Artificial Membrane Permeability Assay (PAMPA)

PAMPA is an *in vitro* assay used in investigating the trans-cellular permeability of a drug. It provides information about the oral absorption capacity of a drug. Briefly, this assay was done in triplicate in 96-well multiscreen filter plates (Millipore, 0.4 µM PCTE Membrane) which have been pre-coated with hexadecane and allowed to dry. Membrane integrity

marker, Lucifer yellow was included in the wells of the donor plate containing buffer (pH 6.5) spiked with 1 µg/mL C60. Donor plate was slotted into the acceptor plate containing phosphate buffer (pH 7.4) to form a sandwich after which incubation was done for at 50 rpm (IKA MS3 Digital shaker, Sigma) for 4 hours at room temperature to permit for passive diffusion of the compound. Subsequently, samples were transferred from the acceptor wells into the analysis plate and quenched with acetonitrile containing 0.0236 µg/mL carbamazepine (internal control) before analysis was done using LC-MS/MS (Agilent Rapid Resolution HPLC, AB SCIEX 4500 MS). Normalised peak areas were used to determine the apparent permeability (P_{app}) of the samples. Membrane integrity was evaluated by calculating the P_{app} of Lucifer yellow using Modulus microplate reader at 490 nm excitation wavelength and 510-570 nm emission wavelength [273].

7.2.15.4. Lipophilicity assay

Lipophilicity assay was used to explore the extent to which C60 dissolves in organic solvents. This assay was done in triplicate using a scaled down shake flask method. Briefly, 10 µL C60 (10 mM) was added to a 1:1 mixture of octanol (495 µL) and 0.1 M phosphate buffer (495 µL) in a microtiter plate. Solutions in microtiter plates were shaken at 1500 rpm (IKA MS3 Digital shaker, Sigma) for 2 hours at room temperature followed by centrifugation to separate the octanol/PBS layers. Aliquots of each layer were analysed by HPLC-DAD (Agilent 1200 Rapid Resolution HPLC with diode array detector) to determine the concentration of C60 in each layer which was eventually used to calculate the partition coefficient (LogD 7.4) [274].

7.2.15.5. Microsomal stability assay

Hepatic metabolic stability assay was done to examine the rate at which C60 is broken down by metabolic enzymes. Metabolism is the enzymatic alteration of compounds, which plays a role in determining oral bioavailability, clearance and *in vivo* half-life. Metabolism occurs majorly in the liver [211]. This assay was performed in duplicate in 96-well microtiter plate. 1 µM C60 was incubated separately in 0.4 mg/mL pooled human, rat and mouse liver microsomes (Sekisui Xenotech, LLC. Kansas City, US) at 37 ˚C at different time points in the presence or absence of 1 mM NADPH (cofactor). Reactions were quenched at different times by adding 300 µL of ice-cold acetonitrile containing 0.0236 µg/mL carbamazepine (internal standard). The half-life and clearance of C60 was determined by analysing the quantity of C60 contained in the supernatant by LC-MS/MS (Agilent Rapid Resolution HPLC, AB SCIEX 4000 QTRAP MS) [274].

7.2.16. *In vivo* studies

7.2.16.1. *In vivo* toxic side effect study

In order to confirm the suitability of C60 for *in* vivo studies in nude mice, toxic side effects of C60 was investigated. Low (10 µg/g), intermediate (30 µg/g) and high (50 µg/g) doses of C60 in PBS were tested and 7.5% DMSO in PBS served as control. 24 mice were randomised into three experimental groups and a control group of 6 mice each. Animals were injected intraperitoneally twice a week for a period of 28 days. Animals were monitored daily for their wellbeing while body mass was monitored four times a week. Mice were euthanised at the end of the study using halothane overdose. An animal technician from the UCT animal unit carried out the autopsies to determine if the drug caused any internal toxic effects.

Signs of toxicity investigated include liver enlargement, inflammation, adherence of organs to each other, discolouration and deposits and the site of injection. The liver of each mouse was excised and weighed.

7.2.16.2. *In vivo* tumour formation assay

Tumourigenesis assay was carried out using cervical (HeLa S3 and CaSki) and oesophageal (WHCO6 and KYSE 30) cancer cell lines. 5 million cells were injected via the subcutaneous route into the hind flank of nude mice. Cells were prepared for inoculation by culturing them in 15 cm dishes until they reached 70-80% confluency. Cells were harvested using trypsin, washed twice with warm PBS and resuspended in PBS to a concentration of 10000 cells/µL. 500 µL of cell suspension was injected subcutaneously into the hind flank of each nude mouse. The mice were monitored daily for welfare and tumour development. Tumour was allowed to reach a palpable size of 5 mm before the commencement of treatment. Tumour formation in KYSE 30, WHCO6 and CaSki cells took approximately 5, 10 and 48 days respectively. Tumour length and width were measured using a digital caliper. Tumour volume was calculated using the formula:

$$\textit{Tumour volume } (mm^3) = \boldsymbol{length} \times \boldsymbol{width} \times \boldsymbol{width}/2$$

7.2.16.3. Tumourigenesis assay

When tumour size reached 5 mm, tumour-bearing mice of each cancer type were randomised into two groups of 6 each. Mice were injected via the intraperitoneal route with either 7.5% DMSO in PBS (vehicle control) or 10 µg/g C60 twice a week for 28 days. Tumour volume was measured on the first day of treatment (Day 0) and twice a week subsequently

using a digital caliper. At the end of each study, tumour-bearing animals were euthanised, following which their tumours excised, weighed, and pictures were taken. Extracted tumours were fixed in formalin to be used for further analysis using immunohistochemistry technique.

7.2.17. Protein purification and small molecule binding kinetics

7.2.17.1. GST-Kpnβ1 protein induction

10 mL *E. coli* starter culture using TB (Terrific Broth) containing 60 µg/mL Ampicillin (Sigma Aldrich) and pGEX-6P1-Kpnβ1 was grown for about 16 hours before transferring to 1 L culture containing Ampicillin in an orbital shaker incubator (LM-510, YIHDER,Taiwan) at 200 rpm. OD_{600} reading was monitored until it reached ˜0.6 before stimulation was done overnight with 0.1 mM IPTG (Dioxane free, Promega). Prior to IPTG stimulation, 100 µL of unstimulated lysate was stored for downstream comparison to IPTG-stimulated sample (crude). The following day, bacteria pellet was collected after centrifugation at 7700 x G for 10 minutes at 4 ˚C. Bacteria pellet was stored at – 80 ˚C for 1 week.

7.2.17.2. Kpnβ1 protein purification using Glutathione spin column

Bacteria pellet stored at – 80 ˚C was allowed to thaw on ice while pre-chilling equilibration/wash buffer (see solutions section). Bacteria pellet was resuspended in 5 mL of equilibration buffer. Three cycles of freeze thawing on liquid nitrogen was done prior to sonication on ice. Centrifugation was done at 12000 x G for 10 minutes at 4 ˚C. Crude lysate was added to the resin (Pierce Glutathione Spin Columns, 1mL resin bed, Thermoscientific,

Rockford, IL, USA) placed on a rotator and kept in the cold room (4 ˚C) for 2 hours. Elution of flow-through and washes were done using a solution of ice-cold equilibration buffer. After washing stage, 2 mL of elution buffer was added to the spin column and HRV 3C Protease (Thermoscientific, Rockford, IL, USA) was added to the mix to cleave off the GST-tagged to Kpnβ1. Incubation was done in the cold room (4 ˚C) overnight. Purified Kpnβ1 protein was eluted after centrifugation and stored at – 80 ˚C.

To elute GST-Kpnβ1, reduced glutathione was included in the equilibration buffer with the absence of HRV 3C protease after the washing steps. Purified GST-Kpnβ1 was stored at – 80 ˚C. Purified protein alongside flowthrough and washes were electrophoresed using SDS-PAGE and stained with coomassie brilliant blue to determine the efficiency of purification. Different concentrations of BSA were electrophoresed alongside the purified protein to determine protein concentration using Image J software.

7.2.17.3. Protein-Small molecule kinetics assay

I. Binding kinetics using GST-Biosensors

Purified GST-Kpnβ1 protein was concentrated and reduced glutathione contained in elution buffer was removed using Amicon ultra 30 KDa spin column (Merck Millipore, Ireland). Concentration was determined using BSA standards. GST-biosensors were hydrated in 200 µL of ligand buffer (Equilibration buffer) contained in a 96-well black, flat-bottom microplate. 200 µL of assay reagents, which are ligand (GST-Kpnβ1), GST-Kpnβ1 assay buffer and the various concentrations of C60 were transferred into the appropriate wells of a black polypropylene assay microplate. Sensor hydration plate was aligned to assay microplate

before the commencement of the kinetics assay. Analysis of data was done using the Octet FortéBio analysis software.

II. Binding kinetics using Super Streptavidin Biosensors

The binding interaction between purified Kpnβ1 (without GST tag) and C60 was investigated using Super Streptavidin (SSA) biosensors. Purified Kpnβ1 was concentrated prior to buffer exchange into PBS using desalting spin columns (2 mL Zeba desalting spin column, ThermoScientific) to remove primary amines such as Tris or glycine. Kpnβ1 in PBS was then biotinylated (EZ-Link NHS-PEG_4-Biotin, ThermoScientific) according to the manufacturer's instruction. Removal of excess biotin was done using a desalting column. Biotinylated Kpnβ1 was used for SSA binding kinetics. SSA-biosensors were hydrated in 200 µL of ligand buffer (PBS) contained in a 96-well black, flat-bottom microplate. 200 µL of assay reagents, which are ligand (Kpnβ1), Kpnβ1 assay buffer and the various concentrations of C60 were transferred into the appropriate wells of a black polypropylene assay microplate. Sensor hydration plate was aligned to assay microplate before the commencement of the kinetics assay. Analysis of data was done using the Octet FortéBio analysis software.

7.2.18. Statistical analysis

Experiments were performed in triplicates or quadruplicates and expressed as mean ± standard error of mean (SEM) unless stated otherwise. All *in vitro* experiments were performed at least two independent times. Data analysis was done using the student's t-test (paired) and a p-value of <0.05 was considered statistically significant. For the i*n vivo* animal study, changes in the body mass of mice and liver mass were analysed using the non-

parametric Mann-Whitney U test, and a p-value of <0.05 was considered statistically significant.

7.3. Solutions

7.3.1. Tissue culture solutions

Trypsin-EDTA (1 L)
0.5 g Trypsin
8 g NaCl
0.2 g KCl
1.45 g Na_2HPO_4 .$2H_2O$
0.2 g KH_2PO_4
10 mM EDTA, pH 8.0
Up to 1 L with PBS

Cell freezing media
90% complete DMEM with P/S (Penicillin/Streptomycin)
10% DMSO

10 X PBS
40 g NaCl
1 g KCl
1 g KH_2PO_4
5.75 g $Na_2HPO_4.7H_2O$
Up to 500 mL with dH_2O
Autoclave

MTT (5 mg/mL)
100 mg MTT
20 L 1 X PBS
Vortex and incubate at 37 ˚C for 15 minutes
Wrap in foil and store at 4 ˚C for up to a month

Solubilisation Solution
25 g SLS
Add 76.6 µL concentrated HCl
Up to 250 mL with dH_2O

Colony fixation solution (160 mL)
Acetic acid (20 mL)
Methanol (140 mL)

Crystal violet 0.5% solution (100 mL)
500 mg crystal violet
25 mL methanol
75 mL dH_2O

7.3.2. Protein solutions

RIPA Buffer
150 mM Sodium Chloride
1 % Triton X-100
1 % Sodium Deoxycholate
0.1 % SDS
10 mM Tris-Cl, pH 7.4

Complete RIPA Buffer
1 mM Na_3VO_4
1 mM NaF
1 X Protease inhibitor cocktail (Roche)

Harvest buffer (Nuclear and cytoplasmic fractionation- 10 mL)
1.72 g Sucrose
100.5 µL 1 M HEPES pH 7.9
502 µL 1 M NaCl
2 µL 500 mM EDTA
50 µL Triton X-100
Up to 10 mL with dH_2O

Buffer A (Nuclear and cytoplasmic fractionation-10 mL)
100 µL 1 M HEPES pH 7.9
100 µL 1 M KCl
2 µL 500 mM EDTA
2 µL 500 mM EGTA
100 µL 0.1 M Na_2VO_3
1 mL 10 X protease inhibitor cocktail
Up to 10 mL with dH_2O

Buffer C (Nuclear and cytoplasmic fractionation-10 mL)
100 µL 1 M HEPES pH 7.9
5 mL 1 M NaCl

10 µL 100 mM EDTA
10 µL 100 mM EGTA
200 µL 5 % NP-40
100 µL 0.1 M Na_2VO_3
1 mL 10 X protease inhibitor cocktail
Up to 10 mL with dH_2O

10 % APS

0.1 g APS
1 mL dH_2O

10 % SDS

20 g SDS
Up to 200 mL with dH_2O (stir on low heat)

1M Tris

60.5 g Tris
300 mL dH_2O
pH with concentrated HCl to desired pH of 6.8 or 8.8
make up to 500 mL with dH_2O

4% Stacking Gel

3.65 mL dH_2O
0.625 mL 1M Tris-Cl pH 6.8
50 µL 10 % SDS
0.65 mL 30 % Acrylamide
60 uL 10 % Ammonium Persulphate (APS)
6 µL TEMED

10 % Separating Gel

2.75 mL dH_2O
3.75 mL 1M Tris-Cl pH 8.8
100 µL 10 % SDS
3.35 mL 30 0% Acrylamide
200 µL 10 % Ammonium Persulphate (APS)
20 µL TEMED

12.5% Separating Gel
5.3 mL dH_2O
5.85mL 1 M Tris-Cl pH 8.8
156.25 µL 10% SDS
4.22 mL 30 % Acrylamide
312.5 µL 10 % Ammonium Persulphate (APS)
31.25 µL TEMED

15 % Separating Gel
2.3 mL dH_2O
2.5 mL 1 M Tris-Cl pH 8.8
100 µL 10 % SDS
5mL 30 % Acrylamide
100 µL 10 % Ammonium Persulphate (APS)
31.25 µL TEMED

4 X Laemmli loading dye (10 mL)
4 mL Glycerol
0.5 mL 0.1% Bromophenol Blue
2.5 mL 1 M Tris-Cl pH 6.8
3 mL 20 % SDS
10 µL 100 % β-mercaptoethanol
Before use, 50 µL of β-mercaptoethanol was added to 450 µL of the dye solution. Solution was kept at room temperature for a maximum period of 1 month

10 X Running Buffer (500 mL)
20 g Glycine
31.6 g Tris
50 mL 10% SDS
Up to 500 mL with dH_2O

1 X Running Buffer
100 mL 10 X Running Buffer
900 mL dH_2O

10 X Transfer Buffer (500 mL)
72 g Glycine
19 g Tris
Up to 500 mL with dH_2O

1 X Transfer Buffer
100 mL 10X Transfer Buffer
200 mL Methanol
700 mL dH_2O

10 X TBS (1 L)
24.23 g Tris
80.06 g NaCl
Adjust pH to 7.6 with concentrated HCl
Up to 1000 mL with dH_2O

1 X TBST
100 mL 10X TBS
900 mL dH_2O
1 mL Tween 20

7.3.3. Flow cytometry solutions

FACS Staining Solution
0.1% Triton X-100
2 mM $MgCl_2$
100 mM NaCl
10 mM PIPES, pH 6.8
10 µg/mL Propidium Iodide

1 M $MgCl_2$
40.66 g $MgCl_2$
200 mL of dH_2O

0.1 M PIPES pH 6.8
6.05 g PIPES
200 mL of dH_2O

5 M NaCl
58.44 g NaCl
200 mL of dH_2O

7.3.4. Immunofluorescence solutions

4% Paraformaldehyde
40 g paraformaldehyde
900 mL PBS
Heat to about 60 ˚C with constant stirring
Clear solution by adding by adding 1 N NaOH in a drop wise manner
Make up to 1 L with PBS
Filter sterilize

0.25% Triton X100 in PBS (250 mL)
625 µL Triton X 100 in 1 X PBS

0.1% PBST (250 mL)
250 µL Tween 20 in 1 X PBS

1% BSA in PBST (100 mL)

1g BSA in PBST

1% BSA in PBST + 0.3 M Glycine (50 mL)
1.1.26 g Glycine in 1% BSA + PBST

Mowiol Mounting Solution
2.4 g Mowiol-488
6 g Glycerol
6 mL dH_2O
Stir vigorously
12 mL 200 mM Tris-Cl, pH 8.5
Heat to about 60 ˚C with constant stirring
Centrifuge at 5000 x G for 15 minutes, collect supernatant into new tube
Store at -20 ˚C

Mowiol Mounting Solution (with anti-fade)
Add very little amount of N-propyl gallate (anti-fade) to 1 mL already thawed Mowiol
Heat at 37 ˚C overnight to dissolve
Spin before use to sediment undissolved anti-fade
Store at 4 ˚C (discard once Mowiol has yellowish colour)

7.3.5. Protein purification solutions

Terrific Broth (1 L)
12 g tryptone
24 g yeast extract
4 mL glycerol
Make up to 900 µL with dH_2O
Autoclave and allow to cool
Add 100 mL of autoclaved 0.17 M KH_2PO_4 and 0.72M K_2HPO_4

Equilibration/Wash Buffer (200 mL)
50 mM Tris
150 mM NaCl
150 mL dH_2O
Adjust pH to 8.0 with HCl
Make up to 200 mL with dH_2O

Elution Buffer
50 mM Tris
150 mM NaCl
150 mL dH_2O
Adjust pH to 8.0 with HCl
Make up to 200 mL with dH_2O
Add 10 mM reduced glutathione before use

GST-Kpnβ1 assay buffer
Equilibration/wash buffer
0.02% Tween 20
1% DMSO

Kpnβ1 assay buffer
1 X PBS
0.02% Tween 20
1% DMSO

Coomassie Blue Staining (1 L)
0.5 g coomassie brilliant blue
500 mL methanol
100 mL acetic acid
400 mL dH_2O

Destaining Solution (1 L)
50 mL methanol
70 mL acetic acid
Make up to 1 L with dH_2O

7.3.6. Others

0.5 M EDTA
186.12 g Na_2 EDTA-$2H_2O$
800 mL dH_2O
Adjust to pH 8.0 with NaOH
Make up to 1 L with dH_2O
Autoclave

0.5 M EGTA
190.18 g EGTA
800 mL dH_2O
Adjust to pH 8.0 with NaOH
Make up to 1 L with dH_2O
Autoclave

1 M Tris-Cl
121 g Tris
800 mL dH_2O
Adjust to pH 8.0 with conc. HCl
Make up to 1 L with dH_2O
Autoclave

1 M HEPES
238.80 g HEPES
800 mL dH_2O
Adjust to desired pH using KOH pellets
Up to 1 L with dH_2O
Filter sterilize

7.3.7. Fluorophores

Maximum excitation and emission wavelengths

Fluorophore	Maximum excitation wavelength (nm)	Maximum excitation wavelength (nm)
Cy3	548	561
PI (Propidium iodide)	540	620
DAPI	359	461
Alexa Fluor 488	495	519
DiI	549	565

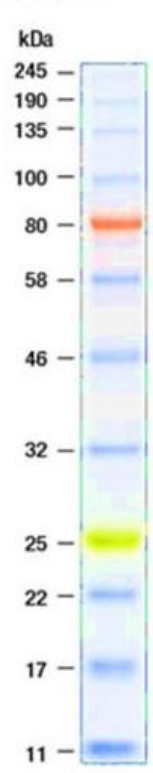

Figure 7.1. Protein molecular weight marker. Colour Prestained Protein Standard (11-245 kDa) was used to determine the molecular weight of proteins electrophoresed on 10-15% SDS-PAGE gels.

References

1. Hanahan D, Weinberg RA. The Hallmarks of Cancer. *Cell*. 2000;100:57-70.
2. Devi P. Basics of Carcinogenesis. *Heal Adm*. 2004;XVII(1):16-24. doi:10.1186/1471-2407-10-175.
3. Malarkey DE, Hoenerhoff M, Maronpot RR. Carcinogenesis: Mechanisms and manifestations. In: *Haschek and Rousseaux's Handbook of Toxicologic Pathology*. 3rd ed. Elsevier; 2013:107-146. doi:10.1016/B978-0-12-415759-0.00005-4.
4. Hanahan D, Weinberg RA. Hallmarks of cancer: The next generation. *Cell*. 2011;144(5):646-674.
5. WHO. Cancer. http://www.who.int/mediacentre/factsheets/fs297/en/. Published 2017. Accessed January 13, 2017.
6. Stewart BW, Wild CP. Rising burden of cancer-Prevention the key. *The Globe*. 2014;1(1):1-24. doi:10.1136/ip.2.2.84.
7. Ferlay J, Soerjomataram I, Dikshit R, et al. Cancer incidence and mortality worldwide : Sources , methods and major patterns in GLOBOCAN 2012. *Int J Cancer*. 2014;136:E359-E386. doi:10.1002/ijc.29210.
8. Stewart B, Wild CP. *Global Battle against Cancer Won't Be Won with Treatment Alone Effective Prevention Measures Urgently Needed to Prevent Cancer Crisis*.; 2014. doi:10.11600/1692715x.1113300812.
9. Ervik M, Lam F, Ferlay J, Mery L, I. Soerjomataram I, Bray F. Cancer today. International Agency for Research on Cancer. http://gco.iarc.fr/today. Published 2016. Accessed January 30, 2018.
10. Jordaan S, Michelow P, Richter K, Simoens C, Bogers J. A Review of Cervical Cancer in South Africa: Previous, Current and Future. *Heal Care Curr Rev*. 2016;4(4):1-6. doi:10.4172/2375-4273.1000180.
11. Nair S, Pillai MR. Human papillomavirus and disease mechanisms: Relevance to oral and cervical cancers. *Oral Dis*. 2005;11(6):350-359. doi:10.1111/j.1601-0825.2005.01127.x.
12. Jaisamrarn U, Castellsagué X, Garland SM, et al. Natural history of progression of HPV infection to cervical lesion or clearance: Analysis of the control arm of the large, randomised PATRICIA study. *PLoS One*. 2013;8(11):1-15.

doi:10.1371/journal.pone.0079260.

13. Castellsagué X, Schneider A, Kaufmann AM, Bosch FX. HPV vaccination against cervical cancer in women above 25 years of age: Key considerations and current perspectives. *Gynecol Oncol*. 2009;115:S15-S23. doi:10.1016/j.ygyno.2009.09.021.
14. Ibeanu OA. Molecular pathogenesis of cervical cancer. *Cancer Biol Ther*. 2011;11(3):295-306. doi:10.4161/cbt.11.3.14686.
15. Stanley MA. Human papillomavirus and cervical carcinogenesis. *Best Pract Res Clin Obstet Gynaecol*. 2001;15(5):663-676. doi:10.1016/S0140-6736(07)61416-0.
16. González Martín A. Molecular biology of cervical cancer. *Clin Transl Oncol*. 2007;9(6):347-354. doi:10.1007/s12094-007-0066-8.
17. Schlecht NF, Platt RW, Duarte-Franco E, et al. Human Papillomavirus Infection and Time to Progression and Regression of Cervical Intraepithelial Neoplasia. *J Natl Cancer Inst*. 2003;95(17):1336-1343. doi:10.1093/jnci/djg037.
18. Schellenbacher C, Roden RBS, Kirnbauer R. Developments in L2-based Human Papillomavirus (HPV) Vaccines. *Virus Res*. 2017;231:166-175. doi:10.1016/j.copsyc.2015.03.007.Current.
19. McCormack PL, Joura EA. Quadrivalent Human Papillomavirus Vaccine (Gardasil) Genital Lesions , Genital Cancer and Genital Warts in Women. *Drugs*. 2010;70(18):2449-2474.
20. Cox JT. The development of cervical cancer and its precursors: what is the role of human papillomavirus infection? *Curr Opin Obstet Gynecol*. 2006;18:S5-S13. doi:10.1097/01.gco.0000216315.72572.fb.
21. Ledwaba T, Dlamini Z, Naicker S, Bhoola S. Molecular genetics of human cervical cancer: Role of papillomavirus and the apoptotic cascade. *Biol Chem*. 2004;385(8):671-682.
22. Zamanian-Azodi M, Rezaei-Tavirani M, Hasanzadeh H, et al. Introducing biomarker panel in esophageal, gastric, and colon cancers; a proteomic approach. *Gastroenterol Hepatol from Bed to Bench*. 2015;8(1):6-18.
23. Sakai M, Sohda M, Miyazaki T, et al. Significance of karyopherin-{alpha} 2 (KPNA2) expression in esophageal squamous cell carcinoma. *Anticancer Res*. 2010;30:851-856.
24. Kgomo M, Elnagar A, Nagel J, Mokoena T. Prevalence of squamous cell carcinoma of the esophagus in a single tertiary center of South Africa: a cross sectional analytic

study. *J Public Health Africa*. 2017;8(563):72-73. doi:10.4081/jphia.2017.

25. Herbst MC. *Fact Sheet on Oesophageal Cancer*.; 2014.
26. Terry Priestman. *Cancer Chemotherapy in Clinical Practice*. Vol 1. London: Springer-Verlag London Limited; 2012. doi:10.1007/978-0-85729-727-3.
27. Absi A, Adelstein DJ, Rice T. Esophageal cancer. Disease management. https://www.clevelandclinicmeded.com/medicalpubs/diseasemanagement/hematology-oncology/esophageal-cancer/. Published 2010. Accessed May 25, 2016.
28. Cancer Council Australia. *Understanding Stomach and Oesophageal Cancer*. 2nd ed. (Wuellner L, ed.). Cancer council Australia; 2013. http://www.cancervic.org.au/downloads/booklets/Stomach-Oesophageal-cancer.pdf.
29. Melhado RE, Alderson D, Tucker O. The changing face of esophageal cancer. *Cancers (Basel)*. 2010;2(3):1379-1404. doi:10.3390/cancers2031379.
30. Pacella-Norman R, Urban MI, Sitas F, et al. Risk factors for oesophageal, lung, oral and laryngeal cancers in black South Africans. *Br J Cancer*. 2002;86(11):1751-1756. doi:10.1038/sj.bjc.6600338.
31. Kahrilas PJ. Gastroesophageal Reflux Disease. *N Engl J Med*. 2008;359(16):1700-1707. doi:10.1016/j.suc.2011.06.004.
32. Howden CW, Chey WD. Gastroesophageal Reflux Disease. *J Fam Pract*. 2003;52(3):240-248.
33. American Cancer Society. *Esophagus Cancer Overview*.; 2014. https://old.cancer.org/acs/groups/cid/documents/webcontent/003049-pdf.pdf.
34. Ullah MF, Aatif M. The footprints of cancer development: Cancer biomarkers. *Cancer Treat Rev*. 2009;35(3):193-200. doi:10.1016/j.ctrv.2008.10.004.
35. Meany DL, Sokoll LJ, Chan DW. Early detection of cancer: Immunoassays for plasma tumor markers. *Expert Opin Diagn*. 2009;3(6):597-605. doi:10.1517/17530050903266830.Early.
36. Shen Z. Cancer biomarkers and targeted therapies. *Cell Biosci*. 2013;3(6):1-2. doi:10.1186/2045-3701-3-6.
37. Sharma S V, Settleman J. Oncogene addiction : setting the stage for molecularly targeted cancer therapy. 2007:3214-3231. doi:10.1101/gad.1609907.
38. Ke X, Shen L. Molecular targeted therapy of cancer: The progress and future prospect. *Front Lab Med*. 2017;1:69-75. doi:10.1016/j.flm.2017.06.001.

39. Padma VV. An overview of targeted cancer therapy. *BioMedicine*. 2015;5(4):1-6. doi:10.7603/s40.
40. Hoelder S, Clarke PA, Workman P. Discovery of small molecule cancer drugs: Successes, challenges and opportunities. *Mol Oncol*. 2012;6(2):155-176. doi:10.1016/j.molonc.2012.02.004.
41. Bozic I, Allen B, Nowak MA. Dynamics of targeted cancer therapy. *Trends Mol Med*. 2012;18(6):311-316.
42. Chari RVJ. Targeted Cancer Therapy : Conferring Specificity to Cytotoxic Drugs. *Acc Chem Res*. 2008;41(1):98-107.
43. Gerber DE. Targeted therapies: A new generation of cancer treatments. *Am Fam Physician*. 2008;77(3):311-319.
44. Sawyers C. Targeted cancer therapy. *Nature*. 2004;432:294-297. doi:10.1038/nature03095.
45. Nicolaides NC, O'Shannessy DJ, Albone E, Grasso L. Co-development of diagnostic vectors to support targeted therapies and theranostics: essential tools in personalized cancer therapy. *Front Oncol*. 2014;4(141):1-14. doi:10.3389/fonc.2014.00141.
46. Vora C, Gupta S. Targeted therapy in cervical cancer. *ESMO Open*. 2019;3:1-8. doi:10.1136/esmoopen-2018-000462.
47. Menderes G, Black J, Schwab CL, Santin AD. Immunotherapy and targeted therapy for cervical cancer : an update. *Expert Rev Anticancer Ther*. 2015;7140. doi:10.1586/14737140.2016.1121108.
48. Kumar L, Harish P, Malik PS, Khurana S. Chemotherapy and Targeted Therapy in the Management of Cervical Cancer. *Curr Probl Cancer*. 2018:1-19. doi:10.1016/j.currproblcancer.2018.01.016.
49. Tambaro R, Scambia G, Di M, et al. The role of chemotherapy in locally advanced , metastatic and recurrent cervical cancer. *Oncol Hematol*. 2004;52:33-44. doi:10.1016/j.critrevonc.2004.05.003.
50. Xu C, Lin SH. Esophageal cancer : comparative effectiveness of treatment options. *Dove Press*. 2016;6:1-12.
51. Janmaat VT, Steyerberg EW, van der Gaast A, et al. Palliative chemotherapy and targeted therapies for esophageal and gastroesophageal junction cancer (Review). *Cochrane Database Syst Rev*. 2017;(11).

doi:10.1002/14651858.CD004063.pub4.www.cochranelibrary.com.

52. Tew WP, Kelsen DP, Ilson DH. Targeted Therapies for Esophageal Cancer. *Oncologist*. 2005;10:590-601.

53. Abdo J, Agrawal DK, Mittal SK. " Targeted " Chemotherapy for Esophageal Cancer. *Front Oncol*. 2017;7(63):1-4. doi:10.3389/fonc.2017.00063.

54. Bachtiary B, Boutros PC, Pintilie M, et al. Gene expression profiling in cervical cancer: An exploration of intratumor heterogeneity. *Clin Cancer Res Cancer Res*. 2006;12(19):5632-5640. doi:10.1158/1078-0432.CCR-06-0357.

55. Van Der Watt PJ, Maske CP, Hendricks DT, et al. The karyopherin proteins, Crm1 and Karyopherin B1, are overexpressed in cervical cancer and are critical for cancer cell survival and proliferation. *Int J Cancer*. 2009;124:1829-1840. doi:10.1002/ijc.24146.

56. Alizadeh AA, Eisen MB, Davis RE, et al. Distinct types of diffuse large B-cell lymphoma identified by gene expression profiling. *Nature*. 2000;403(6769):503-511. doi:10.1038/35000501.

57. Xiang Y-J, Fu Q-Y, Ma Z-B, et al. Screening for candidate genes related to breast cancer with cDNA microarray analysis. *Chronic Dis Transl Med*. 2015;1(2):65-72. doi:10.1016/j.cdtm.2015.02.001.

58. Yin G, Zhuo W, Zhao Y, et al. Converting a microarray signature into a diagnostic test: A trial of custom 74 gene array for clarification and prediction the prognosis of gastric cancer. *PLoS One*. 2013;8(12):1-8. doi:10.1371/journal.pone.0081561.

59. Mosammaparast N, Pemberton LF. Karyopherins: From nuclear-transport mediators to nuclear-function regulators. *Trends Cell Biol*. 2004;14(10):547-556. doi:10.1016/j.tcb.2004.09.004.

60. Forbes DJ, Travesa A, Nord MS, Bernis C. Nuclear transport factors: global regulation of mitosis. *Curr Opin Cell Biol*. 2015;35:78-90. doi:10.1016/j.ceb.2015.04.012.Nuclear.

61. Hung M-C, Link W. Protein localization in disease and therapy. *J Cell Sci*. 2011;124(20):3381-3392. doi:10.1242/jcs.089110.

62. Nakielny S, Dreyfuss G. Transport of Proteins and RNAs in and out of the Nucleus. *Cell*. 1999;99(7):677-690. doi:10.1016/S0092-8674(00)81666-9.

63. Kau TR, Way JC, Silver PA. Nuclear transport and cancer: from mechanism to intervention. *Nat Rev Cancer*. 2004;4:106-117. doi:10.1038/nrc1274.

64. Chahine MN, Pierce GN. Therapeutic targeting of nuclear protein import in

pathological cell conditions. *Pharmacol Rev*. 2009;61(3):358-372. doi:10.1124/pr.108.000620.

65. van der Watt P, Stowell C, Leaner V. The nuclear import receptor KpnB1 and its potential as an anti-cancer therapeutic target. *Crit Rev Eukaryot Gene Expr*. 2013;23(1):1-24.
66. Sorokin A V, Kim ER, Ovchinnikov LP. Nucleocytoplasmic transport of proteins. *Biochem*. 2007;72(13):1439-1457. doi:10.1007/s12250-010-3099-z.
67. Rout MP, Aitchison JD. The Nuclear Pore Complex as a Transport Machine *. *J Biol Chem*. 2001;276(20):16593-16596. doi:10.1074/jbc.R100015200.
68. Wente SR, Rout MP. The Nuclear Pore Complex and Transport. *Cold Spring Harb Perspect Biol*. 2010;2:1-19.
69. Wa S, Kehlenbach RH. The Part and the Whole : functions of nucleoporins in nucleocytoplasmic transport. *Trends Cell Biol*. 2010;20(8):461-469. doi:10.1016/j.tcb.2010.05.001.
70. Pemberton LF, Paschal BM. Mechanisms of receptor-mediated nuclear import and nuclear export. *Traffic*. 2005;6(3):187-198. doi:10.1111/j.1600-0854.2005.00270.x.
71. He S, Miao X, Wu Y, et al. Upregulation of nuclear transporter, KpnB1, contribute to accelerated cell proliferation and cell adhesion-mediated drug resistance (CAM-DR) in diffuse large B-cell lymphoma. *J cancer Res Clin Oncol*. 2015;142(3):562-572. doi:10.1007/s00432-015-2057-4.
72. Goldfarb DS, Corbett AH, Mason DA, Harreman MT, Adam SA. Importin alpha: a multipurpose nuclear-transport receptor. *Trends Cell Biol*. 2004;14(9):505-514. doi:10.1016/j.tcb.2004.07.016.
73. van der Watt PJ, Ngarande E, Leaner VD. Overexpression of KpnB1 and Kpna2 importin proteins in cancer derives from deregulated E2F activity. *PLoS One*. 2011;6(11):1-10. doi:10.1371/journal.pone.0027723.
74. Chook YM, Suel KE. Nuclear import by Karyopherin- β s : recognition and inhibition. *Biochim Biophys Acta*. 2011;1813(9):1593-1606. doi:10.1016/j.bbamcr.2010.10.014.Nuclear.
75. Lee SJ, Imamoto N, Sakai H, et al. The adoption of a twisted structure of importin-beta is essential for the protein-protein interaction required for nuclear transport. *J Mol Biol*. 2000;302(1):251-264. doi:10.1006/jmbi.2000.4055.

76. Azmi AS. Unveiling the Role of Nuclear Transport in Epithelial-to-Mesenchymal Transition. *Curr cancer drugs targets*. 2013;13:906-914.
77. Yuh MC, Blobel G. Karyopherins and nuclear import. *Curr Opin Struct Biol*. 2001;11(6):703-715. doi:10.1016/S0959-440X(01)00264-0.
78. Stelma T, Chi A, Van Der Watt PJ, Verrico A, Lavia P, Leaner VD. Targeting nuclear transporters in cancer: Diagnostic, prognostic and therapeutic potential. *IUBMB Life*. 2016;68(4):268-280. doi:10.1002/iub.1484.
79. Adam EJH, Adam SA. Identification of cytosolic factors required for nuclear location sequence-mediated binding to the nuclear envelope. *J Cell Biol*. 1994;125(3):547-555. doi:10.1083/jcb.125.3.547.
80. Chi NC, Adam EJH, Adam SA. Sequence and characterization of cytoplasmic nuclear protein import factor p97. *J Cell Biol*. 1995;130(2):265-274. doi:10.1083/jcb.130.2.265.
81. Moroianu J. Nuclear import and export pathways. *J Cell Biochem*. 1999;Suppl 32-3:76-83.
82. Görlich D. Nuclear protein import. *Curr Opin Cell Biol*. 1997;9(3):412-419. doi:10.1016/S0955-0674(97)80015-4.
83. Cautain B, Hill R, De Pedro N, Link W. Components and regulation of nuclear transport processes. *FEBS J*. 2015;282(3):445-462. doi:10.1111/febs.13163.
84. Lange A, Mills RE, Lange CJ, Stewart M, Devine SE, Corbett AH. Classical nuclear localization signals: Definition, function, and interaction with importin a. *J Biol Chem*. 2007;282(8):5101-5105. doi:10.1074/jbc.R600026200.
85. Pumroy RA, Cingolani G. Diversification of importin-a isoforms in cellular trafficking and disease states. *Biochem J*. 2015;466(1):13-28. doi:10.1111/obr.12065.Variation.
86. Moroianu J. Distinct nuclear import and export pathways mediated by members of the karyopherin B family. *J Cell Biochem*. 1998;70(2):231-239. doi:10.1002/(SICI)1097-4644(19980801)70:2<231::AID-JCB9>3.0.CO;2-P.
87. Depping R, Jelkmann W, Kosyna FK. Nuclear-cytoplasmatic shuttling of proteins in control of cellular oxygen sensing. *J Mol Med*. 2015;93(6):599-608. doi:10.1007/s00109-015-1276-0.
88. Hutten S, Kehlenbach RH. CRM1-mediated nuclear export: to the pore and beyond. *Trends Cell Biol*. 2007;17(4):193-201. doi:10.1016/j.tcb.2007.02.003.

89. Turner JG, Dawson J, Cubitt CL, Baz R, Sullivan DM. Inhibition of CRM1-dependent nuclear export sensitizes malignant cells to cytotoxic and targeted agents. *Semin Cancer Biol*. 2014;27:62-73. doi:10.1016/j.semcancer.2014.03.001.

90. Nachury M V., Maresca TJ, Salmon WC, Waterman-Storer CM, Heald R, Weis K. Importin B is a mitotic target of the small GTPase ran in spindle assembly. *Cell*. 2001;104(1):95-106. doi:10.1016/S0092-8674(01)00194-5.

91. Jäkel S, Görlich D. Importin B, transportin, RanBP5 and RanBP7 mediate nuclear import of ribosomal proteins in mammalian cells. *EMBO J*. 1998;17(15):4491-4502. doi:10.1093/emboj/17.15.4491.

92. Rensen W, Lavia P. RAN (RAN, member RAS oncogene family). *Atlas Genet Cytogenet Oncol Haematol*. 2011;14(9):834-840. doi:10.4267/2042/44843.

93. Lui K, Huang Y. RanGTPase: A Key Regulator of Nucleocytoplasmic Trafficking. *Changes*. 2009;29(6):997-1003. doi:10.1016/j.biotechadv.2011.08.021.Secreted.

94. Rensen WM, Mangiacasale R, Ciciarello M, Lavia P. The GTPase Ran: regulation of cell life and potential roles in cell transformation. *Front Biosci*. 2008:4097-4121.

95. Gravina G, Senapedis W, McCauley D, Baloglu E, Shacham S, Festuccia C. Nucleo-cytoplasmic transport as a therapeutic target of cancer. *J Hematol Oncol*. 2014;7(85):1-9. doi:10.1186/s13045-014-0085-1.

96. Hill R, Cautain B, de Pedro N, Link W. Targeting nucleocytoplasmic transport in cancer therapy. *Oncotarget*. 2014;5(1):11-28. doi:10.18632/oncotarget.1457.

97. Kimura M, Imamoto N. Biological Significance of the Importin-B Family-Dependent Nucleocytoplasmic Transport Pathways. *Traffic*. 2014;15(7):727-748. doi:10.1111/tra.12174.

98. Hassanein M, Callison JC, Callaway-Lane C, Aldrich MC, Grogan EL, Massion PP. The state of molecular biomarkers for the early detection of lung cancer. *Cancer Prev Res*. 2012;5(8):992-1006. doi:10.1158/1940-6207.CAPR-11-0441.

99. Xia F, Lee CW, Altieri DC. Tumor cell dependence on Ran-GTP-directed mitosis. *Cancer Res*. 2008;68(6):1826-1833. doi:10.1158/0008-5472.CAN-07-5279.

100. Ouellet V, Guyot MC, Le Page C, et al. Tissue array analysis of expression microarray candidates identifies markers associated with tumor grade and outcome in serous epithelial ovarian cancer. *Int J Cancer*. 2006;119:599-607. doi:10.1002/ijc.21902.

101. Abe H, Kamai T, Shirataki H, Oyama T, Arai K, Yoshida KI. High expression of Ran

GTPase is associated with local invasion and metastasis of human clear cell renal cell carcinoma. *Int J Cancer*. 2008;122(10):2391-2397. doi:10.1002/ijc.23400.

102. Faustino RS, Nelson TJ, Terzic A, Perez-Terzic C. Nuclear transport: target for therapy. *Clin Pharmacol Ther*. 2007;81(6):880-886. doi:6100141 [pii]\r10.1038/sj.clpt.6100141.
103. Noske A, Weichert W, Niesporek S, et al. Expression of the nuclear export protein chromosomal region maintenance/exportin 1/Xpo1 is a prognostic factor in human ovarian cancer. *Cancer*. 2008;112(8):1733-1743. doi:10.1002/cncr.23354.
104. Liu X, Chong Y, Tu Y, et al. CRM1/XPO1 is associated with clinical outcome in glioma and represents a therapeutic target by perturbing multiple core pathways. *J Hematol Oncol*. 2016;9(108):1-14. doi:10.1186/s13045-016-0338-2.
105. Van Der Watt PJ, Zemanay W, Govender D, Hendricks DT, Parker MI, Leaner VD. Elevated expression of the nuclear export protein, Crm1 (exportin 1), associates with human oesophageal squamous cell carcinoma. *Oncol Rep*. 2014;32:730-738. doi:10.3892/or.2014.3231.
106. Ishizawa J, Kojima K, Hail N, Tabe Y, Andreeff M. Expression, function, and targeting of the nuclear exporter chromosome region maintenance 1 (CRM1) protein. *Pharmacol Ther*. 2015;153:25-35. doi:10.1016/j.pharmthera.2015.06.001.
107. Luo Y, Wang Z, Tian L, Li X. The function of importin β1 is conserved in eukaryotes but the substrates may vary in organisms. *Plant Signal Behav*. 2013;8(8):8-10. doi:10.4161/psb.25106.
108. Gasiorowski JZ, Dean D a. Mechanisms of nuclear transport and interventions. *Adv Drug Deliv Rev*. 2003;55:703-716.
109. Kosugi S, Hasebe M, Entani T, Takayama S, Tomita M, Yanagawa H. Design of Peptide Inhibitors for the Importin a / b Nuclear Import Pathway by Activity-Based Profiling. *Chem Biol*. 2008;15:940-949. doi:10.1016/j.chembiol.2008.07.019.
110. Parikh K, Cang S, Sekhri A, Liu D. Selective inhibitors of nuclear export (SINE)--a novel class of anti-cancer agents. *J Hematol Oncol*. 2014;7(78):1-8. doi:10.1186/s13045-014-0078-0.
111. Sun Q, Chen X, Zhou Q, et al. Inhibiting cancer cell hallmark features through nuclear export inhibition. *Signal Transduct Target Ther*. 2016;1:1-10. doi:10.1038/SIGTRANS.2016.10.
112. Gravina GL, Tortoreto M, Mancini A, et al. XPO1 / CRM1-Selective Inhibitors of

Nuclear Export (SINE) reduce tumor spreading and improve overall survival in preclinical models of prostate cancer (PCa). *J Hematol Oncol*. 2014;7(46):1-17.

113. Senapedis WT, Baloglu E, Landesman Y. Clinical translation of nuclear export inhibitors in cancer. *Semin Cancer Biol*. 2014;27:74-86. doi:10.1016/j.semcancer.2014.04.005.
114. Crochiere ML, Hannus S, Hansen K, et al. XPO1 target occupancy measurements confirm the selinexor recommended phase 2 dose. *Oncotarget*. 2017;8(66):110503-110516.
115. Wei XX, Siegel AP, Aggarwall R, et al. A Phase II Trial of Selinexor , an Oral Selective Inhibitor of Nuclear Export Compound , in Abiraterone- and / or Enzalutamide-Refractory Metastatic Castration-Resistant Prostate Cancer. *Oncol*. 2018;23:656-664. doi:10.1634/theoncologist.2017-0624.
116. Pollard VW, Michael WM, Nakielny S, Siomi MC, Wang F, Dreyfuss G. A novel receptor-mediated nuclear protein import pathway. *Cell*. 1996;86(6):985-994. doi:10.1016/S0092-8674(00)80173-7.
117. Liang P, Zhang H, Wang G, et al. KPNB1, XPO7 and IPO8 Mediate the Translocation of NF-kB/p65 into the Nucleus. *Traffic*. 2013;14(11):1132-1143. doi:10.1111/tra.12097.
118. Wiese C. Role of Importin-beta in Coupling Ran to Downstream Targets in Microtubule Assembly. *Science (80-)*. 2001;291(5504):653-656. doi:10.1126/science.1057661.
119. Marfori M, Mynott A, Ellis JJ, et al. Molecular basis for specificity of nuclear import and prediction of nuclear localization. *Biochim Biophys Acta - Mol Cell Res*. 2011;1813:1562-1577. doi:10.1016/j.bbamcr.2010.10.013.
120. Aggarwal A, Agrawal DK. Importins and exportins regulating allergic immune responses. *Mediators Inflamm*. 2014;2014:1-14. doi:10.1155/2014/476357.
121. Giubettini M, van der WP, Verrico A, de T V, Leaner V, Lavia P. KPNB1 (karyopherin (importin) beta 1). *Atlas Genet Cytogenet Oncol Haematol*. 2013;17(10):689-698. doi:10.4267/2042/51535.
122. Ström AC, Weis K. Importin-beta-like nuclear transport receptors. *Genome Biol*. 2001;2(6):REVIEWS3008. doi:10.1186/gb-2001-2-6-reviews3008.
123. Soderholm JF, Bird SL, Kalab P, et al. Importazole, a small molecule inhibitor of the transport receptor importin-B. *ACS Chem Biol*. 2011;6(7):700-708.

doi:10.1021/cb2000296.

124. Cimica V, Chen HC, Iyer JK, Reich NC. Dynamics of the STAT3 transcription factor: Nuclear import dependent on ran and importin-B1. *PLoS One*. 2011;6(5):1-11. doi:10.1371/journal.pone.0020188.

125. Muqbil I, Wu J, Aboukameel A, Mohammad RM, Azmi AS. Snail Nuclear Transport: the Gateways Regulating Epithelial-to- Mesenchymal Transition? *Semin Cancer Biol*. 2014;27:1-15. doi:10.1016/j.semcancer.2014.06.003.Snail.

126. Harel A, Forbes DJ. Importin beta: Conducting a much larger cellular symphony. *Mol Cell*. 2004;16(3):319-330. doi:10.1016/j.molcel.2004.10.026.

127. Angus L, Van der Watt PJ, Leaner VD. Inhibition of the nuclear transporter, Kpnß1, results in prolonged mitotic arrest and activation of the intrinsic apoptotic pathway in cervical cancer cells. *Carcinogenesis*. 2014;35(5):1121-1131. doi:10.1093/carcin/bgt491.

128. Zachariae U, Grubmüller H. Importin-β: Structural and Dynamic Determinants of a Molecular Spring. *Structure*. 2008;16(6):906-915. doi:10.1016/j.str.2008.03.007.

129. Zhu Z-C, Liu J-W, Li K, Zheng J, Xiong Z-Q. KPNB1 inhibition disrupts proteostasis and triggers unfolded protein response-mediated apoptosis in glioblastoma cells. *Oncogene*. 2018:1-17. doi:10.1038/s41388-018-0180-9.

130. Kuusisto H V, Jans DA. Hyper-dependence of breast cancer cell types on the nuclear transporter Importin β 1. *Biochim Biophys Acta*. 2015;1853(8):1870-1878. doi:10.1016/j.bbamcr.2015.05.002.

131. Yan W, Li R, He J, Du J, Hou J. Importin β1 mediates nuclear factor-κB signal transduction into the nuclei of myeloma cells and affects their proliferation and apoptosis. *Cell Signal*. 2015;27:851-859. doi:10.1016/j.cellsig.2015.01.013.

132. Yang L, Hu B, Zhang Y, et al. Suppression of the nuclear transporter-KPNB1 expression inhibits tumor proliferation in hepatocellular carcinoma. *Med Oncol*. 2015;32(4):128. doi:10.1007/s12032-015-0559-1.

133. Zhang P, Garnett J, Creighton CJ, et al. EZH2–miR-30d–KPNB1 pathway regulates malignant peripheral nerve sheath tumour cell survival and tumourigenesis. *J Pathol*. 2014;232(3):308-318. doi:10.1002/path.4294.EZH2.

134. Smith ER, Cai KQ, Smedberg JL, et al. Nuclear Entry of Activated MAPK Is Restricted in Primary Ovarian and Mammary Epithelial Cells. *PLoS One*. 2010;5(2):1-9.

doi:10.1371/journal.pone.0009295.

135. Kuusisto H V., Wagstaff KM, Alvisi G, Roth DM, Jans DA. Global enhancement of nuclear localization-dependent nuclear transport in transformed cells. *FASEB J*. 2012;26:1181-1193. doi:10.1096/fj.11-191585.

136. Xiao X, Li BX, Mitton B, Ikeda A, Sakamoto KM. Targeting CREB for cancer therapy: friend or foe. *Curr Cancer Drug Targets*. 2010;10(4):384-391. doi:10.2174/156800910791208535.

137. Forwood JK, Lam MH, Jans DA. Nuclear import of Creb and AP-1 transcription factors requires importin-beta 1 and Ran but is independent of importin-alpha. *Biochemistry*. 2001;40(17):5208-5217. doi:10.1021/bi002732+.

138. Zhu J, Wang Y, Huang H, et al. Upreguation of KpnB1 in gastric cancer cells promotes tumor cell proliferation and predicts poor prognosis. *Tumor Biol*. 2016;37(1):661-672.

139. Kodama M, Kodama T, Newberg JY, et al. In vivo loss-of-function screens identify KPNB1 as a new druggable oncogene in epithelial ovarian cancer. *PNAS*. 2017;114(35):1-10. doi:10.1073/pnas.1705441114.

140. Martens-de Kemp SR, Nagel R, Stigter-van Walsum M, et al. Functional Genetic Screens Identify Genes Essential for Tumor Cell Survival in Head and Neck and Lung Cancer. *Clin Cancer Res*. 2013;19(8):1994-2003. doi:10.1158/1078-0432.CCR-12-2539.

141. Sekimoto N, Suzuki Y, Sugano S. Decreased KPNB1 Expression is Induced by PLK1 Inhibition and Leads to Apoptosis in Lung Adenocarcinoma. *J Cancer*. 2017;8(19):4125-4140. doi:10.7150/jca.21802.

142. van der Watt PJ, Chi A, Stelma T, et al. Targeting the nuclear import receptor, KpnB1 as an anti-cancer therapeutic. *Mol Cancer Ther*. 2016:1-14. doi:doi: 10.1158/1535-7163.MCT-15-0052.

143. Torgerson TR, Colosia AD, Donahue JP, Lin Y, Hawiger J. Regulation of NF-κB, AP-1, NFAT, and STAT1 Nuclear Import in T Lymphocytes by Noninvasive Delivery of Peptide Carrying the Nuclear Localization Sequence of NF-kappa B p50. *J Immunol*. 1998;161:6084-6092. http://www.ncbi.nlm.nih.gov/pubmed/9834092.

144. Lin Y-Z, Yao S, Veach RA, Torgerson TR, Hawiger J. Inhibition of nuclear translocation of transcription factor NFKB by a synthetic peptide containing a cell membrane permeable motif and nuclear localisation sequence. *J Biol Chem*. 1995;270(24):14255-14258.

145. Mahipal A, Malafa M. Importins and exportins as therapeutic targets in cancer. *Pharmacol Ther*. 2016;164:135-143. doi:10.1016/j.pharmthera.2016.03.020.
146. Wagstaff KM, Sivakumaran H, Heaton SM, Harrich D, Jans DA. Ivermectin is a specific inhibitor of importin α/β-mediated nuclear import able to inhibit replication of HIV-1 and dengue virus. *Biochem J*. 2012;443:851-856. doi:10.1042/BJ20120150.
147. Ambrus G, Whitby LR, Singer EL, et al. Small molecule peptidomimetic inhibitors of importin α/β mediated nuclear transport. *Bioorganic Med Chem*. 2010;18(21):7611-7620. doi:10.1016/j.bmc.2010.08.038.Small.
148. Moroianu J, Blobel G, Radu A. Nuclear protein import: Ran-GTP dissociates the karyopherin alphabeta heterodimer by displacing alpha from an overlapping binding site on beta. *Proc Natl Acad Sci U S A*. 1996;93:7059-7062. doi:10.1073/pnas.93.14.7059.
149. Lee SJ, Sekimoto T, Yamashita E, et al. The structure of importin beta bound to SREBP 2: nuclear import of a transcription factor. *Science (80-)*. 2003;302(5650):1571-1575. doi:10.1126/science.1088372.
150. Stelma T, Leaner VD. KPNB1-mediated nuclear import is required for motility and inflammatory transcription factor activity in cervical cancer cells. *Oncotarget*. 2017;8(20):32833-32847.
151. Sangshetti, JN Altamash Ahmad A, Khan F, Zaheer Z. Synthesis and biological activities of substitutes Benzoxazepine. *Mini Rev Org Chem*. 2015;12(4):345-354.
152. Dwivedi SKD, Samanta K, Yadav M, et al. Amino acids derived benzoxazepines: design, synthesis and antitumor activity. *Bioorg Med Chem Lett*. 2013;23(24):6816-6821. doi:10.1016/j.bmcl.2013.10.013.
153. Samanta K, Chakravarti B, Mishra JK, et al. Anti-tumor activity of a new series of benzoxazepine derivatives in breast cancer. *Bioorg Med Chem Lett*. 2010;20(1):283-287. doi:10.1016/j.bmcl.2009.10.115.
154. Kendre B V., Landge MG, Bhusare SR. Synthesis and biological evaluation of some novel pyrazole, isoxazole, benzoxazepine, benzothiazepine and benzodiazepine derivatives bearing an aryl sulfonate moiety as antimicrobial and anti-inflammatory agents. *Arab J Chem*. 2013. doi:10.1016/j.arabjc.2015.01.007.
155. Fiore D, Proto MC, Pisanti S, et al. Antitumor effect of pyrrolo-1,5-benzoxazepine-15 and its synergistic effect with oxaliplatin and 5-FU in colorectal cancer cells. *Cancer*

Biol Ther. 2015;17(8):849-858.

156. Ferreira D, Adega F, Chaves R. The Importance of Cancer Cell Lines as in vitro Models in Cancer Methylome Analysis and Anticancer Drugs Testing. *Oncogenomics Cancer Proteomics- Nov Approaches Biomarkers Discov Ther Targets Cancer*. 2013:139-166. doi:http://dx.doi.org/10.5772/53110.
157. Mouton JW, Dudley MN, Cars O, Derendorf H, Drusano GL. Standardization of pharmacokinetic/pharmacodynamic (PK/PD) terminology for anti-infective drugs: an update. *J Antimicrob Chemother*. 2005;55:601-607. doi:10.1093/jac/dki079.
158. Wardihan, Rusdi M, Alam G, Manggau MA. Selective Cytotoxicity Evaluation in Anticancer Drug Screening of Boehmeria virgata (Forst) Guill Leaves to sveral human cell lines: HeLa, WiDr, T4D7 and Vero. *Dhaka Univ J Pharm Sci*. 2013;12(2):87-90.
159. Liu M, Qi Z, Liu B, et al. {RY-2f,} an isoflavone analog, overcomes cisplatin resistance to inhibit ovarian tumorigenesis via targeting the {PI3K/AKT/mTOR} signaling pathway. *Oncotarget*. 2015;6(28):25281-25294. doi:10.18632/oncotarget.4634.
160. Munshi A, Hobbs M, Meyn RE. Clonogenic cell survival assay. *Methods Mol Med*. 2005;110:21-28. doi:10.1385/1-59259-869-2:021.
161. Guzmán C, Bagga M, Kaur A, Westermarck J, Abankwa D. ColonyArea: An ImageJ plugin to automatically quantify colony formation in clonogenic assays. *PLoS One*. 2014;9(3):1-9. doi:10.1371/journal.pone.0092444.
162. Shapiro, Geoffrey I., Harper WJ. Anticancer drug targets: cell cycle and checkpoint control. *J Clin Invest*. 1999;104(12):1645-1653. doi:10.3109/10409238.2011.575764.
163. Rastogi RP, Sinha RP. Apoptosis : Molecular mechanisms and pathogenicity. *EXCLI*. 2009:155-181.
164. Ke B, Tian M, Li J, Liu B, He G. Targeting Programmed Cell Death Using Small-Molecule Compounds to Improve Potential Cancer Therapy. *Med Res Rev*. 2016;00(0):1-53. doi:10.1002/med.
165. Tait SW, Green DR. Mitochondria and cell death: outer membrane permeabilization and beyond. *Nat Rev Mol Cell Biol*. 2008;11:621-632. doi:10.1038/nrm2952.
166. Fan TJ, Han LH, Cong RS, Liang J. Caspase family proteases and apoptosis. *Acta Biochim Biophys Sin (Shanghai)*. 2005;37(11):719-727. doi:10.1111/j.1745-7270.2005.00108.x.
167. Virag L, Csaba S. The Therapeutic Potential of Poly (ADP-Ribose). *Pharmacol Rev*.

2002;54(3):375-429.

168. Kaufmann SH, Desnoyers S, Ottaviano Y, Davidson NE, Poirier GG. Specific proteolytic cleavage of Poly (ADP-ribose) Polymerase : An early marker of chemotherapy induced apoptosis. *Cancer Res*. 1993;53:3976-3985.
169. Fujise K, Zhang D, Liu J -l., Yeh ETH. Regulation of Apoptosis and Cell Cycle Progression by MCL1: Differential role of proliferating cell nuclear antigen. *J Biol Chem*. 2000;275(50):39458-39465. doi:10.1074/jbc.M006626200.
170. Trepat X, Chen Z, Jacobson K. Cell migration. *Compr Physiol*. 2012;2(4):2369-2392. doi:10.1002/cphy.c110012.Cell.
171. Arribas J, Bech-Serra JJ, Santiago-Josefat B. ADAMs, cell migration and cancer. *Cancer Metastasis Rev*. 2006;25:57-68. doi:10.1007/s10555-006-7889-6.
172. Eccles SA, Box C, Court W. Cell migration/invasion assays and their application in cancer drug discovery. *Biotechnol Annu Rev*. 2005;11:391-421. doi:10.1016/S1387-2656(05)11013-8.
173. Entschladen F, Drell VI TL, Lang K, Joseph J, Zaenker KS. Tumour-cell migration, invasion, and metastasis: Navigation by neurotransmitters. *Lancet Oncol*. 2004;5:254-258. doi:10.1016/S1470-2045(04)01431-7.
174. Alshareeda AT, Negm OH, Green AR, et al. KPNA2 is a nuclear export protein that contributes to aberrant localisation of key proteins and poor prognosis of breast cancer. *Br J Cancer*. 2015;112(12):1929-1937. doi:10.1038/bjc.2015.165.
175. Abdul Razak AR, Mau-Soerensen M, Gabrail NY, et al. First-in-class, first-in-human phase I study of selinexor, a selective inhibitor of nuclear export, in patients with advanced solid tumors. *J Clin Oncol*. 2016;34(34):4142-4150. doi:10.1200/JCO.2015.65.3949.
176. Alexander TB, Lacayo NJ, Choi JK, Ribeiro RC, Pui CH, Rubnitz JE. Phase I study of selinexor, a selective inhibitor of nuclear export, in combination with fludarabine and cytarabine, in pediatric relapsed or refractory acute leukemia. *J Clin Oncol*. 2016;34(34):4094-4101. doi:10.1200/JCO.2016.67.5066.
177. He H, Li D-W, Yang L-Y, et al. A novel bifunctional mitochondria-targeted anticancer agent with high selectivity for cancer cells. *Sci Rep*. 2015;5:1-10. doi:10.1038/srep13543.
178. Deepa PR, Vandhana S, Jayanthi U, Krishnakumar S. Therapeutic and Toxicologic

Evaluation of Anti-Lipogenic Agents in Cancer Cells Compared with Non-Neoplastic Cells. *Basic Clin Pharmacol Toxicol*. 2012;110(6):494-503. doi:10.1111/j.1742-7843.2011.00844.x.

179. Kim C, Hwang K, Choi K. Anti-metastatic potential of resveratrol and its metabolites by the inhibition of epithelial-mesenchymal transition , migration , and invasion of malignant cancer cells. *Phytomedicine*. 2016;23:1787-1796. doi:10.1016/j.phymed.2016.10.016.
180. Vermeulen K, Bockstaele DR Van, Berneman ZN. The cell cycle : a review of regulation , deregulation and therapeutic targets in cancer. *Cell Prolif*. 2003;36:131-149.
181. Malumbres M, Barbacid M. Cell cycle, CDKs and cancer: a changing paradigm. *Nat Rev Cancer*. 2009;9:153-166. doi:10.1038/nrc2602.
182. Yim D, Singh RP, Agarwal C, Lee S, Chi H, Agarwal R. A novel anticancer agent, decursin, induces G1 arrest and apoptosis in human prostate carcinoma cells. *Cancer Res*. 2005;65(3):1035-1044. doi:65/3/1035 [pii].
183. Clohessy JG, Zhuang J, Brady HJM. Characterisation of Mcl-1 cleavage during apoptosis of haematopoietic cells. *Br J Haematol*. 2004;125:655-665. doi:10.1111/j.1365-2141.2004.04949.x.
184. Varin E, Denoyelle C, Brotin E, et al. Downregulation of Bcl-xL and Mcl-1 is sufficient to induce cell death in mesothelioma cells highly refractory to conventional chemotherapy. *Carcinogenesis*. 2010;31(6):984-993. doi:10.1093/carcin/bgq026.
185. Yang C, Kaushal V, Shah S V, Kaushal GP. Mcl-1 is downregulated in cisplatin-induced apoptosis, and proteasome inhibitors restore Mcl-1 and promote survival in renal tubular epithelial cells. *Am J Physiol Renal Physiol*. 2007;292:F1710-7. doi:10.1152/ajprenal.00505.2006.
186. Li Y, He K, Huang Y, et al. Betulin induces mitochondrial cytochrome c release associated apoptosis in human cancer cells. *Mol Carcinog*. 2010;49:630-640. doi:10.1002/mc.20638.
187. Chen R, Guo L, Chen Y, Jiang Y, Wierda WG, Plunkett W. Homoharringtonine reduced Mcl-1 expression and induced apoptosis in chronic lymphocytic leukemia. *Blood*. 2011;117(1):156-164. doi:10.1182/blood-2010-01-262808.
188. Siraj AK, Pratheeshkumar P, Parvathareddy SK. Overexpression of PARP is an independent prognostic marker for poor survival in Middle Eastern breast cancer and

its inhibition can be enhanced with embelin co-treatment. *Oncotarget*. 2018;9(99):37319-37332.

189. Sun S-C. Non-canonical NF-κB signaling pathway. *Cell Res*. 2011;21(1):71-85. doi:10.1038/cr.2010.177.
190. Brown K, Park S, Kanno T, Franzoso G, Siebenlist U. Mutual regulation of the transcriptional activator NF-kappa B and its inhibitor, I kappa B-alpha. *Proc Natl Acad Sci*. 1993;90:2532-2536. doi:10.1073/pnas.90.6.2532.
191. Fagerlund R, Kinnunen L, Ko M, Julkunen I, Mele K. NF- kB Is Transported into the Nucleus by Importin a3 and Importin a4 *. *J Biol Chem*. 2005;280(16):15942-15951. doi:10.1074/jbc.M500814200.
192. Maguire O, Tornatore KM, O' Loughlin K, Venuto RC, Minderman H. Nuclear translocation of Nuclear Factor of Activated T cells (NFAT) as a quantative pharmacodynamic parameter for tacrolimus. *Cytom A*. 2013;83(12):1096-1104. doi:10.1016/j.immuni.2010.12.017.Two-stage.
193. Hessmann E, Ellenrieder V, Koenig A. NFAT in Pancreatic Carcinogenesis. 2014;5(6):1-5. doi:10.4172/2157-2518.1000203.
194. Shou J, Jing J, Xie J, et al. Nuclear factor of activated T cells in cancer development and treatment. *Cancer Lett*. 2015;361(2):174-184. doi:10.1016/j.canlet.2015.03.005.
195. Qin J, Nag S, Wang W, et al. NFAT as a cancer target: Mission possible? *Biochim Biophys Acta*. 2016;1846(2):297-311. doi:10.1016/j.bbcan.2014.07.009.NFAT.
196. Otis KO, Thompson KR, Martin KC. Importin-mediated nuclear transport in neurons. *Curr Opin Neurobiol*. 2006;16:329-335. doi:10.1016/j.conb.2006.05.001.
197. Schneider-poetsch T, Ju J, Eyler DE, et al. Inhibition of eukaryotic translation elongation by Cycloheximide and Lac. *Nat Chem Biol*. 2010;6(3):209-217. doi:10.1038/nchembio.304.Inhibition.
198. Beals CR, Clipstone N a, Ho SN, Crabtree GR. Nuclear localization of NF-ATc by a calcineurin-dependent, cyclosporin-sensitive intramolecular interaction. *Genes Dev*. 1997;4:824-834. doi:10.1101/gad.11.7.824.
199. Miyamoto Y, Hieda M, Harreman MT, et al. Importin α can migrate into the nucleus in an importin β- and Ran-independent manner. *EMBO J*. 2002;21(21):5833-5842. doi:10.1093/emboj/cdf569.
200. Kose S, Imamoto N, Tachibana T, Shimamoto T, Yoneda Y. Ran-unassisted nuclear

migration of a 97-kD component of nuclear pore- targeting complex. *J Cell Biol*. 1997;139(4):841-850. doi:10.1083/jcb.139.4.841.

201. Quensel C, Friedrich B, Sommer T, Hartmann E, Kohler M. In Vivo Analysis of Importin α Proteins Reveals Cellular Proliferation Inhibition and Substrate Specificity. *Mol Cell Biol*. 2004;24(23):10246-10255. doi:10.1128/MCB.24.23.10246.
202. Waldmann I, Wälde S, Kehlenbach RH. Nuclear import of c-Jun is mediated by multiple transport receptors. *J Biol Chem*. 2007;282(38):27685-27692. doi:10.1074/jbc.M703301200.
203. Kenakin TP. *Pharmacology in Drug Discovery*. First. London, United Kingdom: Elsevier; 2012.
204. Zhou W, Wang Y, Lu A, Zhang G. Systems pharmacology in small molecular drug discovery. *Int J Mol Sci*. 2016;17:1-16. doi:10.3390/ijms17020246.
205. Reeves PT, Roesch C, Raghnaill MN. Drug action and pharmacodynamics. Merck veterinary manual. http://www.merckvetmanual.com/pharmacology/pharmacology-introduction/drug-action-and-pharmacodynamics. Published 2016. Accessed June 2, 2017.
206. Wang J. Comprehensive assessment of ADMET risks in drug discovery. *Curr Pharm Des*. 2009;15:2195-2219. doi:10.2174/138161209788682514.
207. Bohnert T, Prakash C. ADME Profiling in Drug Discovery and Development: An overview. In: *Drug Metabolism and Interactions*. First. John Wiley & Sons Inc.; 2012:1-42.
208. Kebamo S, Tesema S. The Role of Biotransformation in Drug Discovery and Development. *J Drug Metab Toxicol*. 2015;06(05):1-13. doi:10.4172/2157-7609.1000196.
209. Iskar M, Zeller G, Zhao XM, van Noort V, Bork P. Drug discovery in the age of systems biology: The rise of computational approaches for data integration. *Curr Opin Biotechnol*. 2011;23:1-8. doi:10.1016/j.copbio.2011.11.010.
210. Parasuraman S. Toxicological screening. *Pharmacol Pharmacother*. 2011;2(2):74-79.
211. Kerns EH, Di L. *Drug-like Properties:Concept,Structure Design and Methods: From ADME to Toxicity Optimization*. 1st ed. Elsevier; 2008. doi:10.1124/mol.105.019547.et.
212. Chen M, Will Y. *Drug Induced Liver Toxicity*. Louisville, Kentucky: Human Press; 2018.

doi:10.1007/978-1-4939-7677-5.

213. Barka T, Popper H. Liver enlargement and drug toxicity. *Medicine (Baltimore)*. 1967;46(2):1-15.

214. van de Waterbeemd H, Gifford E. ADMET in silico modelling: Towards prediction paradise? *Nat Rev Drug Discov*. 2003;2(3):192-204. doi:10.1038/nrd1032.

215. Censi R, Martino P Di. Polymorph Impact on the Bioavailability and Stability of Poorly Soluble Drugs. *Molecules*. 2015;20:18759-18776. doi:10.3390/molecules201018759.

216. Benet LZ, Zia-amirhosseini P. Basic Principles of Pharmacokinetics. *Toxicol Pathol*. 1995;23(2):115-123.

217. Jang GR, Harris RZ, Lau DT. Pharmacokinetics and Its Role in Small Molecule Drug Discovery. *Med Res Rev*. 2001;21(5):382-396.

218. Wang J, Urban L. The impact of early ADME profiling on drug discovery and. *Drug Discov World*. 2004:73-86.

219. le Coutre P, Kreuzer K, Pursche S, et al. Pharmacokinetics and cellular uptake of imatinib and its main metabolite CGP74588. *Cancer Chemother Pharmacol*. 2004;53:313-323. doi:10.1007/s00280-003-0741-6.

220. Alavijeh MS, Chishty M, Qaiser MZ, Palmer AM. Drug Metabolism and Pharmacokinetics , the Blood-Brain Barrier , and Central Nervous System Drug Discovery. *J Am Soc Experimeantal Neurother*. 2005;2:554-571.

221. Peters S, Zimmermann S, Adjei AA. Oral epidermal growth factor receptor tyrosine kinase inhibitors for the treatment of non-small cell lung cancer: Comparative pharmacokinetics and drug-drug interactions. *Cancer Treat Rev*. 2014;40(8):917-926. doi:10.1016/j.ctrv.2014.06.010.

222. Yang J, Bill MA, Young GS, et al. Novel small molecule XPO1/CRM1 inhibitors induce nuclear accumulation of TP53, phosphorylated MAPK and apoptosis in human melanoma cells. *PLoS One*. 2014;9(7). doi:10.1371/journal.pone.0102983.

223. Garzon R, Savona M, Baz R, et al. A Phase I Clinical Trial of Single-Agent Selinexor in Acute Myeloid Leukemia. *Blood J*. 2019:1-21. doi:10.1182/blood-2016-11-750158.

224. Gunaydin H, Altman MD, Ellis JM, et al. Strategy for Extending Half-life in Drug Design and Its Signi fi cance. *ACS Med Chem Lett*. 2018;9:528-533. doi:10.1021/acsmedchemlett.8b00018.

225. Kumar P, Sharma SM. An overview of purification methods for proteins. *Int J Appl Res*.

2015;1(12):450-459.

226. Volkman H. Affinity purification of GST fusion proteins. http://schepartzlab.yale.edu/intranet/protocols/AffinityPurification.pdf. Accessed December 9, 2017.
227. Hedhammar M, Karlstrom A, Hober S. Chromatographic methods for protein purification. http://www.ispybio.com/search/protocols/purification protocol12.pdf. Published 2006.
228. Magdeldin S, Moser A. *Affinity Chromatography: Principles and Applications*. (Magdeldin S, ed.). In Tech; 2012. doi:10.5772/1959.
229. Wood DW. New trends and affinity tag designs for recombinant protein purification. *Curr Opin Struct Biol*. 2014;26:54-61.
230. Pina AS, Lowe CR, Roque AC. Challenges and opportunities in the purification of recombinant tagged proteins. *Biotechnol Adv*. 2014;32(2):366-381.
231. Harper S, Speicher DW. Purification of proteins fused to glutathione S-transferase. *Methods Mol Biol*. 2011;681:259-280. doi:10.1007/978-1-60761-913-0.
232. Young CL, Britton ZT, Robinson AS. Recombinant protein expression and purification: A comprehensive review of affinity tags and microbial applications. *Biotechnol J*. 2012;7:620-634. doi:10.1002/biot.201100155.
233. Davis FP, Sali A. The overlap of small molecule and protein binding sites within families of protein structures. *PLoS Comput Biol*. 2010;6(2):1-10. doi:10.1371/journal.pcbi.1000668.
234. Heller GT, Aprile FA, Vendruscolo M. Methods of probing the interactions between small molecules and disordered proteins. *Cell Mol Life Sci*. 2017;74(17):3225-3243. doi:10.1007/s00018-017-2563-4.
235. Tuffery P, Derreumaux P. Flexibility and binding affinity in protein-ligand, protein-protein and multi-component protein interactions: Limitations of current computational approaches. *J R Soc Interface*. 2012;9(66):20-33. doi:10.1098/rsif.2011.0584.
236. Holdgate G, Geschwindner S, Breeze A, et al. Biophysical Methods in Drug Discovery from Small Molecule to Pharmaceutical. In: Williams M, Daviter T, eds. *Protein-Ligand Interactions: Mrthods and Applications, Methods in Molecular Biology*. Vol 1008. Springer Science; 2013:327-355. doi:10.1007/978-1-62703-398-5.

237. Tobias R. *Biomolecular Binding Kinetics Assays on the Octet Platform*.; 2013.
238. Alsabban AE. Establishing methods to screen novel small molecules targeting insulin-like growth factor/insulin-like growth factor binding protein interaction. 2009.
239. Wartchow CA, Podlaski F, Li S, et al. Biosensor-based small molecule fragment screening with biolayer interferometry. *J Comput Aided Mol Des*. 2011;25(7):669-676. doi:10.1007/s10822-011-9439-8.
240. Buckle P. *Optimising Protein-Protein and Protein-Small Molecule Kinetics Assays*.; 2017.
241. Holdgate G a, Ward WHJ. Measurements of binding thermodynamics in drug discovery. *Drug Discov Today*. 2005;10(22):1543-1550.
242. Kuriyan J, Konforti B, Wemmer D. Molecular Recognition : The Thermodynamics of Binding. In: *The Molecules of Life*. Garland Publisher; 2009:1-58.
243. Pugh DJR, Eiso AB, Faro A, Lutya PT, Hoffmann E, Rees DJG. DWNN, a novel ubiquitin-like domain, implicates RBBP6 in mRNA processing and ubiquitin-like pathways. *BMC Struct Biol*. 2006;6(1):1-12. doi:10.1186/1472-6807-6-1.
244. Gurung AB, Bhattacharjee A, Ali MA, Al-hemaid F, Lee J. Binding of small molecules at interface of protein – protein complex – A newer approach to rational drug design. *Saudi J Biol Sci*. 2017;24(2):379-388. doi:10.1016/j.sjbs.2016.01.008.
245. Kamat V, Rafique A. Designing binding kinetic assay on the bio-layer interferometry (BLI) biosensor to characterize antibody-antigen interactions. *Anal Biochem*. 2017;536:16-31. doi:10.1016/j.ab.2017.08.002.
246. De Lucas Laguna R, Herranz Pinto P, De La Rubio Torre F, et al. Binding affinity and kinetic analysis of targeted small molecule-modified nanoparticles. *Bioconjug Chem*. 2010;21(1):14-19. doi:10.1021/bc900438a.Binding.
247. Abdiche Y, Malashock D, Pinkerton A, Pons J. Determining kinetics and affinities of protein interactions using a parallel real-time label-free biosensor , the Octet. *Anal Biochem*. 2008;377:209-217. doi:10.1016/j.ab.2008.03.035.
248. Aslantürk ÖS. In Vitro Cytotoxicity and Cell Viability Assays : Disadvantages In Vitro Cytotoxicity and Viability Assays : Principles , Advantages , and Disadvantages. *IntechOpen*. 2018:1-18. doi:10.5772/intechopen.71923.
249. Jo HY, Kim Y, Park HW, et al. The Unreliability of MTT Assay in the Cytotoxic Test of Primary Cultured Glioblastoma Cells. *Exp Neurobiol*. 2015;24(3):235-245.

250. Mori S, Chang JT, Andrechek ER, et al. An Anchorage-Independent Cell Growth Signature Identifies Tumors with Metastatic Potential. *Oncogene*. 2009;28(31):2796-2805. doi:10.1038/onc.2009.139.An.

251. Ikenberg K, Valtcheva N, Brandt S, et al. KPNA2 is overexpressed in human and mouse endometrial cancers and promotes cellular proliferation. *J Pathol*. 2014;234(2):239-252. doi:10.1002/path.4390.

252. Huang L, Wang H-Y, Li J-D, et al. KPNA2 promotes cell proliferation and tumorigenicity in epithelial ovarian carcinoma through upregulation of c-Myc and downregulation of FOXO3a. *Cell Death Dis*. 2013;4:e745. doi:10.1038/cddis.2013.256.

253. Karin M, Cao Y, Greten FR, Li Z-W. Nf-Kb in Cancer: From Innocent Bystander To Major Culprit. *Nat Rev Cancer*. 2002;2:301-310. doi:10.1038/nrc780.

254. Mancini M, Toker A. NFAT proteins: emerging roles in cancer progression. *Nat Rev Cancer*. 2009;9(11):810-820. doi:10.1038/nrc2735.

255. Leaner VD, Donninger H, Birrer MJ. Transcription factors as targets for cancer therapy: AP-1 a potential therapeutic target. *Curr Cancer Ther Rev*. 2007;3:1-6. doi:10.1038/nrc906.

256. Masimirembwa CM, Bredberg Ui, Andersson TB. Metabolic stability for drug discovery and development: Pharmacokinetic and biochemical challenges. *Clin Pharmacokinet*. 2003;42(6):515-528. doi:10.2165/00003088-200342060-00002.

257. Zigeuner R, Shariat SF, Margulis V, et al. Tumour Necrosis Is an Indicator of Aggressive Biology in Patients with Urothelial Carcinoma of the Upper Urinary Tract. *Eur Urol*. 2010;57(4):575-581. doi:10.1016/j.eururo.2009.11.035.

258. Inoue H, Kauffman M, Shacham S, et al. CRM1 blockade by selective inhibitors of nuclear export attenuates kidney cancer growth. *J Urol*. 2013;189(6):2317-2326. doi:10.1016/j.juro.2012.10.018.

259. Wettersten HI, Landesman Y, Friedlander S, Shacham S, Kauffman M, Weiss RH. Specific inhibition of the nuclear exporter exportin-1 attenuates kidney cancer growth. *PLoS One*. 2014;9(12):1-15. doi:10.1371/journal.pone.0113867.

260. Du X, Li Y, Xia Y, et al. Insights into Protein – Ligand Interactions : Mechanisms , Models , and Methods. *Int J Mol Sci*. 2016;17(144):1-34. doi:10.3390/ijms17020144.

261. Fabrini R, Luca A De, Stella L, et al. Monomer - Dimer Equilibrium in Glutathione Transferases : A Critical Re-Examination. *Biochemistry*. 2009;48:10473-10482.

doi:10.1021/bi901238t.

262. Hutsell S, Kimple RJ, Siderovski DP, Willard FS, Kimple AJ. High affinity immobilization of proteins using biotin- and GSTbased coupling strategies. *Methods Mol Biol*. 2011;(627):75-90. doi:10.1007/978-1-60761-670-2.

263. Shimada Y, Imamura M, Wagata T, Yamaguchi N, Tobe T. Characterization of 21 newly established esophageal cancer cell lines. *Cancer*. 1992;69(2):277-284. doi:10.1002/1097-0142(19920115)69:2<277::AID-CNCR2820690202>3.0.CO;2-C.

264. Veale R, Thornley A. Increased single class low-affinity Egf receptors expressed by human esophageal squamous carcinoma cell-lines. *S Afr J Sci*. 1989;85(6):375-379.

265. Ichida M, Finkel T. Ras Regulates NFAT3 Activity in Cardiac Myocytes. *J Biol Chem*. 2001;276(5):3524-3530. doi:10.1074/jbc.M004275200.

266. Dong Z, Xu RH, Kim J, et al. AP-1/Jun is required for early Xenopus development and mediates mesoderm induction by fibroblast growth factor but not by activin. *J Biol Chem*. 1996;271(17):9942-9946. doi:10.1074/jbc.271.17.9942.

267. Progatzky F, Dallman MJ, Lo Celso C. From seeing to believing: labelling strategies for in vivo cell-tracking experiments. *Interface Focus*. 2013;3:1-14. doi:10.1098/rsfs.2013.0001.

268. Walker JM. *BCA for Protein Quantitation*. 2nd Editio. Totowa, NJ: Humana Press; 2002.

269. Abcam. A Guide to Fluorochromes. http://docs.abcam.com/pdf/immunology/fluorochrome_guide.pdf. Published 2012. Accessed February 1, 2018.

270. Allard STM, Kopish K. Luciferase Reporter Assays : Powerful , Adaptable Tools for Cell Biology Research. *Cell Notes*. 2008;(21):23-26.

271. Maritz MF, Van Der Watt PJ, Holderness N, Birrer MJ, Leaner VD. Inhibition of AP-1 suppresses cervical cancer cell proliferation and is associated with p21 expression. *Biol Chem*. 2011;392:439-448. doi:10.1515/BC.2011.036.

272. Wohnsland F, Faller B. High-throughput permeability pH profile and high-throughput alkane/water log P with artificial membranes. *J Med Chem*. 2001;44:923-930. doi:10.1021/jm001020e.

273. Alelyunas YW, Pelosi-Kilby L, Turcotte P, Kary MB, Spreen RC. A high throughput dried DMSO Log D lipophilicity measurement based on 96-well shake-flask and atmospheric

pressure photoionization mass spectrometry detection. *J Chromatogr A*. 2010;1217:1950-1955. doi:10.1016/j.chroma.2010.01.071.

274. Obach RS. Prediction of Human Clearance of Twenty-Nine Drugs From Hepatic Microsomal Intrinsic Clearance Data : an Examination of in Vitro Half-Life Approach and Nonspecific Binding To Microsomes. *Drug Metab Dispos*. 1999;27(11):1350-1359.

Appendix 1

A. Cell cycle profile of HeLa cervical cancer cells following C60 treatment at different time points.

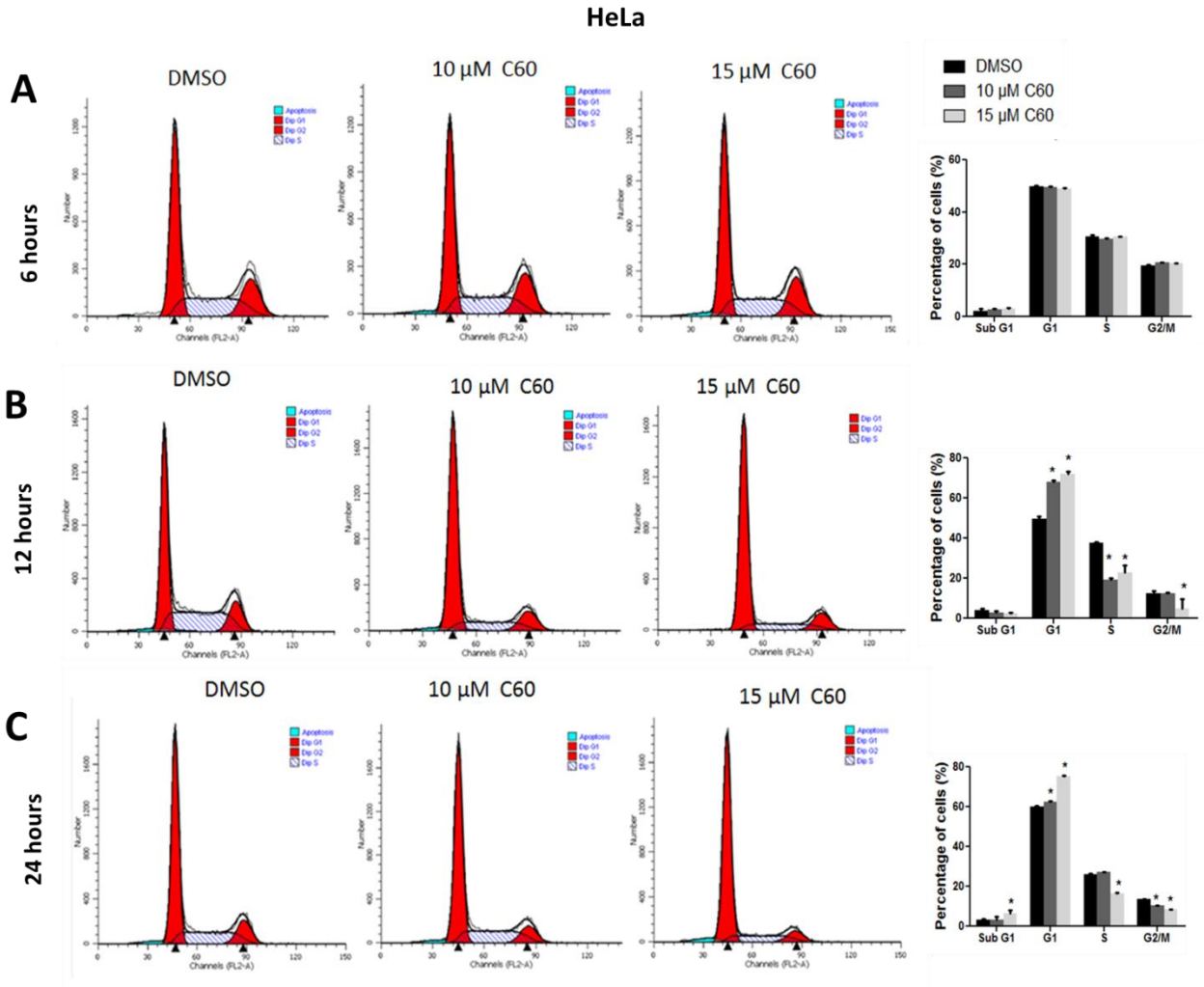

B. Cell cycle profile of WHCO oesophageal cancer cells following C60 treatment at different time points.

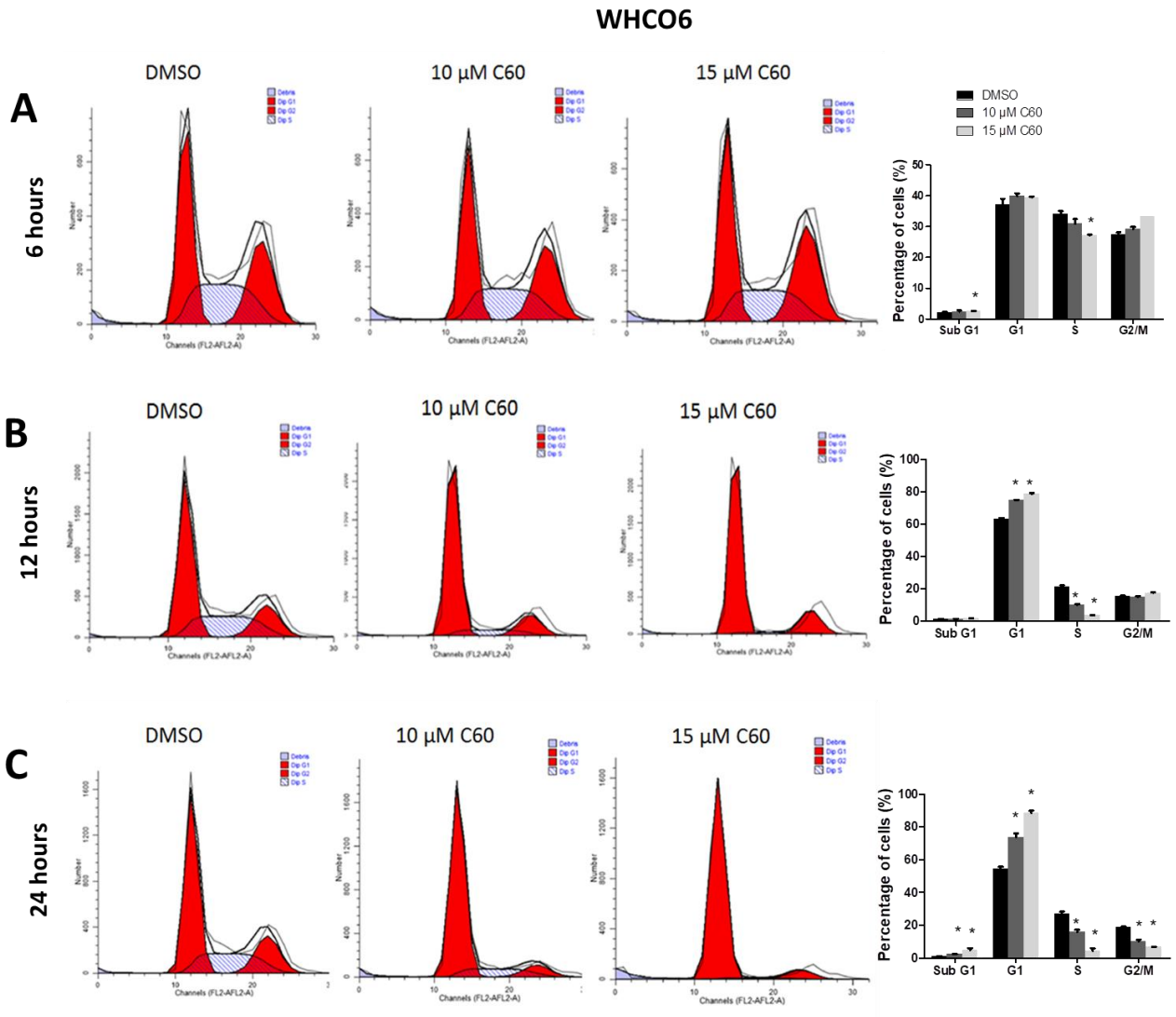

Figure A.1. C60 suppresses cell cycle progression in HeLa and WHCO6 cancer cell lines. Cell cycle analysis done after cells were treated with 10 µM and 15 µM C60 for 6 hours (A), 12 hours (B) and 24 hours (C) showed an increase in the population of cells at the G1 phase of the cell cycle and a significant decrease in the percentage of cells in the S and G2/M phases of the cycle. These resultant changes were observed more at 12 and 24 hours post C60 treatment. Results are shown as a mean ± SEM of experiments performed in triplicate and repeated at least three independent times (*$p \leq 0.05$).

Appendix 2

A. Changes in expression of cell cycle regulatory protein in HeLa cervical cancer cells following C60 treatment

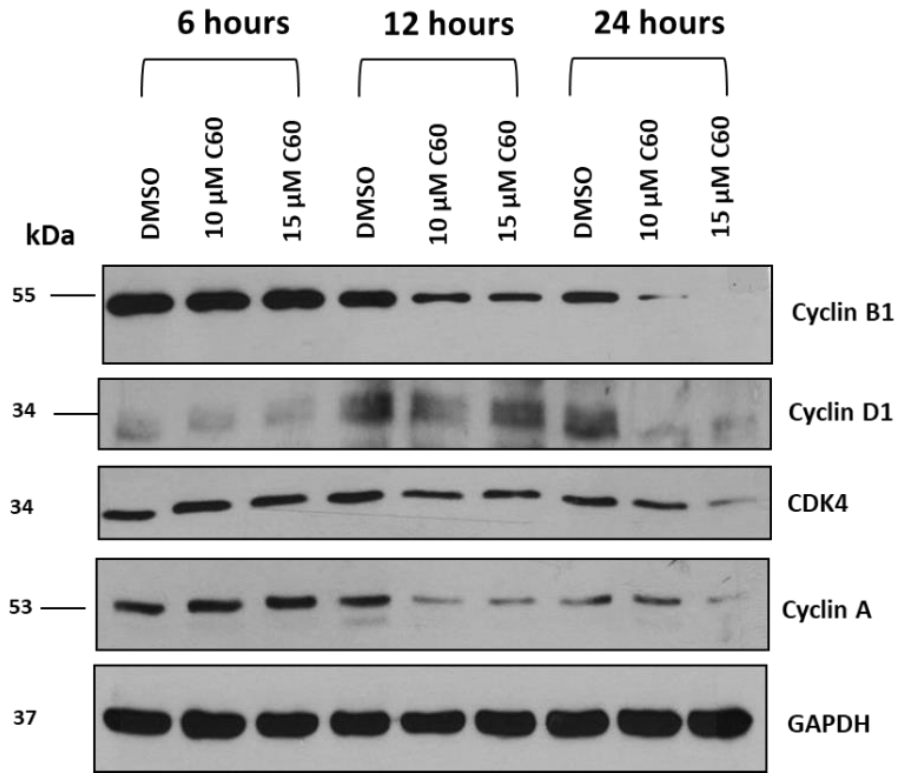

B. Changes in expression of cell cycle regulatory protein in WHCO6 oesophageal cancer cells following C60 treatment

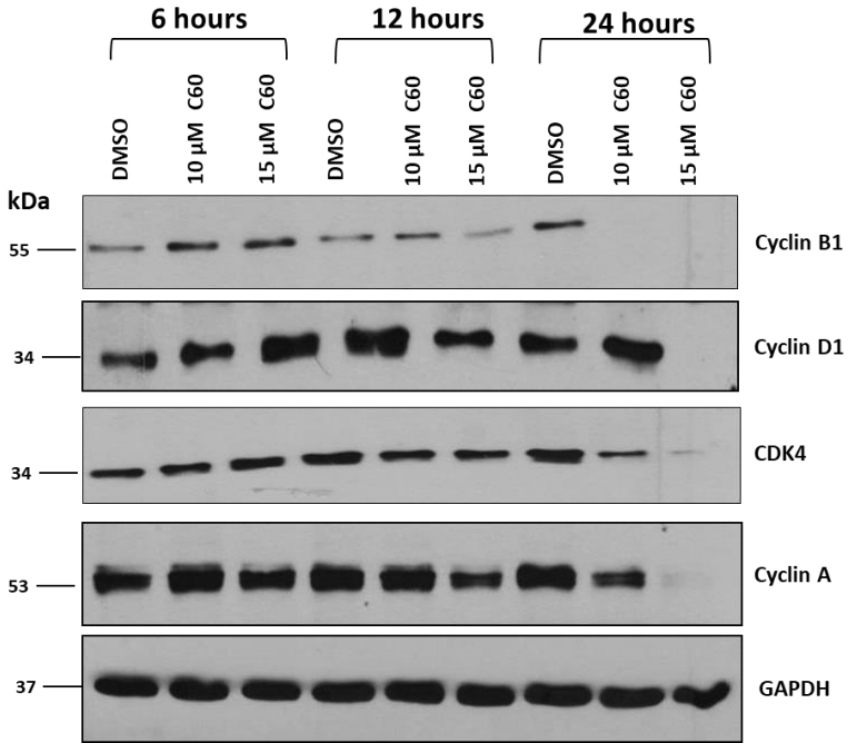

Figure A.2. Effect of C60 treatment on cell cycle regulatory proteins. HeLa cervical cancer cell and WHCO6 oesophageal cancer cells were treated with DMSO (vehicle control), 10 µM or 15 µM C60 for 6, 12 or 24 hours. The effect of treatment on cell cycle markers was investigated via western blot analysis with GAPDH as the loading control. Results shown are representative of experiments performed three independent times.

Appendix 3

A. Effect of C60 treatment on the morphology of HeLa cervical cancer cells.

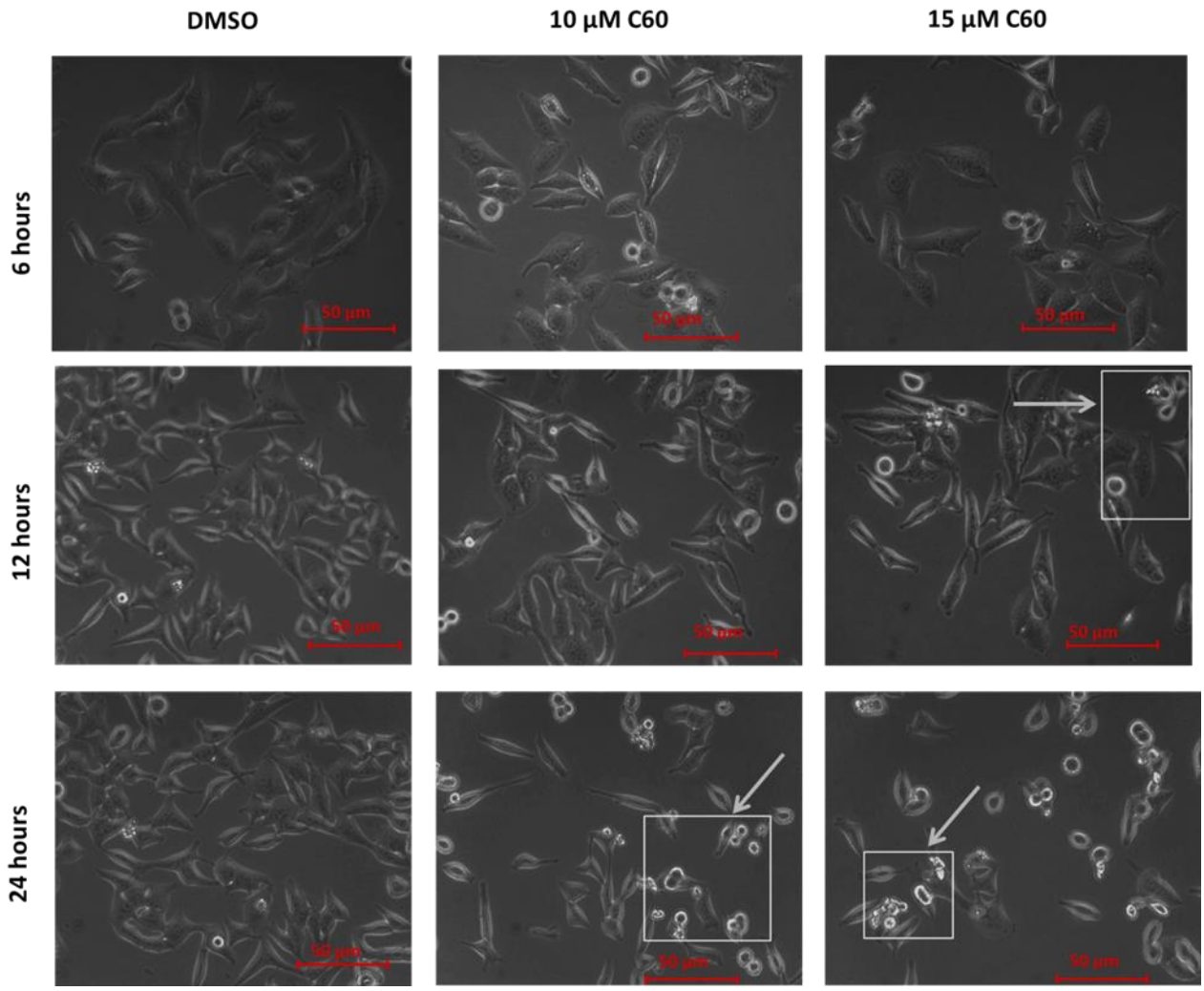

B. Effect of C60 treatment on the morphology of WHCO6 oesophageal cancer cells.

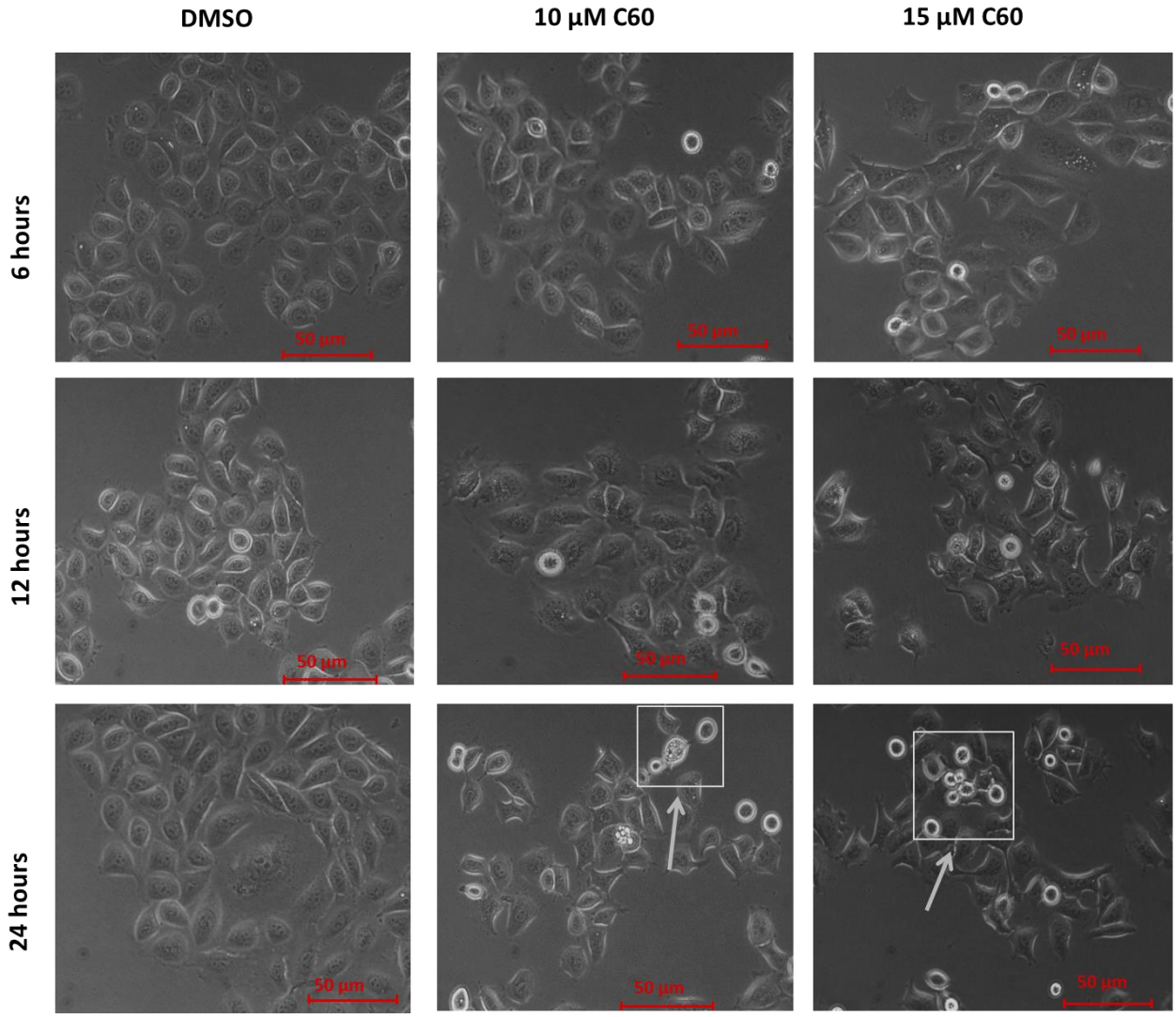

Figure A.3. Effect of C60 treatment on the morphology of HeLa and WHCO6 cancer cells. Images of HeLa cervical cancer cells (A) and WHCO6 oesophageal cancer cells (B) treated with 10 µM and 15 µM C60 or DMSO (vehicle control) at different time points were captured using Primovert inverted microscope with Axio cam ERC 5s (Zeiss, Göttingen, Germany) at 20X magnification.